YANKEE ATOMIC ELECTRIC COMPANY

YAEC-1683-A

MICBURN-3/CASMO-3/TABLES-3/SIMULATE-3 BENCHMARKING OF VERMONT YANKEE CYCLES 9 THROUGH 13

March 1989

Principal Investigators:

B. Y. Hubbard

D. J. Morin

J. Pappas

R. C. Potter

Prepared By: Richard A. Woehlke 3/10/89

R. A. Woehlke, VY Lead Engineer (Date)

Reactor Physics Group

Approved By: R. Cacciapouti 3/14/89

R. J. Cacciapouti, Manager (Date)

Reactor Physics Group

Approved By: Bruce C. Slifer 3/14/89

B. C. Slifer, Director (Date)

Nuclear Engineering Department

Yankee Atomic Electric Company

580 Main Street

Bolton, Massachusetts 01740-1398

UNITED STATES
NUCLEAR REGULATORY COMMISSION
WASHINGTON, D. C. 20555

March 15, 1990

Mr. R. W. Capstick, Licensing Engineer
Vermont Yankee Nuclear Power Corporation
Engineering Office
580 Main Street
Bolton, MA 01740

Dear Mr. Capstick:

SUBJECT: ACCEPTANCE FOR REFERENCING OF TOPICAL REPORT YAEC-1683, "MICBURN-3/CASMO-3/TABLES-3/SIMULATE-3 BENCHMARKING OF VERMONT YANKEE CYCLES 9 THROUGH 13"

The staff has completed its review of the Topical Report YAEC-1683, "MICBURN-3/CASMO-3/TABLES-3/SIMULATE-3, Benchmarking of Vermont Yankee Cycles 9 through 13," submitted for NRC review by the Vermont Yankee Nuclear Power Corporation by letter dated March 27, 1989. Additional information was incorporated into the report by letter dated February 2, 1990. The purpose of this topical report (YAEC-1683) is to demonstrate the suitability of these codes for plant licensing of future Vermont Yankee cycles. Cold critical startup and hot steady state full power operation are modeled. Extensive three dimensional comparisons are made between the calculated and measured in-core detector responses.

We find the application of YAEC-1683 to be acceptable for referencing in license applications to the extent specified, and under the limitations delineated, in YAEC-1683 and the associated NRC technical evaluation. The evaluation defines the basis for acceptance of this topical report.

We do not intend to repeat our review of the matters found acceptable as described in YAEC-1683 when the report appears as a reference in license applications, except to assure that the material presented is applicable to the specific plant involved. Our acceptance applies only to the matters described in the application of YAEC-1683.

In accordance with procedures established in NUREG-0390, it is requested that the Vermont Yankee Nuclear Power Corporation publish accepted versions of this topical report, proprietary and non-proprietary, within three months of receipt of this letter. The accepted versions shall include an -A (designating accepted) following the report identification symbol.

Should our criteria or regulations change so that our conclusions as to the acceptability of the report are invalidated, Vermont Yankee Nuclear Power Corporation and/or the applicants referencing the topical report will be

expected to revise and resubmit their respective documentation, or submit justification for the continued effective applicability of the topical report without revision of their respective documentation.

Sincerely,

A. C. Thadani

Ashok C. Thadani, Director
Division of Systems Technology
Office of Nuclear Reactor Regulation

Enclosure:
YAEC-1683 Evaluation

SAFETY EVALUATION FOR THE TOPICAL REPORT YAEC-1683,
"MICBURN-3/CASMO-3/TABLES-3/SIMULATE-3
BENCHMARKING OF VERMONT YANKEE CYCLES 9 THROUGH 13"

1.0 INTRODUCTION

By letter dated March 27, 1989, the Vermont Yankee Nuclear Power Corporation, the licensee for the Vermont Yankee Nuclear Power plant, submitted the Topical Report YAEC-1683 for NRC review (Refs. 1-5). Additional information was submitted on February 2, 1990 (Ref. 6). This report presents the results of benchmarking of the above code package against several recent cycles of Vermont Yankee (VY) operating data. VY fuel and core models have been used to calculate cold and hot critical eigenvalues and detector response data at various exposure points at which steady state measured data had been collected. It is YAEC's intention to use these codes for reload design, steady state licensing and plant support applications.

The two principal components of the code package, CASMO-3 and SIMULATE-3 are currently under review (Refs. 7 and 8). An overview of the topical report appears in the next section. The technical evaluation is presented in Section 3.0.

The following evaluation incorporates our consultant's, BNL, contribution to this review (FIN No. A-3868 Task No. 14). Restrictions to be observed in the application of this topical report are listed in Section 3.7.

2.0 SUMMARY OF TOPICAL REPORT

The MICBURN-3/CASMO-3/TABLES-3/SIMULATE-3 code package is a simplified version of an earlier code package (Refs. 9-12) which it now replaces. The MICBURN-3 code (Ref. 2) is similar to its predecessor MICBURN (Ref. 9) and calculates the burnup in a fuel rod which contains initially homogeneously distributed gadolinium. This code generates effective microscopic cross sections as a function of burnup for use in the lattice calculation. CASMO-3 (Ref. 3), an

improved version of CASMO (Ref. 10), is a multigroup two-dimensional transport theory code for fuel assembly burnup calculations. This code generates few-group macroscopic cross sections and reaction rates for use in core calculations. TABLES-3 (Ref. 11) is a computer program which provides a link between CASMO-3 and SIMULATE-3. It processes two-group cross sections, generated by CASMO-3, into two- and three-dimensional tables which are used in SIMULATE-3 to develop homogenized two-group cross sections in each node. SIMULATE-3 is a three-dimensional coupled neutronics-thermal hydraulics analysis code. While the functions of this code are essentially the same as those performed by its predecessor, SIMULATE-E (Ref. 12), the physics model uses the QPANDA (Ref. 3) method which solves the three-dimensional two-group neutron diffusion equation and generates a global (homogeneous flux distribution) and a local (heterogeneous assembly flux distribution) solution. This code uses assembly discontinuity factors (ADFs) generated by CASMO-3 in the calculation of neutron currents between nodes. The concept of the ADF is also employed in the treatment of the baffle/reflector nodes. This operation eliminates the need for adjustments of the power distribution. Unlike SIMULATE-E no albedos are used.

Vermont Yankee is a General Electric BWR-3 D-lattice plant with a rated power of 1593 MWt. The VY core consists of 368 fuel assemblies with an 8x8 fuel rod array. The U-235 enrichment, gadolinium loading and active fuel length vary among the designs used in the cycles modeled in the benchmarking. Starting with Cycle-9 the VY core has been operated on longer cycles, thus requiring larger reload batches, higher enrichment and heavier burnable poison loadings.

The data which form the bulk of the measured VY database used in the benchmarking of the codes have been collected from the twenty instrumented locations containing the local power range monitors (LPRM's) and the traversing incore probes (TIPs).

Lattice depletion calculations for each fuel type were carried out at the standard (0%, 40% and 70%) voids for the uncontrolled assemblies and at 0% voids for the controlled assemblies with the appropriate branch cases. Top, bottom and radial reflector cross sections were also obtained from CASMO-3. A separate cold model was used for the generation of cold cross section sets. Both hot and

cold cross sections were processed by TABLES-3 so that cross sections tables as a function of their independent variables, (exposure, void history, moderator temperature and control state) could be accessed by SIMULATE-3. Similarly, two separate SIMULATE-3 models were set up; a hot model and a cold model. In the VY SIMULATE-3 input model there are 27 axial nodes per assembly and one radial node per assembly. Depending on the active fuel length (144 in. or 150 in.) a fuel assembly has either 24 or 25 axial zones. The side reflector is represented by adding a pseudo assembly which consists of reflector material. A node of reflector material is added to each end of a fuel assembly. An extra node is added in the region above the 144-inch fuel assembly. The VY SIMULATE-3 model provides a spacer correction option and, when the location of the spacers in the core is specified, SIMULATE-3 will adjust the thermal-hydraulic calculation downstream to allow for voiding due to the pressure drop in those regions. The thermal-hydraulic model in SIMULATE-3 includes a heat balance derived from actual VY plant measurements. The bypass flow and several other pressure drop parameters are obtained from FIBWR (Refs. 14-15). The standard EPRI void correlation (Ref. 16) is used for the calculation of the void distribution in the channels.

When a SIMULATE-3 depletion calculation has been carried to a cycle exposure at which a TIP measurement had been made, the calculated detector response (simulated TIP reading) is compared with the measured data. Comparisons of measured and calculated TIP data and critical state-points are discussed in the following section.

3.0 EVALUATION

The technical evaluation of YAEC-1683 is based on (1) the review of the application of the MICBURN-3/CASMO-3/TABLE-3/SIMULATE-3 code package to the operation of Cycles 9 through 13 of VY, (2) the review of both hot and cold models and their performance vis-a-vis measured data and (3) the evaluation of the YAEC response to the request for additional information (Ref. 6).

3.1 Fuel Pellet Densities

The fuel pellet stack density is an important CASMO-3 input parameter which varies for each fuel rod type and depends on the gadolinium concentration in the rod. YAEC uses a special procedure to adjust the CASMO-3 pellet density, when the calculated and measured assembly weights for a given fuel type disagree. The procedure consists of running a zero depletion CASMO-3 case for the typical lattice using the nominal pellet stack density as a first guess. The initial CASMO overall weight of the assembly is obtained from the cell area and the active fuel length, and the heavy metal density. This overall weight is then compared to the batch average of the as-loaded weights. The ratio of the as-loaded weight to the CASMO weight serves as the adjustment factor which is used to correct the CASMO-3 input density. This pellet stack density correction procedure is an acceptable method for accounting for the deviations between design and as-built densities.

3.2 Sensitivity Calculations

YAEC has carried out a wide range of sensitivity studies at each stage of the calculational process. The goal in these studies was to determine the effect of changes in specific input parameters on the predictions of the code package. Sensitivity calculations performed with the MICBURN-3 code showed that, except for the gadolinium concentration, the only state variable which had a significant effect on the output was the water density. This parameter directly affects the spectrum which determines the rate of gadolinium burnout. Comparisons with measurement together with this sensitivity study support the practice of using the recommended default value of zero voids in the buffer region when running production calculations. We find this approach acceptable.

Following recent studies indicating preferential channel bowing in D-lattice BWR plants (Reference-17), YAEC performed sensitivity calculations to determine the effects of channel bowing on lattice parameters and core reactivity. There is initially expected to be a small channel deflection, introduced by the orientation of the channels away from the control blade (wide-wide corner gap) to avoid interference between the channel and control blade. This initial

bowing is expected to increase with fuel burnup. The enrichment distribution in the fuel rods of an assembly is such as to provide optimum neutron multiplication and minimum local peaking for the non symmetric arrangement of the interassembly water gaps: lower enrichment adjacent to the wide gaps and higher enrichment next to the narrow gaps. When the channel is bowed, shifting the lattice toward the narrow-narrow corner, the overall reactivity of the fuel assembly is reduced since the loss in reactivity resulting from reduced moderation in the vicinity of the narrow water gaps is greater than the gain in reactivity occurring on the wide side. This effect is more pronounced as the void concentration in the assembly is increased.

In the YAEC sensitivity study a 40-mil (1 mm) channel deflection was assumed and standard depletion calculations were performed for one of the middle lattice sections. YAEC has stated (in Ref. 6) that while the deflection of 40 mils assumed in the analysis, and kept constant throughout the cycle, exceeds the expected initial as-built deflection, this value is believed to provide a more realistic simulation of the expected increase with fuel burnup. The sensitivity results showed that on the average there was a loss in the reactivity of the lattice by approximately 0.5%Δk, an amount of sufficient magnitude to warrant recalculation of the VY lattices with the appropriate branch cases. Since the bundles are fixed near the top and bottom axial nodes, the zones at each end of the fuel assembly were not recalculated. The bowed channel cross sections were incorporated into the SIMULATE-3 input model via TABLES-3. YAEC finds that these bowed channel cross sections significantly improve the agreement between the SIMULATE-3 core reactivity calculation and measurement.

Additional sensitivity calculations were carried out to determine the effect of modeling the channel spacers. When the spacer correction model was implemented in SIMULATE-3 an additional improvement between the calculated and measured core reactivity was observed.

Based on this improved calculation/measurement agreement, the YAEC method of modeling channel bowing and spacers is found acceptable for core reactivity calculations. The effects of channel bowing and spacers on the minimum critical

power ratio (MCPR) and linear heat generation rate (LHGR) are outside the scope of this review and were not considered.

3.3 The SIMULATE-3 Cold Model

YAEC has applied the SIMULATE-3 cold model to cold critical measurements spanning five cycles. These criticals covered a cycle exposure range from 0 to 9,000 MWd/ST and core average exposures ranging from 8,600 to 18,000 MWd/ST. Twenty three of these criticals had in-sequence control rod configurations while one was an adjacent-rod (local) type critical. The adjacent-rod calculation resulted in a k_{eff} outside the standard deviation of the eigenvalues of the 23 in-sequence critical calculations. It is stated in Reference 8 that based on comparisons of eight in-sequence and ten adjacent-rod criticals for Quad Cities 1 Cycles-1 and 2, there is statistical overlap in the calculated cold eigenvalues (Ref. 18, Table 4.2) demonstrating that SIMULATE-3 local critical results are consistent with in-sequence critical data. This severe test of the methodology demonstrates that the VY cold model is adequate for performing cold shutdown margin calculations.

3.4 The Audit Function

Cross section data generated with CASMO-3 for each fuel assembly type is processed by the TABLES-3 code into a tabular form for use in SIMULATE-3. Both cold and hot cross section sets are processed and loaded into a single library accessed by SIMULATE-3. The method used by TABLES-3 is based on defining node-average cross sections expressed as a sum of partial (or differential) cross sections. These partial cross sections are calculated at different statepoints by CASMO-3. The variables used to construct the VY cold model cross sections are exposure, void history, moderator temperature and instantaneous control rod. For the hot model the variables are exposure, void history, instantaneous voids, fuel temperature, instantaneous control and control rod history. To ensure the validity of the cross section data parameterized in TABLES-3, an AUDIT module in SIMULATE-3 provides a means of verifying that the cross section data for each lattice in TABLES-3 have been processed correctly at the specific CASMO-3 conditions. The results of the AUDIT calculation are compared against the

two-group k and M^2 sets and demonstrate that TABLES-3 preserves the CASMO-3 k and M^2 to within 0.1% (Ref. 6). It is concluded that TABLES-3 is an acceptable interface between CASMO-3 and SIMULATE-3.

3.5 Model Validation

SIMULATE-3 has been benchmarked against hot and cold critical statepoints from Cycles 9 through 13. Core eigenvalues and TIP traces generated by SIMULATE-3 have been used in the validation of the VY model. The hot eigenvalue averaged over Cycles 9 through 13 is 0.9989 with a standard deviation of 0.0010, while the cold eigenvalue averaged over the same cycles is 0.9968 with a standard deviation of 0.0017. The hot-to-cold bias is 0.0021. Comparison of these results with those obtained using the earlier YAEC code system (Refs. 9-12) indicates that the MICBURN-3/CASMO-3/TABLES-3/SIMULATE-3 code package can predict hot and cold reactivities with good accuracy.

Extensive comparisons of SIMULATE-3 calculated TIP readings and measured TIP readings were made at each of the 24 axial levels, in each of the 20 TIP locations and at every exposure statepoint. The nodal rms error statistically summed over all statepoints and for all five cycles is 2.94%. This is a slight improvement over the earlier YAEC SIMULATE-2 model which, when applied to the same benchmarked cycles, yielded a nodal rms error of 3.19%.

Axially integrated SIMULATE-3 TIPs were compared to the axially integrated measured TIPs to obtain the error in the radial power distribution. For the five cycles benchmarked, the average error in the radial power distribution is less than 2.2%. Good overall agreement between the model and plant data is also found in the comparison of radially integrated axial traces. A tendency of the SIMULATE-3 model to underpredict the power in the bottom of the core was observed, but this underprediction occurred only in the first few bottom nodes and does not affect the limiting core minimum critical power ratio or linear heat generation rate.

The slight improvement of the nodal rms error of SIMULATE-3 vis-a-vis SIMULATE-2 (2.94% vs 3.19) is noteworthy since the SIMULATE-3 results have been obtained

without any adjustment factors. The performance of SIMULATE-3 in predicting the VY power distributions, as shown in the benchmarking of Cycles 9 through 13, is acceptable.

3.6 Evaluation Summary

The benchmarking of the MICBURN-3/CASMO-3/TABLES-3/SIMULATE-3 code system against operating data from VY Cycles 9 through 13 has been reviewed. This review included the material provided in the YAEC-1683 topical report and supporting information supplied in References 16 and 18. The YAEC methodology is found to be acceptable for performing reload analyses for the Vermont Yankee Nuclear Power Station. This acceptance applies to fuel designs similar to those included in the Vermont Yankee Cycle-9 through Cycle-13 validation data-base. Should new fuel designs that are significantly different from those in the YAEC-1683 data-base be introduced in future cycles, the MICBURN-3/CASMO-3/TABLES-3/SIMULATE-3 code system will require additional validation for this new application.

3.7 Restrictions

The following restrictions are imposed on the use of YAEC-1683.

1. Spacer corrections and bowed channel cross sections should be used in the application of the Vermont Yankee model,

2. Application of the model should be restricted to the range of the operating conditions existing throughout the Vermont Yankee benchmarked Cycles 9-13, and

3. Should new fuel designs be introduced in the future, additional validation will be required for this system of codes.

4.0 REFERENCES

1. Letter, R.W. Capstick (Vermont Yankee Nuclear Power Corporation) to NRC, BVY89-29, dated March 27, 1989.

2. Ahlin, A., et al., MICBURN-3 - Microscopic Burnup in Burnable Absorber Rods, Studsvik/NFA-86/26, dated November, 1986. (Proprietary)

3. Edenius, M., et al., CASMO-3 A Fuel Assembly Burnup Program, Studsvik/NFA-86/7, dated November 1986. (Proprietary)

4. Ver Planck, D.M., et al., TABLES-3P Library Preparation Code for SIMULATE-3P, Studsvik/SOA-88/02, dated February 1988. (Proprietary)

5. Ver Planck, D.M., et al., SIMULATE-3P Advanced Three-Dimensional Two-Group Reactor Analysis Code, Studsvik/SOA-88/01, dated February 1988. (Proprietary)

6. Letter, Tremblay, L.A., Jr. (VYNPC) to Jones, R.C. (NRC), "Response to Request for Additional Information Regarding the Topical Report YAEC-1683 on MICBURN-3/CASMO-3/TABLES-3/SIMULATE-3 Benchmarking," February 2, 1990.

7. Letter, Jones, R.C. (NRC) to Papanic, G. (YAEC), "Request for Additional Information YAEC Topical Report YAEC-1363, dated November 13, 1989.

8. Letter, Jones, R. C. (NRC) to Capstick, R.W., (Vermont Yankee Nuclear Power Corporation), "Request for Additional Information Regarding the Topical Report YAEC-1683 on "MICBURN-3/CASMO-3/TABLES-3/SIMULATE-3," dated December 26, 1989.

9. Edenius, M., and Ahlin, A., "MICBURN: Microscopic Burnup in Gadolinia Fuel Pins," Chapter 7 of ARMP Computer Code Manuals, CCM-3, dated November 1975.

10. Edenius, M., et al., CASMO-2: A Fuel Assembly Burnup Program, Studsvik/NR-81/3, dated March 1981. (Proprietary)

11. Ver Planck, D.M., et al., TABLES-2 Manual, YAEC-1391P, April 1983. (Proprietary)

12. Ver Planck, D.M., et al., SIMULATE-E: A Nodal Core Analysis Program for Light-Water Reactors, EPRI NP-2792-CCM, dated March 1983.

13. Smith, K.S., OPANDA; An Advanced Nodal Method for LWR Analyses, Trans. Am. Soc., 50, 532 (1985).

14. Ansari, A.A.F., Methods for the Analysis of Boiling Water Reactors: Steady-State Core Flow Distribution Code (FBWR), YAEC-1234, December 1980.

15. Ansari, A.A.F., et al., FIBWR: A Steady-State Core Flow Distribution Code Boiling Water Reactors - Code Verification and Qualification Report, EPRI NP-1923, Project 1754-1 Final Report, July 1981.

16. Lellouche, G.S. and Zolotar, B.A., Mechanistic Model for Predicting Two-Phase Void Fraction for Water in Vertical Tube Channels, and Rod Bundles, EPRI NP-2246-SR, February 1982.

17. Gorman, J.A., et.al., Investigation of Large Bows in Reused BWR Fuel Channels, EPRI-NB-5718P, April 1988.

18. DiGiovine, A.S., Gorski, J.P., and Tremblay, L.A., "SIMULATE-3 Validation and Verification," Yankee Atomic Electric Company Topical Report, YAEC-1659, September 1988.

DISCLAIMER

This document was prepared by Yankee Atomic Electric Company for its own use. The use of information contained in this document by anyone other than Yankee Atomic Electric Company is not authorized, and in regard to unauthorized use neither Yankee Atomic Electric Company or any of its officers, directors, agents or employees assumes any obligation, responsibility or liability, or makes any warranty or representation, with respect to the contents of this document, or its accuracy or completeness.

ABSTRACT

The MICBURN-3/CASMO-3/TABLES-3/SIMULATE-3 code package is applied to the five most recent cycles of Vermont Yankee, a General Electric BWR. The purpose of this benchmark is to demonstrate the suitability of these codes for plant support and licensing of future Vermont Yankee cycles. Both cold critical startup and hot steady-state full power operation are modeled. Both exhibit steady, consistent eigenvalues close to unity.

Extensive 3-D comparisons are made between the model-calculated and plant-measured detector responses. The comparisons imply that the code package reproduces the power distributions of the plant with reasonable accuracy. The minor discrepencies that do exist are in a conservative direction as far as licensing applications of the codes are concerned.

TABLE OF CONTENTS

LIST OF TABLES

LIST OF FIGURES

LIST OF FIGURES

ACKNOWLEDGEMENTS

The authors wish to acknowledge contributions by J. P. Gorski and N. Barbetta in the preparation of both text and figures for this manuscript. We also wish to thank D. M. VerPlanck and A. S. DiGiovine of Studsvik of America for their ideas and encouragement in this benchmarking effort.

1.0 INTRODUCTION AND SUMMARY

This report benchmarks the MICBURN-3/CASMO-3/TABLES-3/SIMULATE-3 code package against several recent cycles of Vermont Yankee operating data. The models are used to calculate eigenvalues and detector response data at numerous steady-state exposure points. These calculations are compared to plant measurements; i.e., criticality and Traversing Incore Probe (TIP) data. The consistency and accuracy of the comparisons validate these codes for reload design, steady state licensing and plant support applications.

Section 2 provides a brief overview of the proposed code package. With regard to overall function, MICBURN-3/CASMO-3/TABLES-3/SIMULATE-3 will replace the current physics codes of MICBURN/CASMO-2/TABLES-2/SIMULATE-2. Differences between the two sets of codes are highlighted.

Section 3 describes the Vermont Yankee cores and fuel types covered by the benchmark. Only the later cycles are modeled. The earlier cycles are no longer applicable to future plant operation, because they used low enrichment fuel and a less accurate form of incore instrumentation.

Section 4 describes the construction of the Vermont Yankee model. Included are the results of numerous sensitivity studies performed. Based on these results and our best engineering judgement, the model was kept as simple as possible while including all the major effects. Thus, this benchmark is fully applicable to the intended use of these codes as "production tools."

Section 5 provides the detailed results of the model-to-plant comparisons. Briefly, the hot eigenvalue for the five cycles is 0.9989 with a standard deviation of $\pm$ 0.0010. The cold eigenvalue is 0.9968 with a standard deviation of $\pm$ 0.0017. The model produces nodal instrument readings which are compared to the plant for 223 sets of TIPs. For these comparisons, the RMS differences in nodal TIP readings are 2.9%.

In conclusion, the results of the MICBURN-3/CASMO-3/TABLES-3/SIMULATE-3 benchmark prove that this code package is superior to the current methods. It is suitable for all applications, including licensing, for which the current methods are approved.

2.0 GENERAL CODE PACKAGE DESCRIPTION

The proposed code package benchmarked in this report is intended to replace the current physics codes of MICBURN[1], CASMO-2[2], TABLES-2[3], and SIMULATE-2[4] (also referred to as SIMULATE-E, or SIMULATE-YA). The lattice physics code CASMO-2 is virtually identical in form, function and application to the original CASMO code described in the Reference 5 benchmark. The 3-D nodal code SIMULATE-2 is virtually identical to the original SIMULATE described in the Reference 6 benchmark. TABLES-2 is not actually a physics code; it links CASMO-2 to SIMULATE-2. All of the above codes have been approved by the NRC[7,8] for Yankee Atomic Electric Company use in reload physics analysis of the Vermont Yankee Nuclear Power Station. This analysis includes core design, startup test predictions, generation of physics data for safety analysis as well as the direct safety analysis of certain quasi-static transients.

Figure 2.1 shows the function of, and relationship between each of the current physics codes. Notice that the 3-D nodal code requires discontinuity factors. In the past this was supplied by PDQ.[9] Notice too, the gamma detector (TIP) responses were supplied externally. These were generated with KENO.[10] In addition, user specified "adjustment factors" such as albedos and thermal leakage correction factors were iterated upon to bring the 3-D model's power distribution into alignment with plant data.

In contrast, the proposed MICBURN-3/CASMO-3/TABLES-3/SIMULATE-3 code package, shown in Figure 2.2, is greatly simplified. The functions performed by the codes are virtually the same as their predecessors. However, discontinuity factors, and gamma TIP responses are now provided by CASMO-3. Also, the entire process of normalizing the 3D nodal code has been eliminated. This is because of significant improvements made to several of the codes. These will be discussed briefly below.

2.1 MICBURN-3

The MICBURN-3 code is described in detail in References 10 and 11. Similar to its predecessor, it calculates the burnup in a fuel pin containing an initially homogenous distribution of the burnable absorber, gadolinium. The code supplies CASMO-3 with effective absorption cross sections for the gadolinium, homogenized over the fuel pin.

The upgrade to MICBURN-3 is required because it uses the same library and group structure as CASMO-3. It also has many desirable features its predecessor did not possess, which allow it to model future, more complicated fuel designs.

2.2 CASMO-3

CASMO-3 (also referred to as CASMO-3G) is described in detail in Reference 12. The generic benchmark of the code is provided in Reference 11. Similar to its predecessor, CASMO-3 performs burnup calculations on an entire fuel assembly. The code handles geometry consisting of cylindrical fuel rods of varying composition in a square pitch array. It allows for fuel rods loaded with burnable poison, water gaps, water holes, boron steel curtains, channels and cruciform control rods. Like its predecessor, CASMO-3 uses multi-group transport theory to calculate the 2-D space/energy distribution of flux within the bundle. It performs the depletion calculation and produces two-group cross sections, homogenized over the assembly, for input into SIMULATE-3.

However, CASMO-3 has several advantages over its predecessor. It can generate discontinuity factors for use in SIMULATE-3. The production model uses 40 rather than 25 neutron energy groups. The nuclear library is based on the more modern ENDF/B-IV data rather than ENDF/B-IV. It can calculate gamma detector responses. Finally, CASMO-3 can handle baffle/reflector regions, hafnium control blades, water cross and large water hole assembly designs. Therefore, this upgrade provides the ability to model future, more complicated fuel and control rod designs.

2.3 TABLES-3

The TABLES-3 code (also referred to as TABLES-3P) is described in detail in References 13 and 14. It is a linking code between CASMO-3 and SIMULATE-3. TABLES-3 processes CASMO-3's two-group cross sections into two and three dimensional tables. SIMULATE-3 reads these tables and, according to the local conditions, SIMULATE-3 can reconstruct the appropriate homogenized two-group cross sections in each node.

Unlike its predecessor, TABLES-3 can handle discontinuity factors, gamma detector response data and other data SIMULATE-3 requires. The input format of TABLES-3 is also easier to learn and use than that of its predecessor.

2.4 SIMULATE-3

The SIMULATE-3 code (also called SIMULATE-3P) is described in detail in References 14 and 15. Reference 16 provides the generic benchmark. SIMULATE-3 is a three dimensional nodal analysis code. It models the steady state neutronics and thermal-hydraulic behavior of the core. It provides power, exposure, and void distributions, burnup, fission product and reactivity effects. However, beyond these functions, all similarity with its predecessor ends.

The predecessor, SIMULATE-2, used the same nodalization as the familiar codes FLARE[17] and TRILUX[18]. The neutron balance equation was modified coarse mesh diffusion theory[19]. It was a one-group method with a two-group approximation afforded by the use of thermal leakage correction factors. Calculations were only executed in the fueled region of the core; user adjustable albedos terminated the neutron balance equation at the reflector interfaces.

In contrast, SIMULATE-3 is a true two-group nodal code. This eliminates the need for thermal leakage correction factors. It uses the QPANDA[20] model which solves the three-dimensional, two-group neutron diffusion equation. The QPANDA methodology also assumes that the flux distribution is comprised of two pieces: global shapes (homogeneous smooth flux distribution) and local shapes (heterogeneous assembly flux distributions). This assumption allows assembly discontinuity factors (ADF's) to be edited from the same CASMO-3 calculations that produce two-group cross sections. When used in the QPANDA model, the ADFs alter the neutron currents between nodes, effectively eliminating spatial homogenization errors. The ADF concept is also applied in modeling homogenized baffle/reflector nodes. This eliminates the need for any user adjustments (albedos) in the reflector region.

In summary, SIMULATE-3 provides superior accuracy with fewer user-adjustable inputs than its predecessor. It also runs faster.

FIGURE 2.1

Process Stream of Current Physics Codes

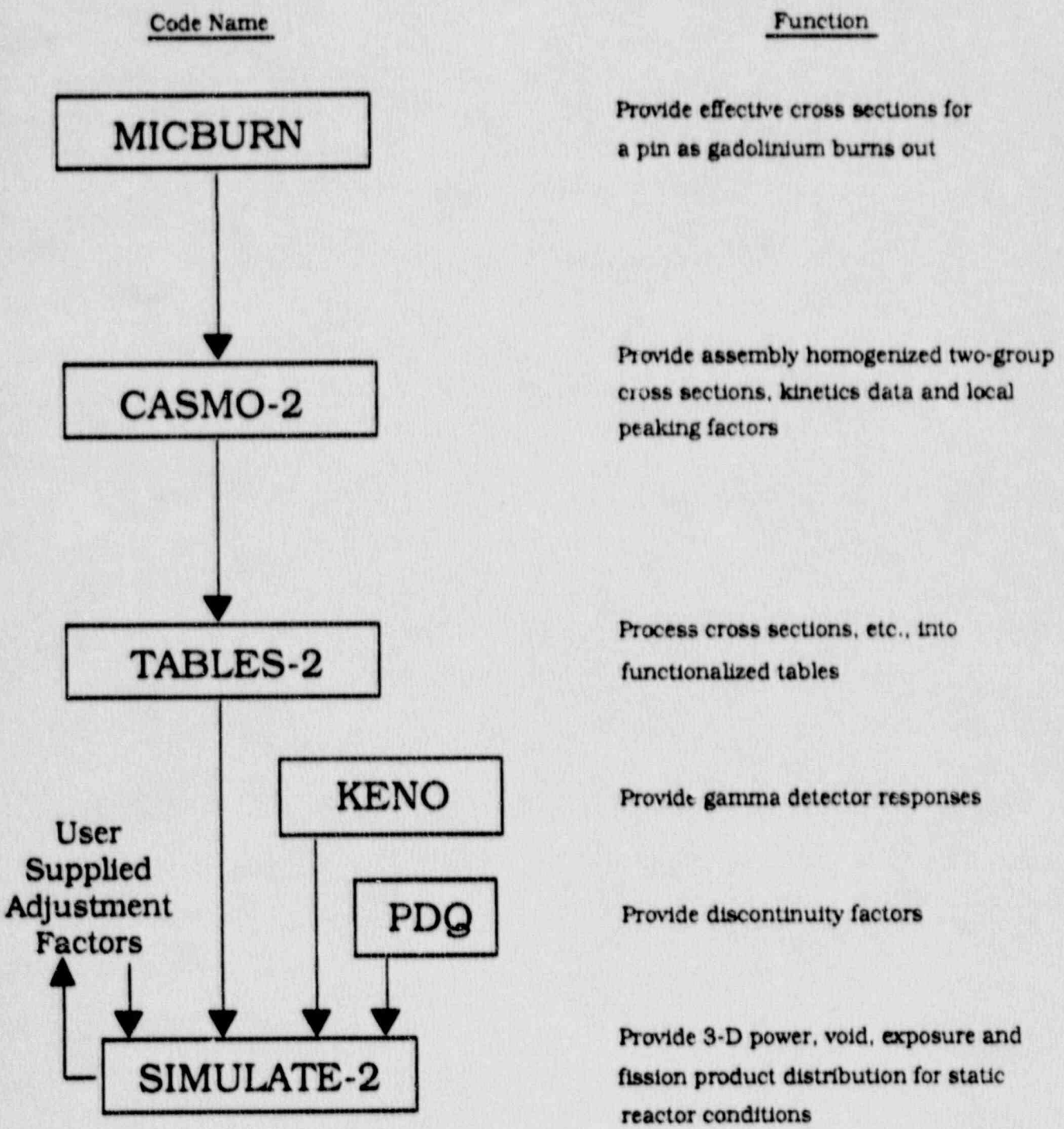

FIGURE 2.2

Process Stream of Proposed New Physics Codes

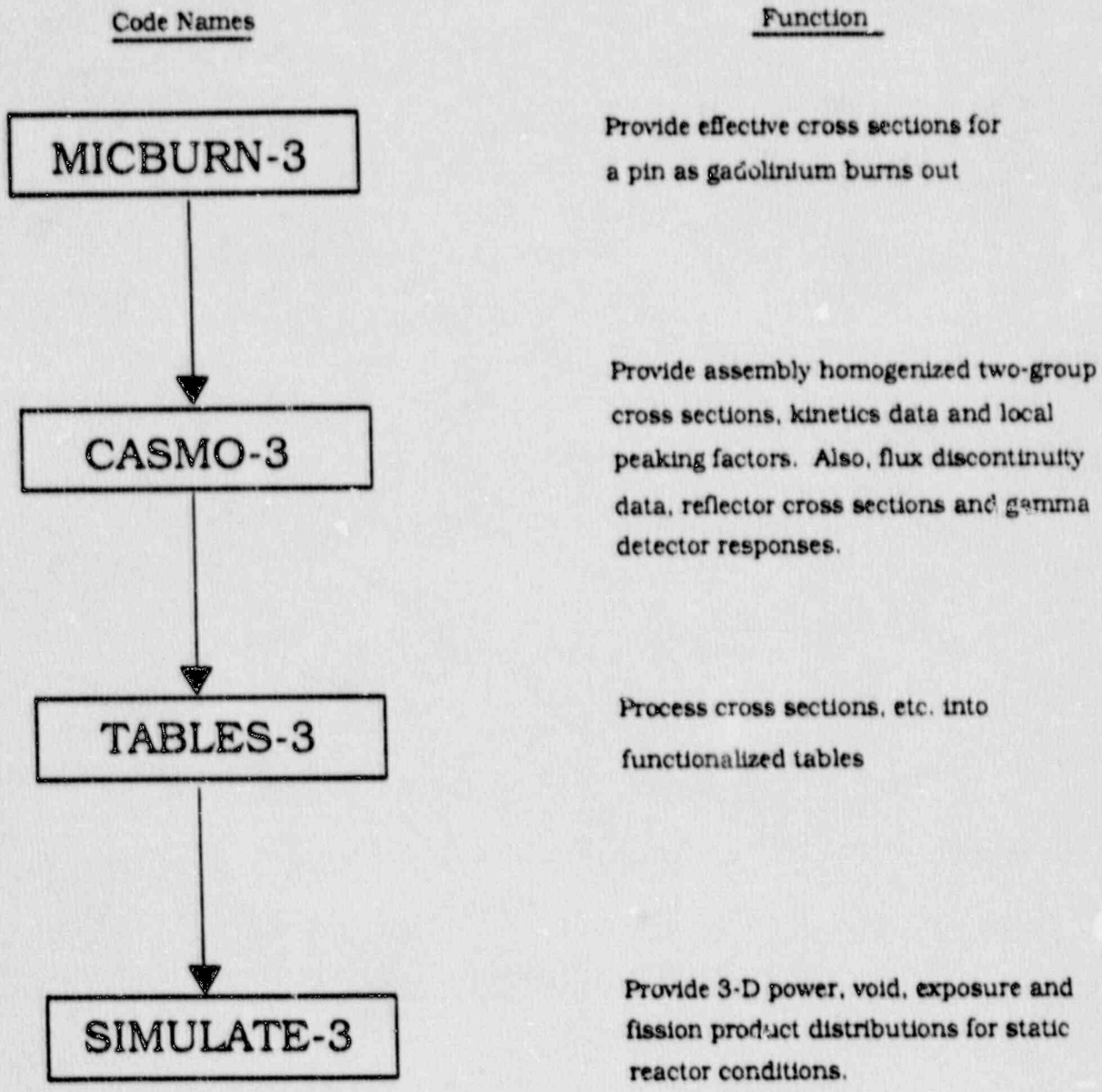

3.0 VERMONT YANKEE OPERATING CHARACTERISTICS

Vermont Yankee (VY) is a General Electric BWR-3 which began commerical operation in 1972. Beginning in Cycle 6 (1978), Vermont Yankee began a transition to axially zoned fuel assemblies with a longer active fuel length. Thus, starting with Cycle 6, all VY cores have been zoned. Also, from Cycles 6 to 9, VY had cores that possessed uneven active fuel at the top. Beginning with Cycle 9 (1981), VY began a transition to longer cycles. This required larger reload batches, and later, higher enrichments and heavier burnable poison loadings. There have also been several changes in the thermo-mechanical design of the fuel rods in the past ten years. All of these changes can be accommodated by the modeling capabilities of the MICBURN-3/CASMO-3/TABLES-3/SIMULATE-3 code package.

3.1 Core Description

Vermont Yankee is a D-lattice plant with a small diameter, high power density core. The rated operating characteristics are provided in Table 3.1. The core description is summarized in Table 3.2. A radial map of the VY core is shown in Figure 3.1. All 368 channeled fuel assemblies are orificed to control flow. The shaded assemblies, shown in Figure 3.1, are tightly orificed to maintain a flow balance between the higher powered core interior and the lower powered edge. The intersections of the dashed lines show the centers of the control blades. Figure 3.1 also shows the locations of the various incore detectors.

The benchmarking effort is primarily interested in the 20 instrumentation locations containing both the Traversing Incore Probes (TIPs) and the local power range monitors (LPRMs). The LPRMs are fixed neutron detectors. At each of these 20 instrument locations there are four LPRMs arranged at four axial levels as shown in Figure 3.2. The LPRMs are calibrated frequently; that is, normalized to their adjacent TIPs. The three TIP machines (A, B, and C) are, in turn, normalized to each other by use of a common core location shown in Figure 3.1. Thus, the TIP readings are the single most important measure of the model's accuracy. All other measures of power distribution, including those at the plant, are either derived or inferred from the TIPs.

Toward the end of Cycle 8 (1981), the TIPs were converted from neutron detectors to gamma sensing detectors. This significantly reduced a major component of measurement uncertainty, namely "TIP asymmetry." TIP asymmetry is caused by a misorientation of the TIP instrument tube within the so called "narrow-narrow corner" of the water gap between the fuel channels (see Figure 3.3). The thermal neutron-TIPs were very sensitive to this orientation, gamma-TIPs are not. In providing an axial shape, the gamma-TIP is less sensitive to uncertainties in the axial variation of voids up the channel. Finally, it is also less sensitive to the possible presence of voids in between the channels (bypass voiding).

Neutron-TIPs detect primarily those neutrons emitted by the four nearest corner pins. The power in the assembly must be inferred from each corner pin by means of a multi-step process. In contrast, the gamma response function receives contributions from deep within each surrounding assembly. The power in adjacent assemblies is more directly inferred.

In conclusion, comparisons between the model-calculated gamma-TIP readings and the plant-measured gamma-TIP readings provide the most direct and accurate test of the model's ability to reproduce the plant's power distribution.

3.2 Description of Cycles Modeled

As discussed, Vermont Yankee converted to gamma-TIPs toward the end of Cycle 8. Thus, Cycle 9 was the first full cycle to use gamma-TIPs. It was also the first transition to longer cycles. Thus, the benchmarking will examine Cycle 9 through the recently completed Cycle 13. The previous cycles have little application to future plant operation and will not be presented here. A summary of the operation of Cycles 9-13 is provided in Table 3.3.

More detail of each Cycle is provided in Appendix A. This includes the reload design of each of the cycles. As shown in Appendix A, Vermont Yankee employs a conventional (not Control Cell Core) loading scheme. This frequently results in very old assemblies alternating with fresh assemblies. The loading schemes are also low leakage; i.e., oldest fuel loaded on the core periphery. Both of these situations, in combination with VY's high power density and small core, result in steep, rapidly varying flux gradients. This can also be handled by the modeling capabilities of the code package.

3.3 Fuel Description

Table 3.3 lists the vendor designation of each fuel type modeled in the complete benchmarking effort. Detailed descriptions of the fuel are proprietary to the vendor and can be found in Reference 21. However, as a general description of the fuel: The fuel types modeled are all D-lattice 8 x 8 arrays as shown in Figure 3.3. They include several different enrichments, gadolinium loadings and active fuel lengths. Some of the fuel is zoned axially, creating several lattices per fuel type. A "lattice" consists of any unique pin distribution of enrichment or gadolinium in an axial slice of an assembly. Each lattice must be explicity modeled.

In addition to the complexity of the fuel designs, the vendor altered the thermo-mechanical properties of the fuel pins several times. For the fuel present in the core during this benchmark, the following is an approximate chronology: a) The vendor introduced helium back-filled pre-pressurized fuel (1979). b) Reduced pellet surface roughness and inside clad roughness (1983). c) Gradually increased pellet density (1983-1985). d) Increased pellet O.D. and decreased pellet/clad gap (1986). These changes were all directed toward reducing fuel failures by reducing average fuel temperatures. The latter affects the overall Doppler defect on a batch by batch basis. This can also be handled by the model.

TABLE 3.1

Vermont Yankee Rated Operating Characteristics

Rated Power (MWth)	1593.0
Average Power Density (kW/l)	49 (1)
Number of Assemblies	368
Equivalent Core Diameter (inches)	129.9
Total Core Rated Flow (Mlb/hr)	48.0
Core Bypass Flow (Mlb/hr)	5.2 (2)
Steam Flow Rate (Mlb/hr)	6.43
Feedwater Flow Rate (Mlb/hr)	6.40
Feedwater Temperature (°F)	372
Nominal Steam Dome Pressure (psia)	1020
Nominal Reactor Average Pressure (psia)	1033
Core Inlet Enthalpy (Btu/lbm)	520
Core Inlet Subcooling (Btu/lbm)	27
Core Exit Quality (% steam)	13.3

Notes: (1) Varies with active length of fuel. A full core of 150 inch fuel equals 48.92 kW/l.

(2) Varies slightly from cycle to cycle. It depends on the number of assemblies with drilled lower tie plates and the number of water rods per assembly. Most later cycles have about 5.2 Mlb/hr of bypass flow.

TABLE 3.2

Vermont Yankee General Core Description

Fuel

Number of Assemblies	368
Cold Assembly Pitch (inches)	6.0
Active Fuel Height (inches)	144-150
Fuel Rod Array	8 x 8
Lattice Type	D
Fuel Pellet Material	Sintered UO_2
Fuel Clad Material	Zr-2
Channel material	Zr-4
Channel Thickness (mils)	80
Spacer Material	Zr-4 and Inconel
Number of Spacers	7

Movable Control Rods

Number of Rods	89
Shape	Cruciform
Cold Control Rod Pitch (inches)	12.0
Control Material Height (inches)	143
Control Material	Compacted B_4C in S.S. tubes and sheath

Incore Instrumentation

Source Range Monitors	4
Intermediate Range Monitors	6
Power Range Detector Locations	20
LPRMs (4 per Location)	80
TIP Machines	3

TABLE 3.3

Summary of Vermont Yankee Cycles Modeled

	Cycle 9	Cycle 10	Cycle 11	Cycle 12	Cycle 13
Operation Dates:					
BOC	12/1/81	6/17/83	8/6/84	6/30/86	10/2/87
EOC	3/5/83	6/15/84	9/21/85	8/7/87	2/11/89
As-Loaded Core Weight (Short Tons):					
Initial H.M.	74.15	74.13	74.25	74.44	74.82
Core Average Burnups (Mwd/St):					
BOC	9,192	10,463	10,418	9,820	8,613
EOFPL	16,595	17,185	16,733	16,358	16,830
EOC	18,137	17,806	18,283	17,949	18,307
Thermal Capacity Factor While Operating:					
CF (%)	90.9	93.6	89.2	94.3	91.4
Number and Type of Fuel Assemblies Loaded:					
Fresh	120	108	104	120	136
Type	P8DPB289	P8DPB289	P8DPB289	P8DPB289	BP8DRB299
1 Cycle	80	120	108	104	120
Type	P8DPB289	P8DPB289	P8DPB289	P8DPB289	P8DPB289
2 Cycle	96	80	120	108	104
Type	P8DPB289	P8DPB289	P8DPB289	P8DPB289	P8DPB289
3 Cycle	60 + 12	60	36	36	8
Type	8DPB289 + 8D274H	P8DPB289	P8DPB289	P8DPB289	P8DPB289

FIGURE 3.1

Radial Map of Vermont Yankee Core

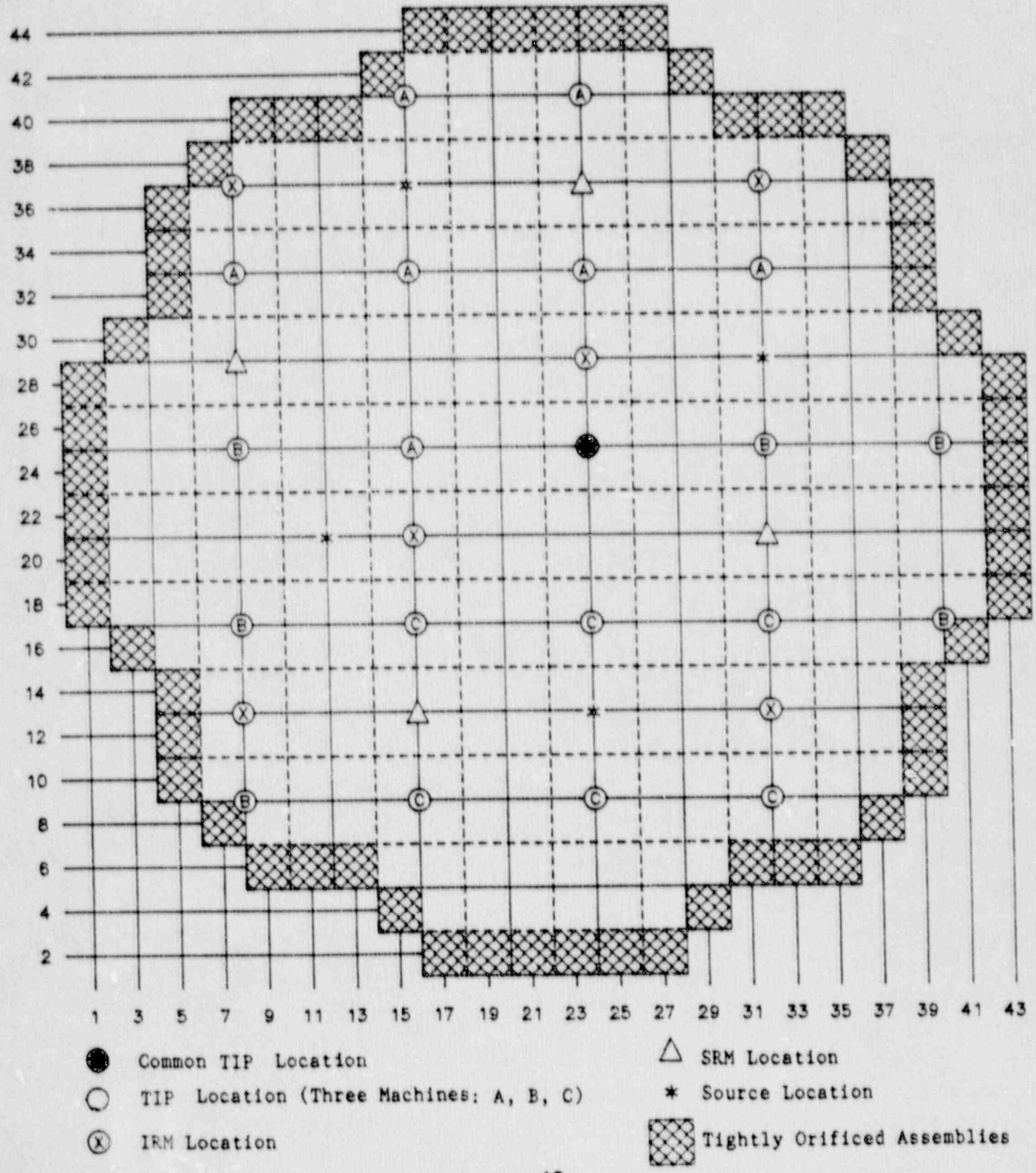

FIGURE 3.2

Axial Relationship of Fuel, Control Rods and Incore Detectors

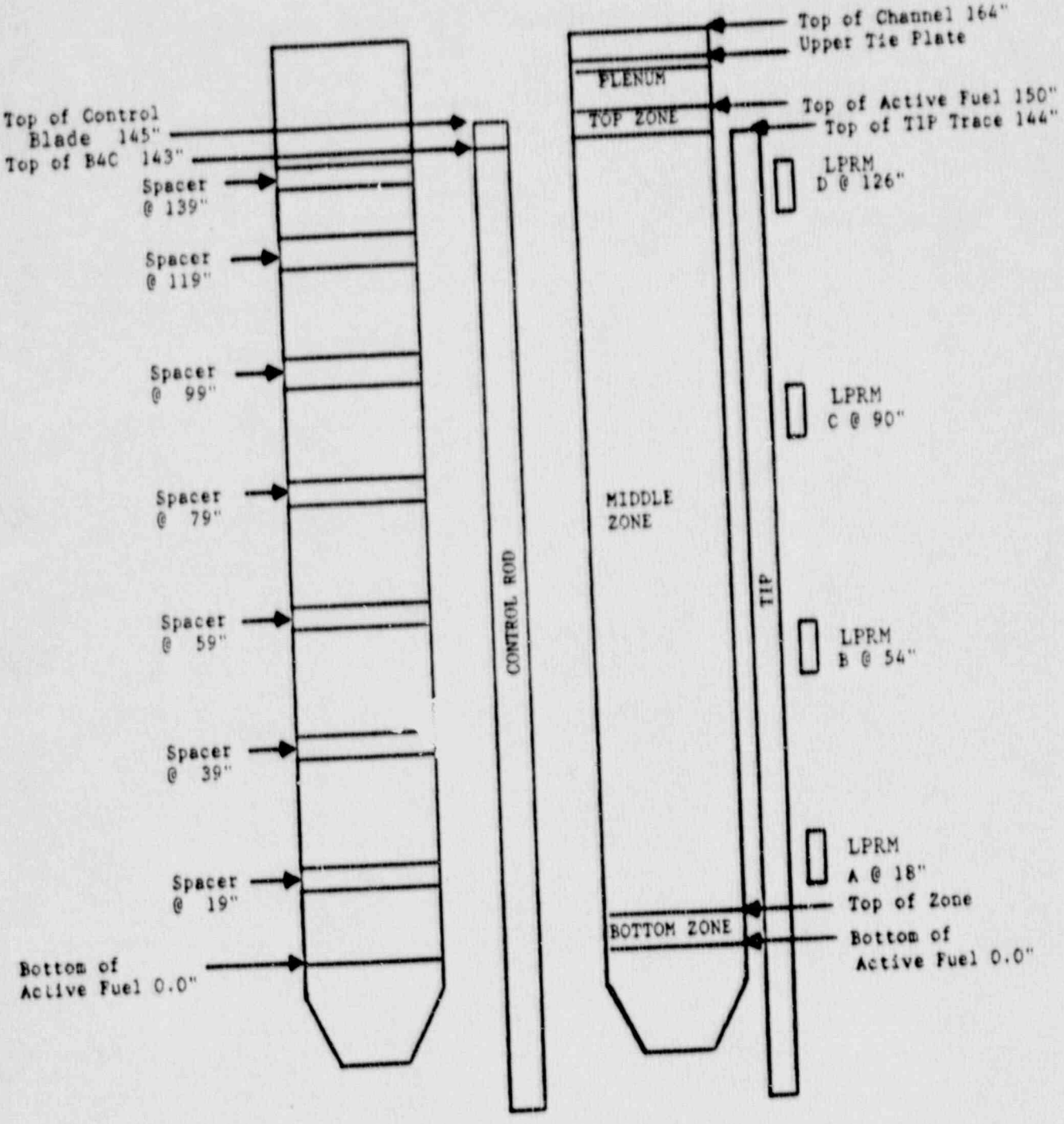

FIGURE 3.3

Detail of Fuel, Control Rod and Incore Instrument Tube

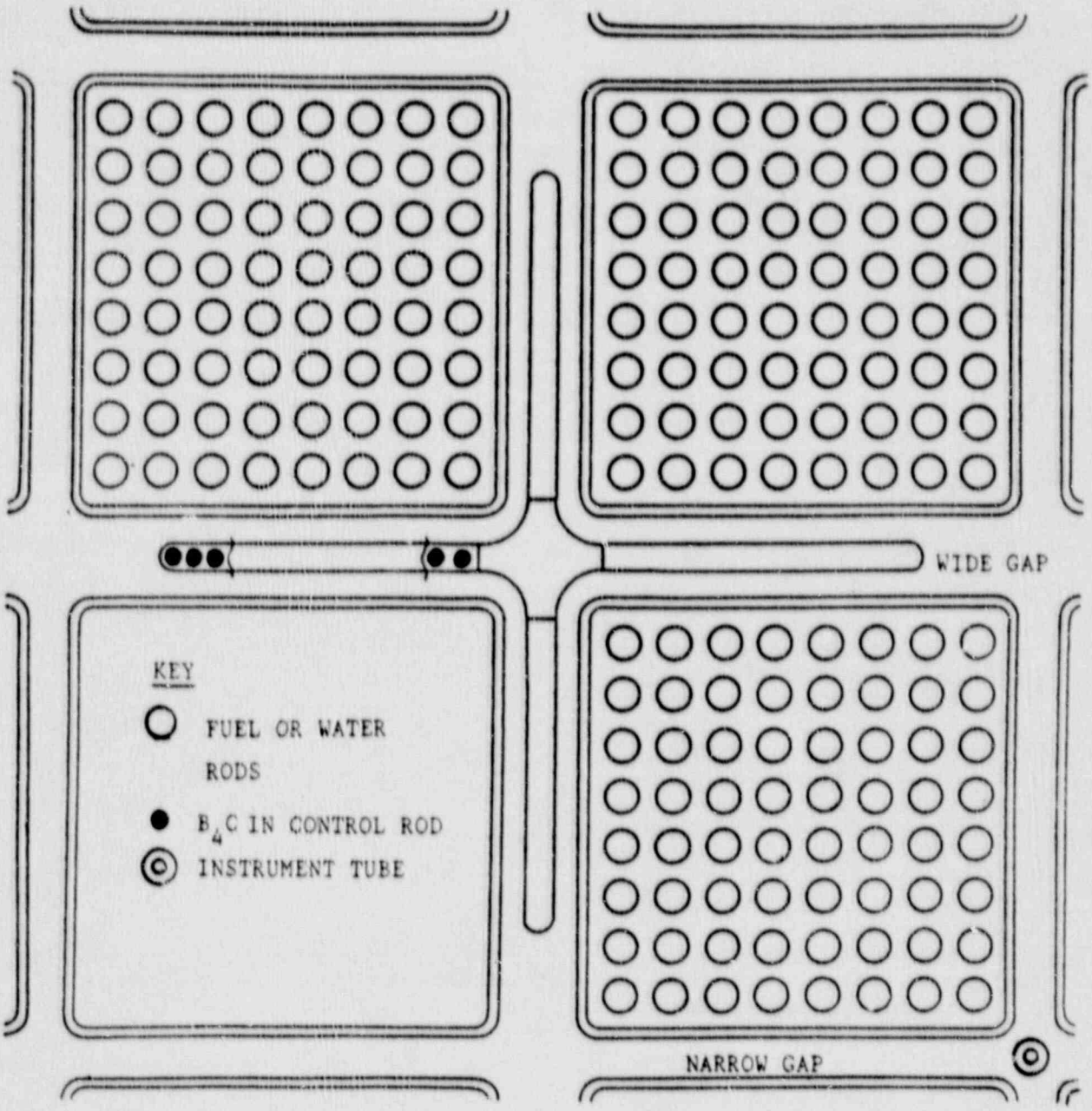

4.0 VERMONT YANKEE SPECIFIC MODEL

The benchmarking of Vermont Yankee was performed with the intention of producing a production tool for reload analysis. Therefore, the input to each of the codes in the package was kept as simple as possible. However, to avoid the trap of oversimplifying, numerous sensitivity studies were performed at each step in the modeling process. Only those details which caused a substantial improvement in the final model were retained.

4.1 MICBURN-3 Model Description

The MICBURN-3 code microscopically depletes the gadolinium in the gad pin. For the fuel types modeled in this benchmark, MICBURN-3 cases were run for each gad pin with a different w/o gadolinium. For the BP8DRB299 fuel type, the same w/o gadolinium existed in two separate U_{235} enrichment pins. Therefore, two separate cases were run. This proved to be unnecessary (see Section 4.1.1, MICBURN-3 Sensitivity Studies).

Figure 4.1 shows the geometry of the Vermont Yankee MICBURN-3 model. In this figure, four separate composition regions can be seen. These regions are defined for the cold (20°C) lattice. MICBURN-3 thermally expands them and modifies the material densities automatically.

The fuel region requires the pellet radius (R_f), the pellet density, the w/o U_{235} and the w/o gadolinium of the gad pin. The VY model uses the default geometric specification for the fuel region: the fuel region has been divided into 10 "macro-regions" for the transport calculation, and 20 "micro-regions" for the burnup calculation. The average fuel temperature specified for the fuel region was generated with the in-house fuel behavior code, FROSSTEY[22, 23, 24].

The cladding region requires the outer radius of the cladding, (R_c). It is defined as a single macro-region.

MICBURN-3 breaks the moderator region into two macro-regions, although the composition is homogeneous. The moderator is specified as saturated water at T_{SAT} = 560°K. The default value of zero voids in the moderator is used. This region represents the water immediately

surrounding the gad rod. The moderator radius, (R_m), creates a circle whose area is equal to the pin pitch squared. Spacer material is ignored in the moderator region and also in the buffer region.

The buffer region is also split into two macro-regions of homogeneous material. The buffer represents everything else surrounding the gad pin and its immediate moderator. The buffer region is created by homogenizing the remaining fuel pins, cladding and water of the fuel assembly into one region. For the VY model, the average uranium enrichment of the assembly is assumed for the remaining fuel pins. The buffer region is assumed to be free of voids and the effects of other gad pins. VY uses the suggested buffer radius (R_b), of 5 cm.

The primary output of MICBURN-3 consists of effective gadolinium microscopic absorption cross sections for the burnable absorber (gad pin) as a function of the absorber number density, N_{BA}. The latter is a pseudo-number density which takes into account the transition chain for the various gadolinium isotopes. The output of the production model is in 40 energy groups, consistent with CASMO-3.

4.1.1 MICBURN-3 Sensitivity Studies

A number of sensitivity studies were performed with MICBURN-3 to determine what significantly altered the output. The output studied was the effective Gd microscopic absorption cross section as a function of N_{BA}. The first study examined the effect of increasing the enrichment of U_{235} in the gadolinium pin by 1.0 w/o. This had negligible impact on the burnable absorber cross sections. A second study examined the effect of increasing the enrichment of U_{235} in the buffer region by 1.0 w/o. This also had negligible impact. Conclusions: MICBURN-3 cases do not need to be run for different enrichment pins having the same gadolinium content. Also, using the bundle average enrichment in the buffer region is a valid input assumption.

The only variable which seems to have the slightest impact on MICBURN-3 (other than w/o gadolinium) is the water density. The water density directly affects the spectrum, which in turn, affects the relative rates at which the various Gd isotopes burn out. Figure 4.2 shows the impact of replacing half the fuel in the buffer region with water rods. This softens the spectrum, which preferentially burns out more Gd_{157} during the early stages of depletion. The

remaining Gd isotopes have smaller thermal absorption cross-sections. Therefore, the microscopic absorption cross section versus N_{BA} is reduced. The fast cross section is not visibly affected.

Hardening the spectrum has just the opposite effect. Figure 4.3 shows that running MICBURN-3 at 40% voids causes a slight change in thermal microscopic cross section in the opposite direction. However, when carried through to the CASMO-3 level, running MICBURN-3 at 40% voids has negligible impact on the results. Therefore, for the production model, we use the recommended default value of zero voids for all MICBURN-3 cases.

4.2 CASMO-3 Model Description

The CASMO-3 code (also called CASMO-3G) is used to calculate the burnup and 2-D flux and energy distributions within each of the lattices required by the benchmark. CASMO-3 can use either a 70 or 40 neutron energy group library. The Vermont Yankee production model uses 40. This is only for calculations at the pin cell level. For the macro-group calculation (see Reference 12), the VY model uses the default collapse to 23 energy groups. For the 2-D calculation, it uses the default collapse to 7 energy groups.

The VY lattice geometry is shown in Figure 4.4. The lattice is symmetrical along the diagonal so only half the bundle is modeled. The bundle is surrounded by a channel of 80 mils. Water outside the channel is specified separately from water inside the channel. The water inside the channel may contain voids, depending on the case. It definitely contains spacers. The amount of spacer material for the assembly is specified as if it is homogenized over all the water inside the channel.

Figure 4.4 shows the mesh spacing of the unit cells for the calculation of the 2-D distribution of flux and local power within the lattice. The mesh spacing is the pin pitch, which is specified cold (20°C). CASMO-3 increases the pitch for hot problems by using the thermal expansion coefficient of the spacers (Zr-4). Likewise, all other dimensions are input for the cold lattice. CASMO-3 uses the T_{FUEL} or T_{MOD} with internal material expansion coefficients to expand the dimensions and adjust the material densities.

The unit cells require several arrays to specify them. One such array distinguishes between fuel rods and water rods. These are treated separately at the pin cell level in CASMO-3. For the fuel rods, the radii of the fuel region, gap region and cladding region are specified. CASMO-3 automatically surrounds the fuel rod with an appropriate moderator, or moderator and buffer region, as required. Water rods require the dimensions of the water inside and the cladding. For VY, the water inside the water rods is specified as being free of voids. Unlike its predecessor, CASMO-3 allows several different size water rods to be specified.

The fuel rods require more than the dimensions. For each fuel rod type, the U_{235} enrichment and, if appropriate, w/o gadolinium is specified. Although CASMO-3 contains an internal Gd library, separate MICBURN-3 cases (see Section 4.1) were run to provide the specific gadolinium cross sections for each lattice/gad pin type.

The pellet stack density of each fuel rod type is required. This varies with the w/o gadolinium, which creates a less dense pellet matrix. For the VY model, the gad pellet density is calculated using a vendor correlation. The final pellet densities for all fuel rods are checked by running a zero depletion CASMO-3 case. This provides a weight for the lattice which is checked against the average bundle weight. The pellet densities are adjusted, as required.

One step up from the pin cell calculation is the macro-group calculation performed on fuel rods along the edge of the assembly. This calculation improves the homogenized cross sections for these rods and provides a neutron source for calculating the channel, gap, and control rod cross sections. Thus, CASMO-3 requires the dimensions of the channel, the narrow and wide water gaps. Only half of each water gap is specified; running through the middle of each water gap is another mirror symmetry line. Together with the diagonal, these form the boundaries of the infinite lattice problem.

When a rodded case is run, half of a control blade is included in the wide water gap as shown in Figure 4.4. The control blade is modeled as two regions. The first region is the central steel shaft; the second region is the active absorber region.

The B_4C powder in the control blade is contained within thin tubes of stainless steel bound by a steel sheath, as shown in Figure 4.5. The blade is modeled in CASMO-3 as follows: The B_4C powder is treated like a strong absorber "pin" placed in the blade matrix according to the

tube pitch. This blade matrix is taken to be a smeared mixture of stainless steel and water as shown in Figure 4.6. In the VY model, the absorbing region is considered to be the area starting with the first B_4C pin and going to the last B_4C pin. The thickness of the tubing is omitted from the first and last B_4C pin. The remaining tube thickness on one end is accounted for as part of the central steel shaft. The little bit of tubing and steel sheath at the very tip of the blade wing is ignored.

4.2.1 CASMO-3 Depletion Cases

Each lattice in the benchmark required four separate depletion cases. Three were uncontrolled; one each, at 0%, 40%, and 70% voids. The fourth case was a control rod history depletion. It was run with the control rod inserted at 0% voids. The void fractions of 0%, 40%, and 70% voids roughly represent conditions at the bottom, middle and top of the core respectively. The control rod history depletion was run at zero voids because the BWR control rods are bottom entry and spend most of their lives in a low void environment.

All depletion cases were run at hot reactor average conditions. The moderator temperature was specified at T_{SAT} = 560°K. This provides the appropriate water density for the water and vapor (voids) mixture specified in the channel and also for the "solid" water specified in the water rods and bypass region (gaps). The fuel temperatures for CASMO-3 were calculated for a typical fuel rod at reactor average power using FROSSTEY. A set of identical depletion cases were performed for each lattice modeled

The depletion cases use the CASMO-3 default timestep scheme. That is, the depletion time steps are close together (.5 GWd/Mtu) until the gadolinium has burned out. Afterwards, the steps are gradually increased (up to 5 GWd/Mtu). The output edited from each of these depletion steps includes: two-group cross sections and infinite multiplication constant, assembly power distribution, conversion ratios, kinetics data (delayed neutron fractions, etc.), gamma detector response data, xenon and samarium yields, and assembly discontinuity factors. These are accessed by TABLES-3 for processing into SIMULATE-3 input.

4.2.2 CASMO-3 Branch Cases

Since the reactor is dynamic, it is not sufficient to run only the depletion cases. These provide appropriate results only if the void fraction, or control rod position remains fixed. The depletion cases provide an average spectral history (so called "void history" or "control history") of a node. However, at any instant in time, the local conditions change. It is germane to the theory of the model, from this point onward, that these "instantaneous effects" are separable. That is, they can be individually calculated and added together later to recreate the proper cross sections, etc., for each individual reactor node.

The instantaneous effects are generated by means of branch cases run from various restart exposure points in the void or control history depletion cases. Essentially, for each void history depletion, branch cases are run to each of the other void levels not covered by the depletion. A lower fuel temperature branch case is run. A rodded branch case is run. From the control rod history depletion, an unrodded branch case is run. All of these changes are assumed to be instantaneous, except that CASMO-3 calculates equilibrium xenon.

In order to model the cold lattice, two uncontrolled and two controlled branch cases were run from each of the 0%, 40% and 70% void history depletions. The moderator for the cold cases is set to zero voids. The moderator and fuel temperatures are set equal to each other. The controlled and uncontrolled cases are run at each of two cold branch temperatures. Control history is ignored in the cold model because the flux, during cold conditions, is peaked at the top of the core. There is almost no control history at the top of the core.

4.2.3 CASMO-3 Reflector Region Model

In order for CASMO-3 to calculate the reflector region cross sections, it needs a source of neutrons. The majority lattice of the 8DPB289 assembly was chosen as the neutron source. The reflector was specified in terms of its thickness and its homogenized material properties.

Data was calculated for the top, bottom, and radial reflectors in the core. The cross-sections at the top of the core were calculated for a 15 cm. section of plenum at three

different voids (0%, 40%, and 70%). The bottom reflector was specified as two adjoining thicknesses. Together, these thicknesses encompassed: lower end plugs, lower tie plate, lower channel and the control blade handle. The coolant in the bottom reflector was specified at 0% voids. The radial reflector was also specified as water at 0% voids. No other material was included in the radial reflector because VY has an oversized core shroud. Therefore, there is no significant structure near the periphery of the core. In a similar manner, reflector cross sections were generated for the cold model at T_{MOD} = 293°K.

4.2.4 CASMO-3 Sensitivity Studies

A few sensitivity studies were performed with the CASMO-3 model. First, the 70 group energy library was tested. (This required a 70 group MICBURN-3 to be run). The two-group K-infinities from the 40 and 70 group cases were virtually the same. The differences between the two are plotted in Figure 4.7. As shown, the differences start at 0.5 milli-K and drop off rapidly. This minor difference is not worth the cost of running in 70 groups.

Another sensitivity study addressed the impact of channel bowing on the lattice physics. A discussion of channel bowing in BWRs is presented in Appendix C. Briefly, the channel bowing, in the interior portion of a D lattice plant, shifts the lattice toward the narrow-narrow corner, affecting the reactivity. For this study, a modest deflection of 40 mils (half the channel thickness) was assumed. This was modeled by simply adding 1 mm to the wide gap and subtracting 1 mm from the narrow gap. The standard depletion cases were re-run for one of the middle lattice sections.

The results were quite remarkable as shown in Figure 4.8. On the average, the deflection resulted in a 5 milli-K decrease in reactivity for the lattice. Figure 4.8 shows the loss in reactivity due to bowing at each of the void levels. As might be expected, the high void region suffers a greater loss. This is because the bypass water makes a greater contribution to the overall moderation when the lattice is voided.

These results were dramatic enough to warrant re-calculation of all the VY lattices, including branch cases. The zones at each end of the fuel assemblies were not re-calculated, since the channel is fixed in the core near the top and bottom. Therefore, bowing will cause

little, if any, deflection of these lattices. The "bowed lattice" cross sections were then checked out in a SIMULATE-3 sensitivity study (Section 4.4.3).

4.3 TABLES-3 Construction

TABLES-3 (also called TABLES-3P) reads user specified CASMO-3 punch files and creates tables of parameterized input for SIMULATE-3. Separate TABLES-3 cases are run for each lattice type used in the benchmark. Because the VY model is segregated into a hot model and a cold model, separate sets of TABLES-3 cases are run for each condition. However, the output from both is loaded into a single library that SIMULATE-3 can access. The hot model and cold model are distinguishable on the basis of "major" and "minor" flags in the library.

The tables stored in the library include two-group cross sections, detector response functions, kinetics data, assembly discontinuity factors, etc. To simplify the remaining discussion, only cross-section data will be referred to. As discussed in Reference 13, TABLES-3 constructs its cross sections according to the general formula:

$$\Sigma\,(A, B, C \ldots Z) = \Sigma_{BASE}\,(Ao, Bo, Co \ldots)$$
$$+ \Delta\,\Sigma\,(A, B, C) + \Delta\Sigma\,(B, C, D) \ldots + \Delta\Sigma\,(X, Y, Z)$$

The user specifies the source of the base cross sections (usually one of the history depletions) and the source of the partial cross sections. Each of the partial cross sections can only have up to three variables. All other variables are fixed. The partial cross sections are derived by comparing various CASMO-3 branch cases to their history depletions, or comparing them to each other.

For the VY hot model, the variables "A ---> Z" which are used to construct the cross sections, Σ(A, B, C .... Z), are exposure, void history, instantaneous voids, fuel temperature, instantaneous control rod, and control rod history. The base case selected for the hot model base cross section set is the unrodded 0% void history depletion.

For the VY cold model, the variables used to construct the cross sections are exposure, void history, moderator temperature, and instantaneous control rod. The base case for the cold model cross section set is the unrodded, cold branch case from the 70% void history depletion.

This case was chosen because most of the flux, during a cold critical, is in the top 1/4 of the core. The void history in the top of the core is closest to 70% voids; therefore, less interpolation will be required in the area of importance.

After TABLES-3 constructed its library of cross sectional tables, the latter were tested out using the "AUDIT" function of SIMULATE-3. The AUDIT function allows the user to exercise the cross sectional variables for each lattice at the specific CASMO-3 depletion or branch case conditions. The results were compared against the CASMO-3 two-group K-infinities and M^2. Overall, the agreement was excellent; this proved that the tables were constructed properly.

4.4 SIMULATE-3 Model Description

SIMULATE-3 (also called SIMULATE-3P) is a sophisticated nodal code with relatively simple input. The simplicity of the input stems from the fact that it allows for few user adjustments when setting up a model. Unlike its predecessor, SIMULATE-2, there are no adjustable neutronics parameters in SIMULATE-3. In essence, the user specifies the actual reactor geometry, fuel assembly characteristics, and operational data when developing the model. Nearly all variations in model design are introduced by means of the cross sections. Some minor leeway exists in the specification of the thermal-hydraulics parameters.

The SIMULATE-3 model of VY is developed in two parts. These are the hot and the cold model. They differ in the temperature range at which the cross sections were generated, and in the thermal-hydraulics of the core. In both cases, the geometry and fuel specifications of the reactor are identical.

The geometry of the core begins with the nodalization: The core is divided into 27 axial nodes per assembly and one radial node per assembly. The nodes are 6" on a side. A single node of reflector material is added around the sides of the core by specifying a pseudo-assembly consisting of nothing but reflector material. The SIMULATE-3 system allows for the possibility of modeling an uneven height active core by means of a flexible fuel assembly definition. Figure 4.9 gives two examples: The 150" fuel is defined as having a bottom reflector node, a bottom fuel zone node, 23 nodes of middle fuel zone and a top fuel zone node followed by a single top reflector node. The 144" fuel, on the other hand, has a bottom reflector node,

24 nodes of fuel zone and two nodes of top reflector. By means of these zones (including reflector zones) the appropriate cross sections can be associated with each part of the core.

The cross-sections for the SIMULATE-3 model are loaded from the library created by TABLES-3 using a library specification card. This library specification associates a cross section set with each zone of fuel (and reflector) specified in the fuel definition cards.

In addition to the nodalization of the model and the specification of the fuel types, several other parameters are required. For VY, the following were specified: serial number and location of each fuel type; fuel batch assignments (for fuel management editing); locations and hydraulic specification of core orificing; and, the location of control rods and in-core instrumentation.

The control rods were specified as being 144" long even though the control material only reaches to 143" (see Figure 3.2). This approximation introduces very little error because there are at least two inches of steel above the B_4C region of the control rod which provide significant epithermal absorption.

The in-core instrumentation (TIPs) cover only 144" of the active fuel length of the core (see Figure 3.2). Thus, the top node of the active fuel region is not instrumented. The SIMULATE-3 code expects all the fueled region of the core to be instrumented. The standard Vermont Yankee TIP string reading has 24 values. SIMULATE-3 would "stretch" these 24 values over the 25 axial nodes if we did not supply a dummy 25th value at the end of each data string. This dummy value is ignored when calculating the statistics of the plant-to-model TIP comparisons in Section 5.4. However, SIMULATE-3 continues to calculate a pseudo-TIP reading for the 25th node. The latter is visible in some of the plots.

If the user specifies the location of the spacers in the core, SIMULATE-3 will use the "spacer correction" model. When the spacer correction model is turned on, SIMULATE-3 adjusts the thermal-hydraulic calculation down stream of each spacer to account for voiding caused by the pressure drop in those areas. The SIMULATE-3 model was tested without, and with, spacer correction.

4.4.1 SIMULATE-3 Hot Model

The hot model performs thermal-hydraulics calculations. SIMULATE-3's internal heat balance is input by means of interpolation tables of various reactor water flows, temperatures, pressure drops, etc. The heat balance for the VY model was largely derived from fits to actual plant measurements. Some of the values, such as carry-under fraction, were inferred. The fraction of bypass flow and several other pressure drop parameters were calculated by FIBWR[25, 26].

Based on this heat balance, the SIMULATE-3 model calculates inlet subcooling. As an alternative, the subcooling calculated by the plant process computer can be input directly. In this case, the hot model requires a pressure correction to convert plant subcooling (calculated at steam dome pressure) to SIMULATE-3 subcooling (calculated at reactor average pressure). SIMULATE-3 was tested both ways.

For the calculation of voids up the channel, the Vermont Yankee model uses the standard EPRI-Void correlation[27]. For fuel temperatures, the VY model uses fuel temperatures generated with FROSSTEY. These can be input to SIMULATE as a function of exposure on the assembly. However, to keep the model simple, the fuel temperature in the VY model is kept fixed with exposure, it only varies with fuel type and relative nodal power.

The test of the VY hot model consists of a TIP to TIP depletion of the five cycles of the benchmark. On the order of 50 TIP sets were used for each cycle. They are all gamma TIP measurements and nearly all are at equilibrium xenon. Appendix A contains the details of each depletion TIP step as well as descriptions for each core.

The input to SIMULATE-3 for each depletion step includes: core average exposure, power, flow rate, inlet subcooling, steam dome pressure, and control rod positions. SIMULATE-3 depletes to where a TIP set was taken and calculates a corresponding detector response. This response can then be compared to the plant measured data. Appendix D presents the comparisons of the model to plant TIP measurements. Section 5.3 summarizes the hot model eigenvalue behavior.

4.4.2 SIMULATE-3 Cold Model

The cold model uses the thermal-hydraulics of the hot model. However, it is not sensitive to the heat balance, except for the following: Some flow and pressure must be specified. This is required, because the SIMULATE-3 model insists on a tiny amount of core thermal power to provide a neutron source. For a given core moderator temperature, voiding will be calculated to occur unless some flow and pressure (greater than the saturation pressure) is specified.

The test of the VY cold model consists of statepoint benchmarks to plant measured cold criticals. Each cold benchmark is done as a branch SIMULATE-3 case following the hot model depletion to the appropriate exposure point in the cycle. A fission product depletion step always precedes the cold case, to account for the shutdown period before the critical was measured. This is necessary to get the right xenon and samarium concentrations.

Each cold benchmark case is modeled at the plant measured conditions of: core average exposure, reactor average temperature (fuel and moderator are at the same temperature), and control rod positions. Reactor pressure is usually atmospheric; however, some of the criticals required a higher saturation pressure because they took place above 212°F. The reactor period, recorded at the time of the critical, is converted to worth and used to correct the model's eigenvalue.

A total of 24 cold criticals occurred at VY during the five cycles modeled in the benchmark. Every one of them was modeled. Appendix B gives the details of each cold critical. The model's accuracy in the cold benchmark is determined by a steady consistent eigenvalue among all the cold critical cases. Section 5.2 of this report presents the SIMULATE-3 model results for all the cold benchmarks.

4.4.3 SIMULATE-3 Sensitivity Studies

A number of sensitivity studies were performed with SIMULATE-3. The first two merely confirmed the accuracy of our means of constructing the model. The last three illustrate what the model is sensitive to. This helps identify those areas which require caution when analyzing

future fuel designs or changes to those codes (FROSSTEY and FIBWR) which supply auxiliary input for the SIMULATE-3 model.

SIMULATE-3 will either accept fuel bundle weights, or it will calculate the same based on a pass-through of the CASMO-3 lattice weights. As discussed (see Section 4.2) the CASMO-3 stack densities were explicitly adjusted to give weights very close to the long term average weights of the various fuel types involved in the benchmark. Yet, batches of the same fuel type, loaded at different times in the benchmark, varied from 182.4 KgHM in early cycles, up to 184.3 KgHM in later cycles. This was caused by the fuel vendor gradually increasing the pellet density (see Section 3.3). As a test, the actual fuel batch weights were installed in SIMULATE-3. This did not improve the results of the model relative to the pass-through of CASMO-3 lattice weights. Therefore, the production model will continue to use the generalized CASMO-3 weights.

Another sensitivity study tested whether using the internal heat balance in SIMULATE-3 altered the benchmark results relative to direct input of the plant subcooling. Again, the results were virtually indistinguishable. Therefore, the plant subcooling will be used when it is available; the heat balance will be used when it is not.

One input parameter that does affect the SIMULATE-3 results significantly is the fuel temperature. Based on the user's definition of average fuel temperature in SIMULATE-3, the latter will interpolate (or extrapolate) between the CASMO-3 fuel temperature results to get less (or more) Doppler feedback. FROSSTEY is used to calculate individual fuel temperatures for each fuel type. This was input to SIMULATE-3 as a value which varies only with power. To test the importance of the fuel temperatures, the VY model was exercised by simply increasing the values of the average fuel temperature assigned to each fuel type by 80°C. The Doppler feedback of the model behaved predictably and produced a 2.3 milli-K reduction in core K-effective.

Conclusion: It is very important to be aware of any changes to the fuel behavior modeling code, FROSSTEY. Likewise, any future fuel vendor changes to the fuel thermo-mechanical design which may affect average fuel temperature need to be evaluated. Even subtle changes, such as producing a smoother pellet surface can significantly affect the gap conductance and thereby change the average fuel temperature.

The last two sensitivity studies were a test of the spacer correction model in SIMULATE-3 and a test of the channel bowing cross sections developed at the CASMO-3 level (see Section 4.2.4). These both had significant impact on the eigenvalue behavior of the model. Figure 4.10 gives an example of how the eigenvalue of Cycle 10 behaved as the two changes were made in succession. Each one tended to bring the average eigenvalue closer to 1.0. The channel bowing cross sections tended to flatten the "eigenvalue drift" the model exhibits as the cycle progresses.

Figures 4.11 and 4.12 illustrate the impact of the spacer correction model on the axial average of all the TIP readings. Notice in Figure 4.11 the obvious location of spacers in the plant data. The plain, uncorrected, EPRI-void thermal hydraulic model, however, is smoothly varying. Notice in Figure 4.12 that the spacer correction model does, to some degree, exhibit the characteristic dips in the TIP readings, especially at the top of the core.

Conclusions: The SIMULATE-3 model with spacer correction and bowed channel cross sections is the preferred method of modeling Vermont Yankee. In the next section the results of this final model will be reported.

FIGURE 4.1

Composition Regions Specified for Vermont Yankee MICBURN-3 Model

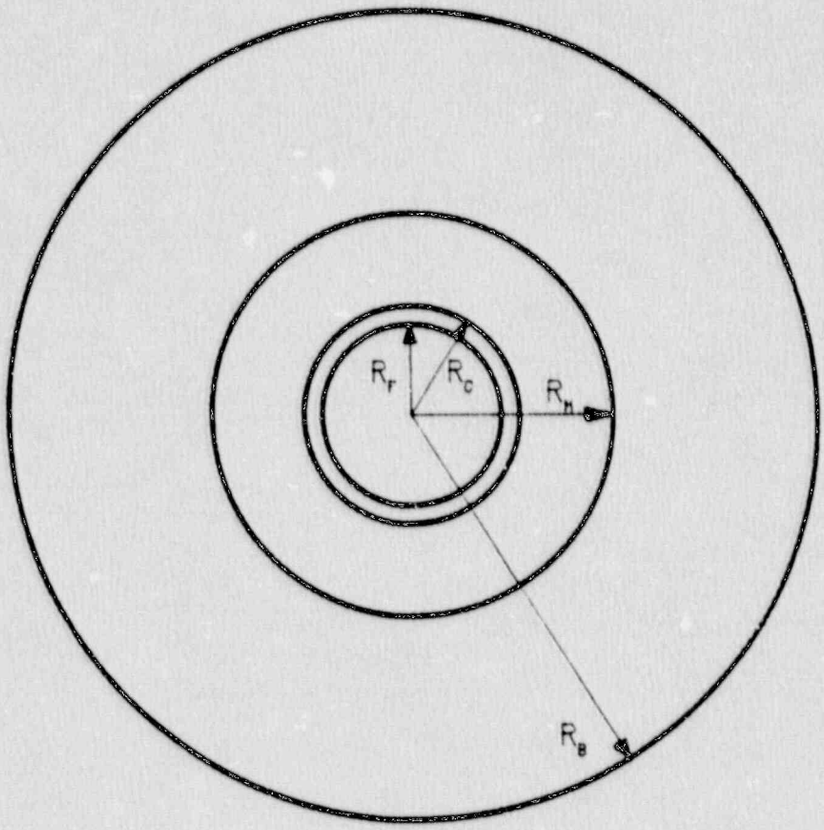

Notes	Macro-Regions	Micro-Regions
R_f = Fuel Pellet Composition	10	20
R_c = Fuel Cladding Composition	1	N/A
R_M = Pin Moderator Composition	2	N/A
R_B = Buffer Region Composition	2	N/A

FIGURE 4.2

MICBURN-3 Sensitivity: Adding Water to the Buffer Region

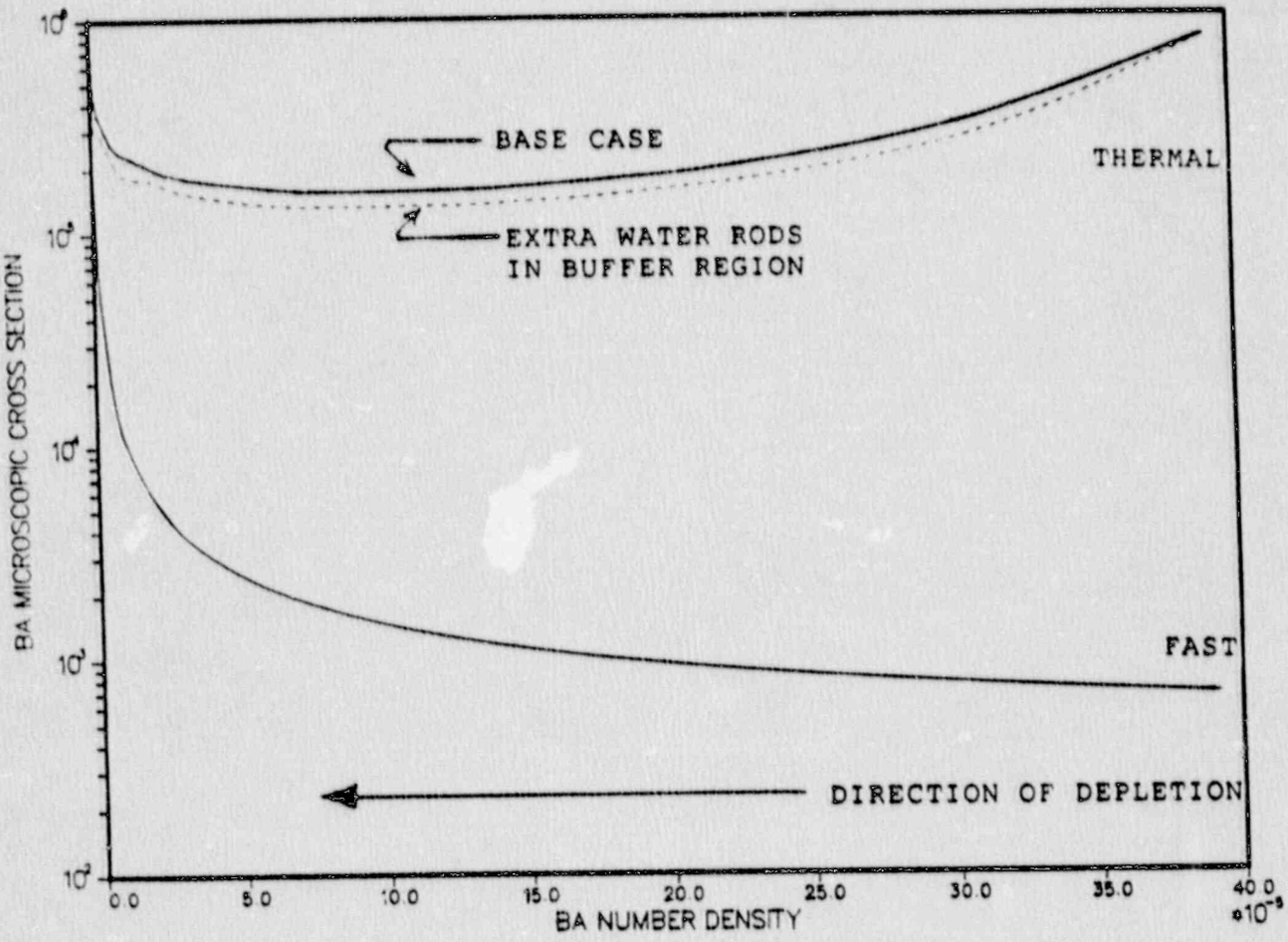

FIGURE 4.3

MICBURN-3 Sensitivity: Adding Voids to the Moderator Region

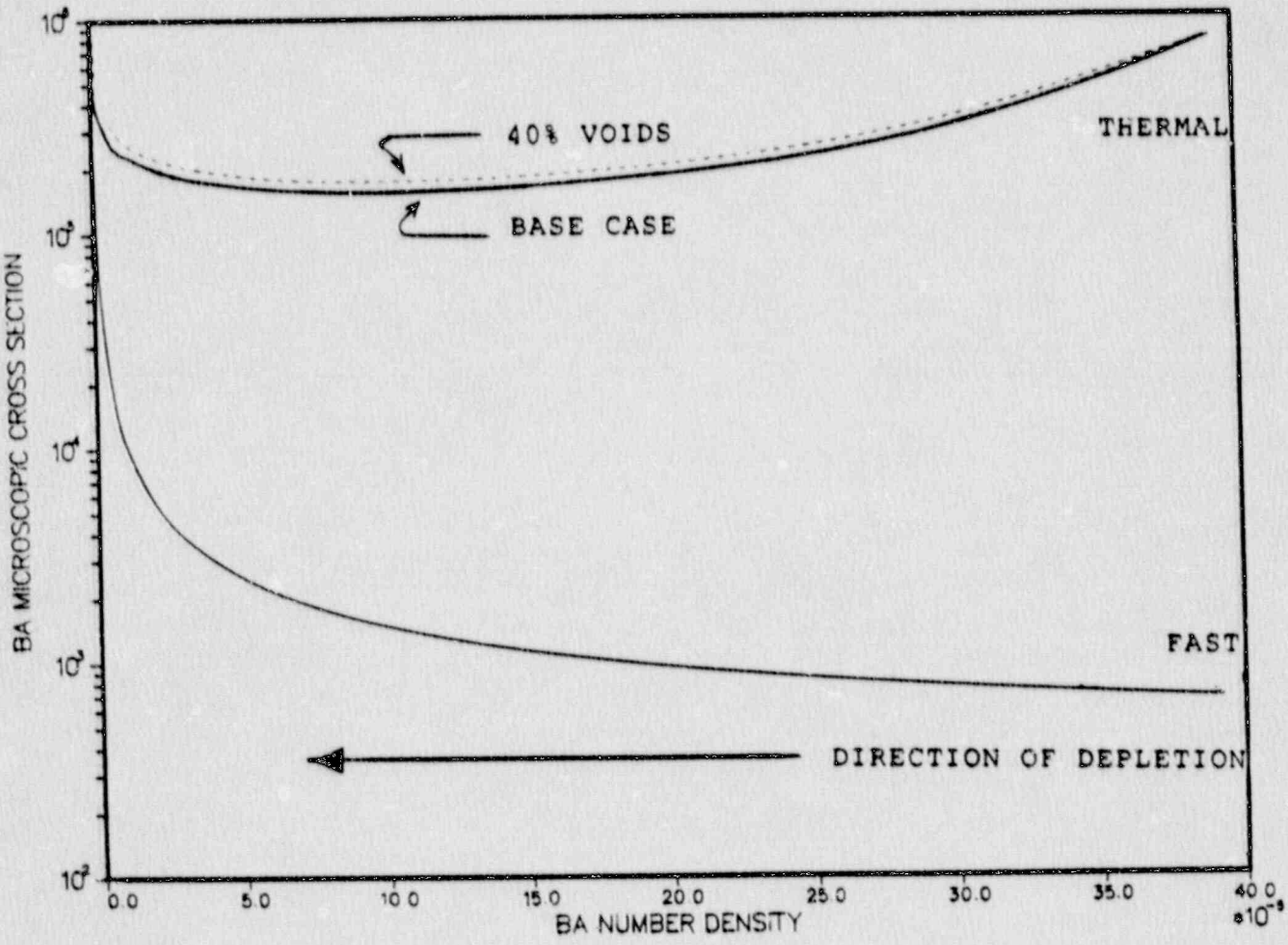

FIGURE 4.4

CASMO-3 Representation of the Vermont Yankee Lattice

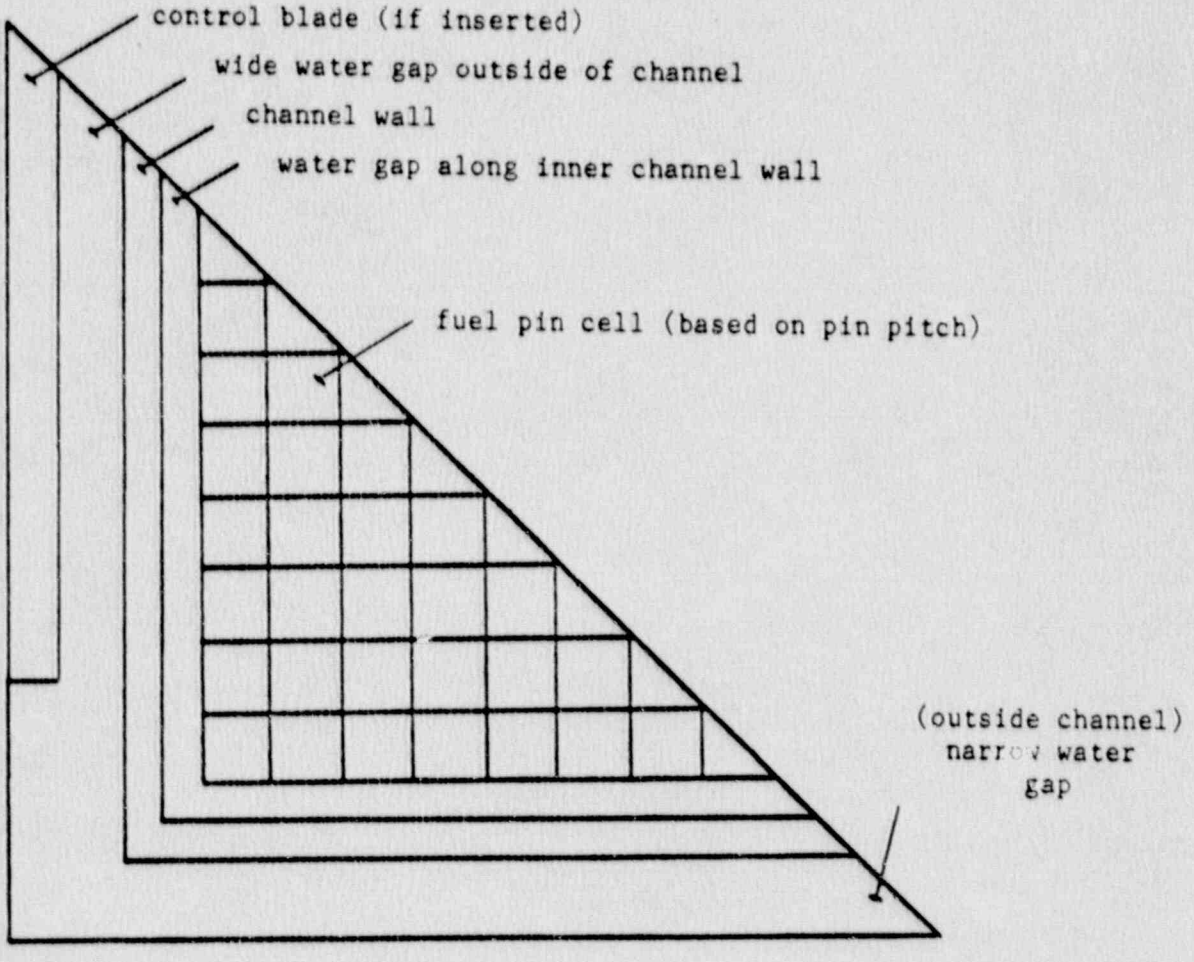

FIGURE 4.5

Cross Section View of the Vermont Yankee Control Rod Wing

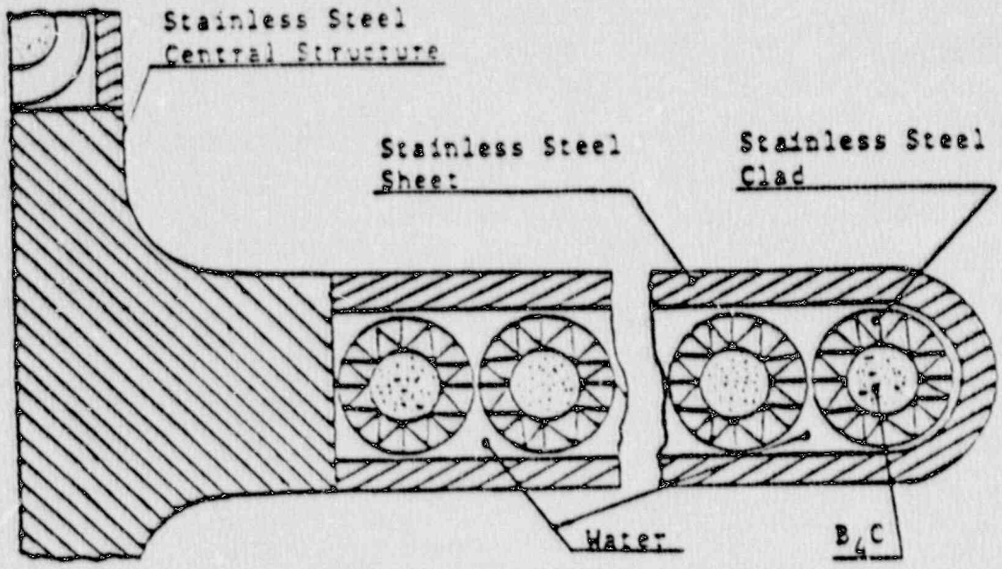

FIGURE 4.6

CASMO-3 Representation of the Control Rod Wing

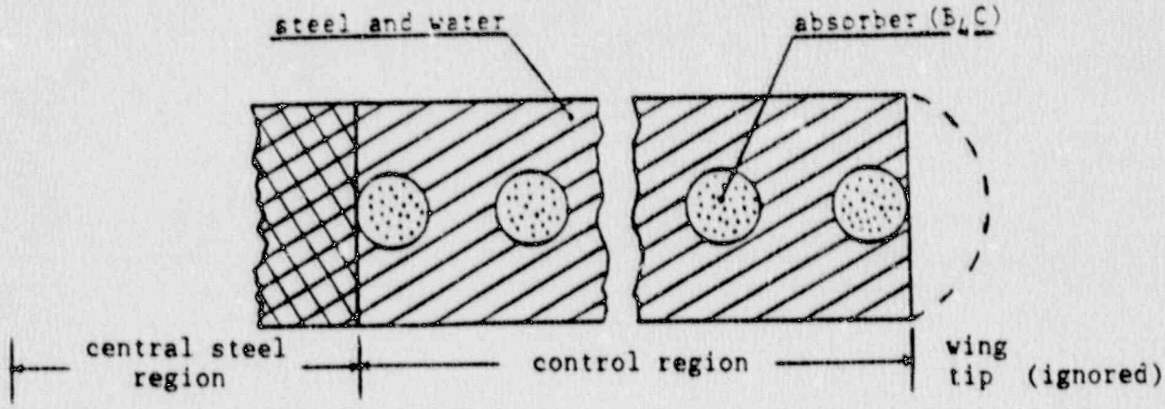

FIGURE 4.7

CASMO-3 Sensitivity: Change in K_∞ Between 40 and 70 Groups

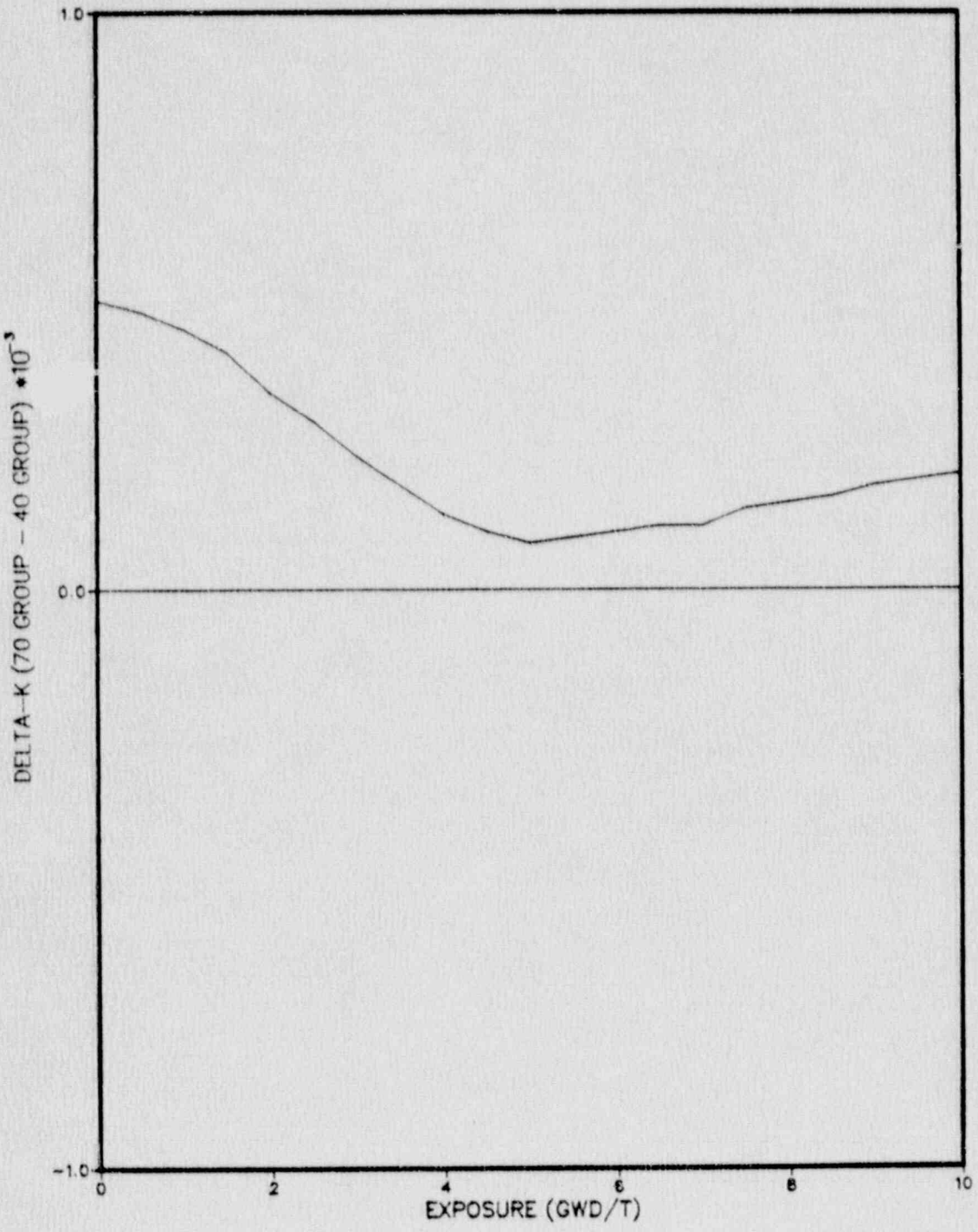

FIGURE 4.8

CASMO-3 Sensitivity: Change in K_∞ Caused by 40 mil Channel Bow

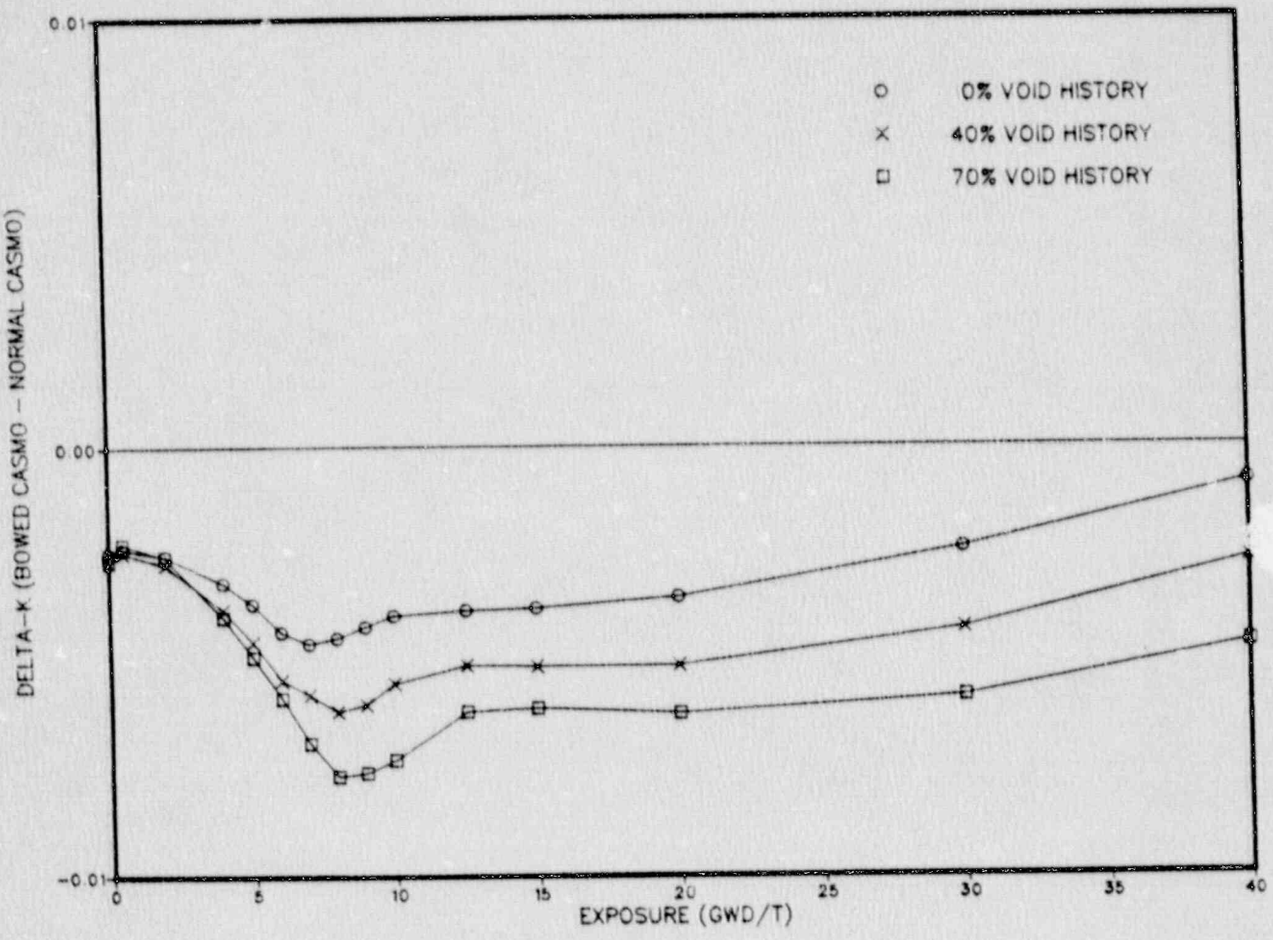

FIGURE 4.9

SIMULATE-3 Axial Representation of Vermont Yankee Fuel

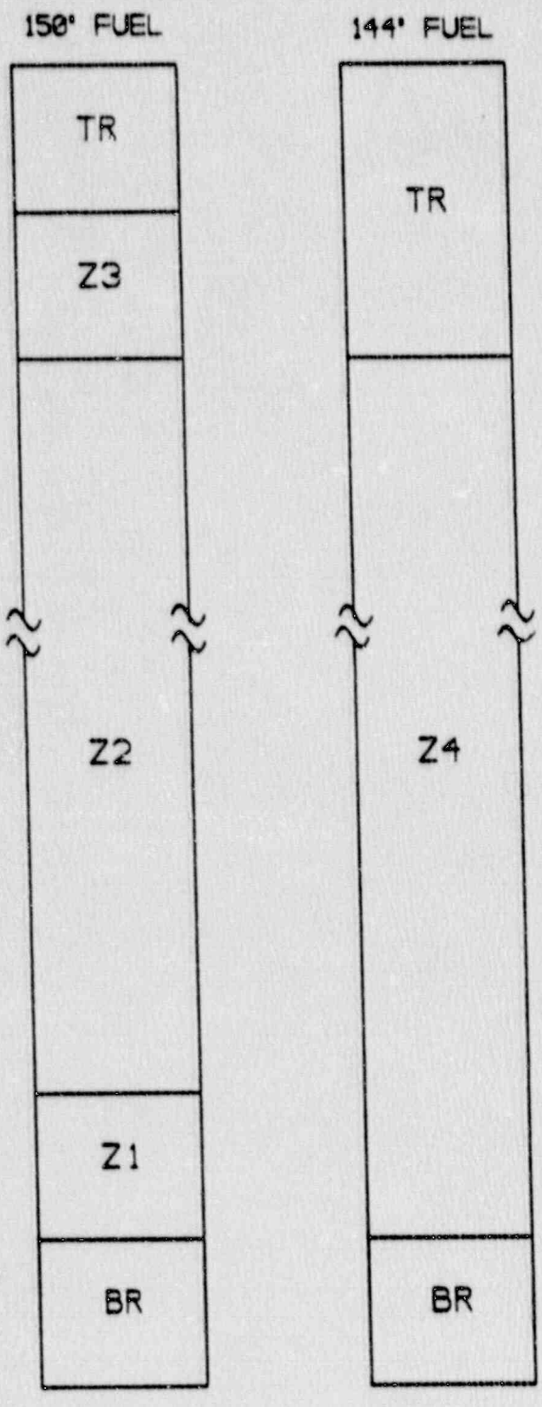

KEY

TR = TOP REFLECTOR 'ZONE'
BR = BOTTOM REFLECTOR 'ZONE'
Z1 = BOTTOM FUEL ZONE, 150" FUEL
Z2 = MIDDLE FUEL ZONE, 150" FUEL
Z3 = TOP FUEL ZONE, 150" FUEL
Z4 = ACTIVE FUEL, 144" FUEL

FIGURE 4.10

Impact of Spacer Correction and Channel Bowing on SIMULATE-3 Eigenvalue

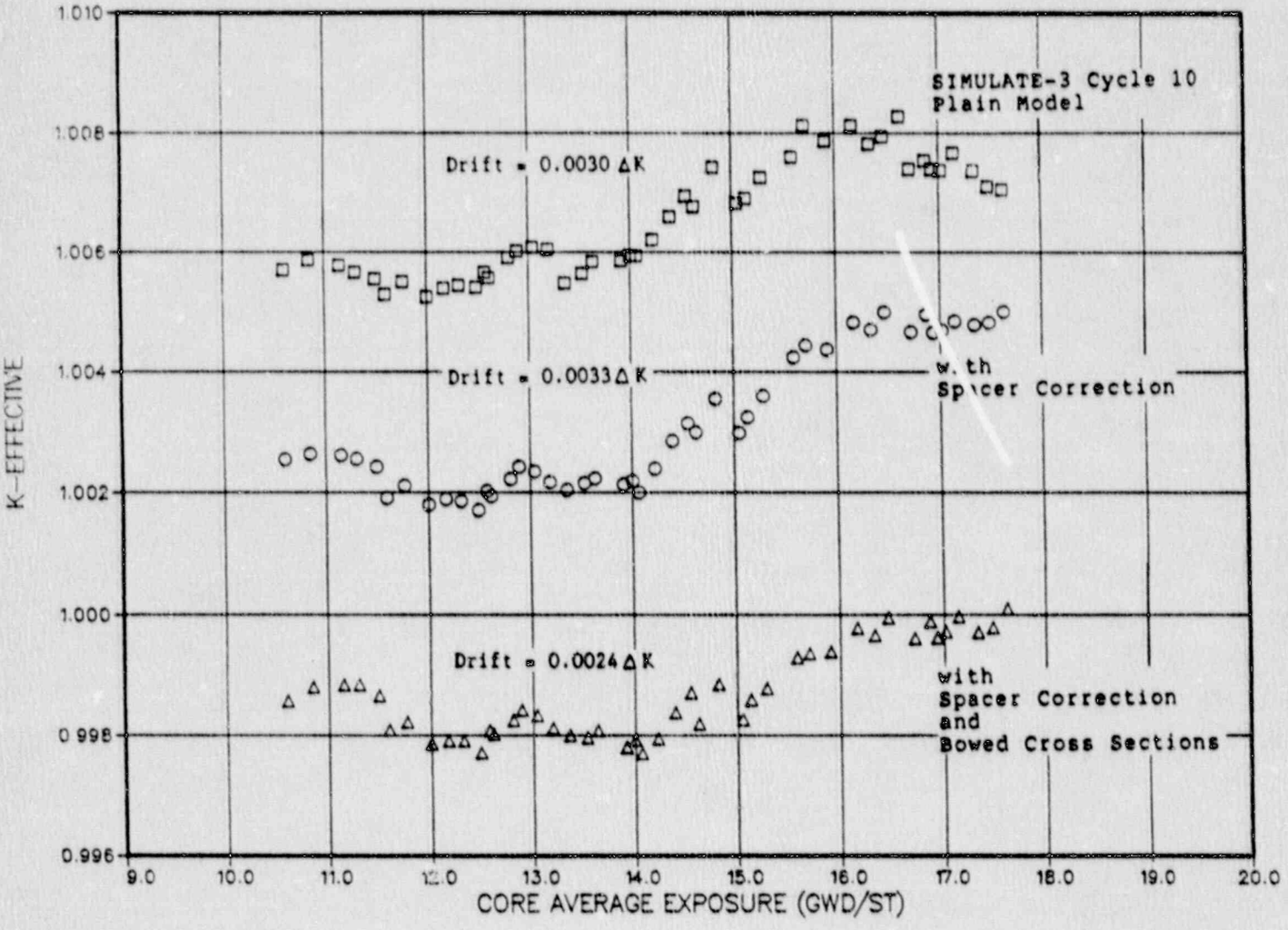

FIGURE 4.11

Plant Average Axial TIP Trace vs. Plain SIMULATE-3 Model

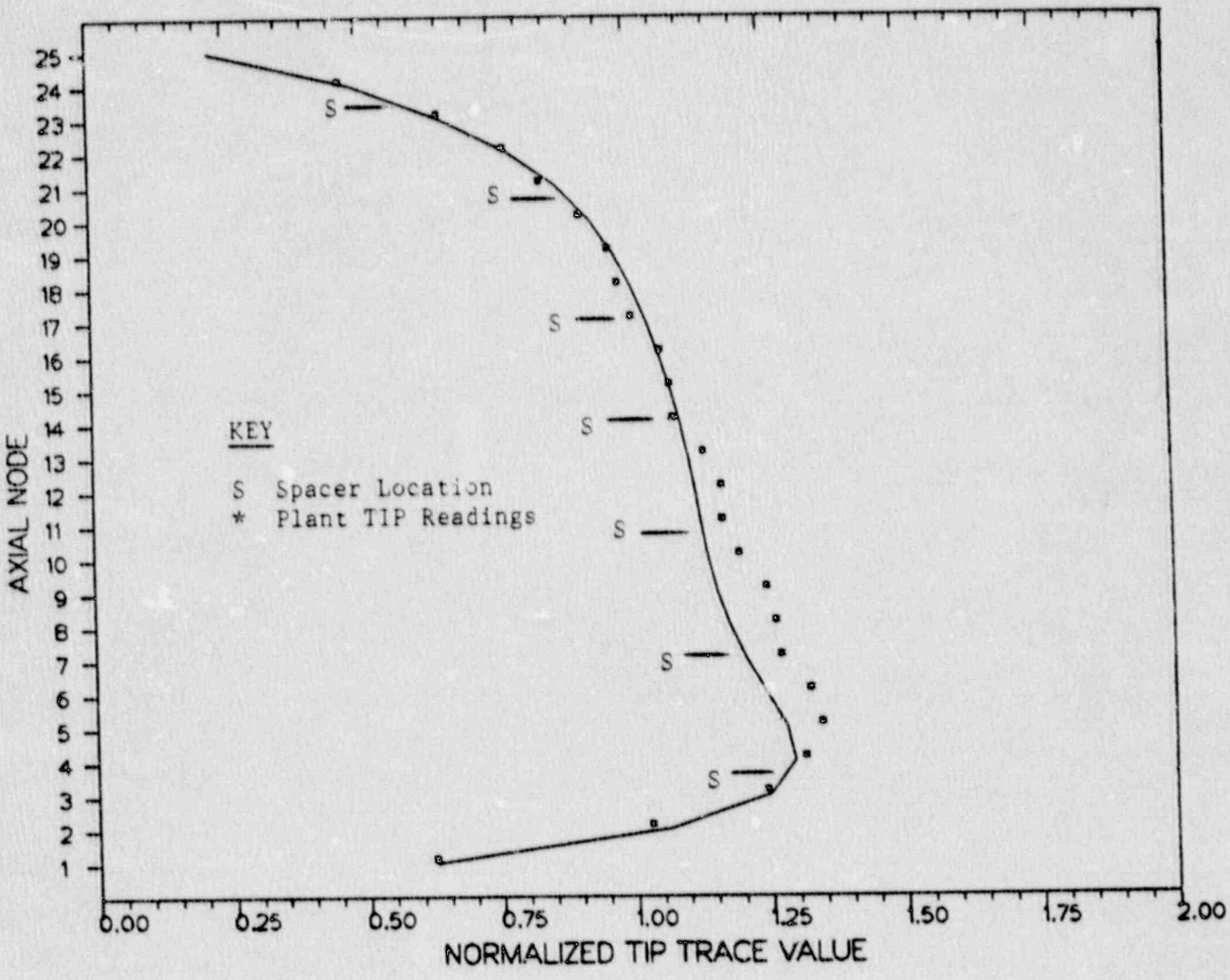

FIGURE 4.12

Plant Average Axial TIP Trace vs. SIMULATE-3 Spacer Correction Model

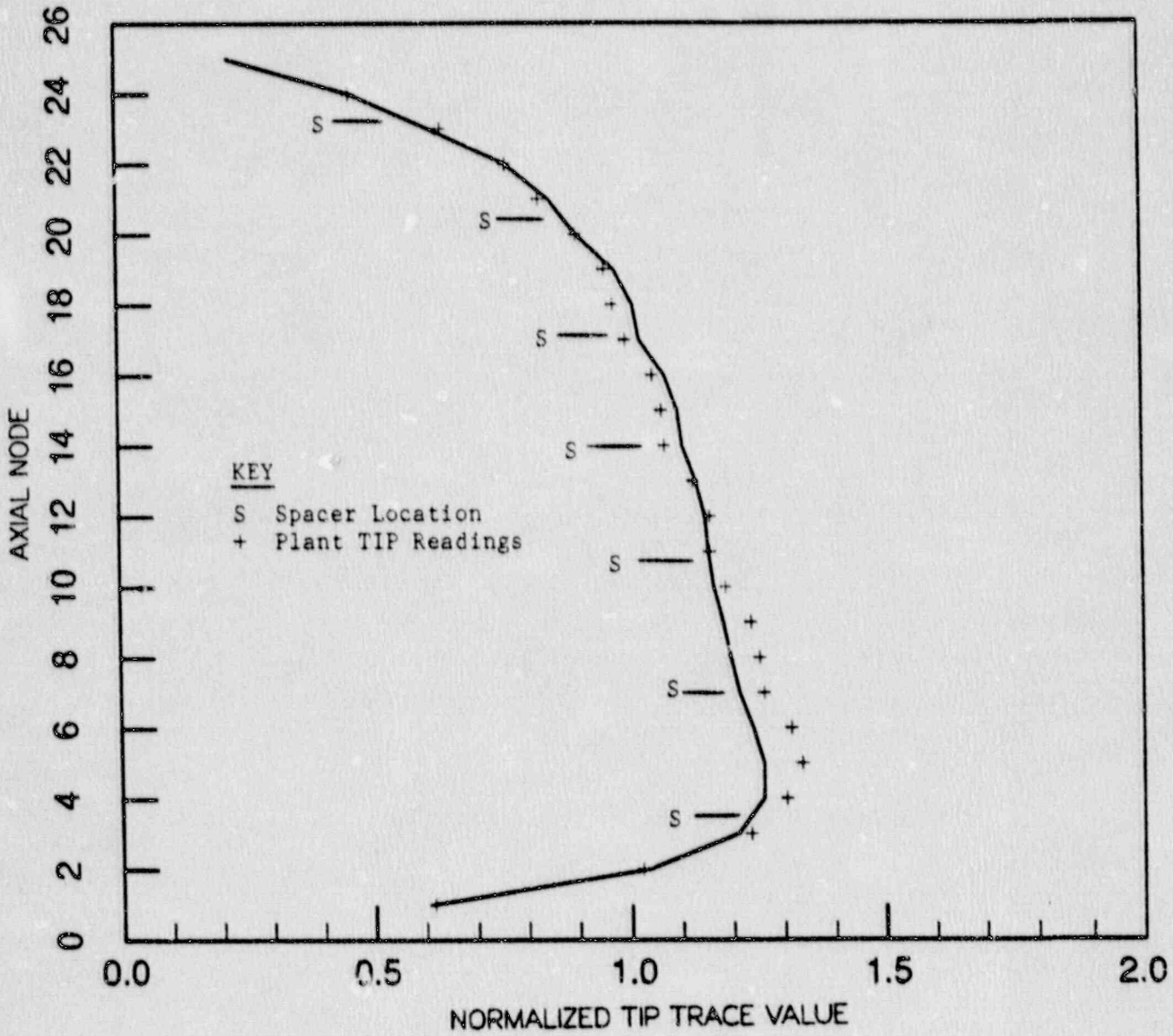

5.0 VERMONT YANKEE PHYSICS MODEL RESULTS

The final evaluation of the entire code package is based upon the performance of the SIMULATE-3 code. The final Vermont Yankee model contains cross sections which reflect the shift due to channel bowing. The thermal hydraulics model uses the EPRI-void model, corrected for local spacer effects. SIMULATE-3 is benchmarked against hot and cold critical statepoints from Cycles 9-13. The model is judged on two main figures of merit:

- **Eigenvalues** - must be reasonably close to 1.0. They must be steady, with small standard deviations. Any trends exhibited must be gradually varying.

- **TIP Traces** - generated by the model must compare closely to the plant TIP traces, both radially and axially. The errors must be small and steady. Any trend exhibited in the errors must be gradually varying.

A model that meets both these figures of merit is suitable for making predictions. These can be short range, as in plant support; or, long range, as in licensing.

5.1 Hot Model Eigenvalues

The benchmark went back to the end of Cycle 8 to pick up a set of exposure, void, and control history arrays. The latter were developed during the benchmark of the old CASMO/SIMULATE model presented in Reference 6. As such, the EOC8 history arrays loaded into SIMULATE-3 were slightly inconsistent with the new CASMO-3 cross sections. The differences, however, proved not to be that great. The old cross section history effects disappeared rapidly during the depletion of Cycle 9. Therefore, the beginning of Cycle 9 results are included in the total model results. With over 200 statepoints modeled, the impact of the BOC9 results on the statistics is negligible.

Figure 5.1 shows the eigenvalues for the five cycles of the benchmark. The data is consistent and tightly packed. There is a slight upward "drift" in the eigenvalues that starts in the middle of each cycle. However, this drift meets the criterion that any trends be slowly varying. It will not affect our ability to make critical predictions with the model.

Table 5.1 shows the average hot eigenvalue for each cycle with the standard deviation. The average hot eigenvalue for all cycles is 0.9989 ±.0010. This meets the figure of merit of being reasonably close to unity. The overall standard deviation is small and consistent within the individual cycles. The standard deviations, for each cycle, primarily reflect the little amount of drift in the eigenvalue over each cycle. Within a given cycle, the eigenvalue is very well behaved. It varies gradually with exposure as the previous example in Figure 4.10 illustrates. Therefore, this model is suitable for hot critical predictions during plant operation.

Table 5.2 shows the hot startup eigenvalue at the beginning of each cycle. This was derived by averaging the first five equilibrium statepoints of each cycle. The average of the BOC hot eigenvalues is 0.9985, for all the cycles, with a standard deviation of ± 0.0005. This small standard deviation indicates good consistency among the cycles. In licensing applications, this provides a high level of confidence in the calculation of BOC hot excess reactivity. Thus, predictions of startup control rod patterns will be quite accurate.

Table 5.3 shows the hot eigenvalue at EOFPL in each cycle. This was the eigenvalue of the depletion statepoint nearest to the start of coastdown. As with the BOC eigenvalues, the EOFPL values are consistent among all the cycles. The average of all the EOFPL hot eigenvalues is 0.9998 with a standard deviation of ± 0.0006. Consistency in these eigenvalues is important for predicting the EOFPL exposure when doing a licensing analysis, because the results of certain licensing transients, especially the pressurization transients, are sensitive to the EOFPL calculated.

5.2 Cold Model Eigenvalues

As stated in Section 5.1, the beginning of Cycle 9 was initiated using old cross section histories. The impact this had on the hot model results was negligible because of the large number of hot statepoints. However, because of VY's exceptional operation, there are very few cold statepoints to benchmark against. The BOC9 statepoints represent a significant portion of available cold criticals. Therefore, the three cold criticals near BOC9 are given half the weighting of the remaining cold critical comparisons in deriving the cold model eigenvalue.

The results of the cold critical benchmark are presented in Table 5.4. The actual control rod patterns for the criticals are given in Appendix B. The weighted cold critical eigenvalue for the SIMULATE-3 model is .9968 with a standard deviation of ±.0017. To be sure that there is no bias in the cold model, the eigenvalues were grouped by A sequence and B sequence. The results of the A sequence cases are .9968 ± .0015. The results of the B sequence cases are .9971 ± .0018. Statistically, there is no meaningful difference between sequences.

The cold eigenvalue is also plotted against core temperature and core average exposure in Figures 5.2 and 5.3. There are no obvious trends in the cold model, with regard to either of these two variables.

5.3 Hot Model Detector Comparisons

As described in Section 3.1, all plant "measurements" of power distribution ultimately depend on the TIP traces. SIMULATE-3 produces a set of gamma based detector responses at specific instrument locations. These can be compared with the plant-measured gamma-TIP traces, at the same locations.

The simplest comparison is a one-for-one comparison, or nodal comparison. Each of the 20 plant TIP traces has 24 readings, spaced evenly over the 144" of the TIP tube. This works out to one reading for every six inch node. SIMULATE-3, however, has 25 six inch nodes. It produces, and expects to receive for plant data, 25 TIP readings per trace. To prevent inconsistency, the plant data is supplied to SIMULATE-3 with a dummy 25th value at the top of each trace. The dummy value is zero. Therefore, at the top of each trace, the code always calculates 100% error.

In the following statistical comparisons of model-to-plant, the 25th node "readings" are ignored. With the 25th node values removed, both the plant and SIMULATE-3 TIP traces were normalized. That is, all 20 x 24 nodal values were summed and divided by 480 to obtain one global normalization factor for the plant and one for SIMULATE-3. This was divided into each nodal instrument reading. This normalization is necessary because the plant uses arbitrary units for its TIP readings which differ from SIMULATE-3's units by a factor of about 100.

Following the normalization, comparisons were made between the SIMULATE-3 TIP readings and the plant TIP readings at each of the 480 nodal (24 x 20) locations. The 480 comparisons provide an RMS error for each "TIP set"; i.e., each exposure statepoint where TIPs were taken. The nodal RMS errors were statistically summed for each cycle and for all five cycles. The results are given in Table 5.5. For the five cycles the total RMS nodal error is 2.94%.

This RMS error is beginning to approach the accuracy limitations of the TIPs themselves. A measure of the instrumentation accuracy is the "Total TIP Uncertainty" provided in the VY Startup Test Reports[28, 29, 30, 31, 32]. Total TIP uncertainty is simply half of the RMS differences observed between mirror symmetric TIPs when the plant starts up in a symmetric rod pattern. Table 5.6 provides the plant total TIP uncertainty measured at BOC for the cycles included in the benchmark. Statistically combining the results for all cycles produces a five cycle TIP uncertainty of 1.74%.

The model's 2.94% RMS error is very close to the intrinsic average instrumentation uncertainty of 1.74%. On the surface, this agreement appears to be sufficient. However, the nodal RMS errors do not provide enough information to judge the accuracy of the model. There may still be some residual problems, either radially or axially, which get lost in the nodal RMS statistics, because the vast majority of comparison points are good. To judge the model further, the radial and axial shapes of the instrument readings were individually examined for each TIP set.

5.3.1 Radial Comparisons

Integrated TIP readings were created at each of the 20 instrument locations by adding up the 24 normalized nodal readings for each individual string. The resulting integral reading for the given string is almost proportional to the relative reactor power in the four adjacent assemblies. By comparing the SIMULATE-3 integrated TIPs to the plant integrated TIPs, a map may be constructed showing the radial error.

The integral TIP errors at each TIP location for each TIP set have been averaged and mapped for each cycle. These radial maps can be found in Appendix D. The errors at each location can also be averaged for all five cycles. The resulting map is shown in Figure 5.4 The

average radial errors are very close to zero. Therefore, on the average, the SIMULATE-3 model is reproducing the plant radial power distribution quite well. However, the errors at any given location will make random step changes in going from cycle to cycle. This may be seen in the specific cycle maps found in Appendix D. Once the step change is established, at BOC, the variation at any given TIP location is small and slowly varying with exposure.

In theory, this step change at BOC is caused by random shifts in the orientation of the TIP string and random variations in adjacent channel bowing created during fuel shuffling. This changes the TIP asymmetry from cycle to cycle. Thus, the TIP integral errors shift at each location following refueling. Over the long haul (say, these five cycles), the impact of random TIP asymmetry should cancel. This is shown by the small average errors of Figure 5.4. Most radial locations in Figure 5.4 show an average error less than 1%. The worst location (near the periphery) is less than 2.2%.

As far as future predictions are concerned, any model of a future cycle may exhibit the magnitude of errors shown in the radial maps of Appendix D. At any given location, this could run 4-5%. Most of this error is due to TIP asymmetry.

5.3.2 Axial Average Comparisons

In a manner similar to the creation of integrated TIP readings, the TIP readings may be integrated for axial planes of the core. The resulting reading is almost proportional to the relative power in the given plane of the core. The SIMULATE-3 core average (planar) TIP readings may then be compared to the plant core average (planar) TIP readings. Appendix D provides axial average comparisons for all TIP sets in the benchmark.

The axial average comparisons, given in Appendix D, show good overall agreement between the model and the plant. However, there is a trend in the axial shapes exhibited by each cycle modeled. The SIMULATE-3 model tends to underpredict the power in the bottom of the core, especially toward end of full power life.

Figure 5.5 summarizes the results of the axial average TIP trace comparisons made over all five cycles. Figure 5.5 plots the average axial error in the planar TIP readings versus axial node. The $\pm$ standard deviations are also plotted. The broadening of the standard deviations

near the bottom of the model is caused by the aforementioned tendency of the model to underpredict the bottom. The direction of the arrow indicates the general direction of the trend from beginning of cycle to end of full power life. (Note: the relatively large errors in the very bottom node should not cause any alarm. The power in the bottom of the core varies between 30% and 40% of reactor average. Therefore, it is never significant from a margin-to-limits standpoint.)

The trend shown in Figure 5.5 was also exhibited by the previous SIMULATE-2 model. It does not affect the licensing applications of the code. The limiting licensing transients near EOFPL are the pressurization transients. These transients are most sensitive to the scram reactivity function. The model's tendency to lose power in the bottom towards EOFPL will simply weaken the calculated (bottom entry) scram reactivity. The net result is that the pressurization transients will be calculated to be more severe than reality; more conservative licensing limits will be generated.

5.4 Comparison of New Model to Current Model

One of the means of judging the new code package is to compare it to the current code package of: MICBURN/CASMO-2/TABLES-2/SIMULATE-2. The latter code package is also judged by the performance of the final code in the process stream; namely, SIMULATE-2. Therefore, to be concise, we will refer to the comparison of the code packages as SIMULATE-3 versus SIMULATE-2.

With regard to eigenvalues, Table 5.7 summarizes the behavior of both packages benchmarked over the same five cycles. SIMULATE-3 is clearly superior. It is closer to 1.0 for the hot model eigenvalue. The latter also exhibits a much smaller standard deviation. This is because the eigenvalue drift has been cut by a factor of 3.

The BOC and EOFPL average hot K-effectives for the SIMULATE-3 model are close to one another. This again indicates the small amount of eigenvalue drift. The same is not true of SIMULATE-2. For the latter, the spread between BOC and EOFPL is almost 0.7%ΔK. While this amount of drift has been an inconvenience, it really does not affect the licensing applications of SIMULATE-2. This is because of the relative tightness of the BOC and EOFPL K-effectives as shown by the standard deviations. The BOC hot excess predictions and EOFPL

cycle length predictions can still be made with SIMULATE-2 with a good degree of accuracy. However, the degree of accuracy will be improved upon by using SIMULATE-3.

The cold eigenvalues are roughly comparable. However, SIMULATE-3 holds a slight advantage in standard deviation. Less uncertainty in the cold eigenvalue produces better cold critical predictions. Also notice that the hot-to-cold bias is significantly reduced.

With regard to accuracy of the power distributions, the codes are comparable with a slight edge given to SIMULATE-3. The nodal RMS errors for the five cycles for SIMULATE-2 are 3.19%. For SIMULATE-3 they are 2.94%. While this improvement is marginal, it is important to keep in mind that these results for SIMULATE-3 were achieved without the use of adjustment factors. In the future, the elimination of adjustment factors will considerably simplify the building of models which have new fuel types.

TABLE 5.1

SIMULATE-3 Cycle Average Hot Eigenvalues

Cycle	Number of TIP Set Statepoints	Average Eigenvalue	± Standard Deviation
9	49	0.99920	0.00077
10	45	0.99870	0.00075
11	39	0.99931	0.00115
12	43	0.99956	0.00069
13	47	0.99802	0.00071
5 Cycles	223	0.99893	0.00098

TABLE 5.2

SIMULATE-3 Beginning of Cycle Hot Eigenvalues

Cycle	Number of TIP Set Statepoints	Average BOC Eigenvalue
9	5	0.99837
10	5	0.99874
11	5	0.99807
12	5	0.99924
13	5	0.99811
BOC Average		0.99851
± Standard Deviation		.00049

TABLE 5.3

SIMULATE-3 End of Full Power Life Hot Eigenvalues

Cycle	Number of TIP Set Statepoints	EOFPL Eigenvalue
9	1	0.99931
10	1	0.99972
11	1	1.00055
12	1	1.00027
13	1	0.99904
EOFPL Average		0.99978
± Standard Deviation		0.00063

TABLE 5.4

VY Cold Critical Case Conditions and SIMULATE-3 Results

Date	Cycle Number	Cycle Exposure (MWd/St)	Core Average (MWd/St)	Control Rod Sequence	Recirc. Temp. (°F)	Reactor Period (Sec)	K-effective Adjusted for Period
11/25/81	9	0	9,192	Local	91	226	.99258
11/26/81	9	0	9,192	A1	96	78	.99717
12/07/81	9	91	9,283	A1	180	100	.99595
01/28/82	9	976	10,168	B2	250	45	.99635
06/10/82	9	3,700	12,892	A1	200	400	.99499
08/31/82	9	5,329	14,521	B2	240	400	.99616
03/09/83	9	8,945	18,137	A2	100	105	.99983
03/09/83	9	8,945	18,137	B1	101	58	.99927
05/28/83	10	0	10,463	A1	103	223	.99681
06/17/83	10	0	10,463	A1	189	75	.99818
01/06/84	10	4,085	14,548	A1	225	120	.99729
06/19/84	10	7,343	17,806	A2	126	100	.99681
06/19/84	10	7,343	17,806	B1	127	200	.99697
07/27/84	11	0	10,418	A1	94	160	.99662
08/06/84	11	0	10,418	A1	161	197	.99634
09/29/84	11	633	11,051	A1	227	120	.99839
06/05/86	12	0	9,820	A2	83	185	.99850
06/30/86	12	0	9,820	B2	158	87	.99841
07/02/86	12	0	9,820	B2	165	118	.99882
08/27/87	13	0	8,613	A2	87	55	.99628
10/02/87	13	0	8,613	A2	197	72	.99498
07/02/88	13	5,386	13,999	B2	209	70	.99406
08/26/88	13	6,329	14,942	A1	228	142	.99473
08/28/88	13	6,329	14,942	A1	234	96	.99513

Average: .99680

Standard Deviation: ±.00168

TABLE 5.5

SIMULATE-3 Nodal TIP Reading RMS Errors

Cycle	Number of TIP Set Statepoints	RMS Error (%)
9	49	2.955
10	45	2.618
11	39	3.201
12	43	2.557
13	47	3.293
5 Cycles	223	2.939

TABLE 5.6

VY Total TIP Uncertainties at Beginning of Cycle

Cycle	Number of TIP Set Statepoints	Total TIP Uncertainty (%)
9	1	1.46
10	1	2.12
11	1	1.98
12	1	1.52
13	1	1.52
5 Cycles	5	1.74

TABLE 5.7

Results of SIMULATE-3 Compared to SIMULATE-2

Benchmark Figure of Merit	Benchmark Results for Cycles 9-13 New Code Package (SIMULATE-3)	Current Code Package (SIMULATE-2)
Hot Eigenvalue	.99893	1.00839
Hot Standard Deviation	±.00098	±.00281
BOC Average Hot K-eff	.99851	1.00539
BOC ± Standard Deviation	±.00049	±.00081
EOFPL Average Hot K-eff	.99978	1.01223
EOFPL ± Standard Deviation	±.00063	±.00078
Hot ΔK BOC to EOFPL	.00127	.00684
Cold Eigenvalue	.99680	.99775
Cold Standard Deviation	±.00168	±.00262
Hot-to-Cold Bias	.00213	.01064
Nodal RMS Error (%)	2.939	3.185

FIGURE 5.1

SIMULATE-3 Hot Eigenvalues for Cycles 9-13 vs. Core Exposure

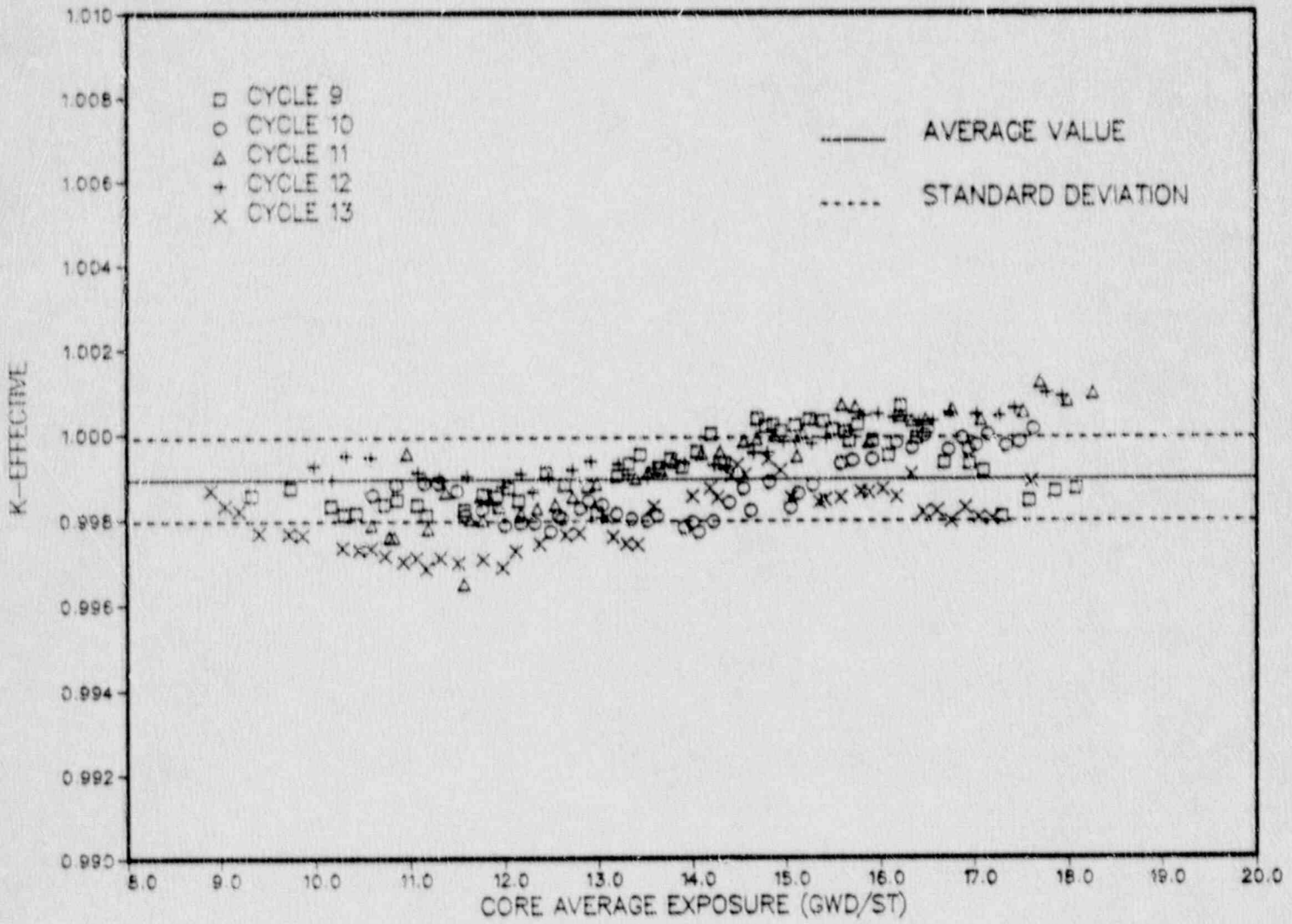

FIGURE 5.2

SIMULATE-3 Cold Eigenvalues for Cycles 9-13 vs. Core Temperature

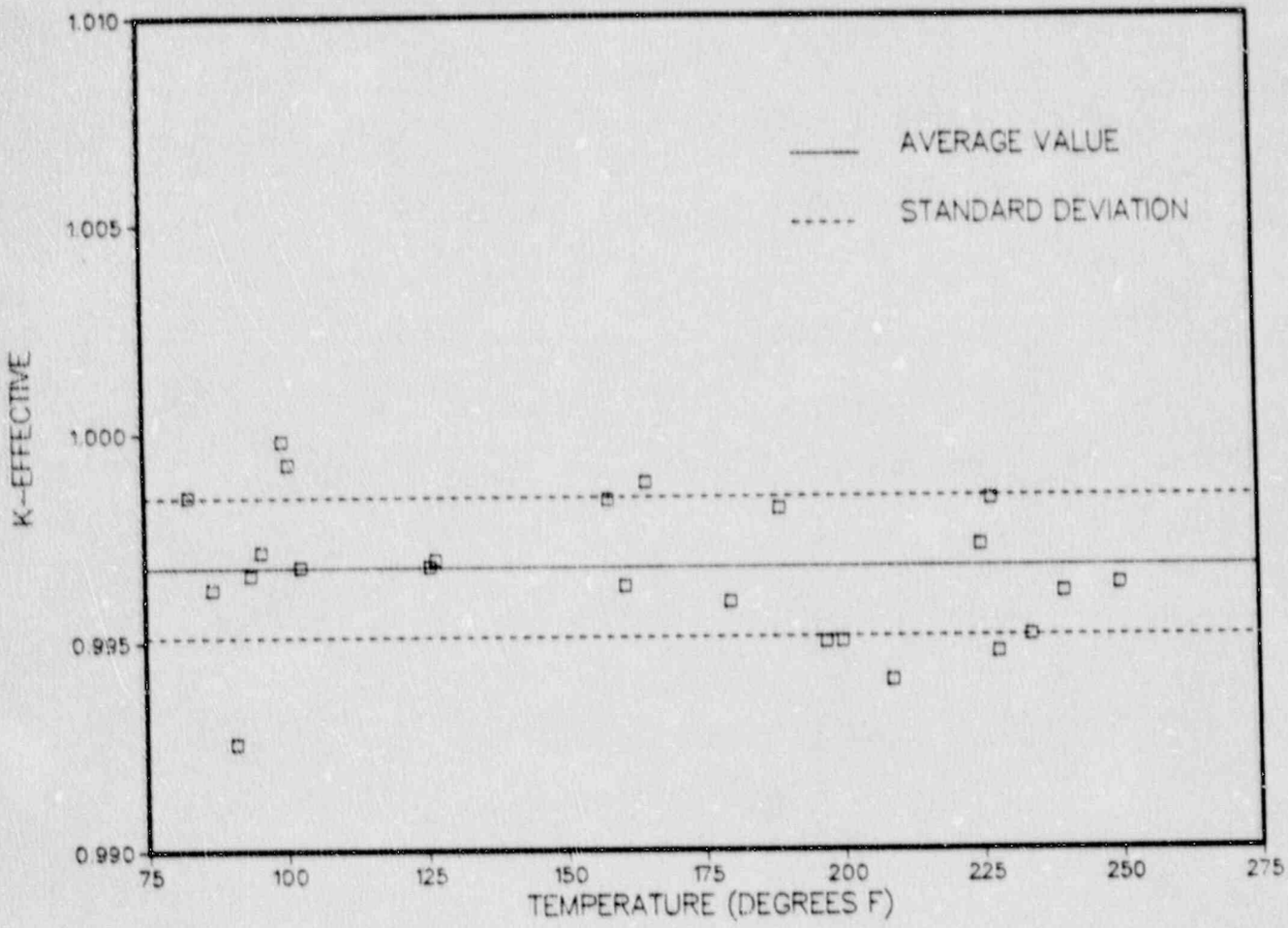

FIGURE 5.3

SIMULATE-3 Cold Eigenvalues for Cycles 9-13 vs. Core Exposure

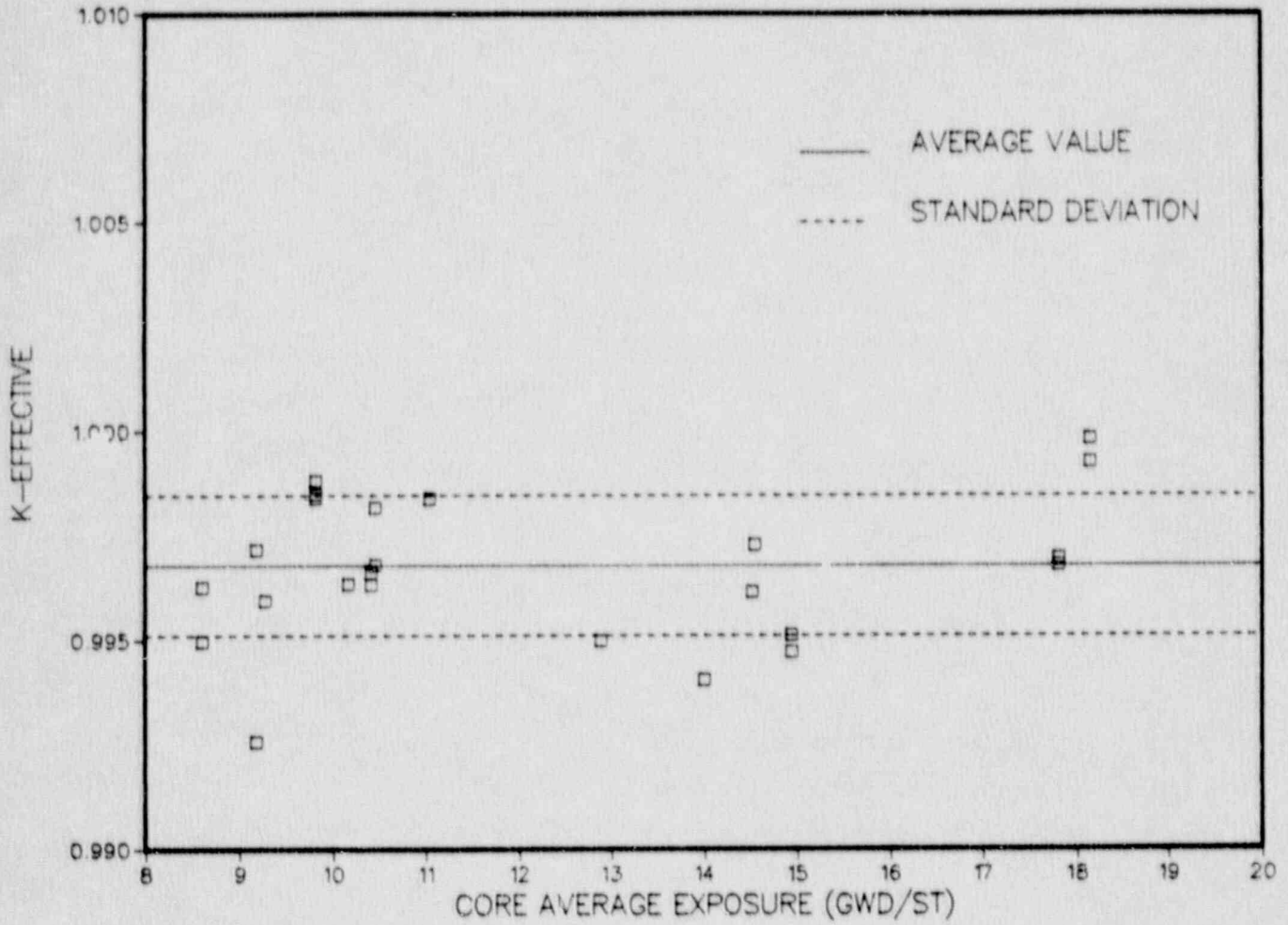

FIGURE 5.4

SIMULATE-3 Averaged TIP Integral Errors, S. D., and RMS Errors for Cycles 9-13

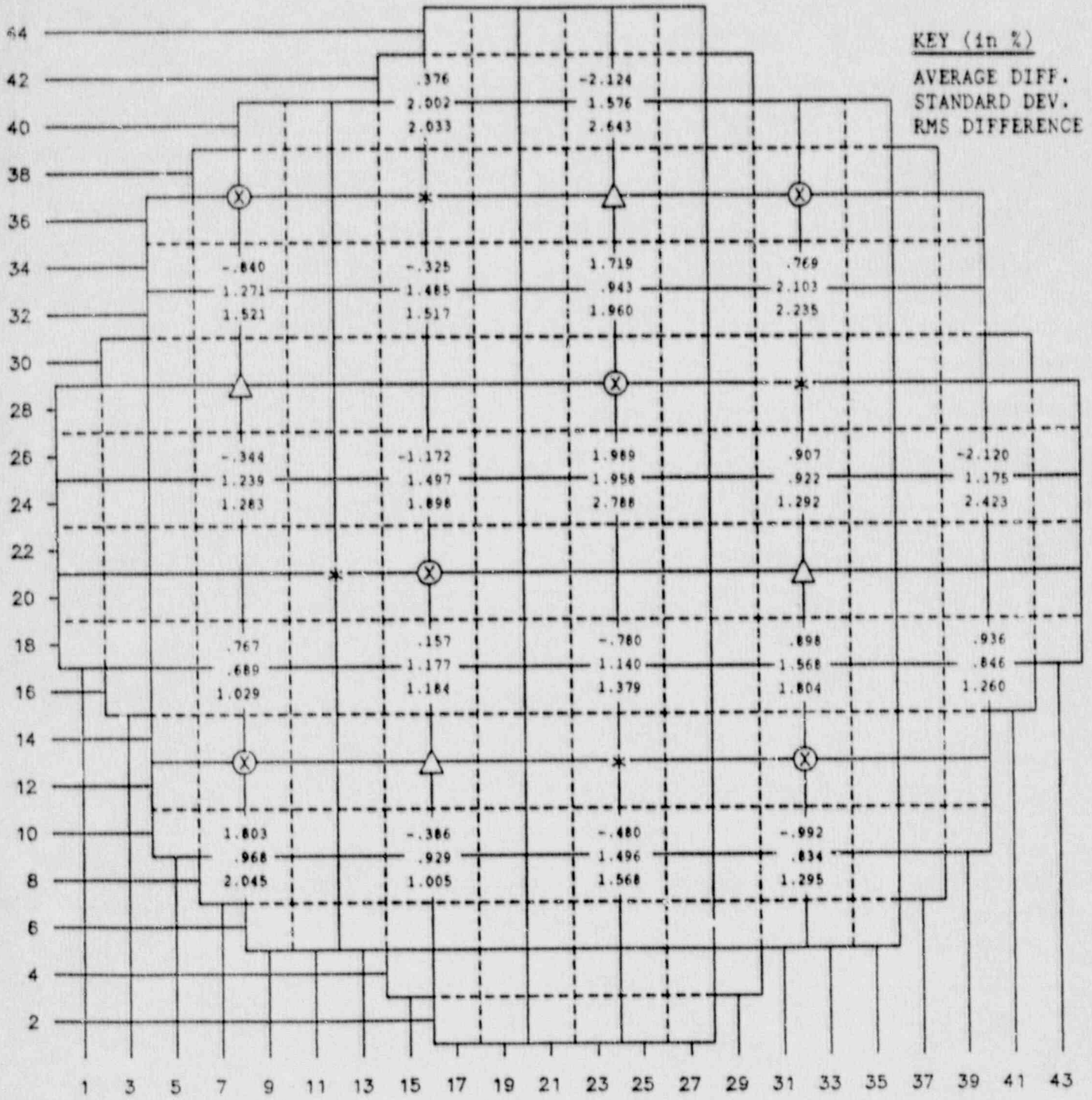

FIGURE 5.5

SIMULATE-3 Core Average Axial TIP Errors and S.D. for Cycles 9-13

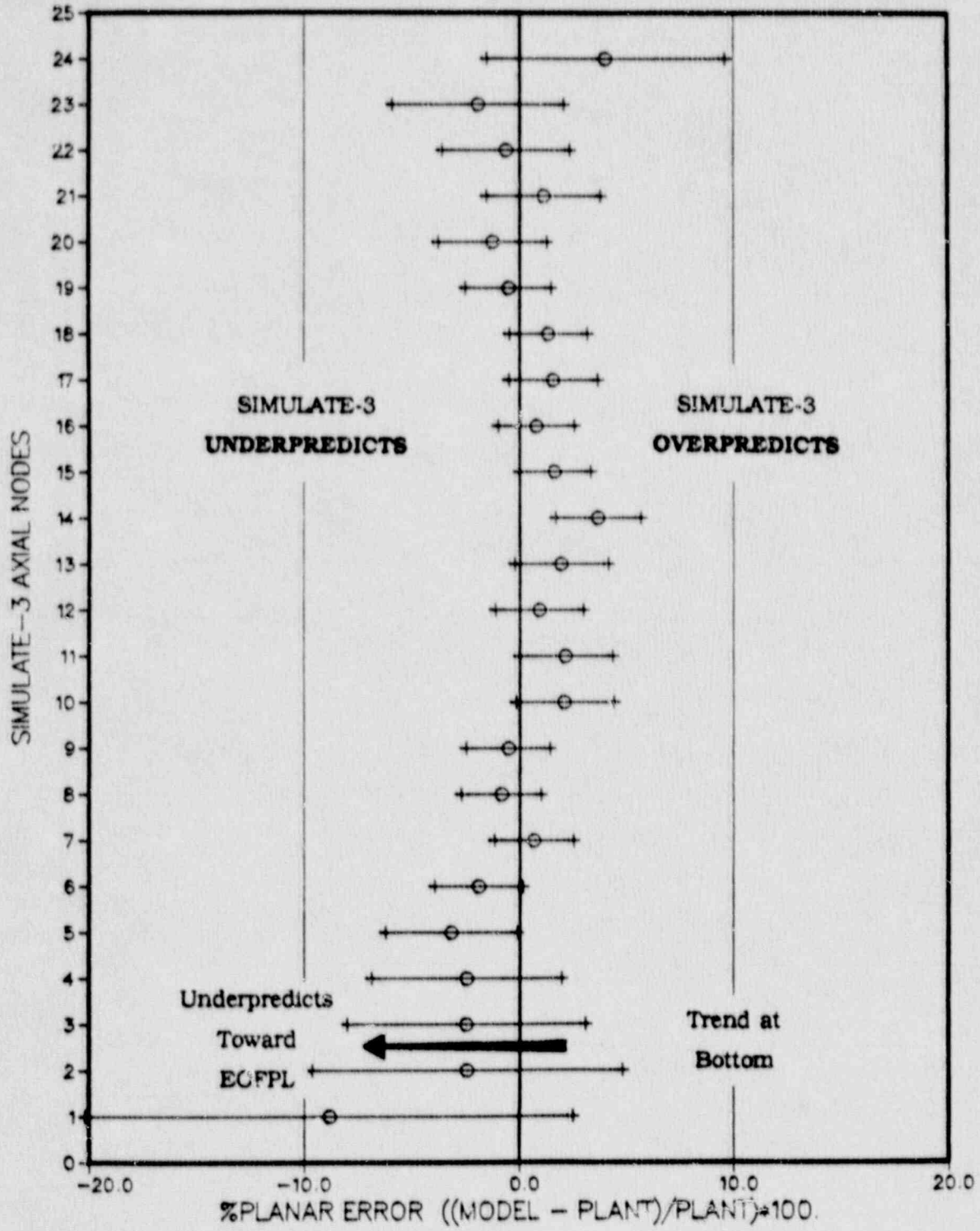

6.0 CONCLUSIONS

When the program to upgrade the Vermont Yankee physics codes began, the goal was to produce a model superior to that currently used to support and license the plant. By the figures of merit discussed in Section 5, this goal has been achieved.

In terms of hot and cold eigenvalue behavior, the new code package of MICBURN-3/CASMO-3/TABLES-3/SIMULATE-3 is clearly superior to its predecessor. In terms of reproducing the plant TIP traces, the new code package is slightly improved. The radial comparisons are excellent. They are very close to the accuracy limitations that TIP asymmetry imposes upon the plant measurements. Axially, there are some consistent errors; however, what errors remain, will not hamper the plant support or licensing applications of the codes. The trend in the axial errors leads to more conservative licensing transient results.

Finally, the investigators unanimously agree that the new code package of MICBURN-3/CASMO-3/TABLES-3/SIMULATE-3 is easier to learn and set up. The codes provide tracking functions for QA purposes, and they run faster on both the CYBER and VAX computer systems.

7.0 REFERENCES

1. Edenius, M. and Ahlin, A., "MICBURN: Microscopic Burnup in Gadolinia Fuel Pins," Chapter 7 of ARMP Computer Code Manuals, CCM-3, dated November 1975.

2. Edenius, M., et al., CASMO-2: A Fuel Assembly Burnup Program, Studsvik/NR-81/3, dated March 1981. (Proprietary)

3. Ver Planck, D. M., TABLES-2 Manual, YAEC-1391P, April, 1983. (Proprietary)

4. VerPlanck, D. M., SIMULATE-E: A Nodal Core Analysis Program for Light-Water Reactors, EPRI NP-2792-CCM, dated March 1983.

5. Pilat, E. E., Methods for the Analysis of Boiling Water Reactors Lattice Physics, YAEC-1232, dated December 1980.

6. Ver Planck, D. M., Methods for the Analysis of Boiling Water Reactors, Steady State Core Physics, YAEC-1238, dated March 1981.

7. Letter and SER, USNRC to J. B. Sinclair, "Acceptance for Referencing in Licensing Actions for the Vermont Yankee Plant of Reports: YAEC-1232, YAEC-1238, YAEC-1239P, YAEC-1299P, and YAEC-1234," NVY 82-157, dated September 15, 1982.

8. Letter and SER, USNRC to R. W. Capstick, "Safety Evaluation by the Office of NRR Supporting Amendment 100 to Facility Operating License No. DPR-28," NYV 87-148, dated September 18, 1987.

9. Harris, D. R., and Hebert, M. J., Methodology for Incore Gamma Effects, YAEC-1456P, June 1985. (Proprietary)

10. Ahlin, A., et al., MICBURN-3 - Microscopic Burnup in Burnable Absorber Rods, Studsvik/NFA-86/26, dated November, 1986. (Proprietary)

11. DiGiovine, A. S., et al., CASMO-3G Validation, YAEC-1363, April, 1988.

12. Edenius, M., et al., CASMO-3, A Fuel Assembly Burnup Program, Studsvik/NFA-86/7, dated November 1986. (Proprietary)

13. Ver Planck, D. M., et al., TABLES-3P Library Preparation Code for SIMULATE-3P, Studsvik /SOA-88/02, dated February, 1988. (Proprietary)

14. DiGiovine, A. S., et al., McGuire Unit 2 SIMULATE-3 Benchmark Analysis Cycles 1 through 3, YAEC-1608, dated October 1987.

15. VerPlanck, D. M., et al., SIMULATE-3P Advanced Three-Dimensional Two-Group Reactor Analysis Code, Studsvik/SOA - 88/01, dated February, 1988. (Proprietary)

16. DiGiovine, A. S., et al., SIMULATE-3 Validation and Verification, YAEC-1659, dated September 1988.

17. Delp, D. L., et al., FLARE, A Three-Dimensional Boiling Water Reactor Simulator, GEAP-4598 (1964).

18. Goldstein, L., et al., "Calculation of Fuel-Cycle Burnup and Power Distribution of Dresden-1 Reactor with the TRILUX Fuel Management Program," Trans. Am. Nuc. Soc., 10, 300 (1967).

19. Borrensen, S., "A Simplified, Coarse Mesh, Three-Dimensional Diffusion Scheme for Calculating the Gross Power Distribution in a Boiling Water Reactor," Nuclear Science and Engineering, 44, 37-43 (1971).

20. Smith, K. S., Rempe, K. R., "Testing and Applications of the QPANDA Nodal Model," Proceedings International Meeting on Advances in Reactor Physics and Computation, Volume 2, p. 861, Paris, France, dated April, 1987.

21. General Electric Standard Application for Reactor Fuel (GESTARII), NEDE-24011-P-A-9, GE Company Proprietary, February 1988, as amended.

22. Schultz, S. P. and St. John, K. E., Methods for the Analysis of Oxide Fuel Rod Steady-State Thermal Effects (FROSSTEY) Code/Model Description Manual, YAEC-1249P, April 1981.

23. Schultz, S. P. and St. John, K. E., Methods for the Analysis of Oxide Fuel Rod Steady-State Thermal Effects (FROSSTEY) Code Qualification and Application, YAEC 1265P, June 1981.

24. Letter and SER, USNRC to R. W. Capstick, "Approval of Use of Fuel Performance Code FROSSTEY," NVY 85-205, September 27, 1985.

25. Ansari, A. A. F., Methods for the Analysis of Boiling Water Reactors: Steady-State Core Flow Distribution Code (FIBWR), YAEC-1234, December 1980.

26. Ansari, A. A. F., et al., FIBWR: A Steady-State Core Flow Distribution Code for Boiling Water Reactors - Code Verification and Qualification Report, EPRI NP-1923, Project 1754-1 Final Report, July 1981.

27. Lellouche, G. S. and Zolotar, B. A., Mechanistic Model for Predicting Two-Phase Void Fraction for Water in Vertical Tubes Channels, and Rod Bundles, EPRI NP-2246-SR, February, 1982.

28. Letter, E. W. Jackson to USNRC (Region I), "Cycle 9 Startup Test Report," FVY82-21, dated February 25, 1982.

29. Letter, W. P. Murphy to USNRC (Region I), "Cycle 10 Startup Test Report," FVY83-100, dated September 15, 1983.

30. Letter, W. P. Murphy to USNRC (Region I), "Cycle 11 Startup Test Report," FVY84-132, dated November 6, 1984.

31. Letter, R. W. Capstick to USNRC (Region I), "Cycle 12 Startup Test Report," FVY86-92, dated October 6, 1986.

32. Letter, R. W. Capstick to USNRC (Region I), "Cycle 13 Startup Test Report," FVY88-1, dated January 4, 1988.

33. Personal Communcation (1988) with D. M. VerPlanck, Studsvik of America, 1087 Beacon Street, Newton, Massachusetts 02159.

34. Two papers, W. A. Golub, "Effects of Channel Bow," and T. Rausch, "Effects of Channel Bow," Station Nuclear Engineer's Conference, June 20-24, 1988, San Jose, Califronia.

35. Gorman, J. A. and Lipsey, G. W., An Assessment of BWR Fuel Channel Lifetimes, EPRI NP-2483, July 1982.

36. Gorman, J. A., et al., Fuel Channel Lifetimes: Statistical Predictive Models, EPRI NP-3937 and NP-3938, February 1984.

37. Gorman, J. A., et al., Fuel Channel Lifetimes: Expansion of Statistical Predictive Models, Final Report, EPRI NP-4225M, September 1985.

38. Gorman, J. A., and Turner, A. P. L., Investigation of Large Bows in Reused BWR Fuel Channels, EPRI NP-5718P, April 1988.

39. Telecon, J. W. Heard with D. T. Weiss (GE), February 1, 1989.

APPENDIX A

HOT DEPLETION STATEPOINTS

During the five cycles modeled here, some 630 complete sets of TIP data were taken at the plant. To reduce the number of comparisons to a manageable number, most non-equilibrium xenon TIP sets were eliminated from the benchmark. What follows is a description of each cycle and the depletion steps used to model it.

Generally, the depletion progressed from TIP set to TIP set, using the plant conditions of the concluding TIP set. The preferred depletion interval between TIP sets was two weeks, but it often varied from one to three weeks. The length of the interval roughly coincided with the frequency of rod moves. When the TIP machine was broken for an extended period, or a TIP set was not taken near the end of a sequence, a depletion step was inserted at suitable plant conditions. In these instances, no comparison to plant data was made in the benchmark.

Figure A.1 shows the reload design for the beginning of Cycle 9. The darker the shading, the older the batch of fuel. Figure A.2 shows the plant power versus exposure for Cycle 9. The statepoints where TIP data set comparisons were made are indicated. The plant ran close to full capacity at all times, so most statepoints are near full power, except during coastdown. Figure A.3 shows the rod inventory for the cycle with the modeled statepoints indicated. The statepoints are evenly distributed among A and B sequences. Finally, Figure A.4 provides the reactor conditions at the comparison statepoints. Also shown are the additional depletion steps where no comparisons were made.

Figures A.5-A.8 provide similar information for Cycle 10. Figures A.9-A.12 for Cycle 11. Figures A.13-A.16 for Cycle 12. Figures A.17-A.20 for Cycle 13.

FIGURE A.1

Reload Design of Cycle 9

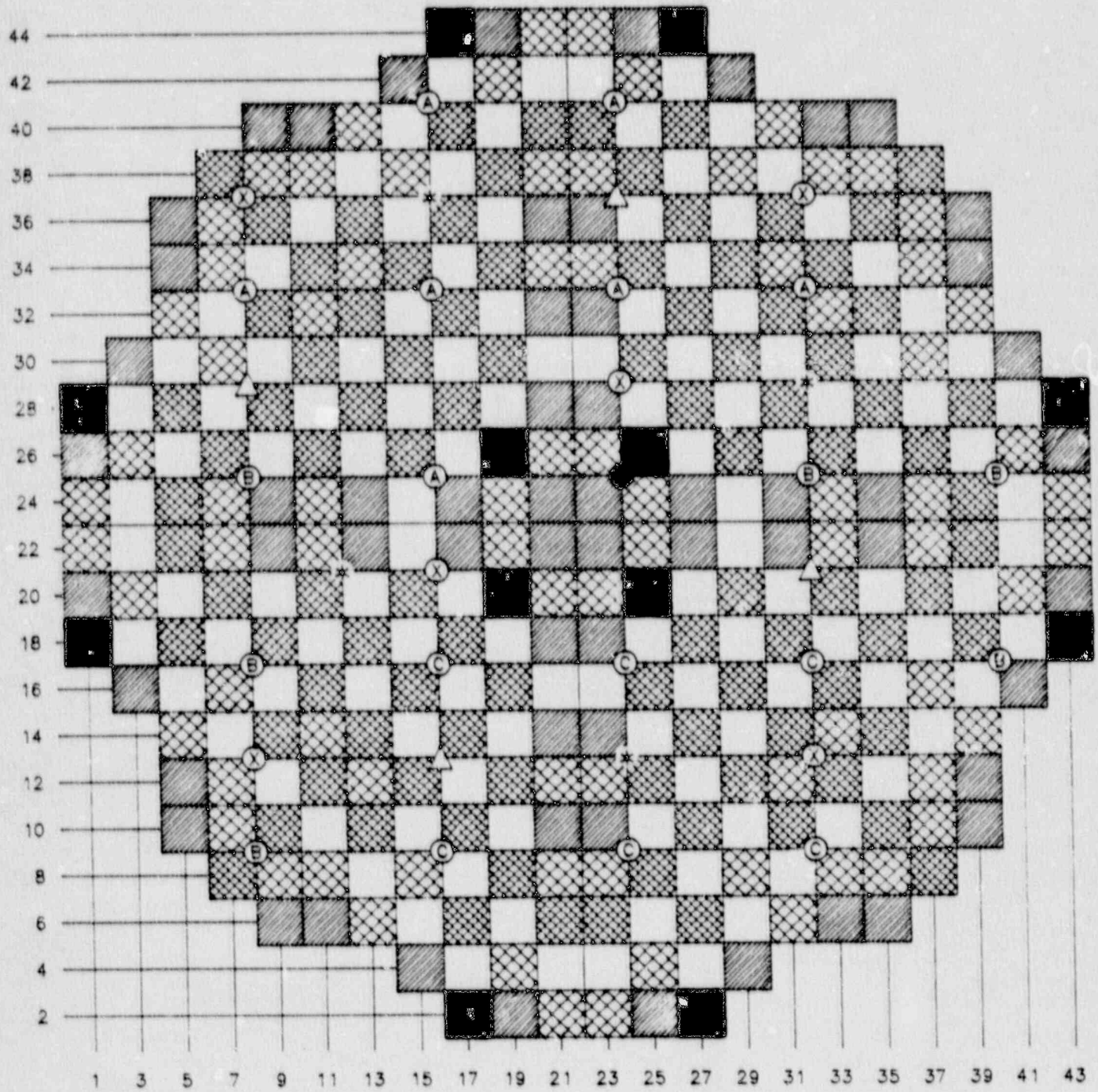

FIGURE A.2

Power History of Cycle 9 Showing TIP Statepoints

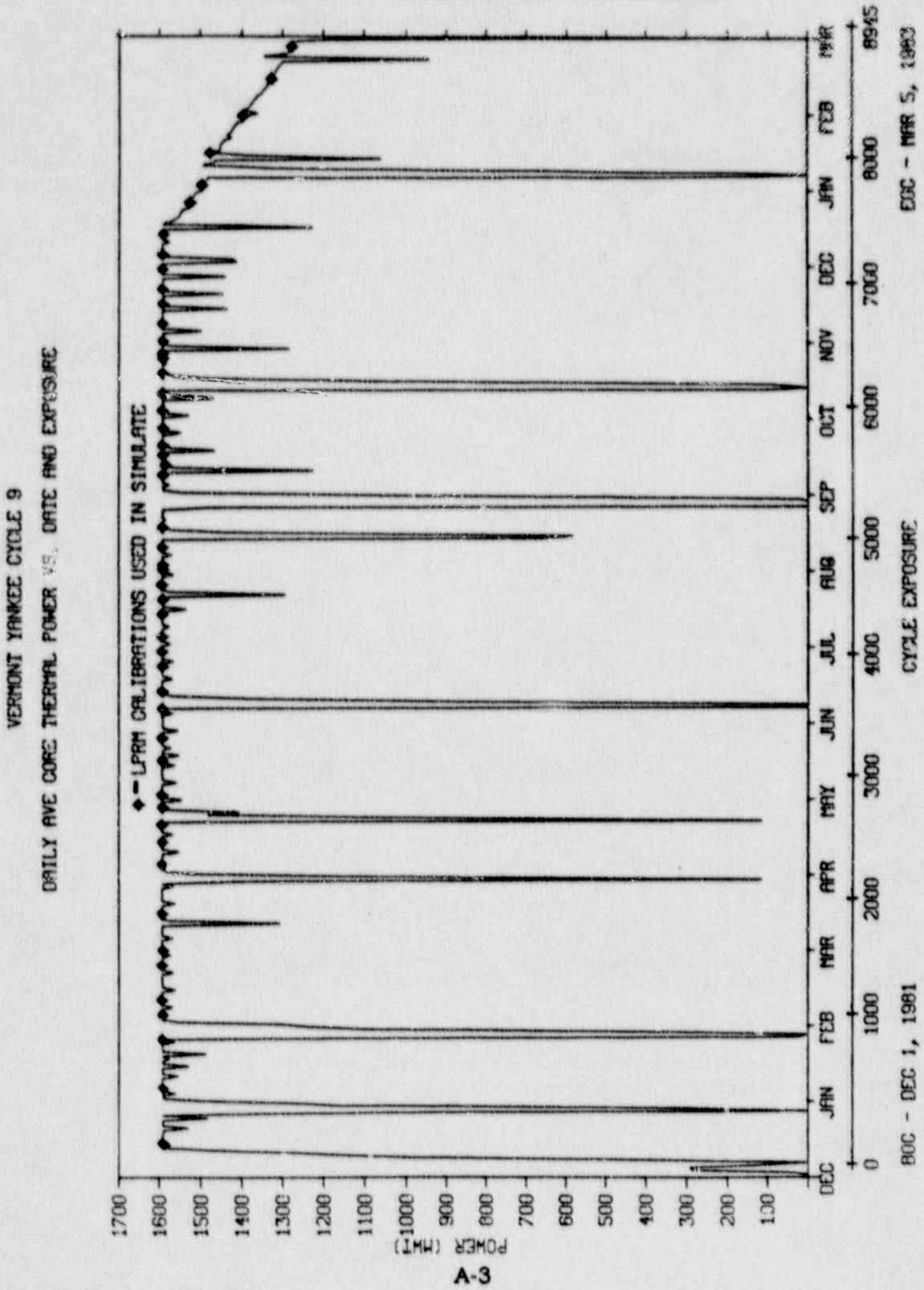

FIGURE A.3

Control Rod Inventory of Cycle 9 Showing TIP Statepoints

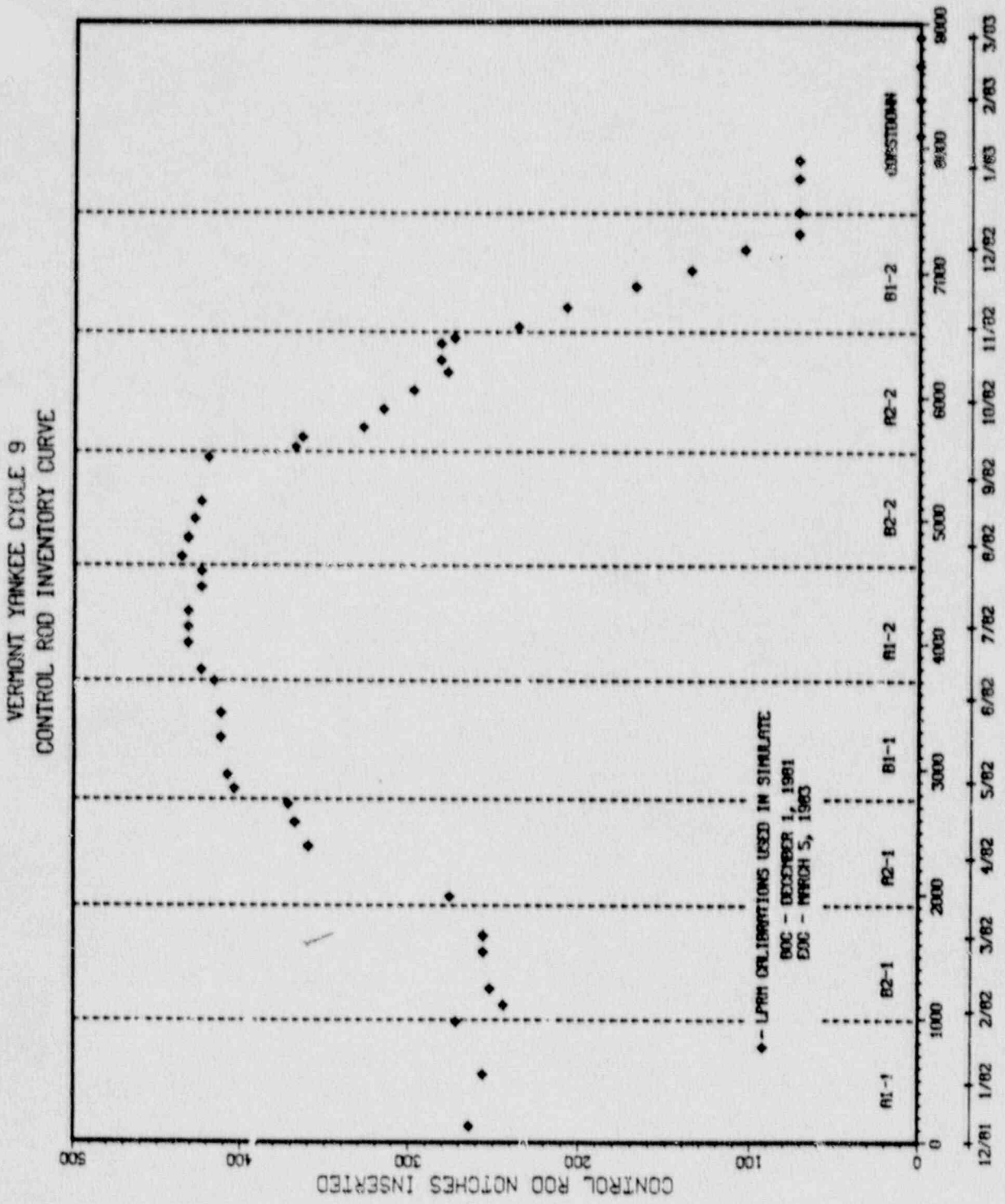

FIGURE A.4

Reactor Conditions for Cycle 9 Depletion Steps

Step	TIP No.	Date	Rod Pattern	Power	Flow	Exposure
0	No TIP	12/1/81	BOC Startup	NA	NA	9192
1	631	12/14/81	A1-1, Deep @ 14	1589	45.6	9324
2	640	1/5/82	A1-1, Deep @ 14	1593	45.6	9742
3	641	1/25/82	A1-1, Deep @ 10	1591	47.3	10168
4	654	2/4/82	B2-1, Deep @ 10	1589	45.2	10302
5	655	2/10/82	B2-1, Deep @ 10	1592	46.6	10434
6	656	2/24/82	B2-1, Deep @ 08	1593	46.7	10731
7	658	3/2/82	B2-1, Deep @ 08	1590	45.9	10863
8	No TIP	3/13/82	B2-1, Deep @ 08	1592	44.7	11077
9	664	3/17/82	A2-1, Deep @ 04	1592	45.5	11177
10	671	4/6/82	A2-1, Deep @ 04	1592	46.9	11579
11	672	4/15/82	A2-1, Deep @ 00	1590	46.7	11772
12	673	4/22/82	A2-1, Deep @ 00	1593	47.4	11918
13	679	4/29/82	B1-1, Deep @ 08	1584	45.8	12037
14	681	5/4/82	B1-1, Deep @ 06	1592	46.7	12148
15	682	5/18/82	B1-1, Deep @ 04	1591	47.1	12444
16	684	5/27/82	B1-1, Deep @ 04	1591	46.3	12640
17	685	6/8/82	B1-1, Deep @ 04	1591	46.2	12892
18	692	6/15/82	A1-2, Deep @ 06	1591	45.9	12980
19	693	6/25/82	A1-2, Deep @ 06	1592	47.2	13197
20	695	7/1/82	A1-2, Deep @ 06	1592	47.4	13325
21	696	7/7/82	A1-2, Deep @ 06	1591	47.4	13450
22	697	7/16/82	A1-2, Deep @ 06	1591	46.4	13647
23	698	7/22/82	A1-2, Deep @ 06	1591	46.6	13774
24	701	7/28/82	B2-2, Deep @ 04	1593	47.6	13894
25	702	8/4/82	B2-2, Deep @ 06	1592	47.1	14043
26	703	8/4/82	B2-2, Deep @ 06	1591	47.1	14046
27	704	8/11/82	B2-2, Deep @ 06	1591	47.2	14198

FIGURE A.4 (Continued)

Reactor Conditions for Cycle 9 Depletion Steps

Step	TIP No.	Date	Rod Pattern	Power	Flow	Exposure
28	709	8/19/82	B2-2, Deep @ 04	1590.	45.8	14339
29	716	9/9/82	B2-2, Deep @ 06	1589	47.5	14696
30	719	9/13/82	A2-2, Deep @ 04	1585	47.9	14784
31	720	9/17/82	A2-2, Deep @ 04	1589	47.6	14862
32	722	9/21/82	A2-2, Deep @ 04	1588	46.8	14943
33	723	9/28/82	A2-2, Deep @ 04	1587	46.0	15093
34	725	10/5/82	A2-2, Deep @ 06	1589	46.2	15245
35	727	10/12/82	A2-2, Deep @ 06	1589	46.1	15394
36	734	10/20/82	A2-2, Deep @ 06	1591	46.3	15490
37	735	10/26/82	A2-2, Deep @ 06	1588	47.5	15623
38	736	10/28/82	A2-2, Deep @ 06	1589	47.3	15666
39	739	11/2/82	B1-2, Deep @ 10	1589	47.2	15758
40	741	11/9/82	B1-2, Deep @ 12	1589	45.8	15915
41	743	11/17/82	B1-2, Deep @ 12	1589	45.6	16084
42	745	11/23/82	B1-2, Deep @ 20	1588	46.9	16211
43	747	12/1/82	B1-2, Deep @ 24	1590	46.1	16380
44	749	12/7/82	B1-2, Deep @ 30	1589	46.7	16506
45	750	12/15/82	B1-2, Deep @ 30	1590	47.8	16676
46	751	12/28/82	B1-2, Deep @ 30	1524	47.8	16944
47	753	1/4/83	B1-2, Deep @ 30	1493	47.9	17092
48	762	1/17/83	ARO	1470	47.9	17291
49	765	2/1/83	ARO	1397	47.7	17581
50	766	2/16/83	ARO	1327	47.7	17853
51	No TIP	3/1/83	ARO	1277	47.6	18077
52	No TIP	3/5/83	ARO to EOC	1263	48.0	18137

FIGURE A.5

Reload Design of Cycle 10

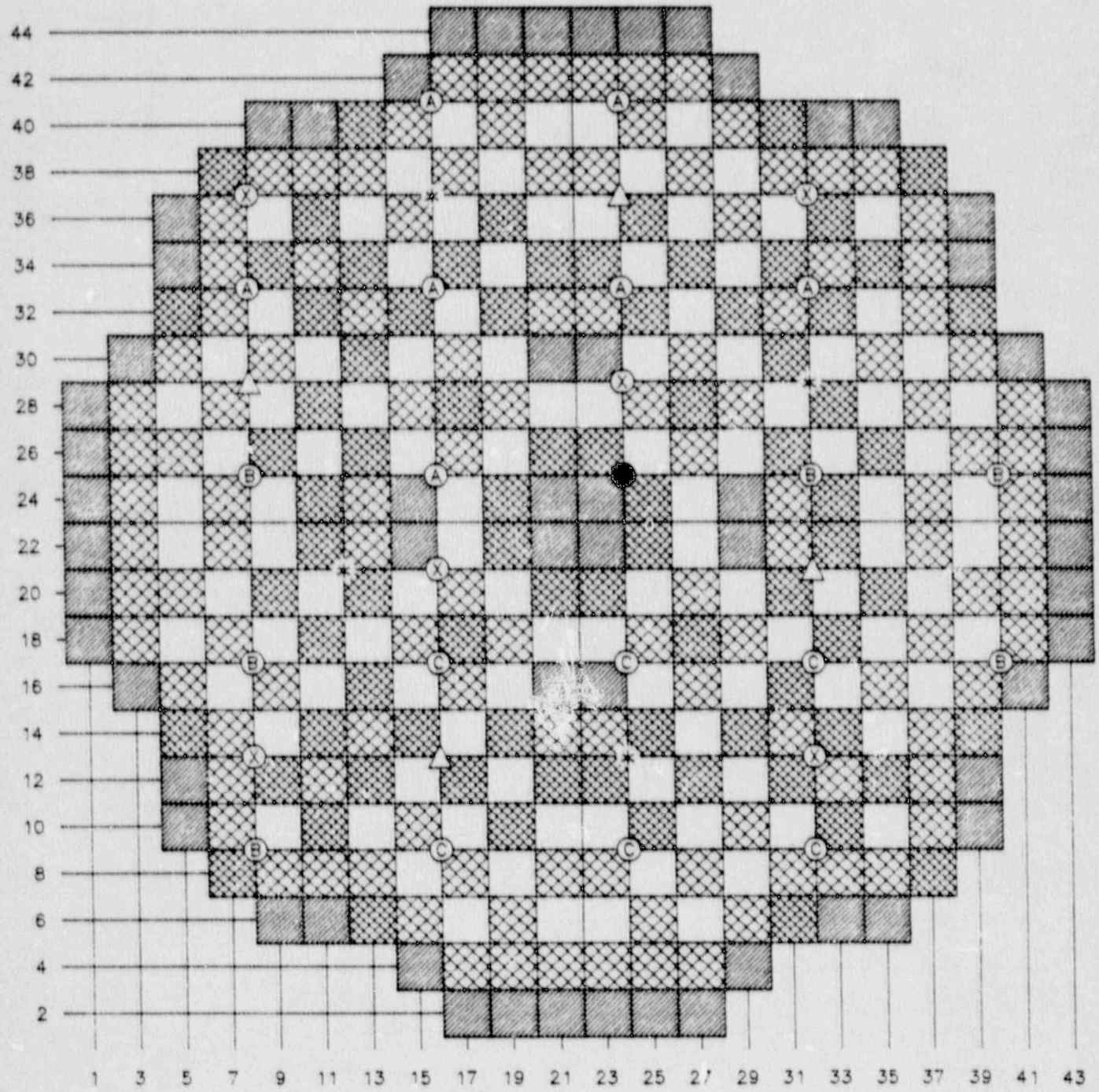

FIGURE A.6

Power History of Cycle 10 Showing TIP Statepoints

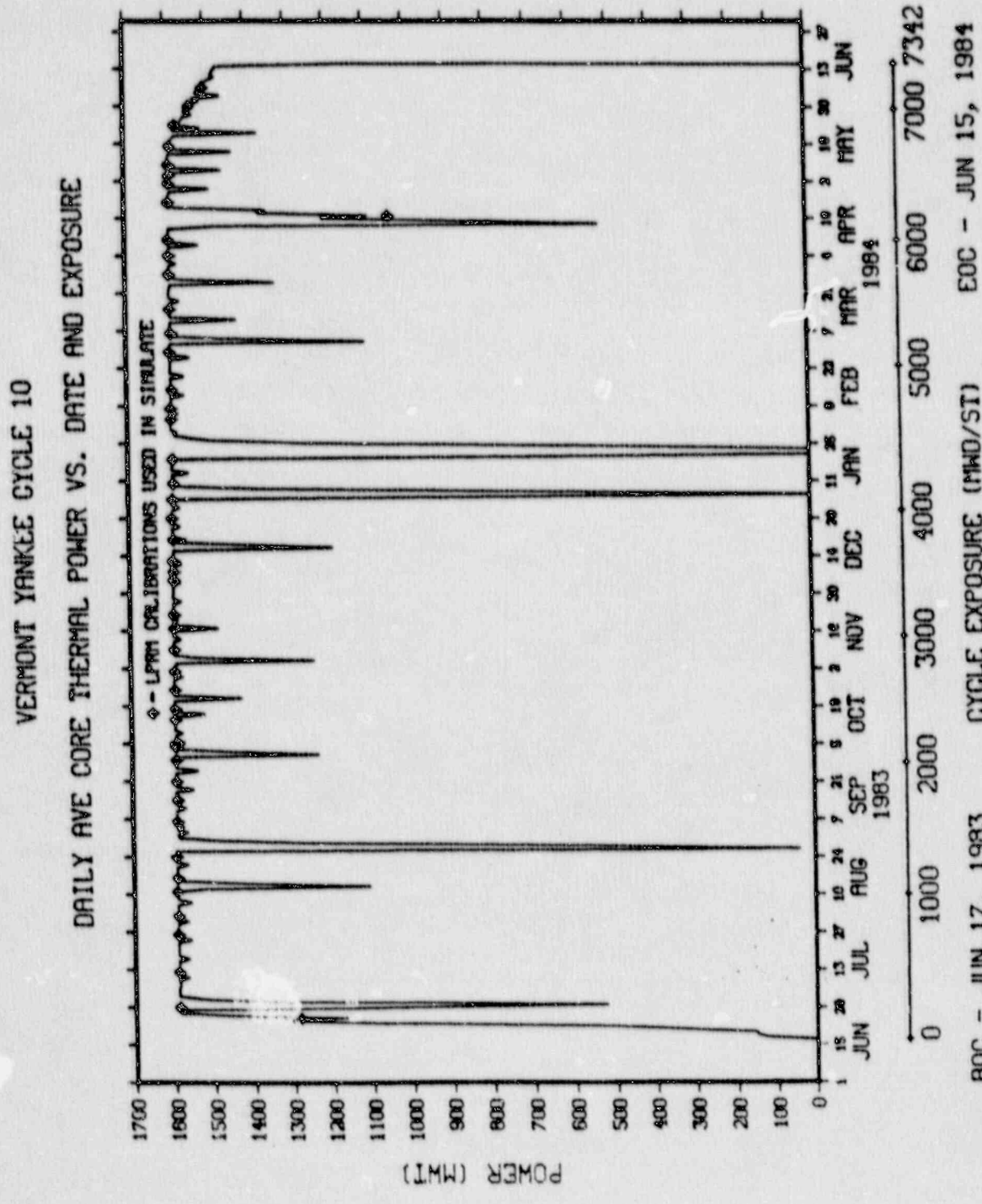

FIGURE A.7

Control Rod Inventory of Cycle 10 Showing TIP Statepoints

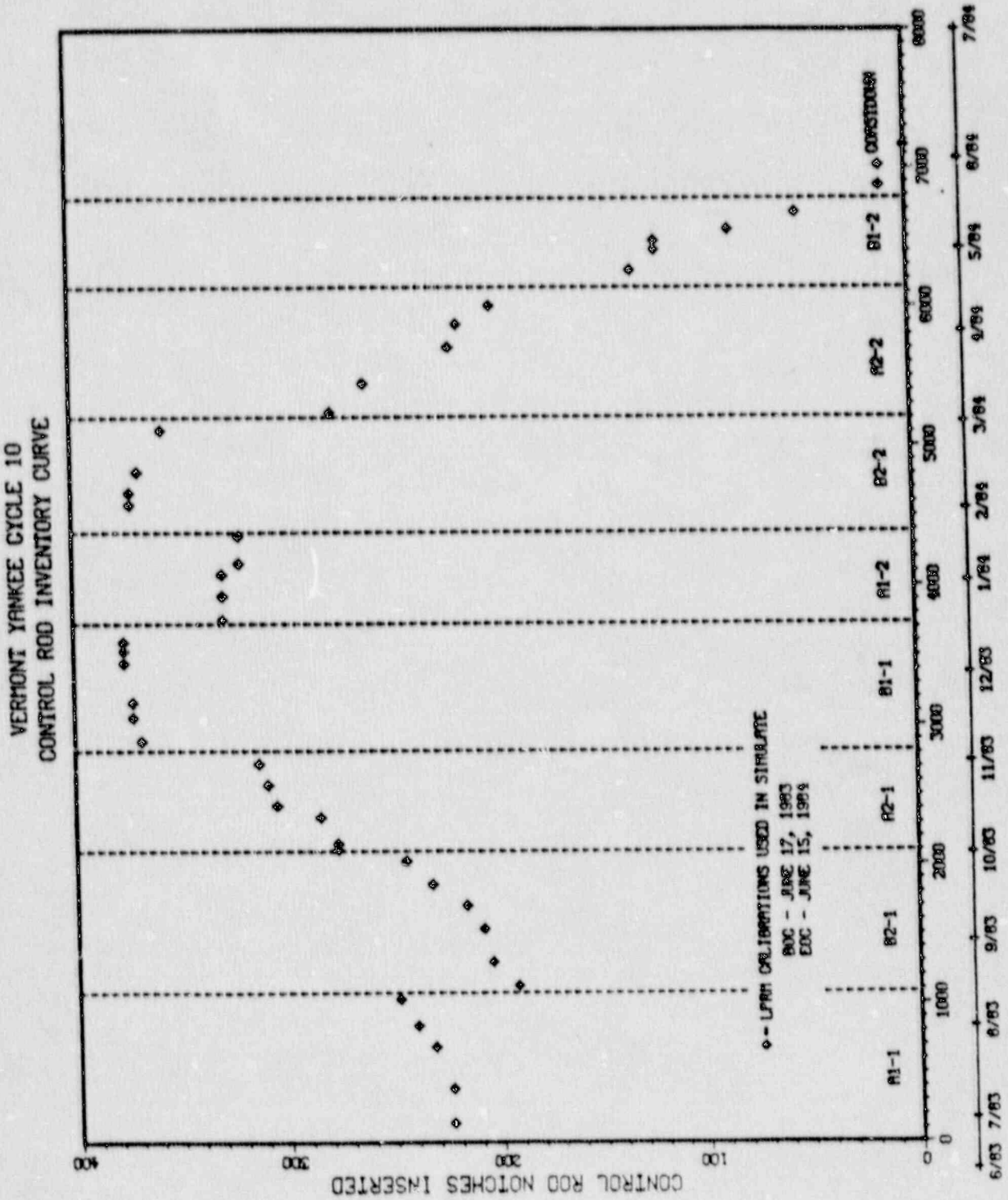

FIGURE A.8

Reactor Conditions for Cycle 10 Depletion Steps

Step	TIP No.	Date	Rod Pattern	Power	Flow	Exposure
0	No TIP	6/17/83	BOC Startup	NA	NA	10463
1	777	6/29/83	A1-1, Deep @ 18	1590	46.7	10602
2	785	7/12/83	A1-1, Deep @ 18	1591	47.8	10850
3	786	7/26/83	A1-1, Deep @ 18	1592	46.9	11150
4	788	8/2/83	A1-1, Deep @ 18	1591	46.5	11304
5	789	8/11/83	A1-1, Deep @ 16	1592	47.3	11496
6	793	8/16/83	B2-1, Deep @ 12	1591	44.5	11592
7	794	8/24/83	B2-1, Deep @ 10	1592	46.6	11765
8	803	9/6/83	B2-1, Deep @ 08	1590	46.0	12002
9	804	9/14/83	B2-1, Deep @ 08	1588	46.5	12170
10	805	9/21/83	B2-1, Deep @ 08	1590	46.0	12320
11	806	9/29/83	B2-1, Deep @ 06	1590	46.3	12490
12	810	10/4/83	A2-1, Deep @ 04	1591	47.1	12574
13	812	10/5/83	A2-1, Deep @ 04	1589	46.6	12615
14	813	10/14/83	A2-1, Deep @ 04	1591	46.5	12807
15	814	10/18/83	A2-1, Deep @ 08	1592	46.6	12890
16	815	10/25/83	A2-1, Deep @ 04	1590	46.9	13040
17	817	11/1/83	A2-1, Deep @ 00	1590	46.6	13191
18	821	11/9/83	B1-1, Deep @ 10	1591	46.4	13354
19	822	11/17/83	B1-1, Deep @ 08	1591	47.2	13524
20	823	11/22/83	B1-1, Deep @ 08	1591	47.0	13631
21	824	12/5/83	B1-1, Deep @ 06	1591	46.9	13914
22	826	12/8/83	B1-1, Deep @ 06	1591	46.8	14002
23	827	12/12/83	B1-1, Deep @ 06	1592	46.6	14064
24	831	12/20/83	A1-2, Deep @ 10	1590	46.9	14222
25	832	12/28/83	A1-2, Deep @ 10	1593	47.3	14394
26	834	1/4/84	A1-2, Deep @ 10	1590	47.4	14548
27	840	1/10/84	A1-2, Deep @ 10	1587	45.5	14626

FIGURE A.8 (Continued)

Reactor Conditions for Cycle 10 Depletion Steps

Step	TIP No.	Date	Rod Pattern	Power	Flow	Exposure
28	841	1/19/84	A1-2, Deep @ 10	1588	46.0	14822
29	849	2/3/84	B2-2, Deep @ 06	1591	46.1	15048
30	851	2/7/84	B2-2, Deep @ 06	1592	46.6	15132
31	853	2/14/84	B2-2, Deep @ 08	1588	46.0	15282
32	855	2/28/84	B2-2, Deep @ 10	1593	45.8	15580
33	859	3/6/84	A2-2, Deep @ 06	1588	47.1	15702
34	861	3/15/84	A2-2, Deep @ 06	1591	46.5	15909
35	863	3/28/84	A2-2, Deep @ 10	1592	46.4	16167
36	864	4/4/84	A2-2, Deep @ 12	1591	46.8	16333
37	866	4/10/84	A2-2, Deep @ 14	1592	46.7	16466
38	872	4/24/84	B1-2, Deep @ 12	1591	46.7	16722
39	874	5/1/84	B1-2, Deep @ 18	1590	46.2	16870
40	875	5/4/84	B1-2, Deep @ 18	1588	46.9	16936
41	877	5/8/84	B1-2, Deep @ 24	1590	46.2	17016
42	879	5/15/84	B1-2, Deep @ 30	1587	47.2	17141
43	881	5/23/84	B1-2, Deep @ 42	1573	48.0	17333
44	882	5/30/84	B1-2, Deep @ 42	1538	47.7	17478
45	884	6/6/84	ARO	1502	47.7	17623
46	No TIP	6/15/84	ARO to EOC	1457	48.0	17806

FIGURE A.9

Reload Design of Cycle 11

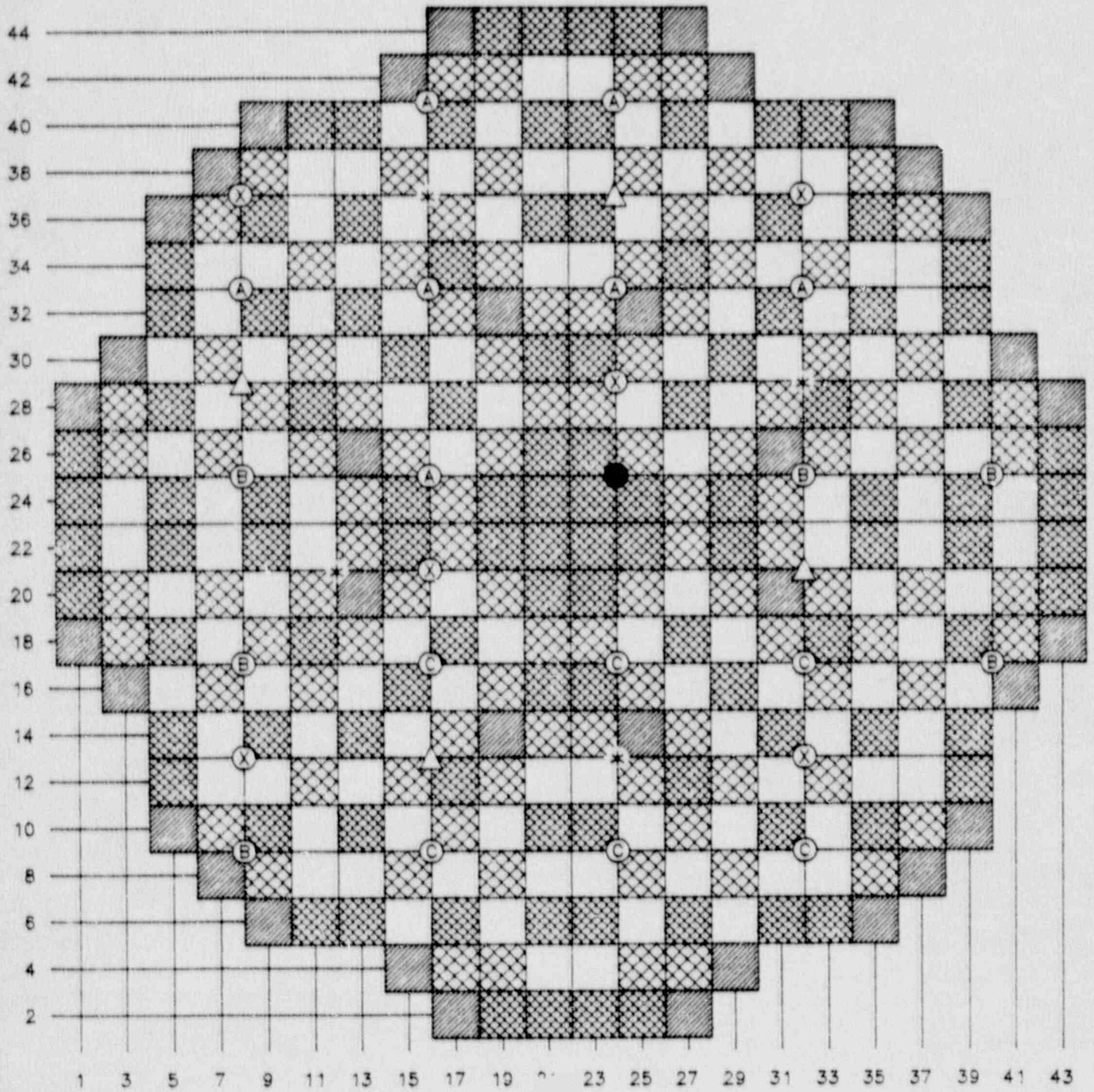

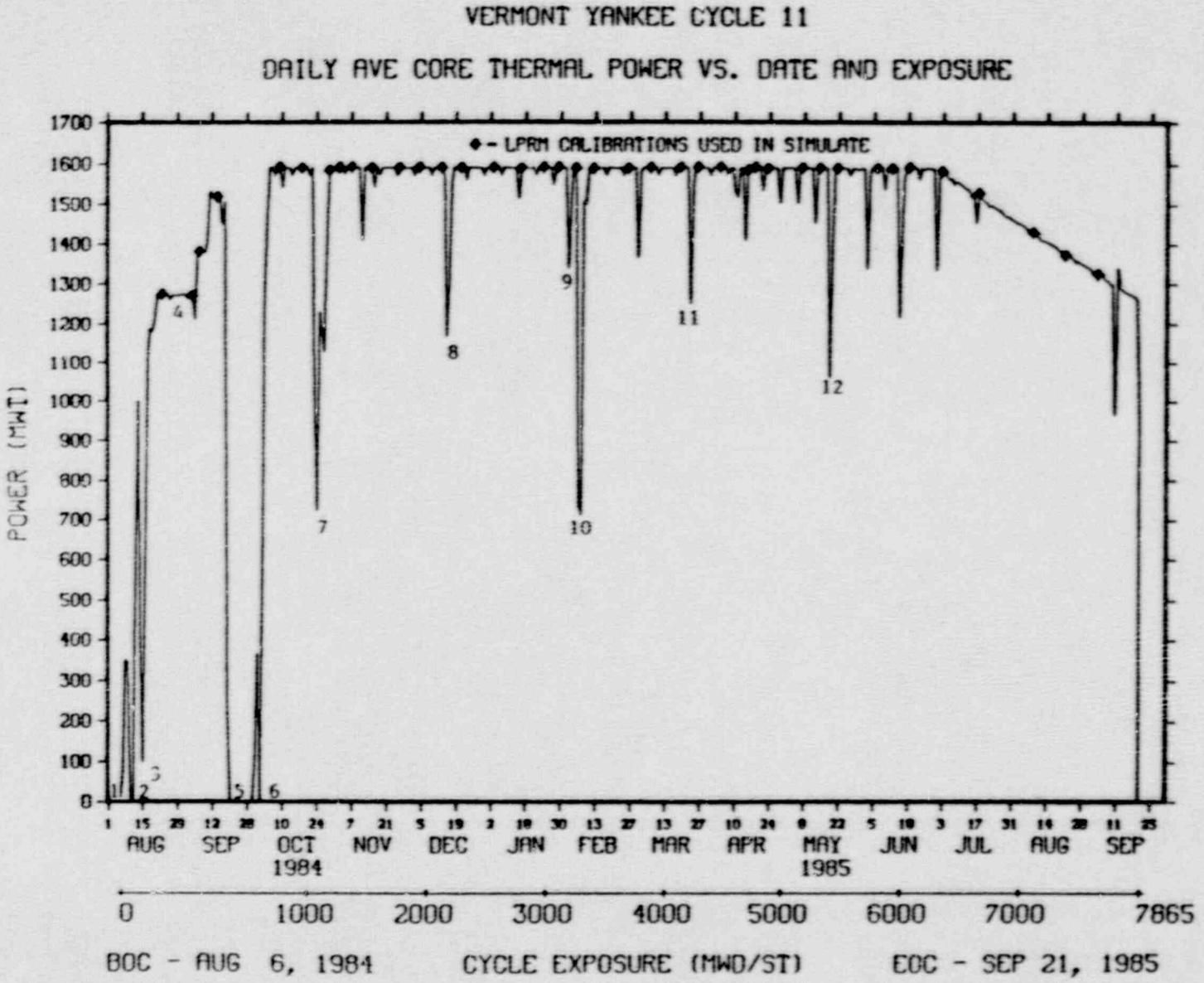

FIGURE A.10

Power History of Cycle 11 Showing TIP Statepoints

FIGURE A.11

Control Rod Inventory of Cycle 11 Showing TIP Statepoints

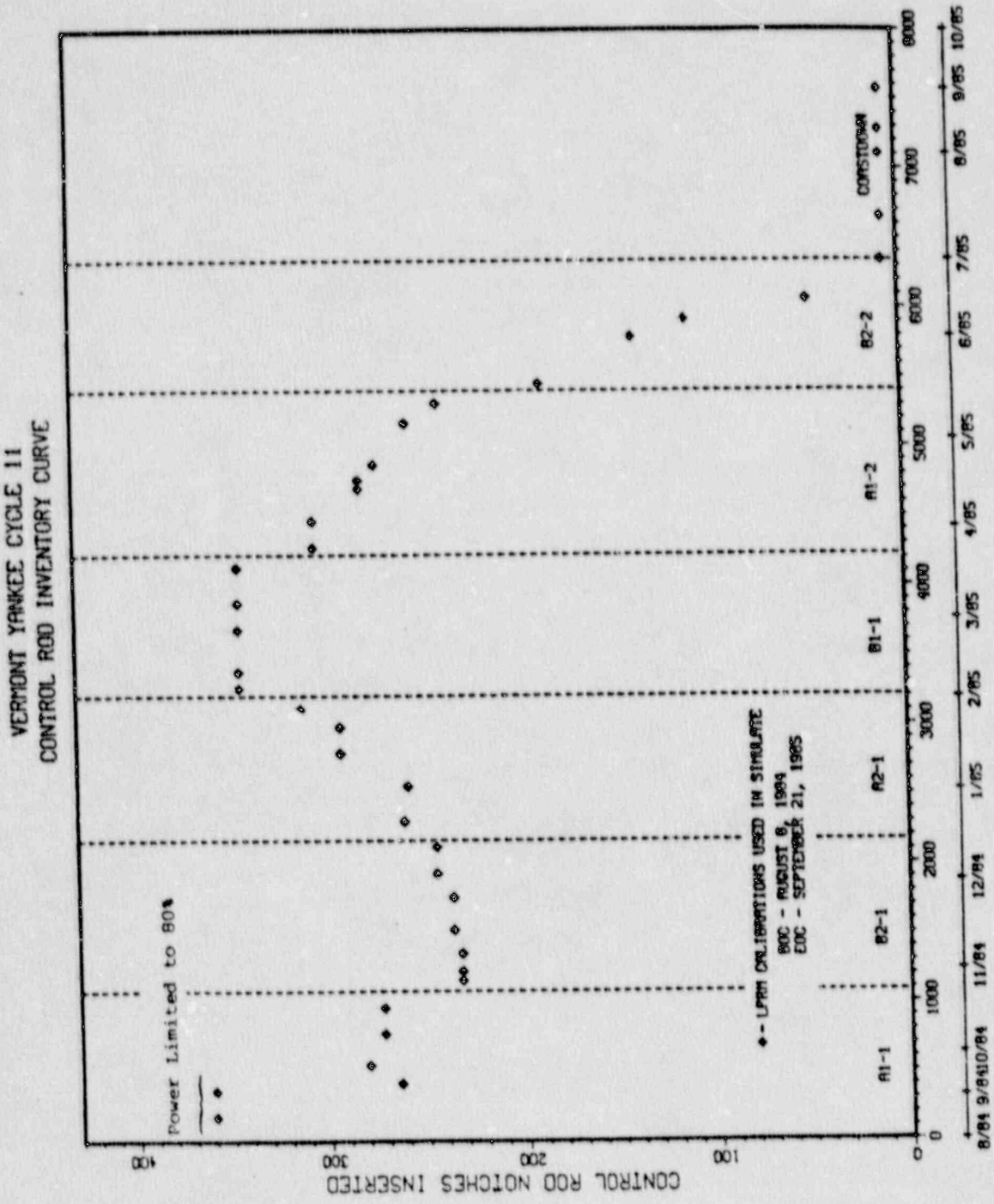

FIGURE A.12

Reactor Conditions for Cycle 11 Depletion Steps

Step	TIP No.	Date	Rod Pattern	Power	Flow	Exposure
0	N/A	8/6/84	BOC Startup	NA	NA	10418
1	894	8/23/84	Power Ascent	1274	44.1	10592
2	895	9/4/84	Power Ascent	1272	44.3	10780
3	897	9/4/84	Power Ascent	1381	33.3	10832
4	898	9/14/84	A1-1, Deep @ 14	1519	46.8	10965
5	904	10/9/84	A1-1, Deep @ 14	1593	46.8	11192
6	907	10/18/84	A1-1, Deep @ 14	1590	46.6	11379
7	917	10/29/84	B2-1, Deep @ 06	1584	44.0	11576
8	918	11/2/84	B2-1, Deep @ 06	1591	46.7	11641
9	920	11/7/84	B2-1, Deep @ 06	1592	46.5	11773
10	921	11/15/84	B2-1, Deep @ 04	1590	47.2	11943
11	922	11/26/84	B2-1, Deep @ 04	1591	46.2	12176
12	924	12/04/84	B2-1, Deep @ 00	1592	46.8	12348
13	925	12/13/84	B2-1, Deep @ 00	1591	46.2	12540
14	927	12/21/84	A2-1, Deep @ 04	1591	47.7	12724
15	929	1/3/85	A2-1, Deep @ 06	1592	47.0	12977
16	931	1/23/85	A2-1, Deep @ 04	1593	46.4	13402
17	932	1/29/85	A2-1, Deep @ 04	1592	46.1	13530
18	937	2/5/85	B1-1, Deep @ 10	1590	46.4	13681
19	943	02/12/85	B1-1, Deep @ 10	1589	46.2	13799
20	944	02/26/85	B1-1, Deep @ 10	1590	46.4	14101
21	947	03/07/85	B1-1, Deep @ 10	1591	46.4	14295
22	948	03/19/85	B1-1, Deep @ 10	1592	46.7	14551
23	951	03/26/85	A1-2, Deep @ 12	1593	46.2	14692
24	952	04/04/85	A1-2, Deep @ 12	1593	46.9	14884
25	955	04/15/85	A1-2, Deep @ 12	1585	45.5	15118
26	956	04/18/85	A1-2, Deep @ 12	1593	46.9	15179

FIGURE A.12 (Continued)

Reactor Conditions for Cycle 11 Depletion Steps

Step	TIP No.	Date	Rod Pattern	Power	Flow	Exposure
27	957	04/23/85	A1-2, Deep @ 14	1590	45.6	15289
28	959	05/07/85	A1-2, Deep @ 16	1590	46.0	15588
29	960	05/14/85	A1-2, Deep @ 18	1590	45.5	15732
30	963	05/21/85	B2-2, Deep @ 10	1590	44.9	15871
31	966	06/06/85	B2-2, Deep @ 14	1590	46.5	16210
32	968	06/12/85	B2-2, Deep @ 24	1589	44.4	16338
33	971	06/19/85	B2-2, Deep @ 32	1592	45.4	16481
34	974	07/02/85	ARO*, Deep @ 46	1583	47.6	16760
35	975	07/17/85	ARO*, Deep @ 46	1529	47.7	17069
36	976	08/08/85	ARO*, Deep @ 46	1430	47.7	17523
37	978	08/21/85	ARO*, Deep @ 46	1372	47.6	17697
38	980	09/03/85	ARO*, Deep @ 46	1326	47.8	17989
39	981	09/19/85	ARO*, Deep @ 46	1261	47.7	18260
40	No TIP	09/21/85	ARO* to EOC	1260	48.0	18283

* In Cycle 11 VY had a single rod "impeded" at 46; that is, it gave no settle indication at 48. The mirror symmetric rods were also driven to 46. Therefore, during coastdown the model was nearly ARO.

FIGURE A.13

Reload Design of Cycle 12

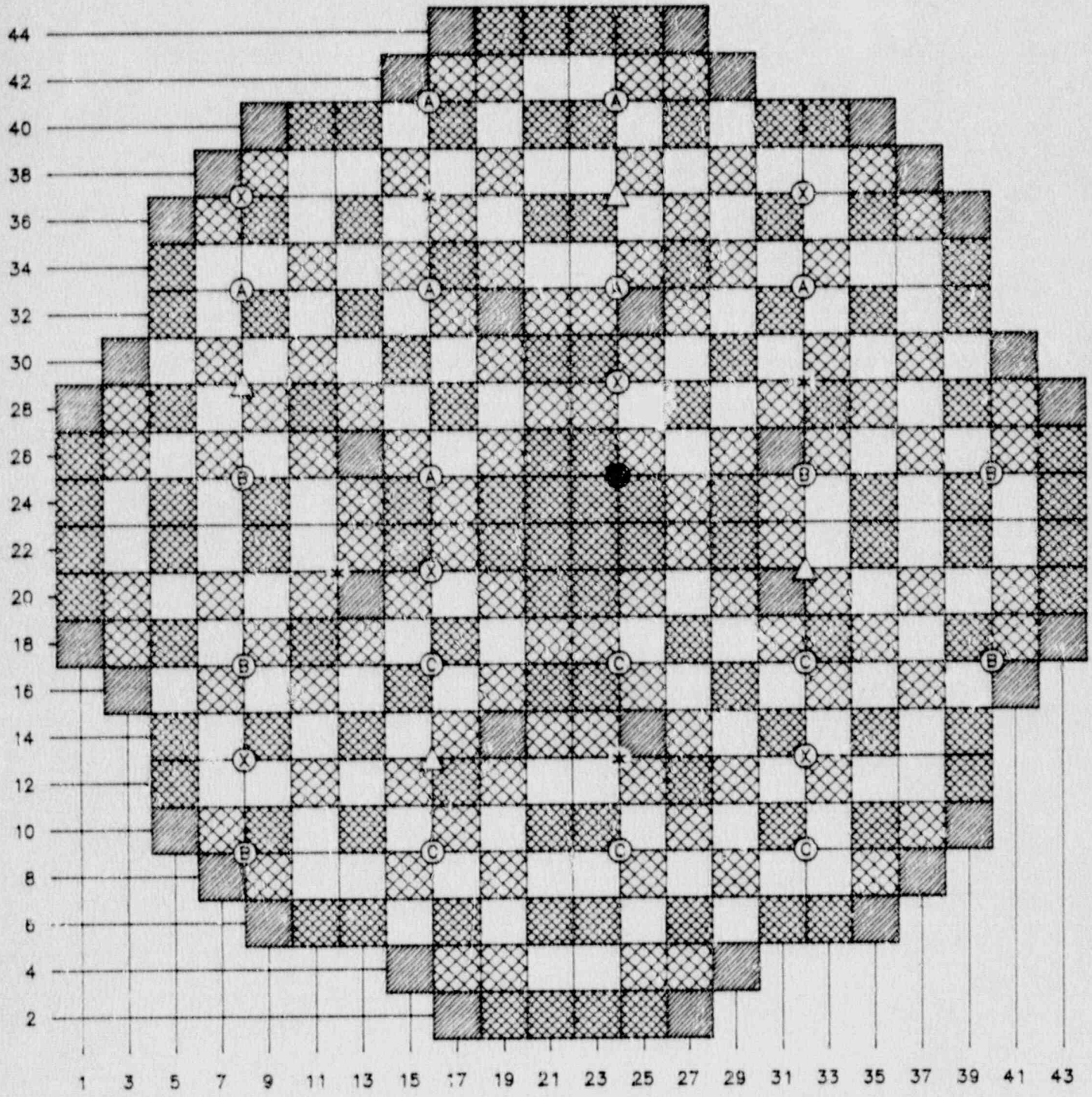

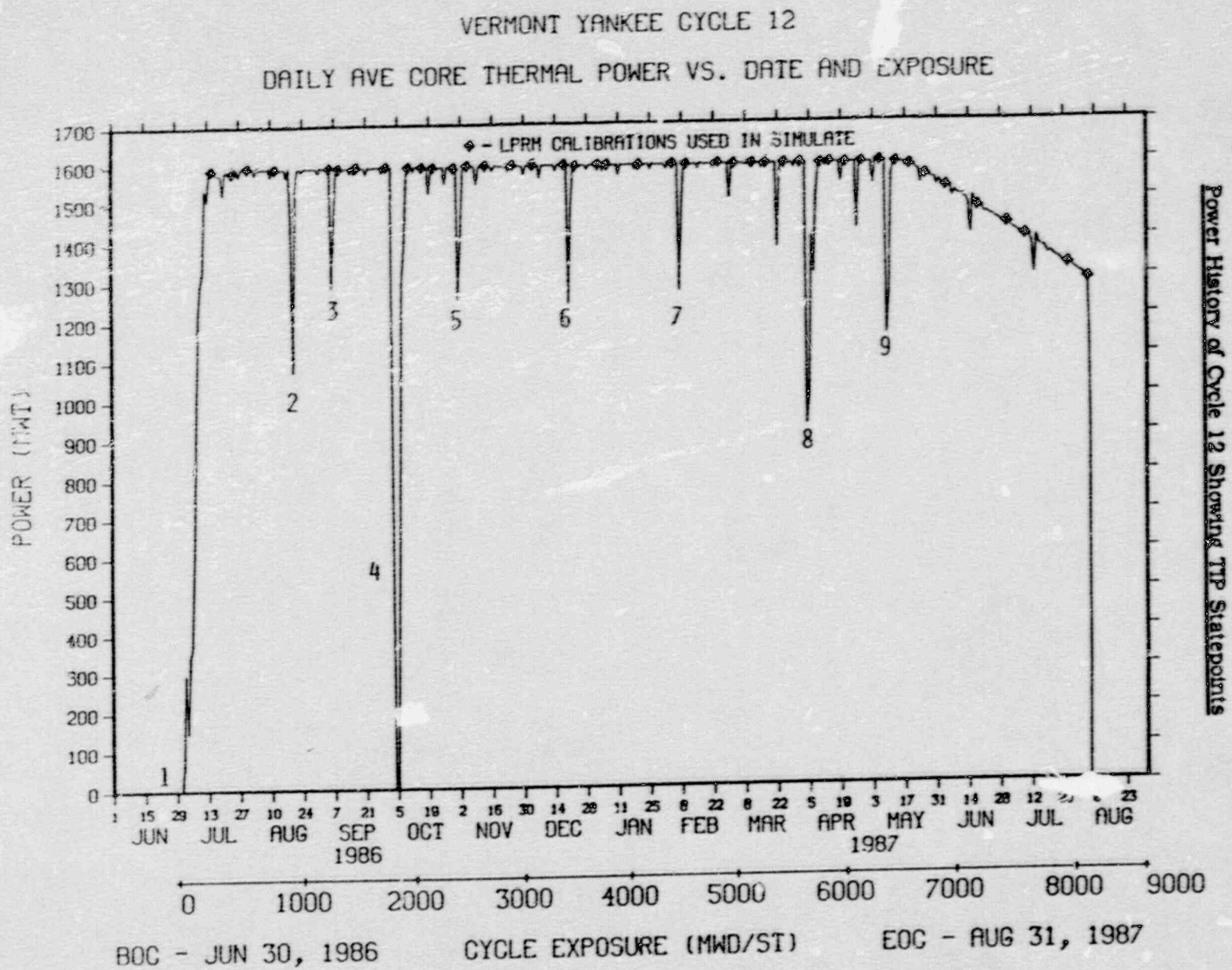

FIGURE A.14

Power History of Cycle 12 Showing TIP Statepoints

FIGURE A.15

Control Rod Inventory of Cycle 12 Showing TIP Statepoints

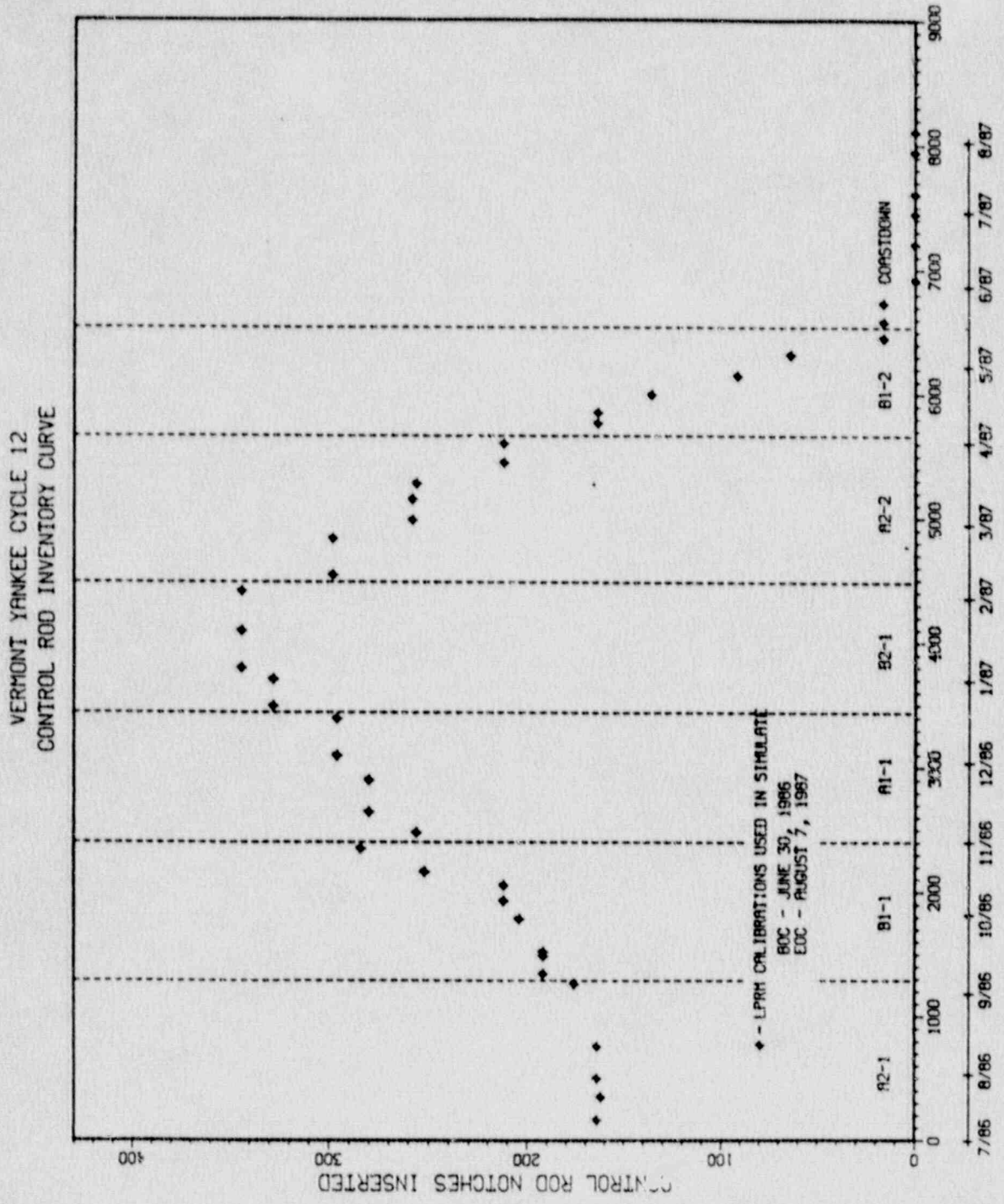

FIGURE A.16

Reactor Conditions for Cycle 12 Depletion Steps

Step	TIP No.	Date	Rod Pattern	Power	Flow	Exposure
0	No TIP	06/30/86	BOC Startup	NA	NA	9820
1	995	07/15/86	A2-1, Deep @ 12	1588	46.1	9983
2	996	07/24/86	A2-1, Deep @ 14	1581	45.6	10170
3	997	07/31/86	A2-1, Deep @ 12	1594	46.9	10320
4	999	08/12/86	A2-1, Deep @ 12	1590	45.6	10580
5	1002	09/05/86	A2-1, Deep @ 12	1591	45.2	11082
6	1005	09/09/86	B1-1, Deep @ 10	1589	46.4	11162
7	1006	09/16/86	B1-1, Deep @ 10	1590	46.0	11307
8	1007	09/17/86	B1-1, Deep @ 10	1592	46.0	11341
9	1008	09/30/86	B1-1, Deep @ 10	1592	45.9	11606
10	1017	10/10/86	B1-1, Deep @ 10	1591	45.4	11751
11	1018	10/16/86	B1-1, Deep @ 10	1590	45.0	11875
12	1020	10/21/86	B1-1, Deep @ 10	1589	46.2	11983
13	1021	10/30/86	B1-1, Deep @ 10	1588	47.0	12173
14	1024	11/05/86	A1-1, Deep @ 12	1593	46.1	12298
15	1026	11/13/86	A1-1, Deep @ 12	1593	46.8	12465
16	1027	11/25/86	A1-1, Deep @ 12	1593	46.2	12721
17	1029	12/04/86	A1-1, Deep @ 12	1592	46.7	12916
18	1030	12/18/86	A1-1, Deep @ 12	1593	45.6	13213
19	1033	12/23/86	B2-1, Deep @ 06	1589	46.2	13312
20	1034	01/02/87	B2-1, Deep @ 06	1592	45.7	13525
21	1036	01/06/87	B2-1, Deep @ 04	1591	47.1	13615
22	1037	01/20/87	B2-1, Deep @ 04	1591	46.8	13913
23	1038	02/04/87	B2-1, Deep @ 04	1593	46.8	14230
24	1043	02/10/87	A2-2, Deep @ 06	1591	45.9	14358
25	1044	02/24/87	A2-2, Deep @ 06	1593	47.2	14653
26	1046	03/03/87	A2-2, Deep @ 06	1591	45.6	14804

FIGURE A.16 (Continued)

Reactor Conditions for Cycle 12 Depletion Steps

Step	TIP No.	Date	Rod Pattern	Power	Flow	Exposure
27	1047	03/11/87	A2-2, Deep @ 06	1592	46.7	14970
28	1048	03/17/87	A2-2, Deep @ 08	1591	46.9	15098
29	1050	03/25/87	A2-2, Deep @ 08	1591	45.7	15267
30	1052	04/01/87	A2-2, Deep @ 08	1591	46.8	15421
31	1063	04/14/87	B1-2, Deep @ 10	1593	46.8	15669
32	1064	04/21/87	B1-2, Deep @ 14	1590	46.4	15818
33	1066	04/28/87	B1-2, Deep @ 18	1591	46.1	15970
34	1068	05/06/87	B1-2, Deep @ 24	1594	46.4	16137
35	1072	05/13/87	B1-2, Deep @ 40	1590	46.7	16273
36	1073	05/19/87	B1-2, Deep @ 40	1583	47.4	16402
37	1074	05/26/87	B1-2, Deep @ 40	1557	47.4	16555
38	1076	06/04/87	ARO	1526	48.0	16740
39	1078	06/18/87	ARO	1473	47.6	17021
40	1079	07/01/87	ARO	1430	47.8	17265
41	1081	07/09/87	ARO	1398	48.0	17426
42	1082	07/28/87	ARO	1324	47.8	17763
43	1083	08/06/87	ARO	1285	47.7	17926
44	No TIP	08/07/87	ARO to EOC	1280	48.0	17949

FIGURE A.17

Reload Design of Cycle 13

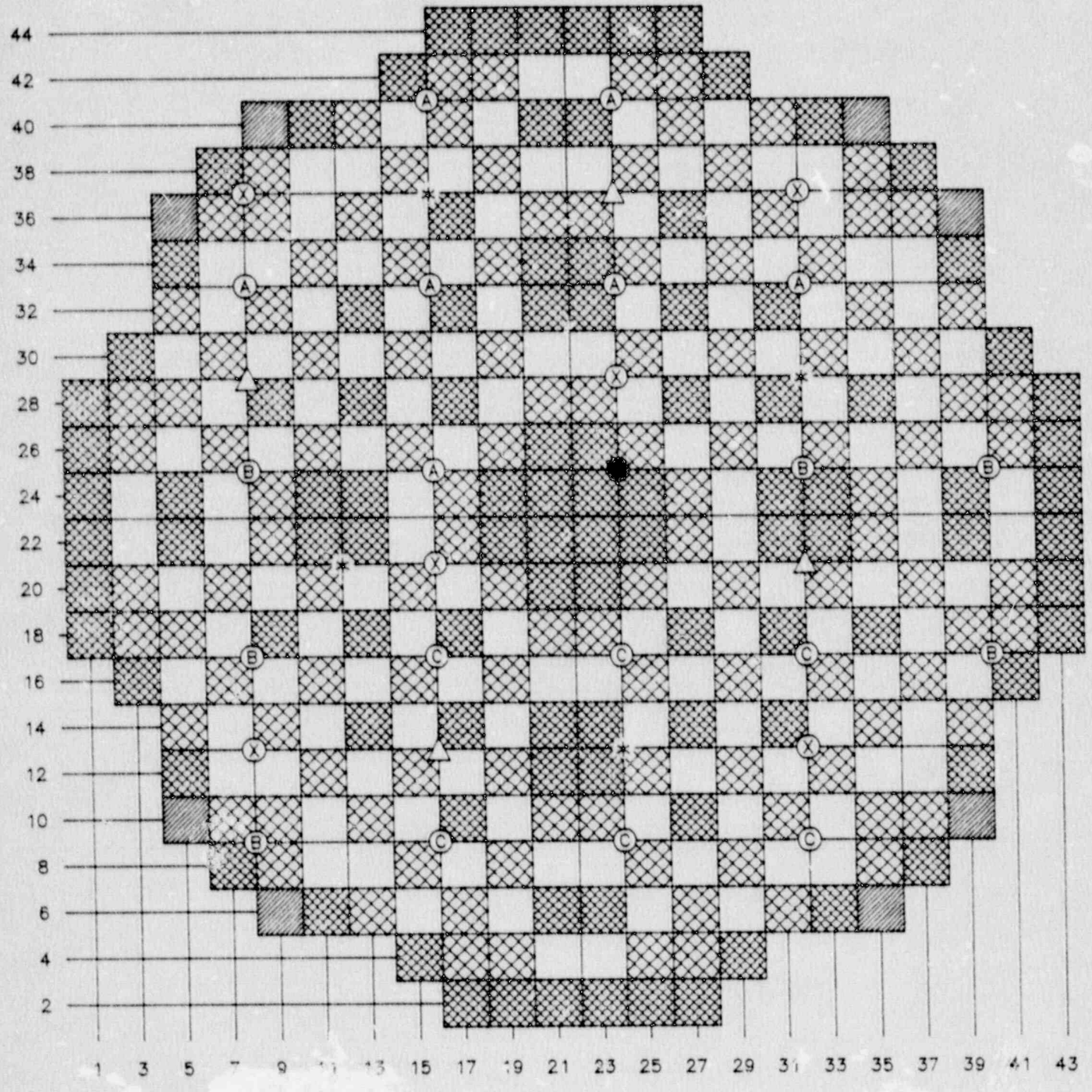

FIGURE A.18

Power History of Cycle 13 Showing TIP Statepoints

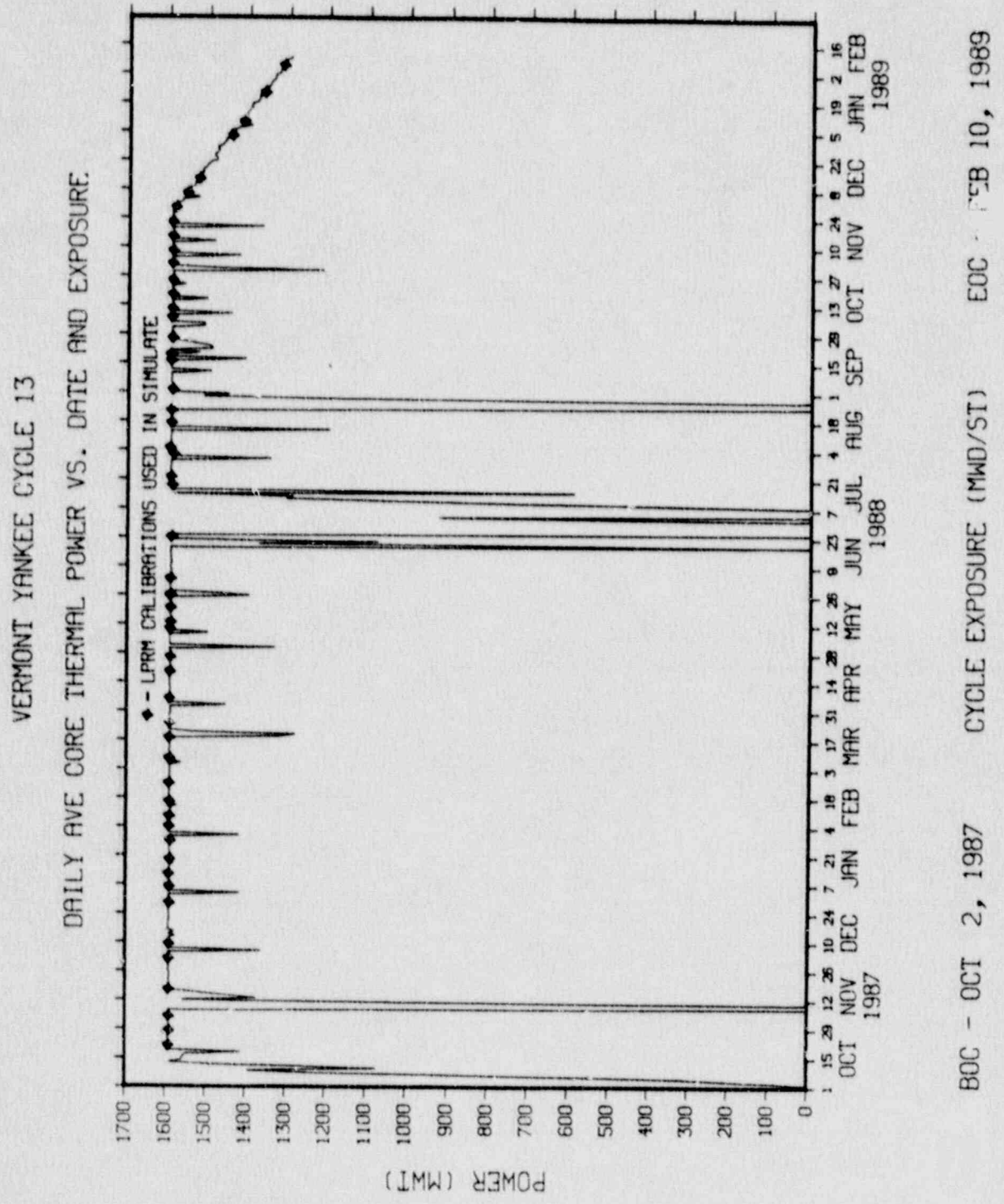

FIGURE A.19

Control Rod Inventory of Cycle 13 Showing TIP Statepoints

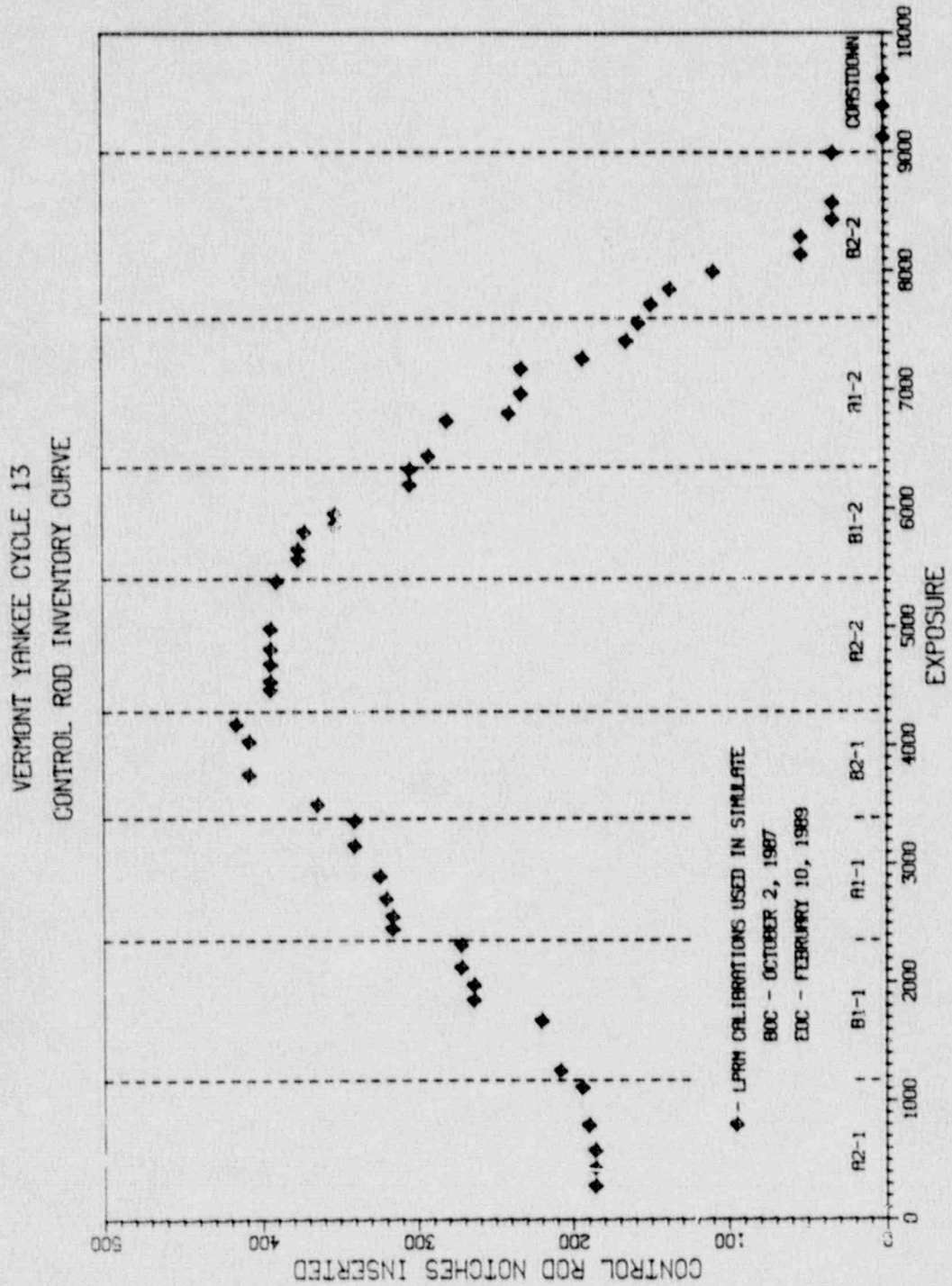

FIGURE A.20

Reactor Conditions for Cycle 13 Depletion Steps

Step	TIP No.	Date	Rod Pattern	Power	Flow	Exposure
0	No Tip	N/A	BOC Startup	N/A	N/A	8613
1	1103	10/21/87	A2-1, Deep @ 18	1592	47.6	8897
2	1104	10/28/87	A2-1, Deep @ 18	1590	47.5	9047
3	1105	11/04/87	A2-1, Deep @ 18	1591	46.8	9195
4	1116	11/17/87	A2-1, Deep @ 16	1592	45.8	9406
5	1118	12/02/87	A2-1, Deep @ 16	1592	45.2	9725
6	1123	12/09/87	B1-1, Deep @ 12	1591	45.7	9866
7	1127	12/29/87	B1-1, Deep @ 10	1591	45.9	10288
8	1130	01/06/88	B1-1, Deep @ 08	1591	46.3	10463
9	1131	01/12/88	B1-1, Deep @ 08	1593	45.8	10588
10	1132	01/19/88	B1-1, Deep @ 08	1590	46.3	10737
11	1134	01/26/88	B1-1, Deep @ 08	1589	44.9	10929
12	1138	02/04/88	A1-1, Deep @ 12	1592	46.2	11068
13	1140	02/09/88	A1-1, Deep @ 12	1592	45.4	11173
14	No TIP	02/16/88	A1-1, Deep @ 12	1592	46.1	11322
15	1142	02/25/88	A1-1, Deep @ 10	1593	46.3	11514
16	1144	03/08/88	A1-1, Deep @ 10	1592	46.6	11772
17	1146	03/18/88	A1-1, Deep @ 10	1593	45.6	11980
18	1151	03/25/88	B2-1, Deep @ 06	1592	46.4	12118
19	1153	04/06/88	B2-1, Deep @ 04	1593	46.8	12370
20	1155	04/19/88	B2-1, Deep @ 04	1592	46.0	12649
21	1156	04/26/88	B2-1, Deep @ 00	1591	46.9	12796
22	1161	05/10/88	A2-2, Deep @ 10	1593	46.6	13085
23	1163	05/13/88	A2-2, Deep @ 10	1591	46.5	13154
24	1164	05/20/88	A2-2, Deep @ 10	1591	46.2	13299
25	1165	05/26/88	A2-2, Deep @ 10	1593	46.1	13425
26	1166	06/03/88	A2-2, Deep @ 10	1592	46.6	13596

FIGURE A.20 (Continued)

Reactor Conditions for Cycle 13 Depletion Steps

Step	TIP No.	Date	Rod Pattern	Power	Flow	Exposure
27	1174	06/23/88	A2-2, Deep @ 10	1590	46.0	13999
28	No TIP	07/18/88	B1-2, Deep @ 04	1588	46.3	14186
29	1193	07/22/88	B1-2, Deep @ 04	1592	46.7	14268
30	1194	05/26/88	B1-2, Deep @ 06	1591	46.9	14415
31	1197	08/02/88	B1-2, Deep @ 06	1586	46.0	14481
32	1198	08/05/88	B1-2, Deep @ 06	1595	46.6	14564
33	1201	08/17/88	B1-2, Deep @ 08	1592	46.1	14814
34	1202	08/23/88	B1-2, Deep @ 08	1592	46.5	14942
35	1213	09/02/88	A1-2, Deep @ 08	1589	45.9	15054
36	No TIP	09/16/88	A1-2, Deep @ 08	1593	47.9	15352
37	1219	09/19/88	A1-2, Deep @ 10	1595	46.1	15413
38	1220	09/27/88	A1-2, Deep @ 12	1590	45.4	15578
39	1223	10/07/88	A1-2, Deep @ 12	1592	47.4	15787
40	1225	10/11/88	A1-2, Deep @ 14	1591	46.3	15871
41	1227	10/18/88	A1-2, Deep @ 16	1590	46.3	16020
42	1228	10/25/88	A1-2, Deep @ 18	1591	45.9	16169
43	1232	11/02/88	B2-2, Deep @ 16	1591	47.5	16327
44	1234	11/08/88	B2-2, Deep @ 18	1590	46.3	16454
45	1237	11/15/88	B2-2, Deep @ 24	1591	46.1	16602
46	1239	11/22/88	B2-2, Deep @ 38	1592	46.4	16748
47	1240	11/29/88	B2-2, Deep @ 38	1584	48.0	16898
48	1241	12/06/88	B2-2, Deep @ 40	1554	47.8	17045
49	1242	12/13/88	B2-2, Deep @ 40	1525	47.8	17187
50	1244	01/03/89	B2-2, Deep @ 40	1442	47.8	17606

Note: The Cycle 13 Benchmark was concluded in January, prior to shutdown. VY continued to operate until 2/11/89 and shutdown at 18,307 MWd/St.

APPENDIX B

COLD CRITICAL STATEPOINTS

The following figures give the control rod patterns for the cold criticals performed at Vermont Yankee during the period of the benchmark. All but one of the criticals are in-sequence criticals.

There is only one local critical. The latter is, a critical performed in a localized region of the core by pulling two adjacent control rods. VY Technical Specifications do not allow the pulling of "face-adjacent" control rods in either shutdown margin or cold critical demonstrations. The beginning of Cycle 9 was the only time, in recent history, that criticality could be achieved using diagonally adjacent rods.

Figure B.1 provides the cold critical patterns for Cycle 9. Figures B.2-B.5 provide the same for Cycles 10 through 13, respectively. Also provided are the approximate hours of xenon depletion at zero power which preceeded the cold critical. This information is important to the quality of the data. It is not sufficient to run these cases at zero xenon. In some instances, the time between scram and recovery was sufficiently short that failure to model the xenon depletion shifts the eigenvalue significantly.

FIGURE B.1

Cycle 9 Cold Critical Patterns

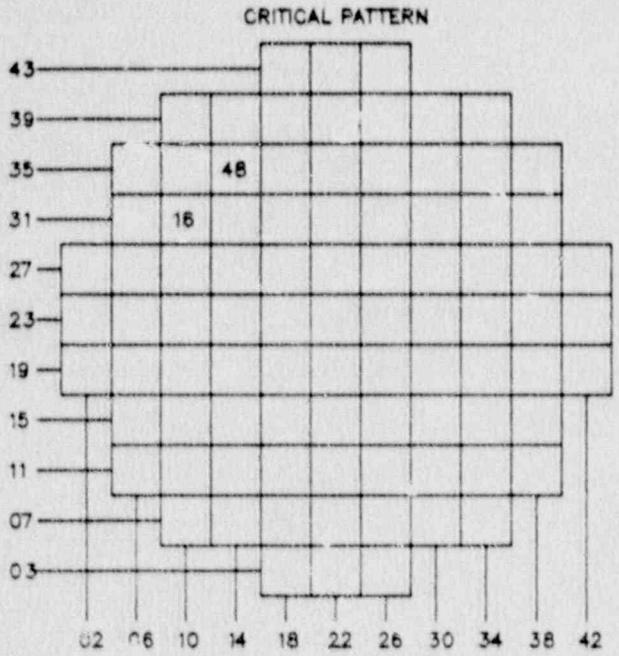

DATE: 11/25/81 PERIOD: 226 SEC. XE HRS: >1000

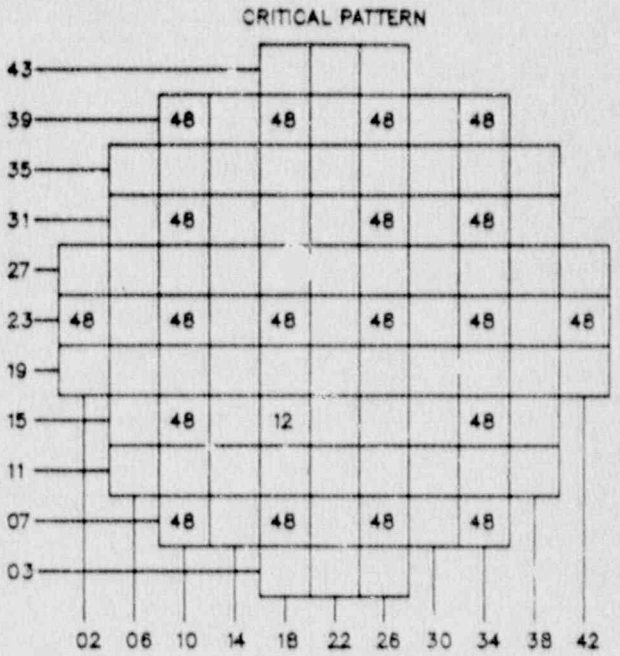

DATE: 11/26/81 PERIOD: 78 SEC. XE HRS: >1000

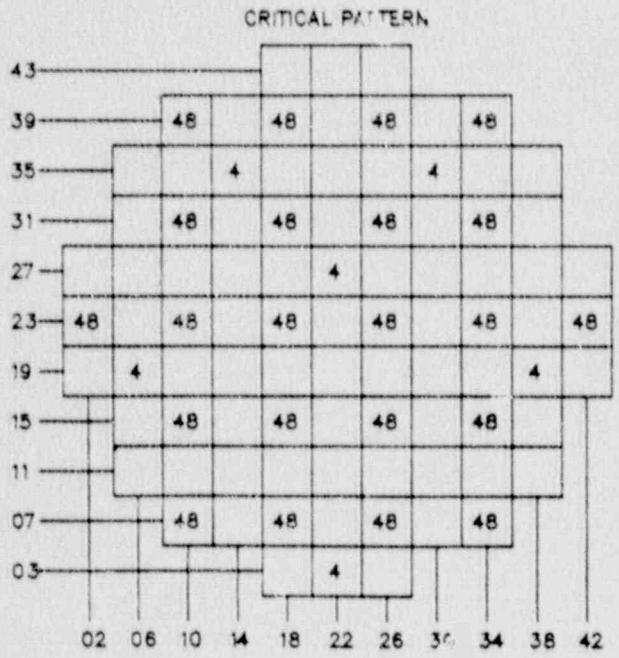

DATE: 12/07/81 PERIOD: 100 SEC. XE HRS: 48

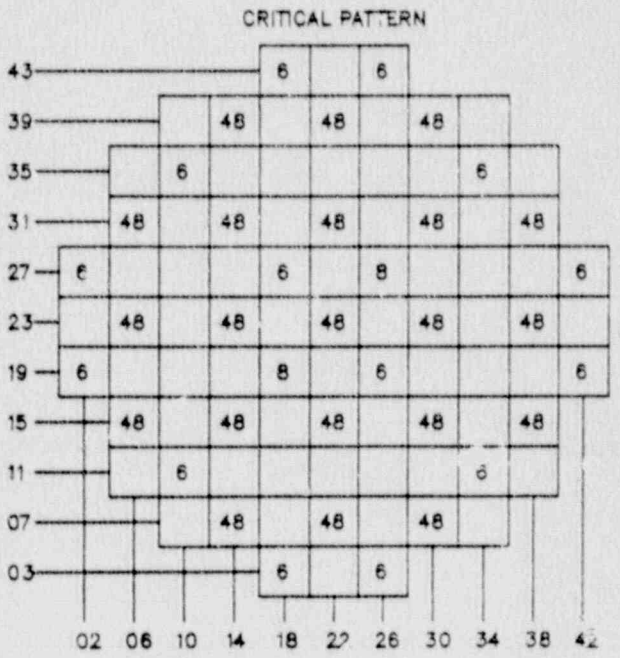

DATE: 01/28/82 PERIOD: 45 SEC. XE HRS: 48

FIGURE B.1 (Continued)

Cycle 9 Cold Critical Patterns

CRITICAL PATTERN

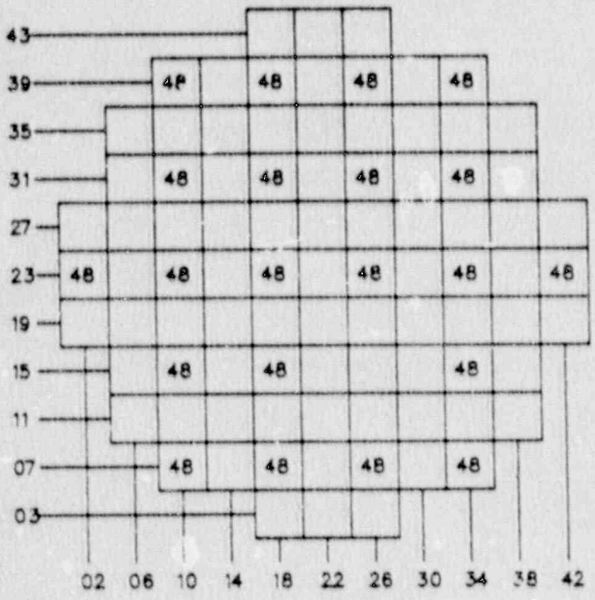

DATE: 06/10/82 PERIOD: 400 SEC. XE HRS: 47

CRITICAL PATTERN

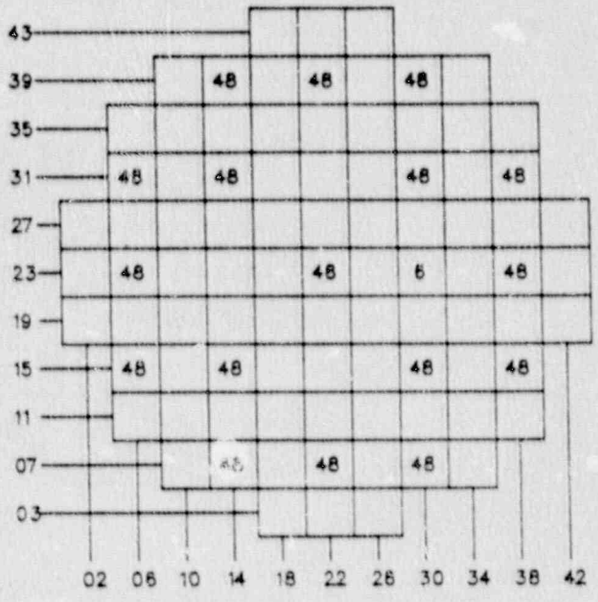

DATE: 08/31/82 PERIOD: 400 SEC. XE HRS: 88

CRITICAL PATTERN

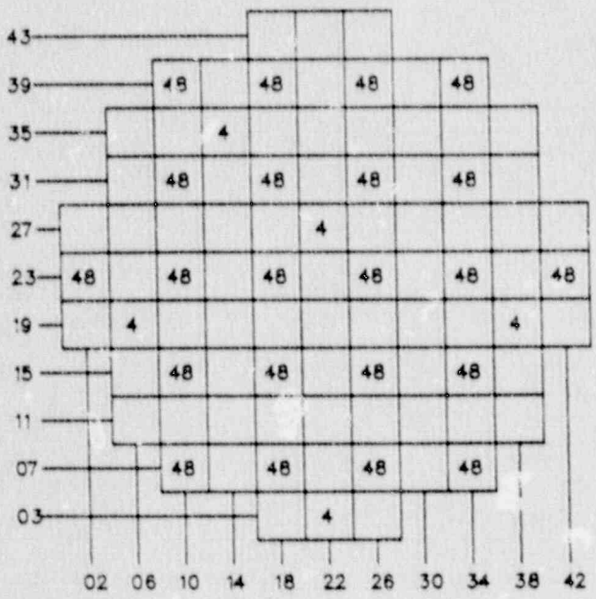

DATE: 03/09/83 PERIOD: 105 SEC. XE HRS: 108

CRITICAL PATTERN

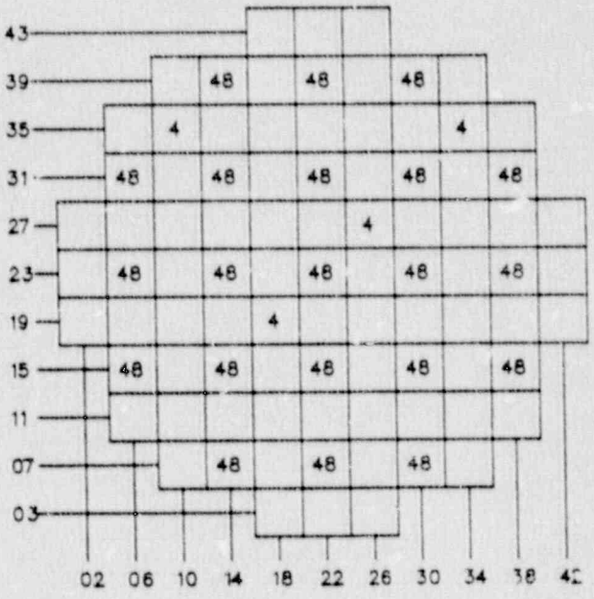

DATE: 03/09/83 PERIOD: 58 SEC. XE HRS: 110

FIGURE B.2

Cycle 10 Cold Critical Patterns

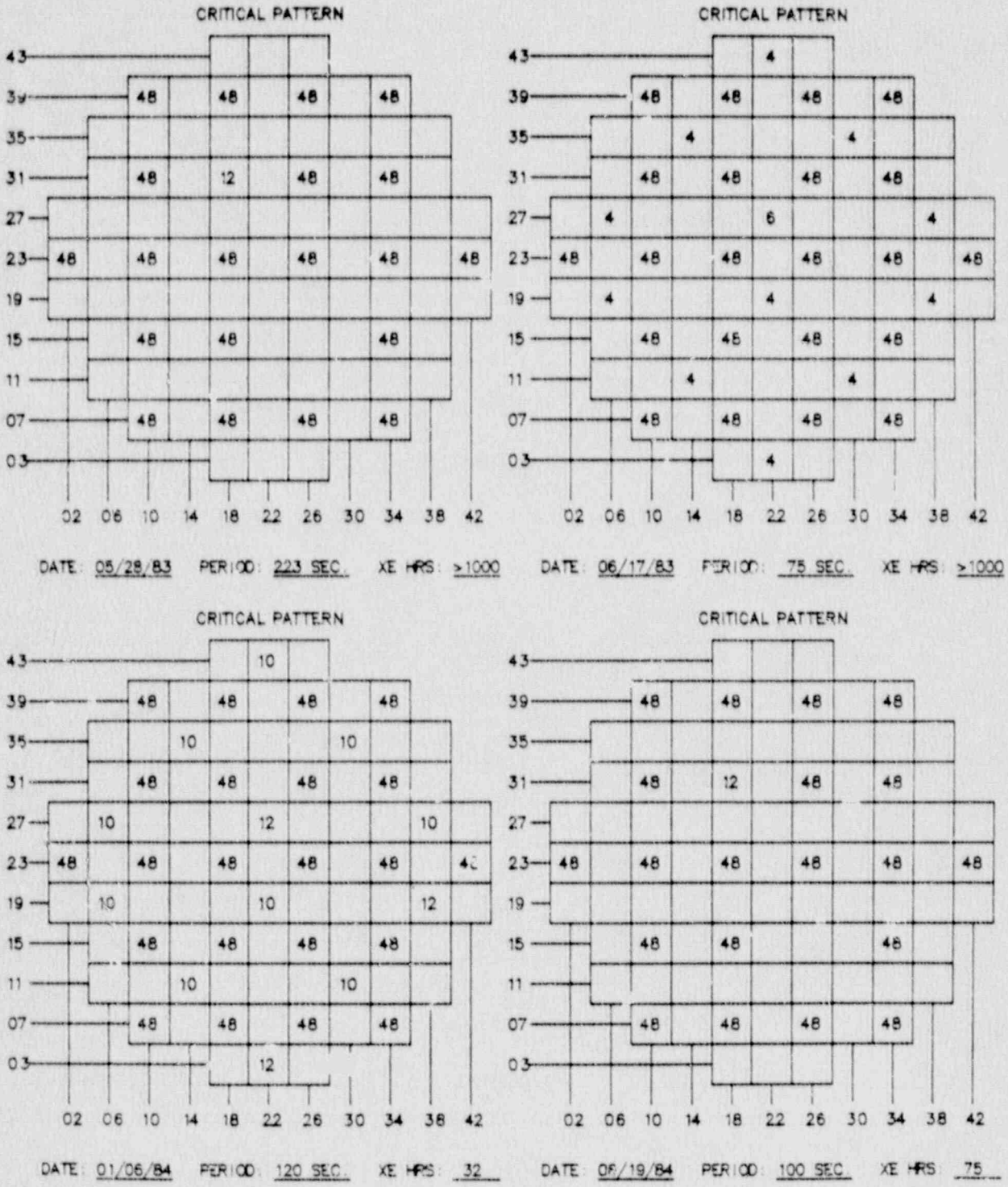

FIGURE B.2 (Continued)

Cycle 10 Cold Critical Patterns

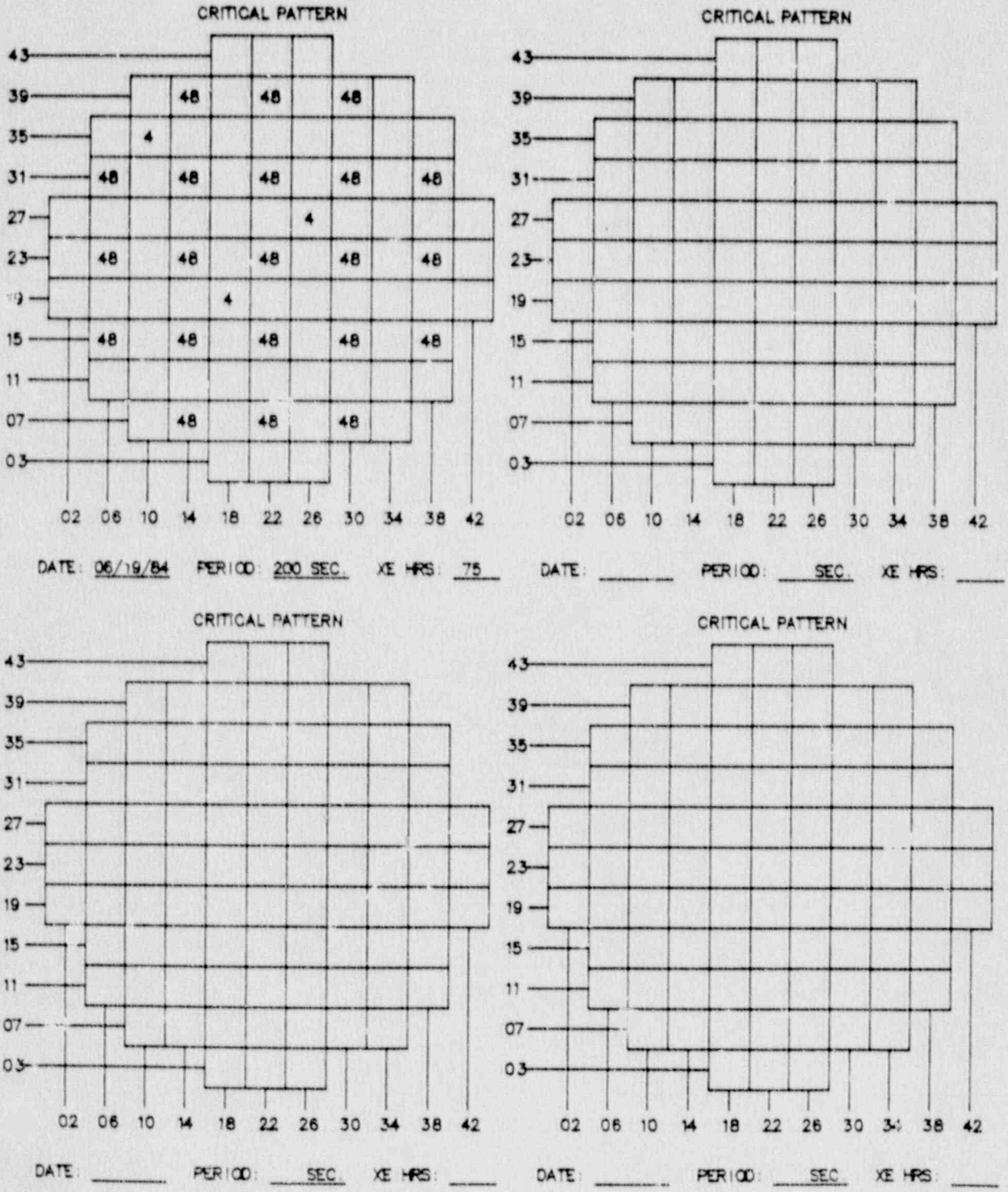

FIGURE B.3

Cycle 11 Cold Critical Patterns

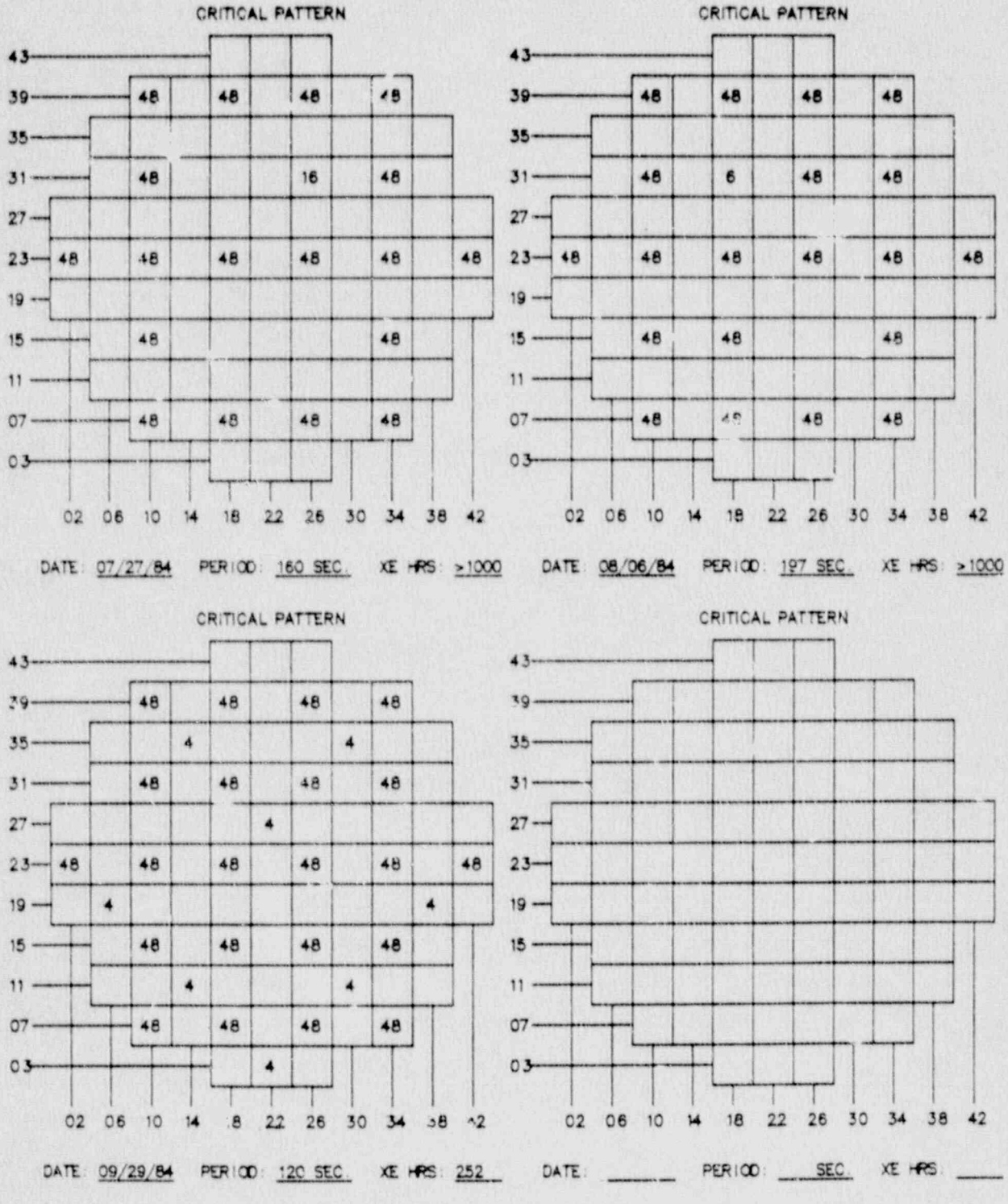

FIGURE B.4

Cycle 12 Cold Critical Patterns

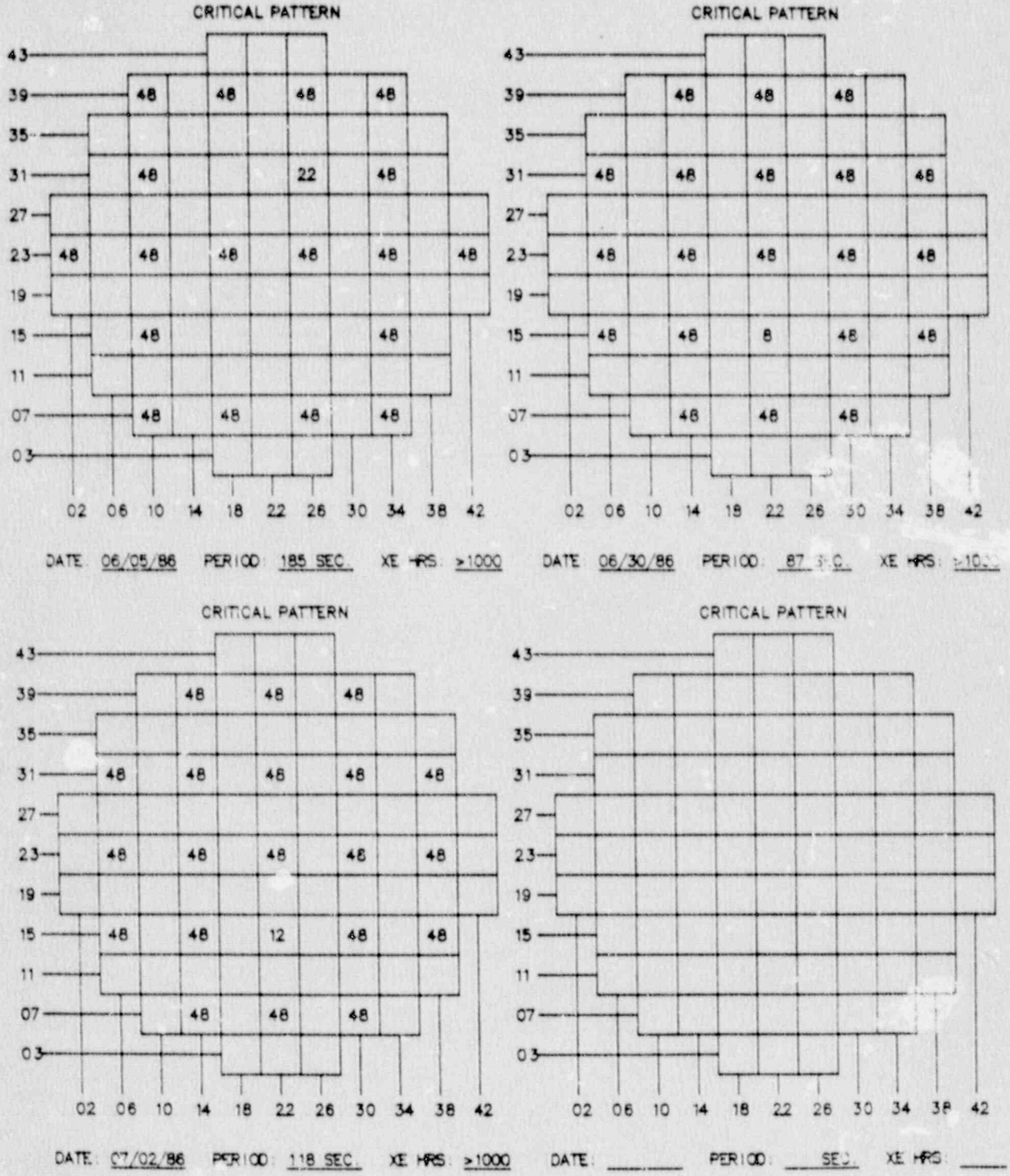

FIGURE B.5

Cycle 13 Cold Critical Patterns

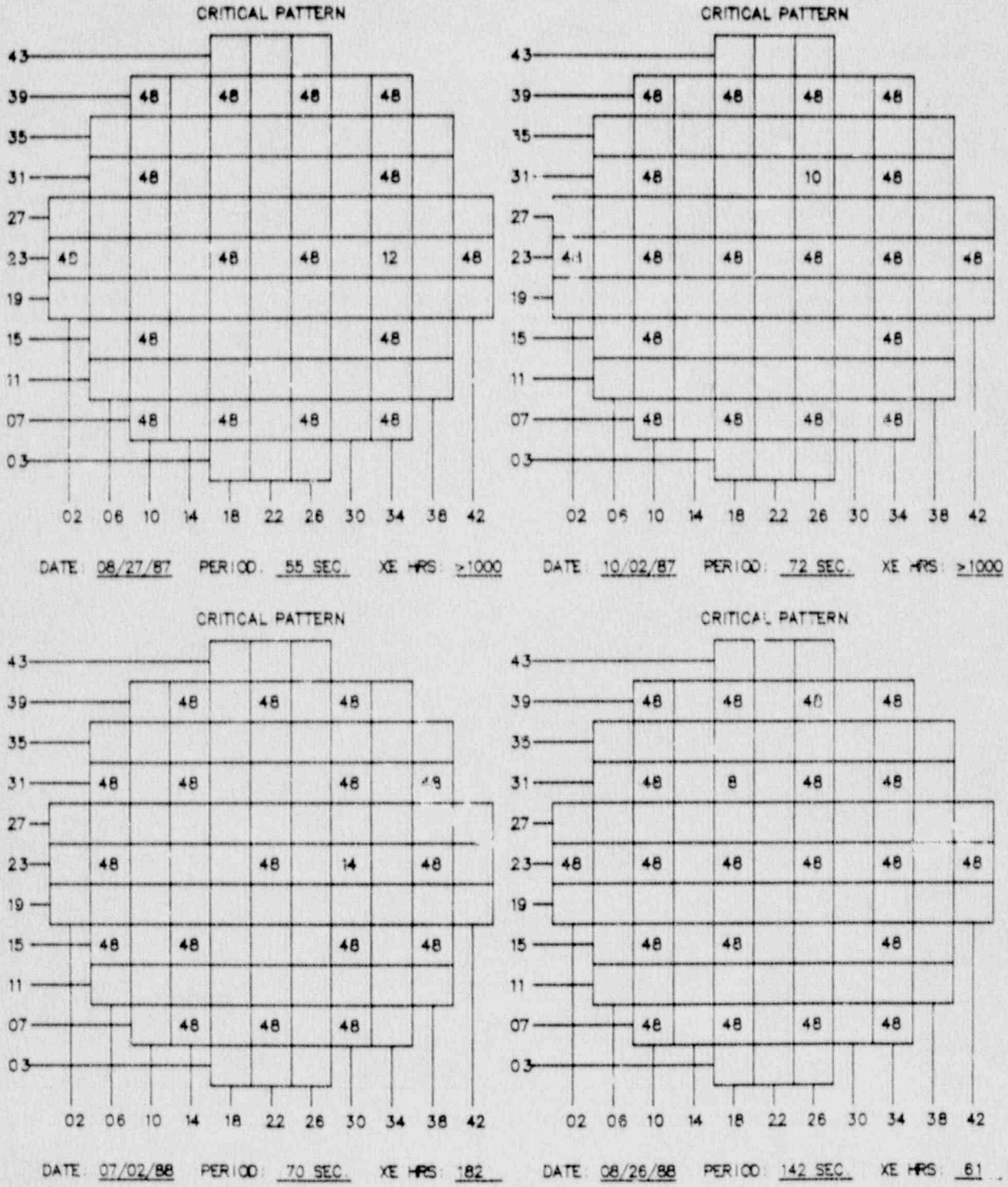

FIGURE B.5 (Continued)

Cycle 13 Cold Critical Patterns

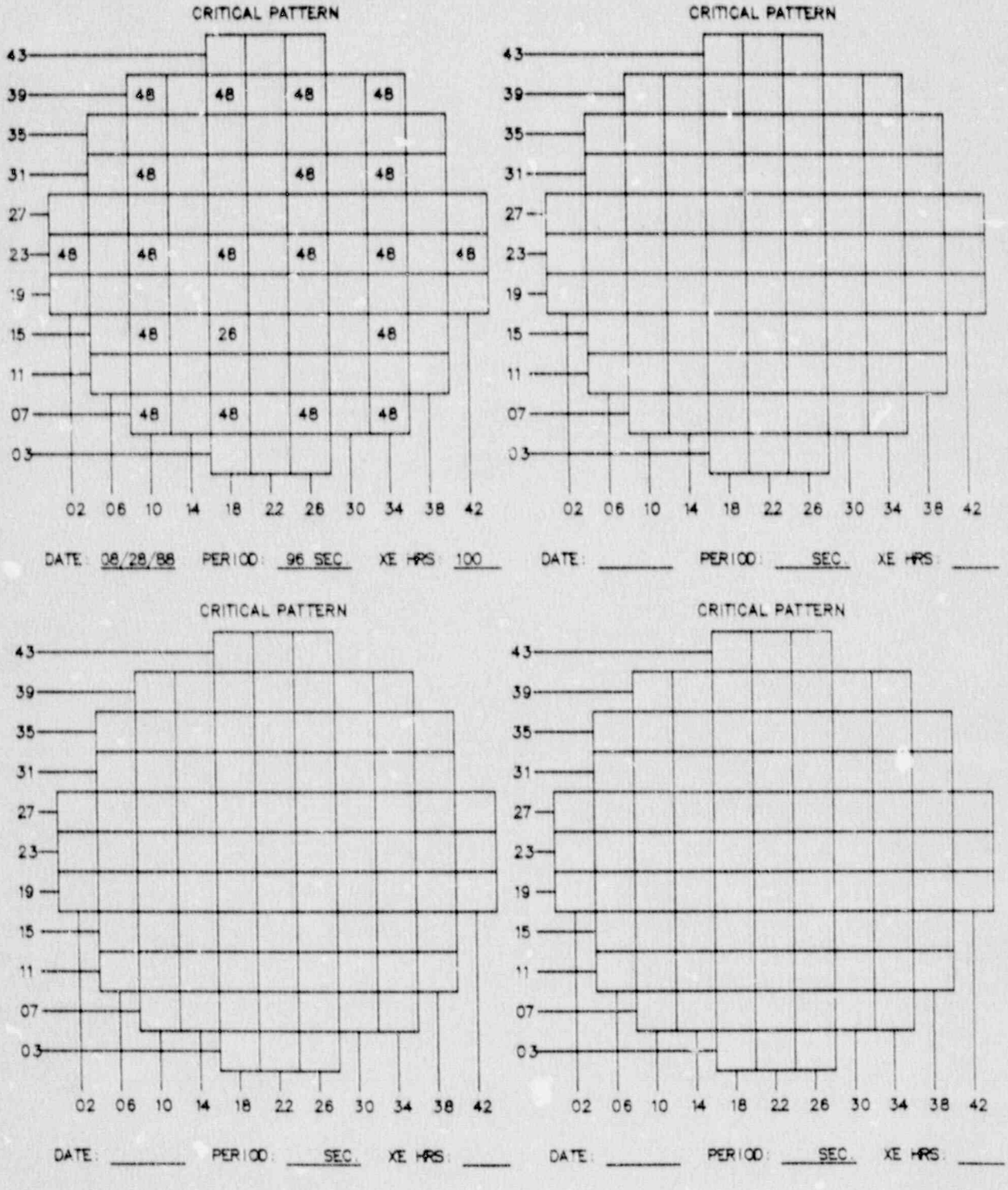

APPENDIX C

CHANNEL BOWING AT D-LATTICE PLANTS

Early in the benchmarking process, the code vendor, Studsvik of America (SOA), advised us that the eigenvalues appeared too high. They had performed numerous benchmarks for other foreign BWR's which produced consistently lower eigenvalues. When reviewing this data with SOA[33] it came to light that all the units in question were C-lattice plants. Subsequent investigation by SOA of a D-lattice reactor revealed high eigenvalues similar to Vermont Yankee's results.

This led to a search for the possible differences between D-lattice and C-lattice plants. The most fruitful discovery was that of preferential channel bowing in D-lattice plants. This issue first came to our attention at the 1988 Station Nuclear Engineers Conference[34]. Subsequent investigation of EPRI channel measurement studies[35, 36, 37, 38] revealed that the channel bowing effect is unique to D-lattices and is quite prevalent across the industry.

Reference 35 provides a good overview of the mechanism causing the bow and the range of possible channel deflections. The primary mechanism is the fast flux gradient across the channel. In the interior of the core, the wide water gaps significantly soften the spectrum. Thus, the gradient results in a higher fast flux on the narrow sides. The higher fast flux results in a higher rate of differential growth on the narrow sides of the channel, bowing the channel away from the wide side as shown in Figure C.1. There is also some contribution from differential oxide growth on the channel, but the impact is in the same direction: Channels deflect away from the wide-wide corner (i.e., the control blade location) as the burnup on the channel (fluence) increases.

The amount of deflection, with burnup, is a function of the initial channel materials and the initial channel deflection. For typical channel material, Commonwealth Edison[36] calculated deflections away from the control blade as a function of initial deflection on the as-built channel. This is presented in Table C.1. From Table C.1 it is obvious that channel bowing exhibits positive feedback. That is, a wider than usual wide water gap results in greater fast flux gradients, further increasing the rate of bowing.

As far as Vermont Yankee is concerned, it is difficult to determine what the average amount of channel bow in the reactor is. We do know that the majority channel vendor[39] has preoriented channels away from the control blade (wide-wide corner) since 1974. This is to prevent channel interference with blade scram times. Thus, even fresh channels start with some average bow greater than zero.

Vermont Yankee has also been reusing channels during the period of the benchmark. The very process of selecting channels for reuse eliminates any channels which might be bowed in the direction of the blade. Thus, it is relatively certain that average bowing on the order of 40 mils, or more exists at VY.

A value of 40 mils was arbitrarily selected by the investigators. It represents half of a channel thickness and is considered to be quite reasonable, since it lies in the middle of the vendor's channel pre-selection criterion. While not such a big deflection, the impact it has on the D-lattice assembly is significant. The reason for this is that the lattice gets its rigidity from the channel being in contact with the spacers. As the channel deflects (see Figure C.2) so do all the pins in the lattice.

As shown in Figure C.2, the enrichment distribution in a D-lattice is not symmetrical. It is tuned for the size of the water gaps. When the narrow gap is narrowed further, the medium enrichment pins on the narrow side suffer from a reduction in thermal utilization. The increase in thermal utilization in the low enrichment pins along the wide side do not take up the slack. The net result is a loss of assembly reactivity.

For C-lattice plants bowing is not a problem. The water gaps in a C-lattice are nearly the same. This reduces the fast flux gradient across the channel to practically zero, eliminating the feedback mechanism that causes bowing. Moreover, even with preorientation of new channels, the reactivity impact is negligible because the C-lattice has a symmetrical enrichment distribution.

TABLE C.1

Channel Bowing vs. Burnup as a Function of Initial Bowing

Initial Deflection (mils) Away from Control Rod (Wide-Wide Corner)	Deflection (mils) Away from Control Rod After 25,000 MWd/St	Change (mils) in Deflection After 25,000 MWd/St
0.0	56	56
50	130	80
100	204	104
150	278	128

FIGURE C.1

Axial Representation of Channel Bowing (Exaggerated)

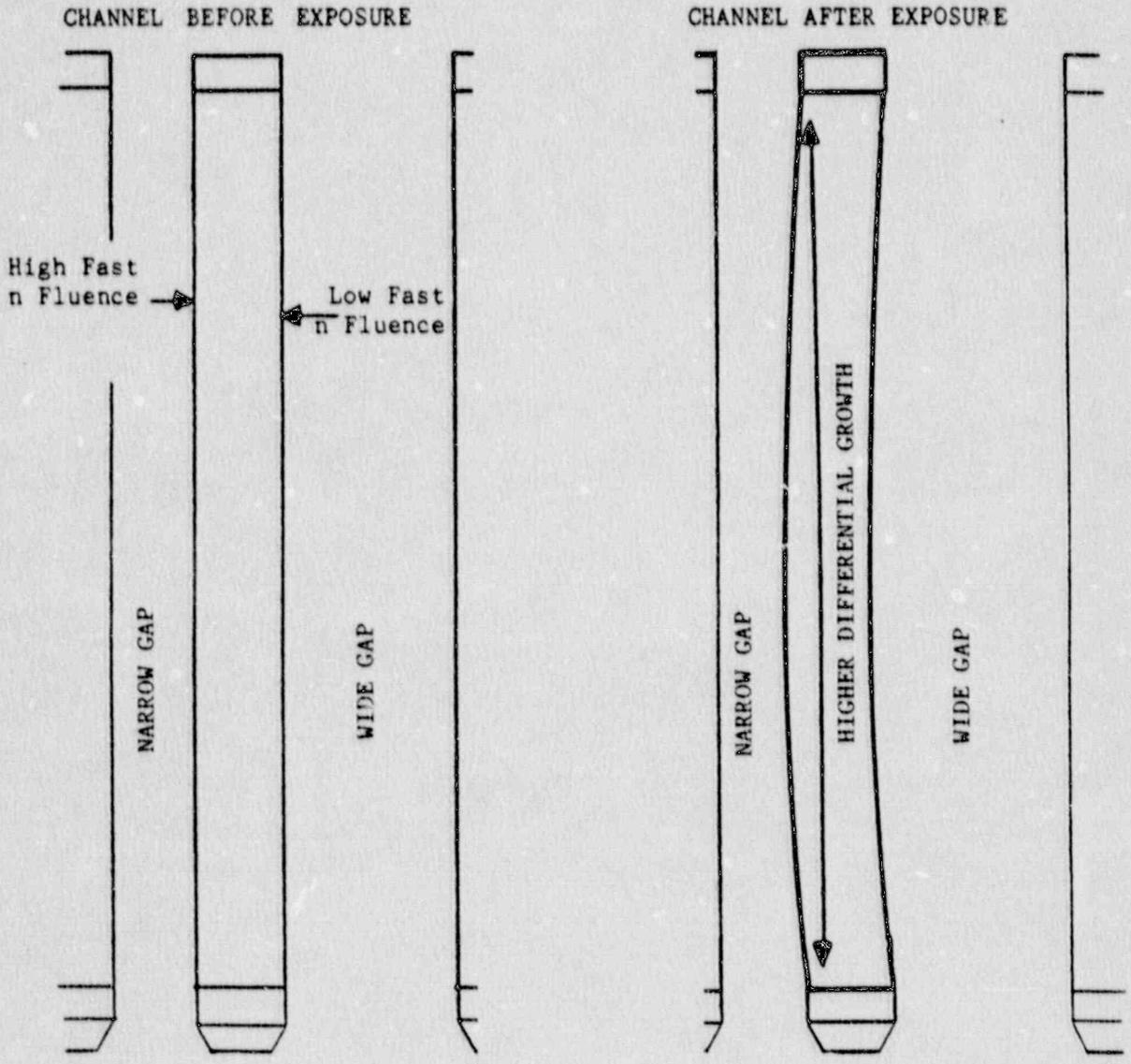

FIGURE C.2

Impact of Channel Bowing on Lattice (Exaggerated)

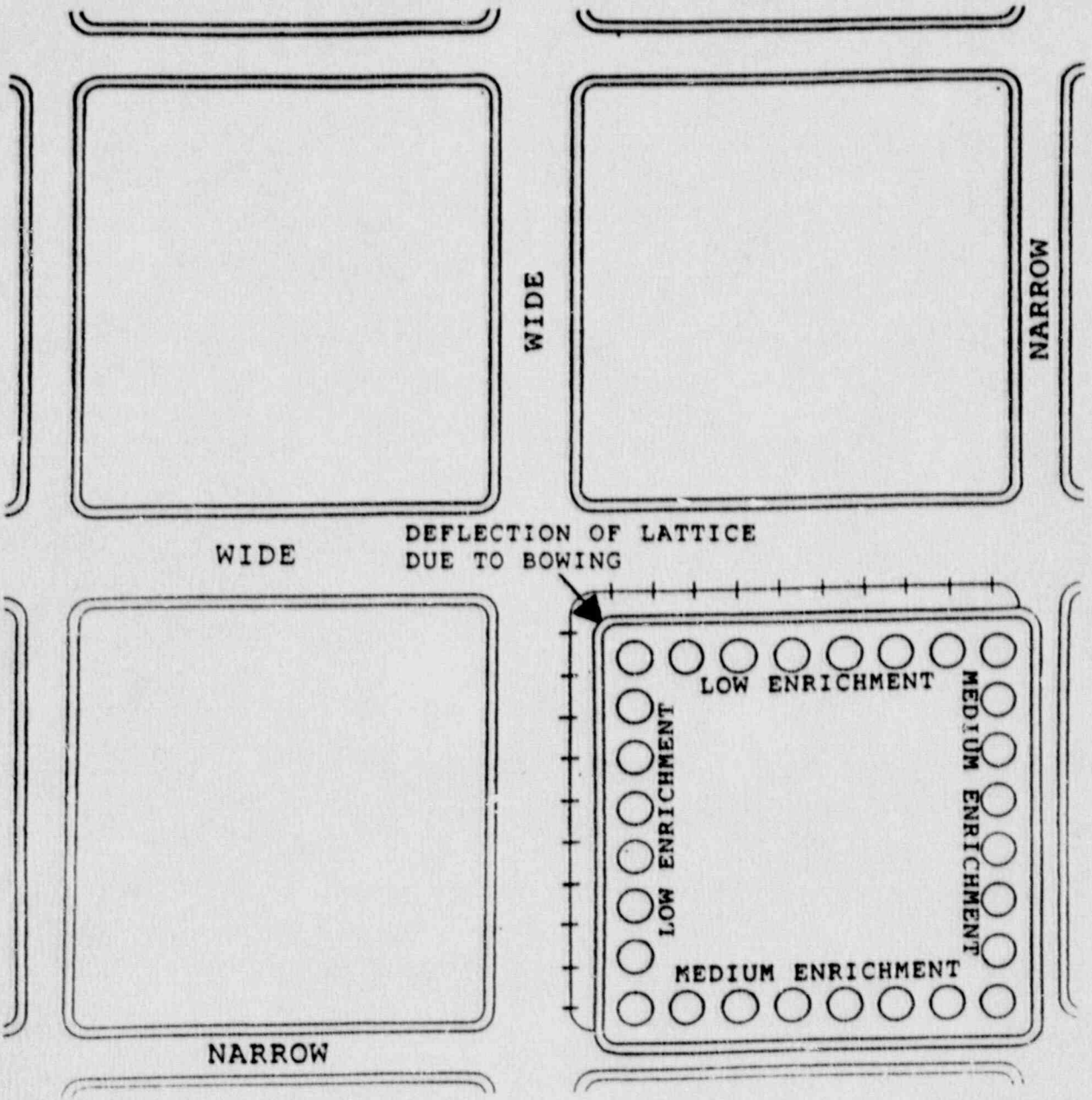

APPENDIX D

HOT MODEL-TO-PLANT DETECTOR COMPARISONS

The five cycles modeled in this benchmark produced comparisons between the hot model and the plant gamma detector readings at 223 TIP set statepoints. With 20 instrument strings per set and 24 data points per string, the number of comparison points exceeds 100,000. To reduce this to a manageable, yet presentable form, the data was normalized and summed radially and axially as explained in Section 5.3. The summations at each radial location are called the "TIP integrals." The summations for each planar slice, when plotted axially, produce the "core average axial TIPs."

This appendix presents the plant to model comparisons for each cycle. For Cycle 9, Figure D.1 shows the average error and standard deviation in the TIP integrals at each location. Note: percent error is always defined as 100*(Model-Plant)/Plant. Figure D.1 also shows the RMS error in the TIP integrals at each location. Figure D.2 shows the core average axial TIPs for the model (lines) compared to the plant (+). The axially averaged TIPs are shown for each TIP set modeled in the Cycle 9 depletion. The order of the TIP sets can be identified by either the TIP set number or the cycle exposure. As the cycle progresses, the model exhibits the following axial trend: The model begins to underpredict the power in the bottom of the core towards EOFPL. This same trend can be observed in all the cycles benchmarked.

Figures D.3 and D.4 present similar information for Cycle 10. Figures D.5 and D.6 for Cycle 11. Figures D.7 and D.8 for Cycle 12. Figures D.9 and D.10 for Cycle 13.

FIGURE D.1

Cycle 9 Averaged TIP Integral Errors, Standard Deviations, and RMS Errors

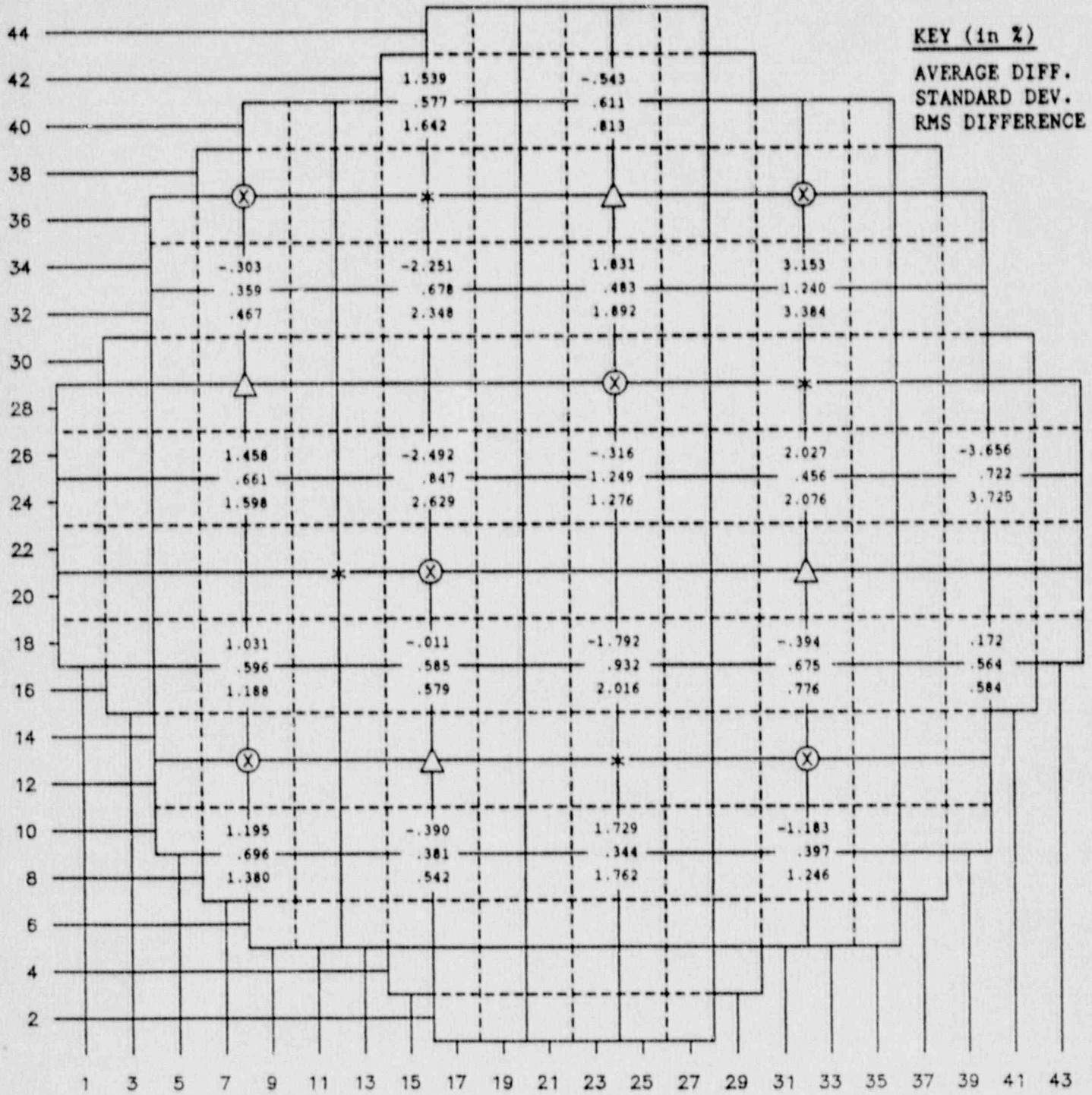

VY CYCLE 09 DEPLETION

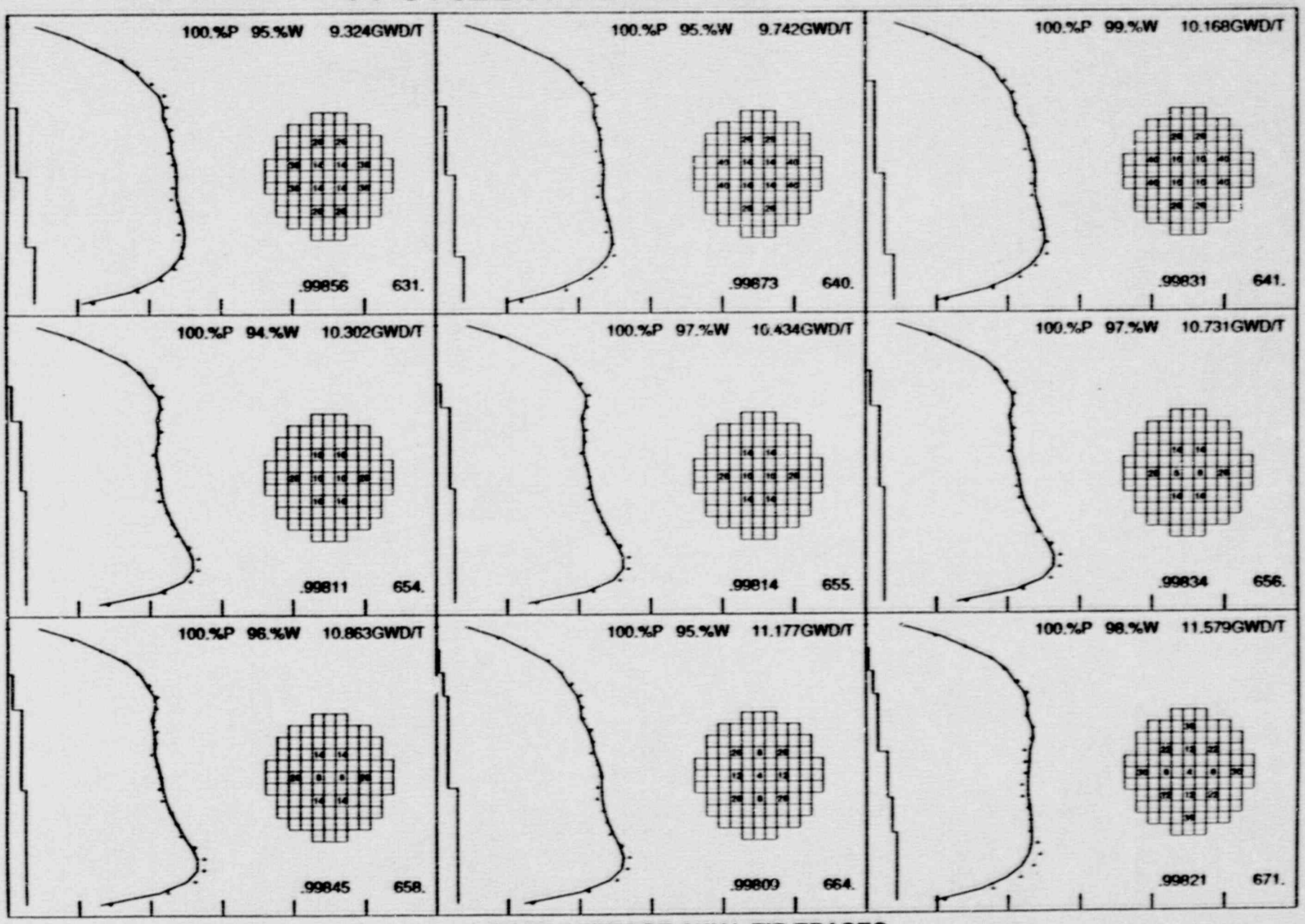

CORE AVERAGE AXIAL TIP TRACES

(*) $USER.DEP8.CYCLE09.S3S9008B S3I908X VERMONT YANKEE 02/25/89 14:45:02 2.30-SUN 88/09/09
(X) $USER.DEP8.CYCLE09.S3D0068 S3I908X VERMONT YANKEE 02/25/89 14:45:02 2.30-SUN 88/09/09

FIGURE D.2
Cycle 9 Core Average Axial TIP Comparisons by TIP Set

VY CYCLE 09 DEPLETION

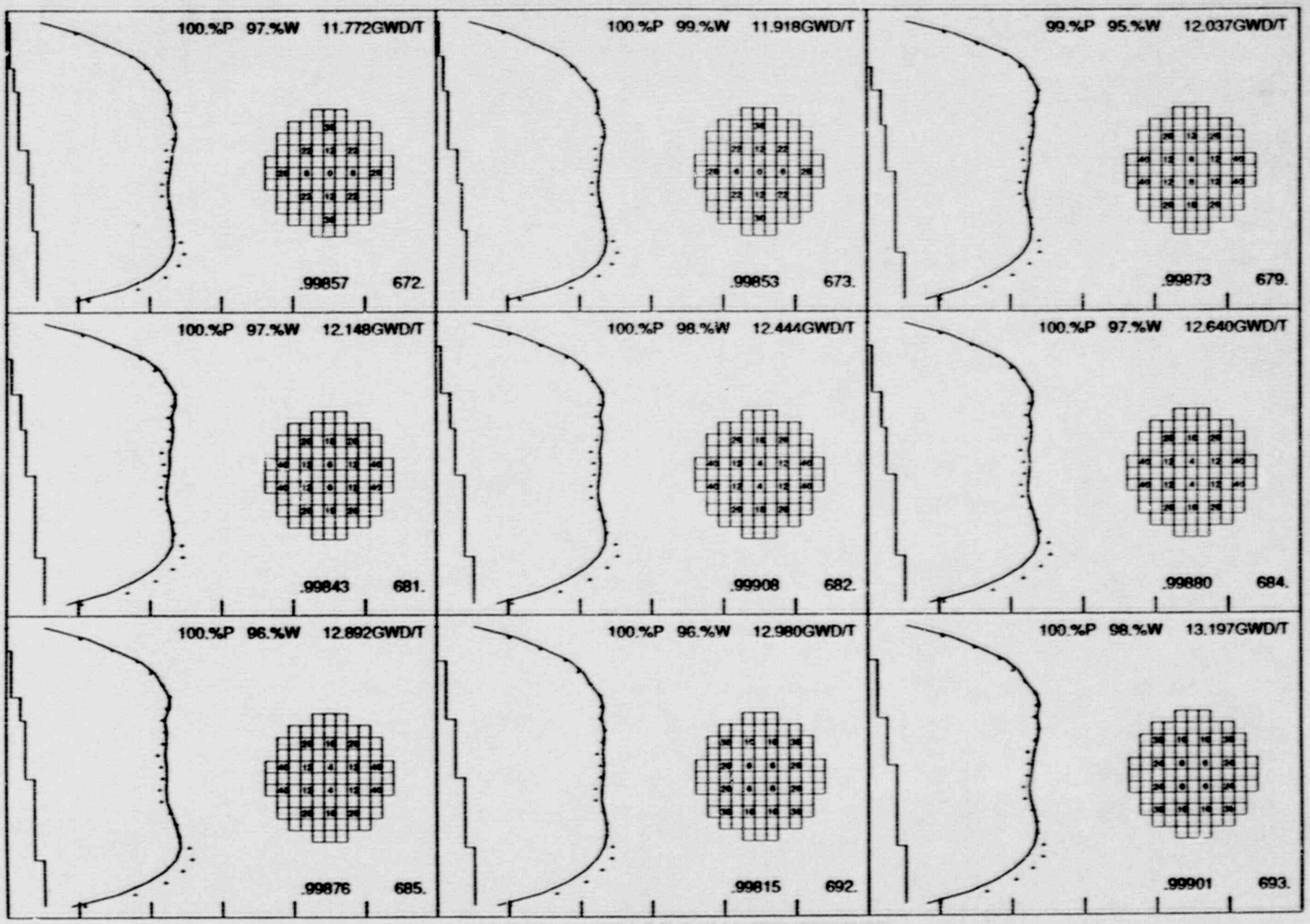

CORE AVERAGE AXIAL TIP TRACES

(*) $USER.DEP8.CYCLE09.S3S908B S3908X VERMONT YANKEE 02/25/89 14:45:02 2.30-SUN 89/09/09
(X) $USER.DEP8.CYCLE09.S3D908B S3908X VERMONT YANKEE 02/25/89 14:45:02 2.30-SUN 89/09/09

FIGURE D.2 (Continued)

VY CYCLE 09 DEPLETION

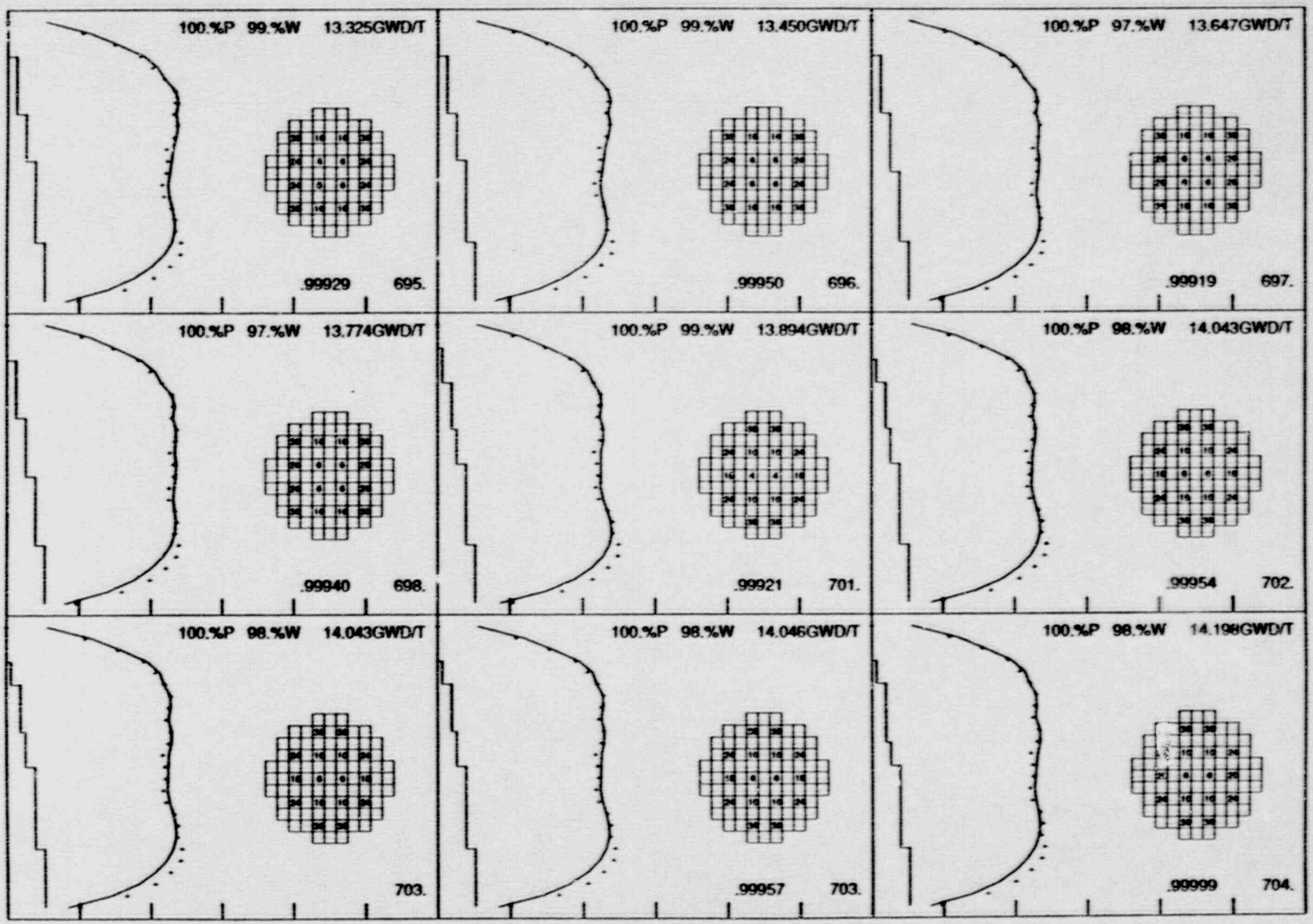

CORE AVERAGE AXIAL TIP TRACES

(*) $USER.DEP8.CYCLE09.S399088 S3808X VERMONT YANKEE 02/25/89 14:45:02 2.30-SUN 88/09/09
(X) $USER.DEP8.CYCLE09.S3D8088 S3808X VERMONT YANKEE 02/25/89 14:45:02 2.30-SUN 88/09/09

FIGURE D.2 (Continued)

VY CYCLE 09 DEPLETION

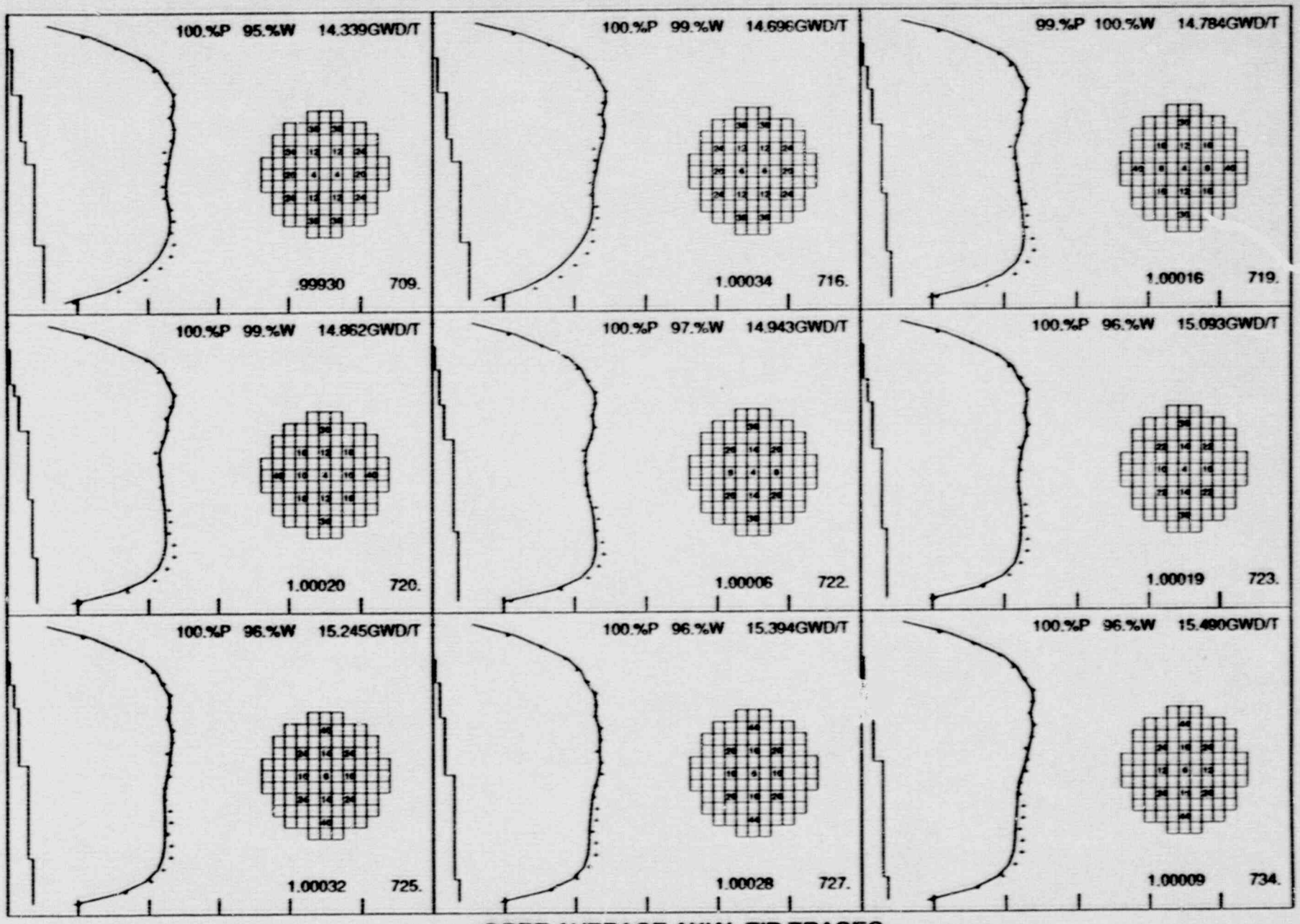

CORE AVERAGE AXIAL TIP TRACES

(*) $USER.DEP8.CYCLE09.S3S9068 S3I908X VERMONT YANKEE 02/25/89 14:45:02 2.30-SUN 88/09/09
(X) $USER.DEP8.CYCLE09.S3D9068 S3I908X VERMONT YANKEE 02/25/89 14:45:02 2.30-SUN 88/09/09

FIGURE D.2 (Continued)

VY CYCLE 09 DEPLETION

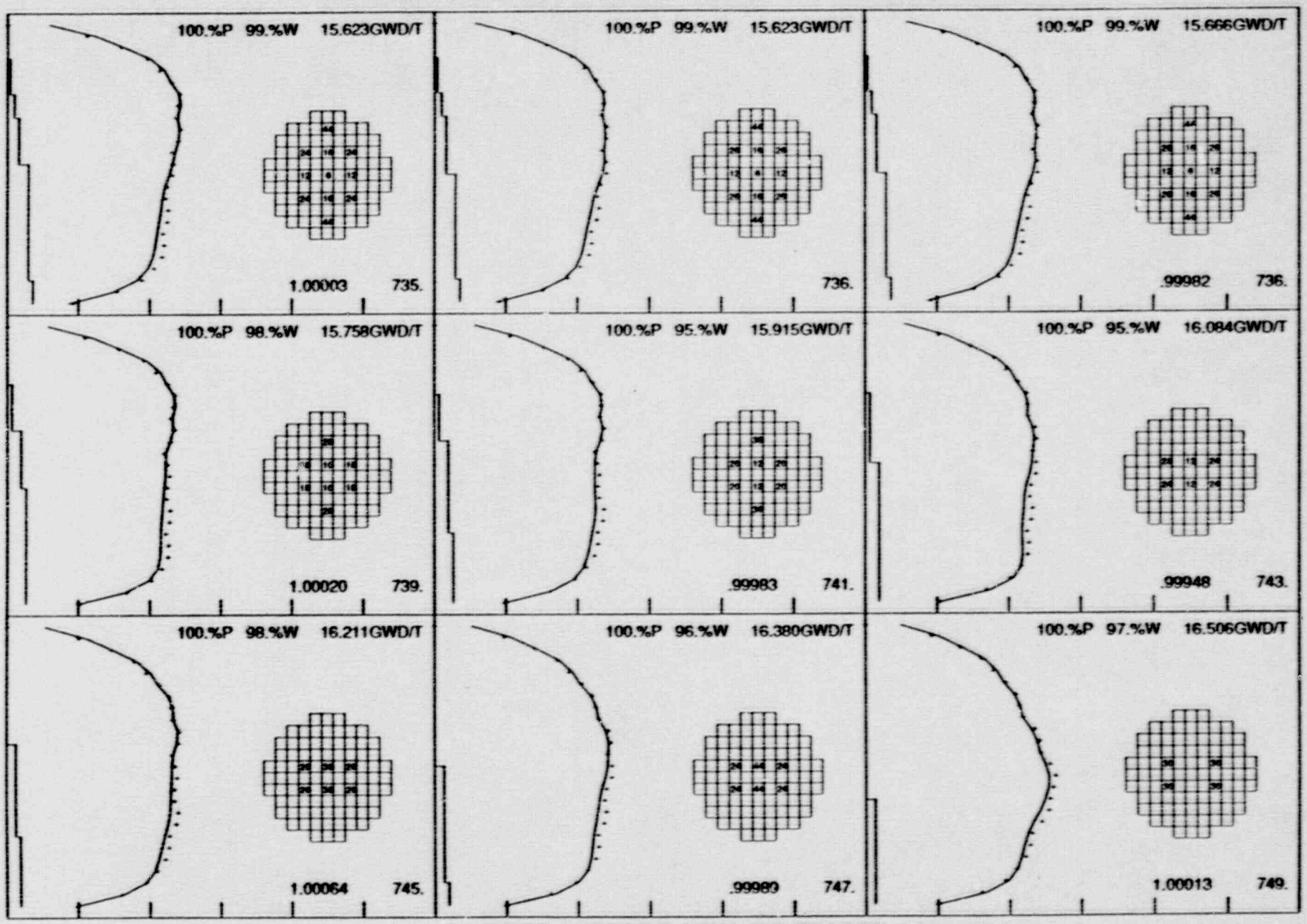

CORE AVERAGE AXIAL TIP TRACES

(*) $USER.DEP8.CYCLE09.S3S9068 S3I906X VERMONT YANKEE 02/25/89 14:45:02 2.30-SUN 89/09/09
(X) $USER.DEP8.CYCLE09.S3D9068 S3I906X VERMONT YANKEE 02/25/89 14:45:02 2.30-SUN 89/09/09

FIGURE D.2 (Continued)

VY CYCLE 09 DEPLETION

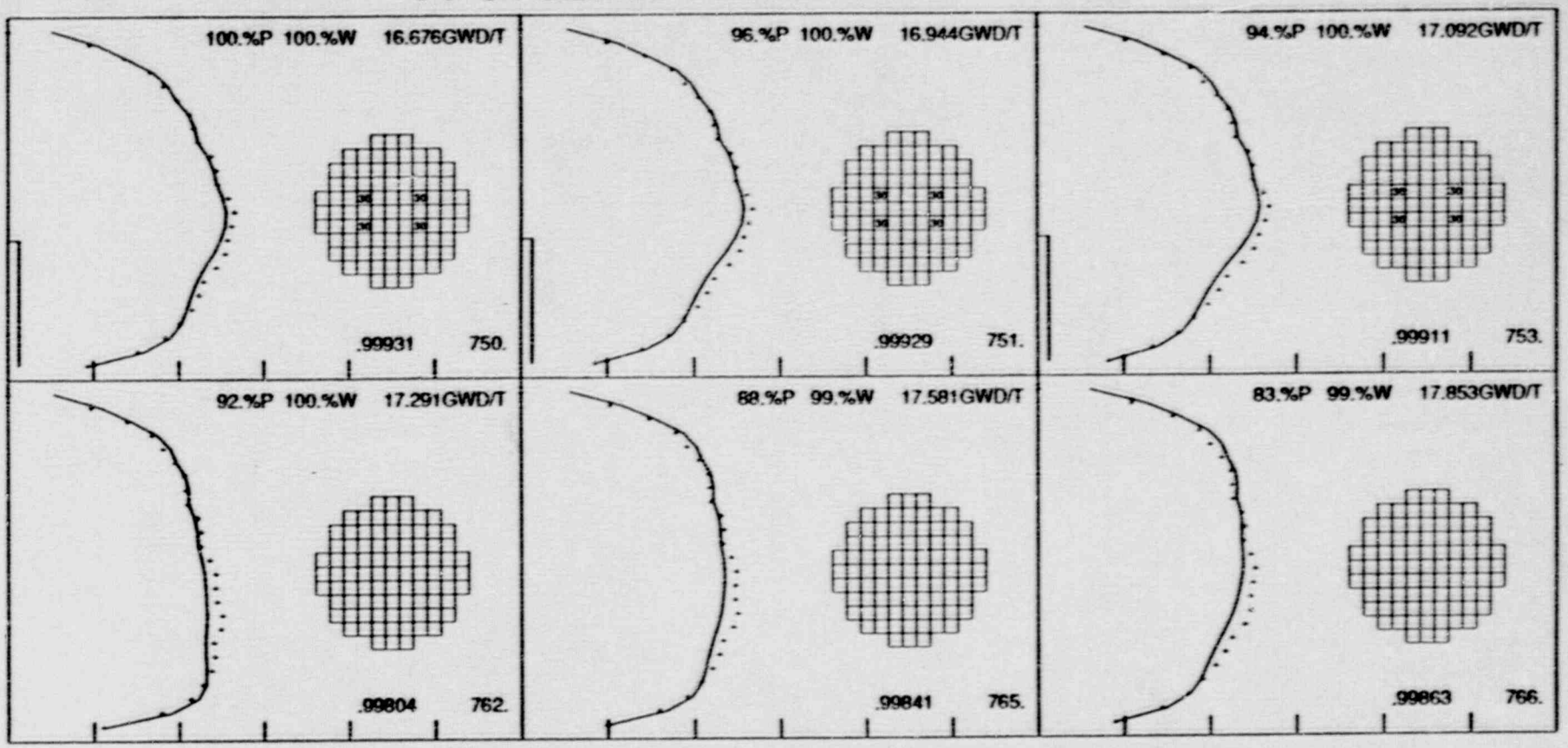

FIGURE D.2 (Continued)

CORE AVERAGE AXIAL TIP TRACES

(*) $USER.DEP8.CYCLE09.S399068 S3I906X VERMONT YANKEE 02/25/89 14:45:02 2.30-SUN 88/09/09
(X) $USER.DEP8.CYCLE09.S3D9068 S3I906X VERMONT YANKEE 02/25/89 14:45:02 2.30-SUN 88/09/09

FIGURE D.3

Cycle 10 Averaged TIP Integral Errors, Standard Deviations, and RMS Errors

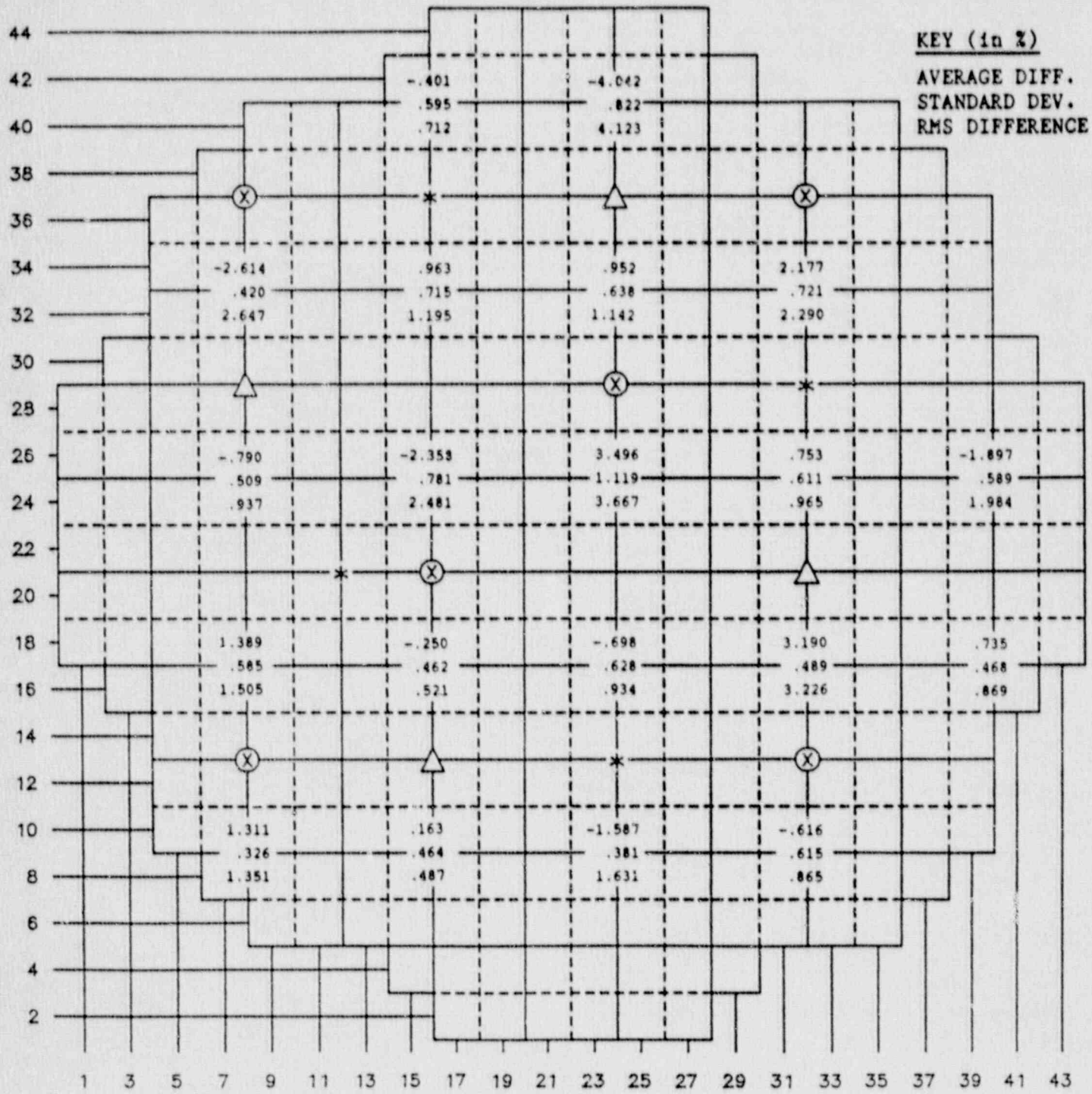

VY CYCLE 10 DEPLETION

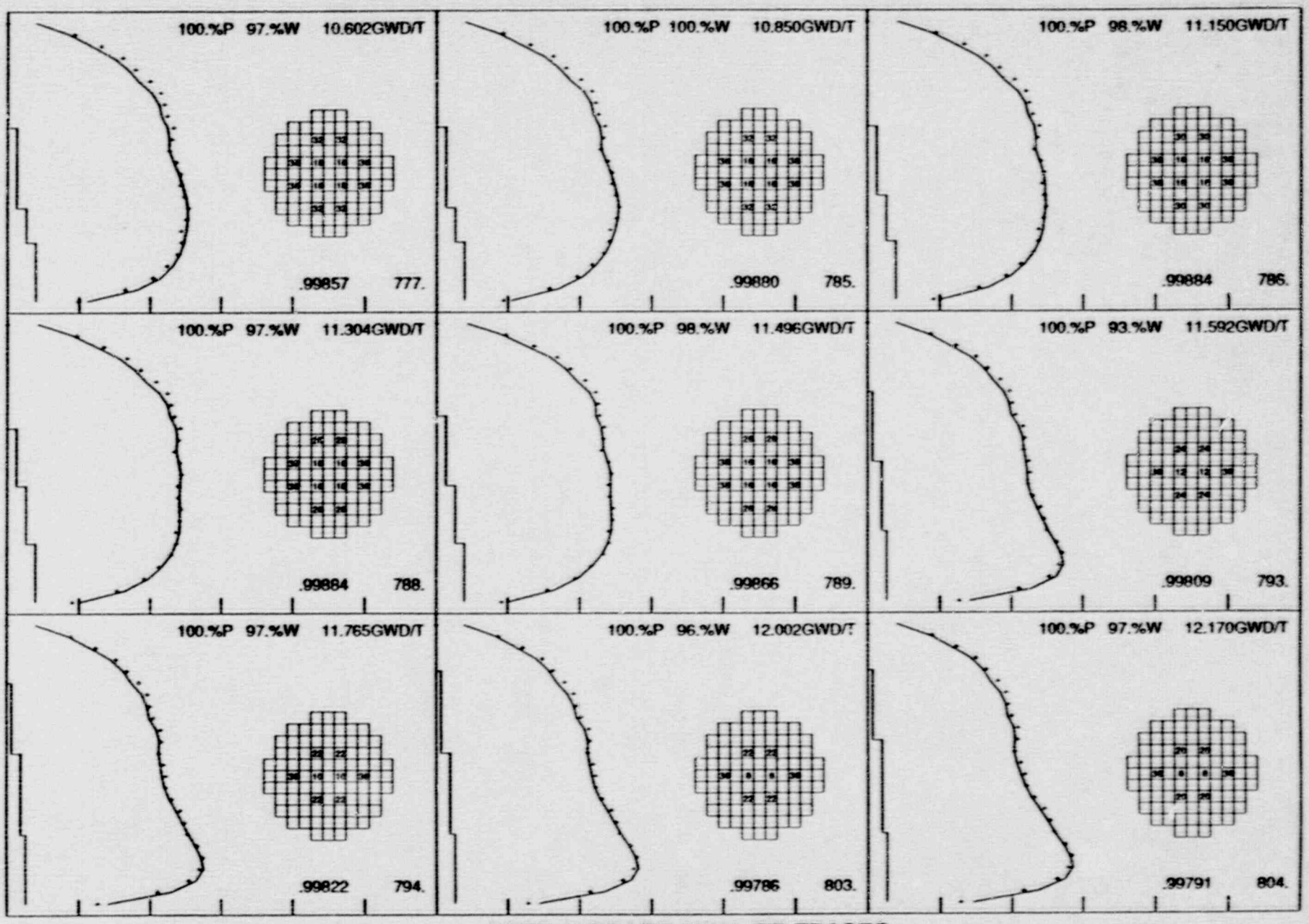

CORE AVERAGE AXIAL TIP TRACES

(*) $USER.DEP8.CYCLE10.S3I0008B S3I008B VERMONT YANKEE 01/24/89 17:04:55 2.30-SUN 88/09/09

(X) $USER.DEP8.CYCLE10.S3I0006B S3I008B VERMONT YANKEE 01/24/89 17:04:55 2.30-SUN 88/09/09

FIGURE D.4

Cycle 10 Core Average Axial TIP Comparisons by TIP Set

VY CYCLE 10 DEPLETION

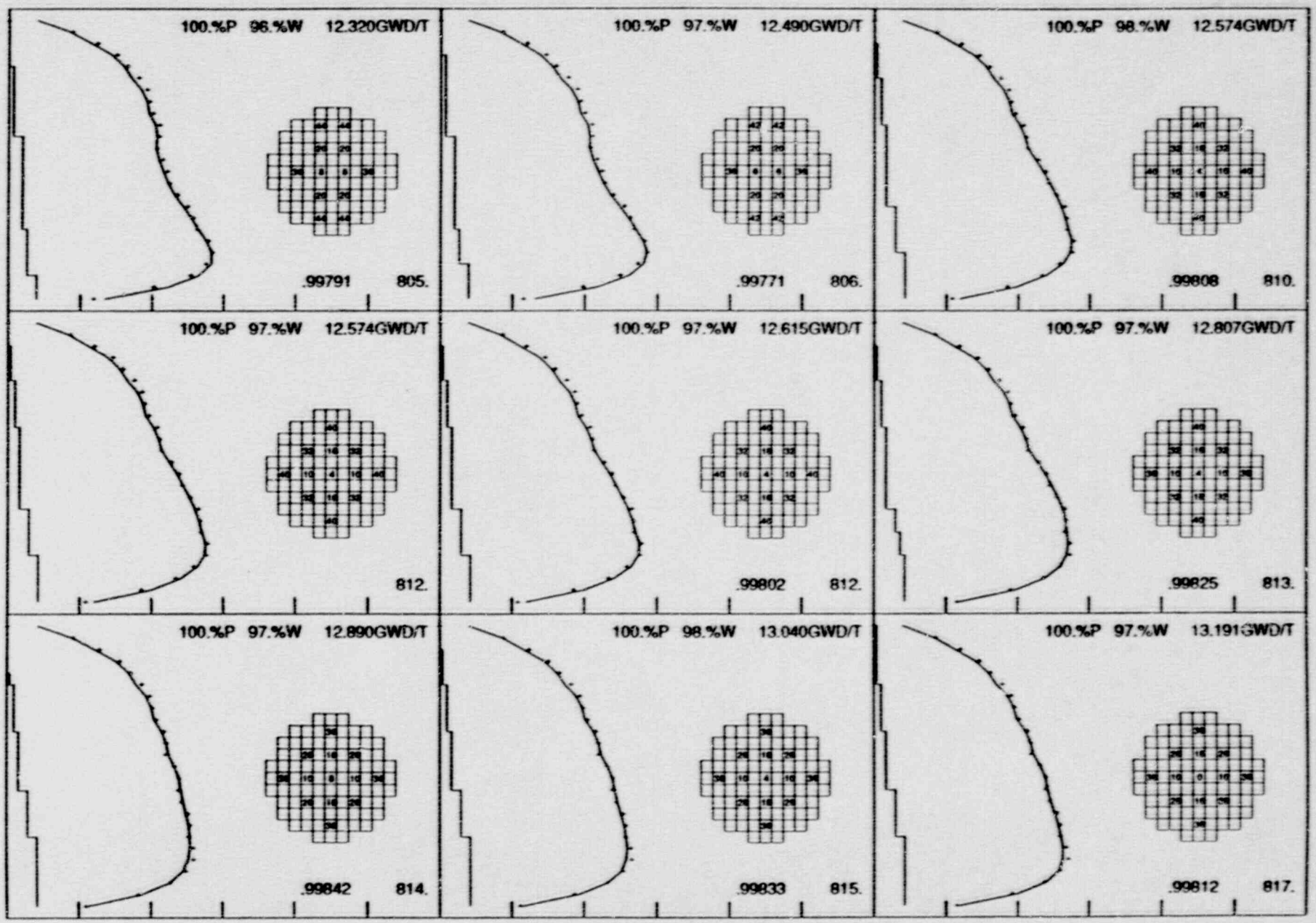

CORE AVERAGE AXIAL TIP TRACES

(*) $USER.DEP6.CYCLE10.S3D006B S3D006B VERMONT YANKEE 01/24/89 17:04:55 2.30-SUN 88/09/02
(X) $USER.DEP6.CYCLE10.S3D006B S3D006B VERMONT YANKEE 01/24/89 17:04:55 2.30-SUN 88/09/09

FIGURE D.4 (Continued)

VY CYCLE 10 DEPLETION

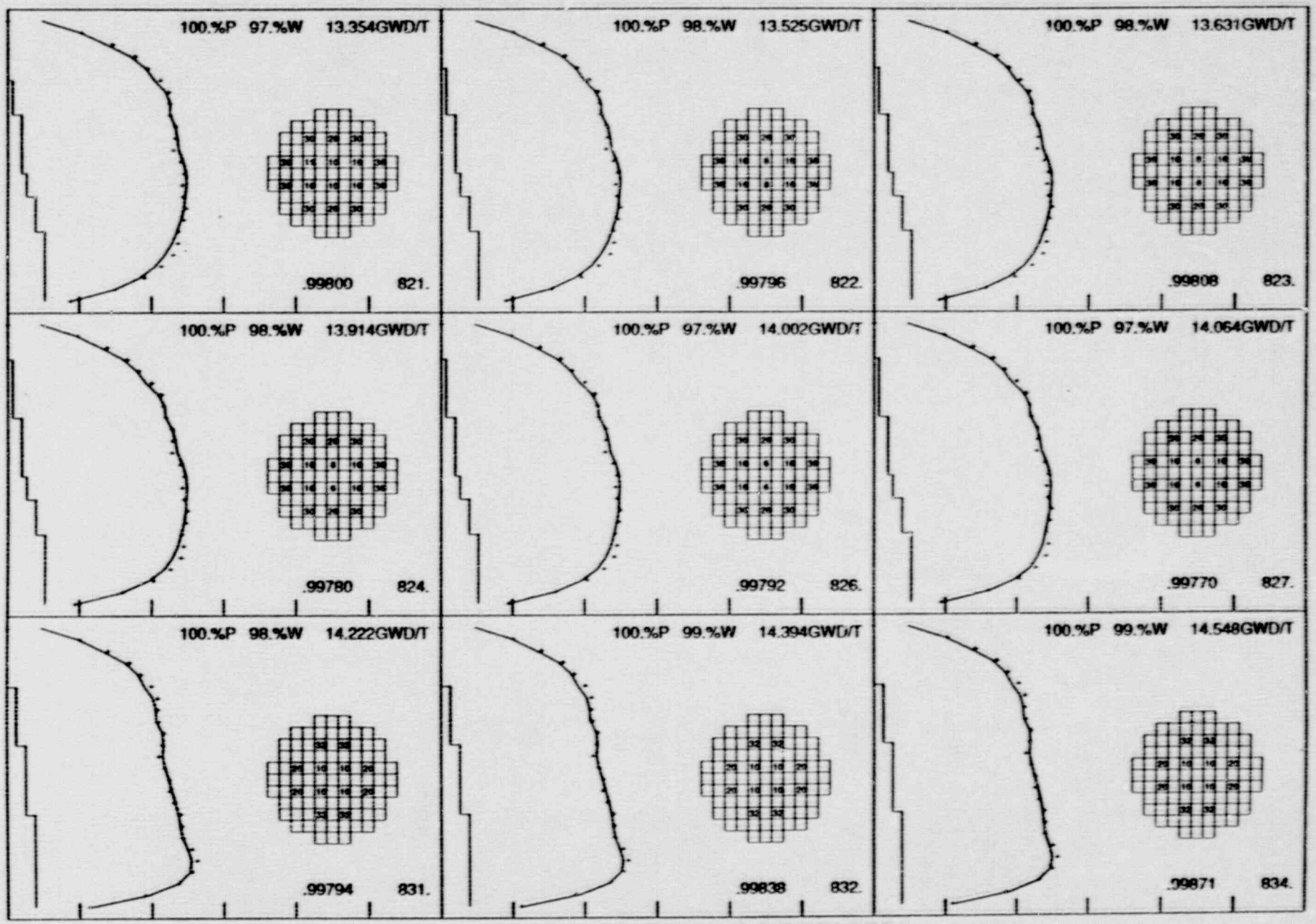

CORE AVERAGE AXIAL TIP TRACES

(*) $USER.DEP8.CYCLE10.S3300068 S300068 VERMONT YANKEE 01/24/89 17:04:55 2.30-SUN 88/09/09
(X) $USER.DEP8.CYCLE10.S3300068 S300068 VERMONT YANKEE 01/24/89 17:04:55 2.30-SUN 88/09/09

FIGURE D.4 (Continued)

VY CYCLE 10 DEPLETION

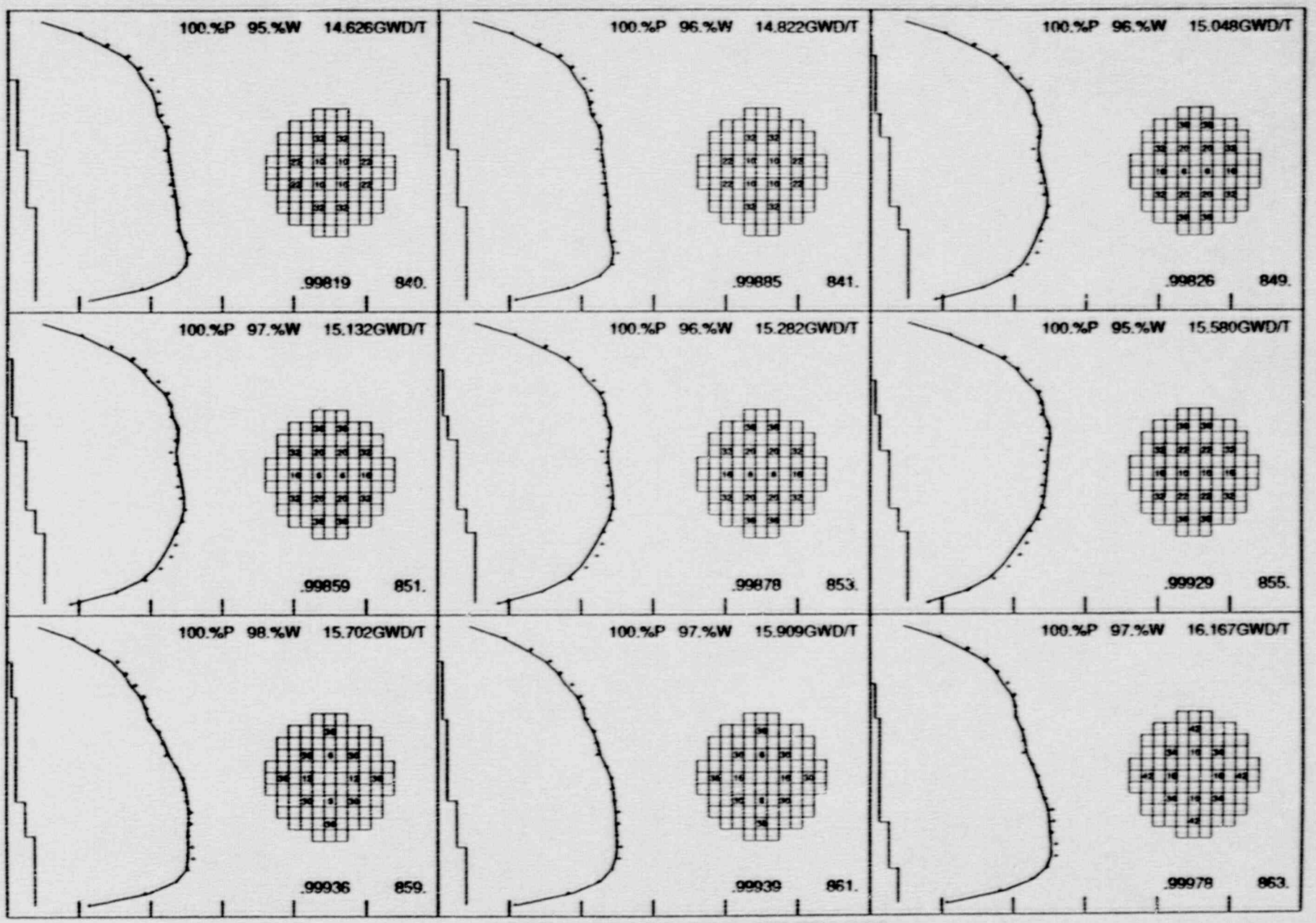

CORE AVERAGE AXIAL TIP TRACES

(*) $USER.DEP8.CYCLE10.S3S006B S3I006B VERMONT YANKEE 01/24/89 17:04:55 2.30-SUN 88/09/09
(X) $USER.DEP8.CYCLE10.S3D006B S3I006B VERMONT YANKEE 01/24/89 17:04:55 2.30-SUN 88/09/09

FIGURE D.4 (Continued)

VY CYCLE 10 DEPLETION

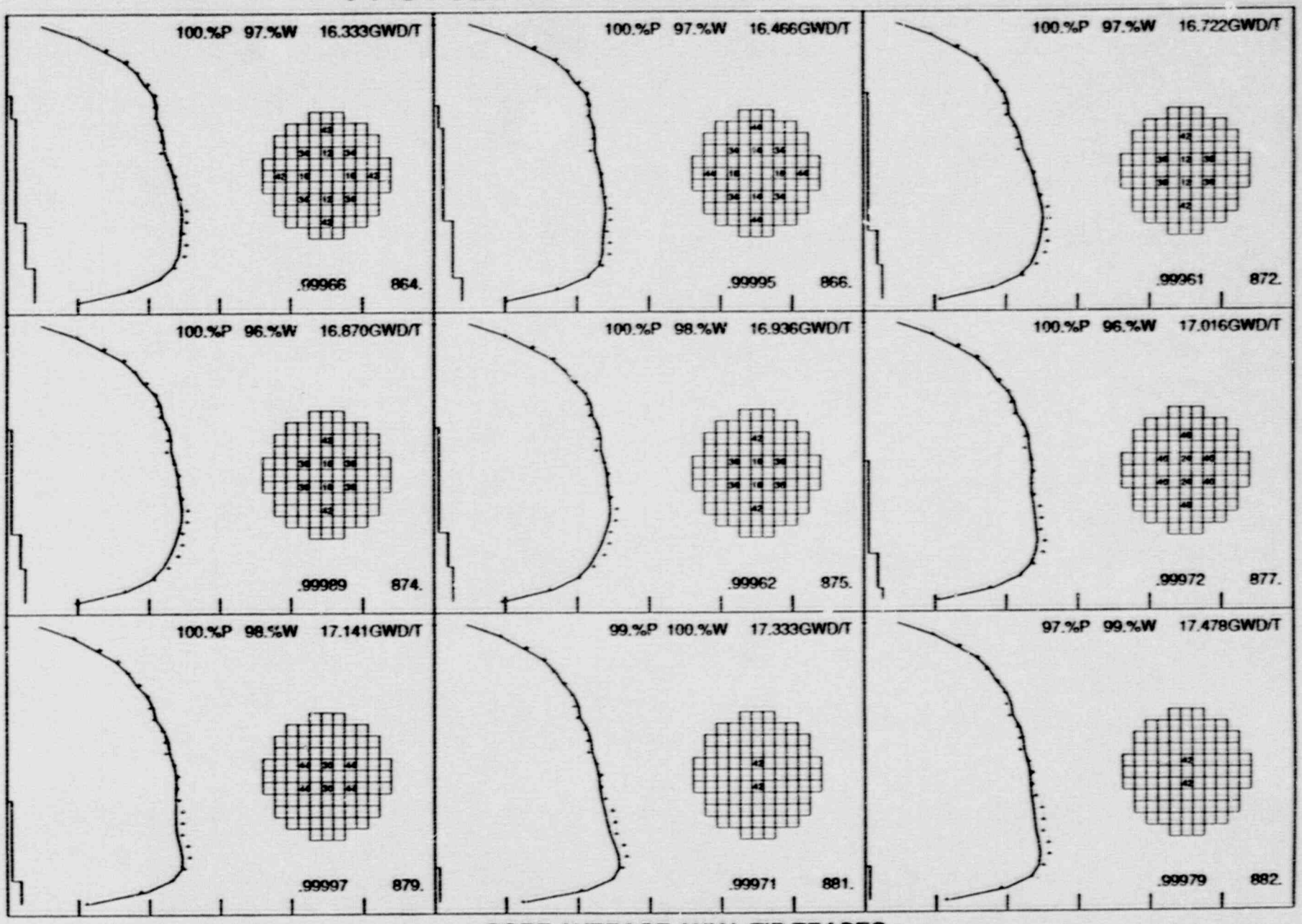

CORE AVERAGE AXIAL TIP TRACES

(*) $USER.DEP8.CYCLE10.S3S0068 S3I0068 VERMONT YANKEE 01/24/89 17:04:55 2:30-SUN 88/09/09
(X) $USER.DEP8.CYCLE10.S3I0068 S3I0068 VERMONT YANKEE 01/24/89 17:04:55 2:30-SUN 88/09/09

FIGURE D.4 (Continued)

VY CYCLE 10 DEPLETION

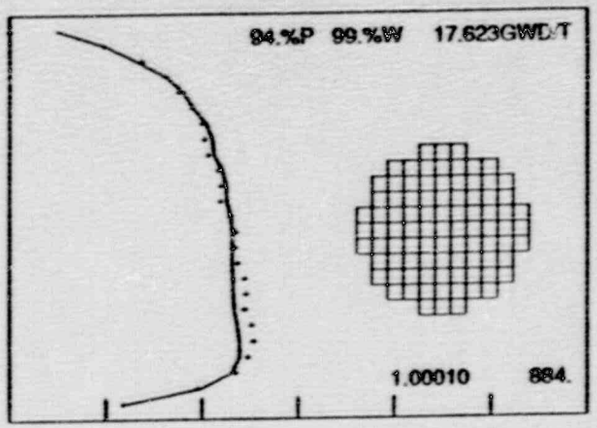

FIGURE D.4 (Continued)

CORE AVERAGE AXIAL TIP TRACES

(*) $USER.DEP8.CYCLE10.S3D0088 S3D088 VERMONT YANKEE 01/24/99 17:04:55 2.30-SUN 02/07/09
(X) $USER.DEP8.CYCLE10.S3D0088 S3D088 VERMONT YANKEE 01/24/99 17:03:55 2.30-SUN 02/07/09

FIGURE D.5

Cycle 11 Averaged TIP Integral Errors, Standard Deviations, and RMS Errors

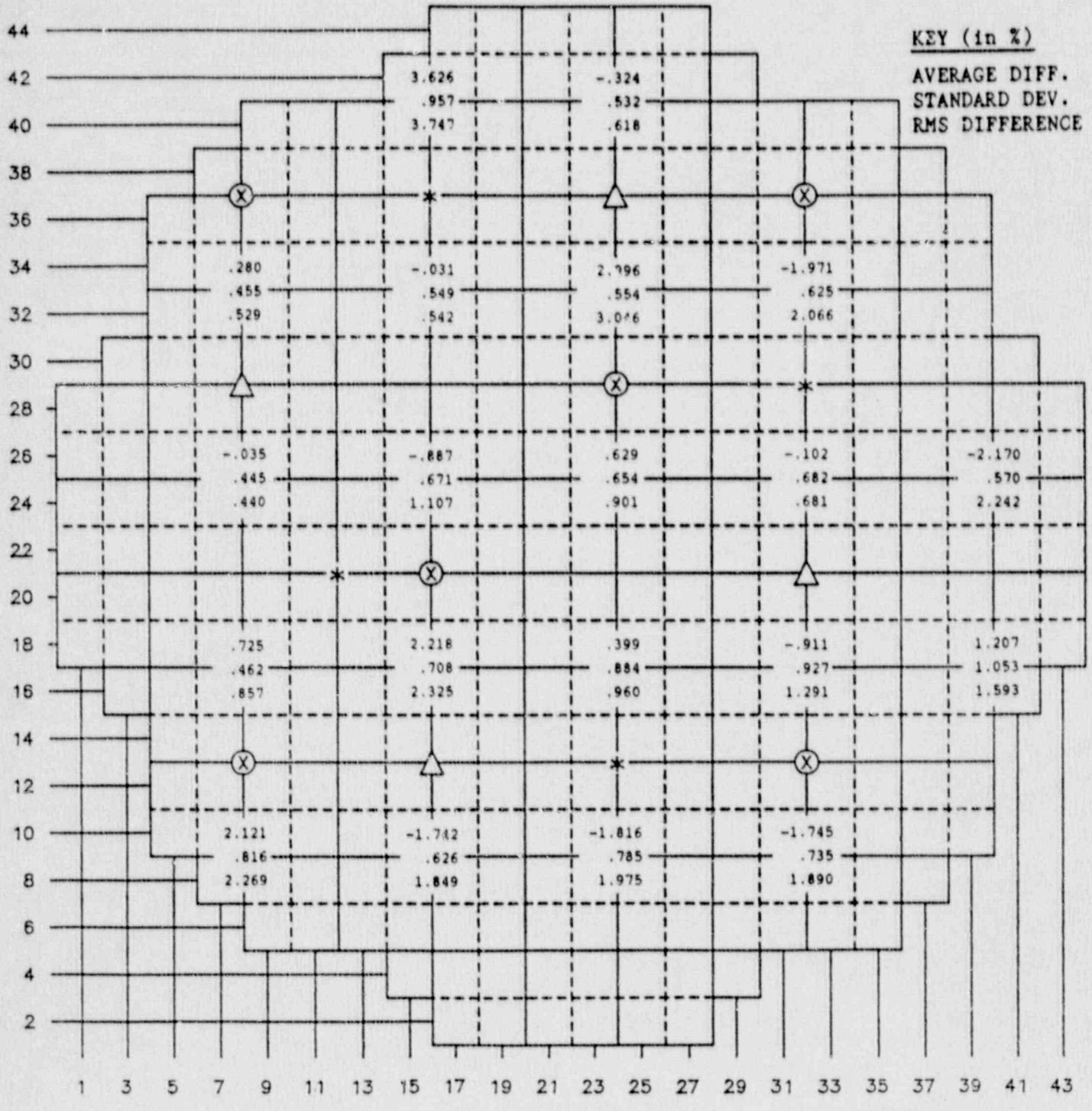

VY CYCLE 11 DEPLETION

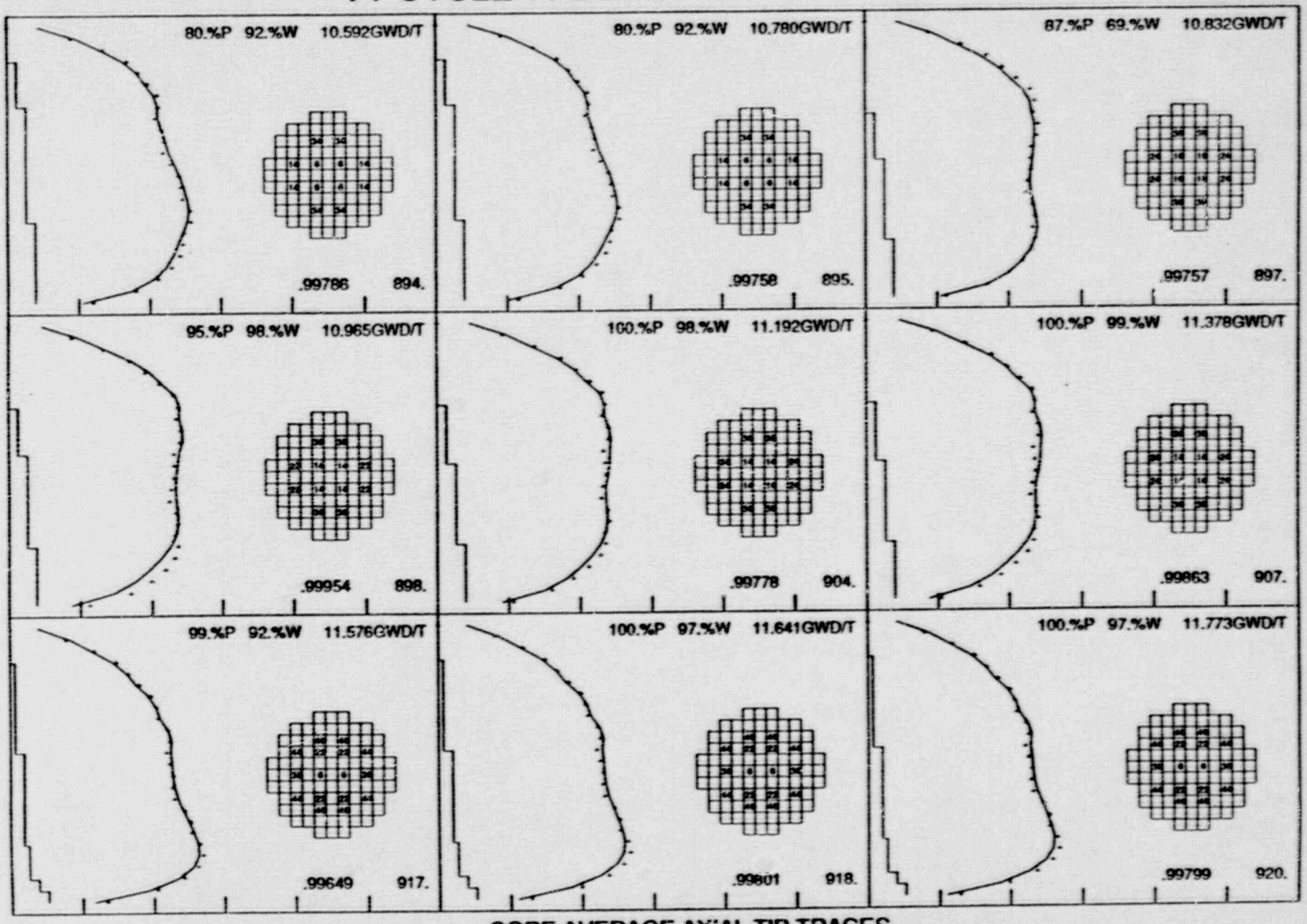

CORE AVERAGE AXIAL TIP TRACES

(*) $USER.DEP8.CYCLE11.S3S108B S3I108B VERMONT YANKEE 01/25/89 11:35:42 2.30-SUN 89/09/09
(X) $USER.DEP8.CYCLE11.S3D108B S3I108B VERMONT YANKEE 01/25/89 11:35:42 2.30-SUN 89/09/09

FIGURE D.6
Cycle 11 Core Average Axial TIP Comparisons by TIP Set

VY CYCLE 11 DEPLETION

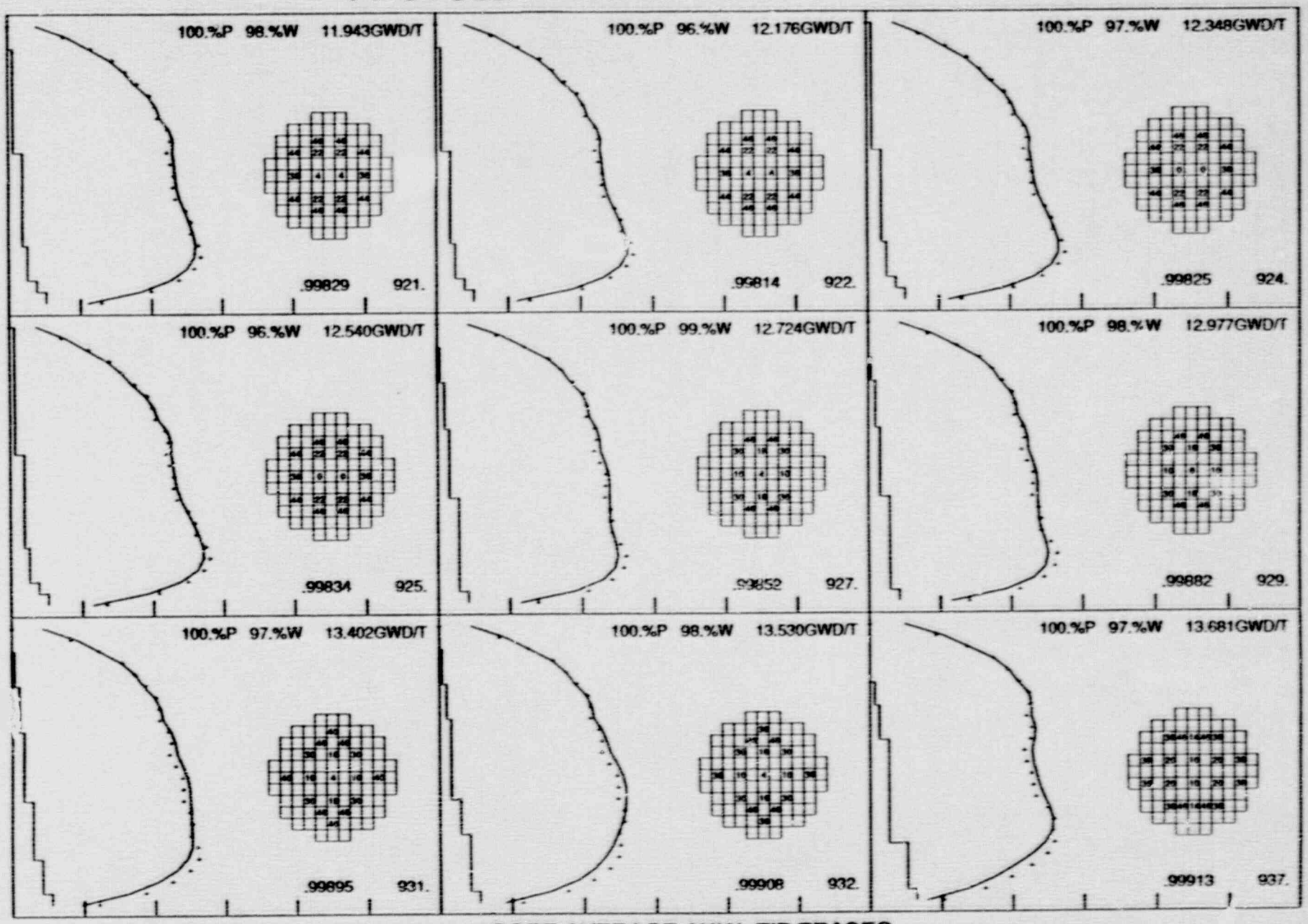

CORE AVERAGE AXIAL TIP TRACES

(') $USER.DEP8.CYCLE11.S3S106B S3I106B VERMONT YANKEE 01/25/89 11:35:42 2.30-SUN 88/09/09
(X) $USER.DEP8.CYCLE11.S3D106B S3I106B VERMONT YANKEE 01/25/89 11:35:42 2.30-SUN 88/09/09

FIGURE D.6 (Continued)

VY CYCLE 11 DEPLETION

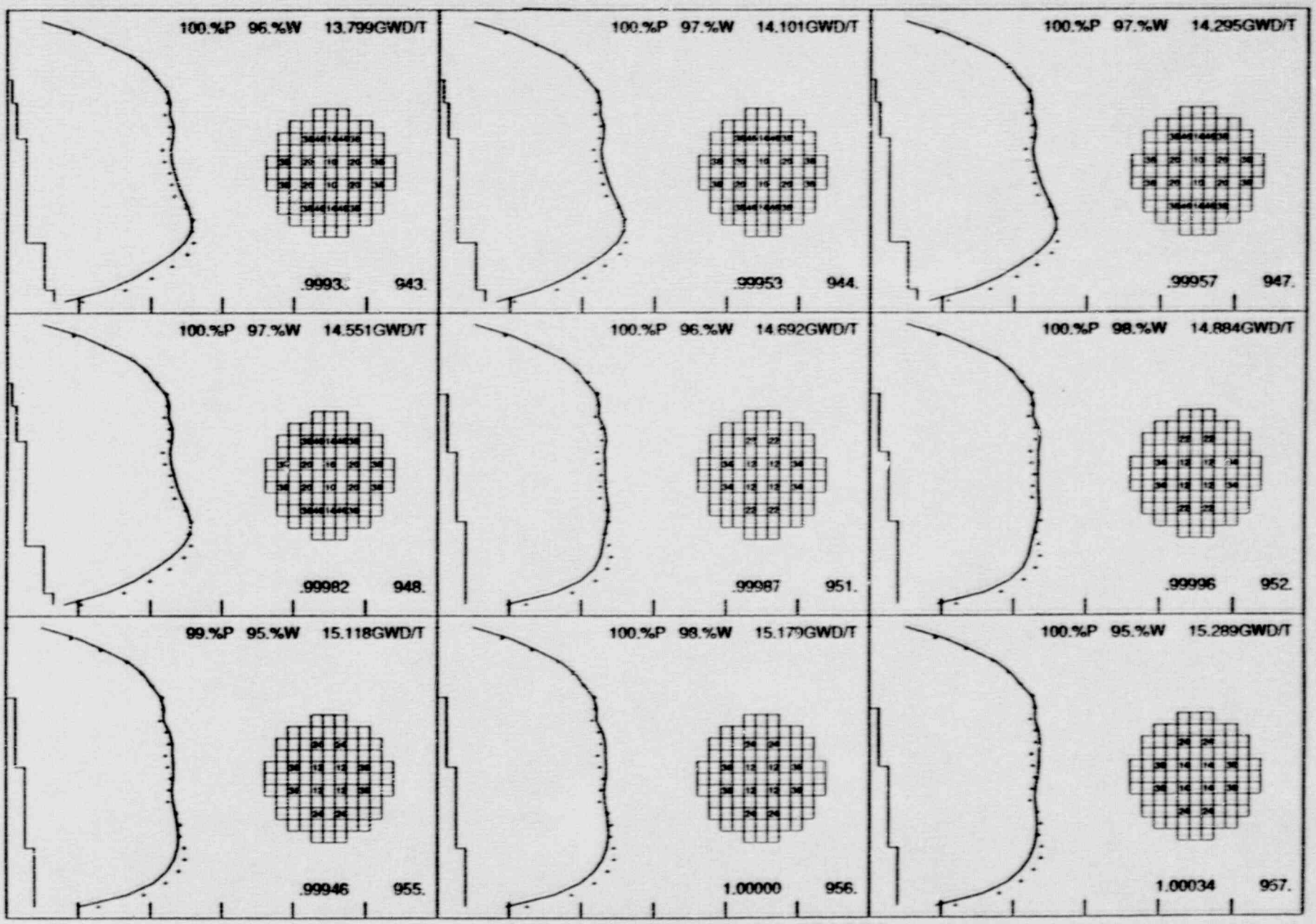

CORE AVERAGE AXIAL TIP TRACES

(*) $USER.DEP8.CYCLE11.S3S106B S3I106B VERMONT YANKEE 01/25/89 11:35:42 2.30-SUN 88/09/09
(X) $USER.DEP8.CYCLE11.S3D106B S3I106B VERMONT YANKEE 01/25/89 11:35:42 2.30-SUN 88/09/09

FIGURE D.6 (Continued)

VY CYCLE 11 DEPLETION

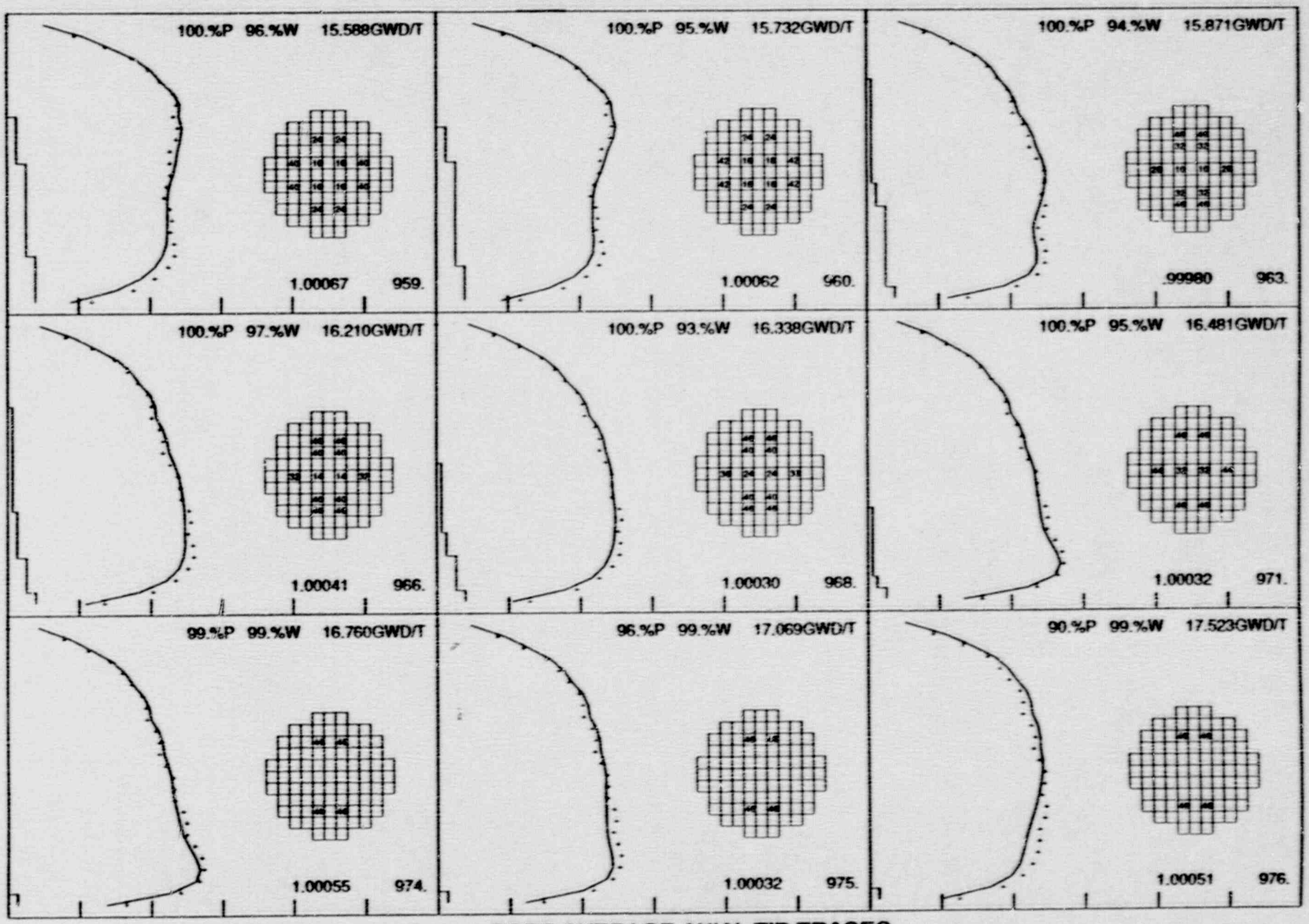

CORE AVERAGE AXIAL TIP TRACES

(*) $USER.DEP8.CYCLE11.S3S108B S3I108B VERMONT YANKEE 01/25/89 11:35:42 2.30-SUN 88/09/09
(X) $USER.DEP8.CYCLE11.S3O108B S3I108B VERMONT YANKEE 01/25/89 11:35:42 2.30-SUN 88/09/09

FIGURE D.6 (Continued)

VY CYCLE 11 DEPLETION

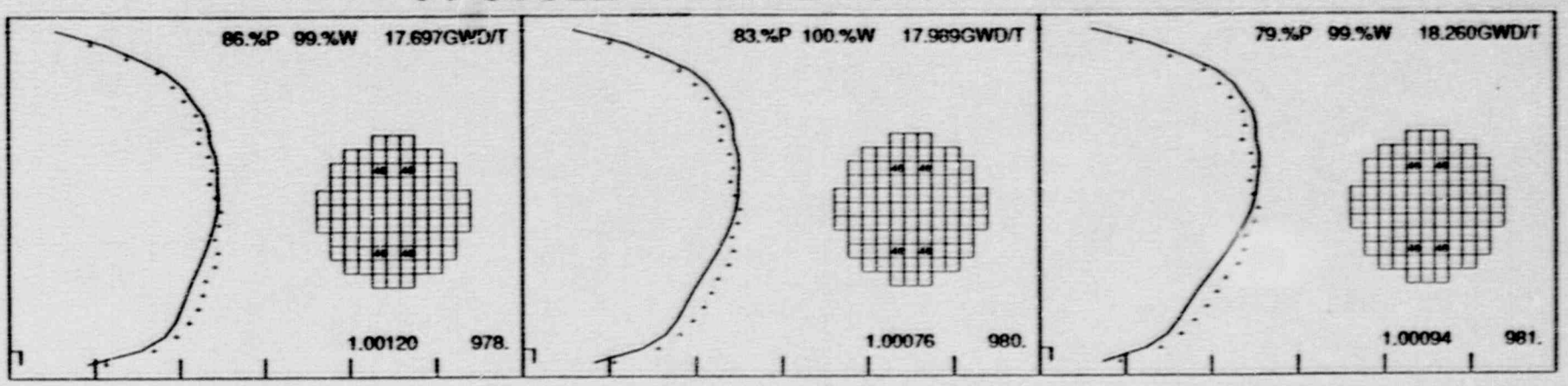

FIGURE D.6 (Continued)

CORE AVERAGE AXIAL TIP TRACES

(*) $USER.DEP8.CYCLE11.S3S1088 S3I1088 VERMONT YANKEE 01/25/89 11:35:42 2.30-SUN 88/09/09
(X) $USER.DEP8.CYCLE11.S3D1088 S3I1088 VERMONT YANKEE 01/25/89 11:35:42 2.30-SUN 88/09/09

FIGURE D.7

Cycle 12 Averaged TIP Integral Errors, Standard Deviations, and RMS Errors

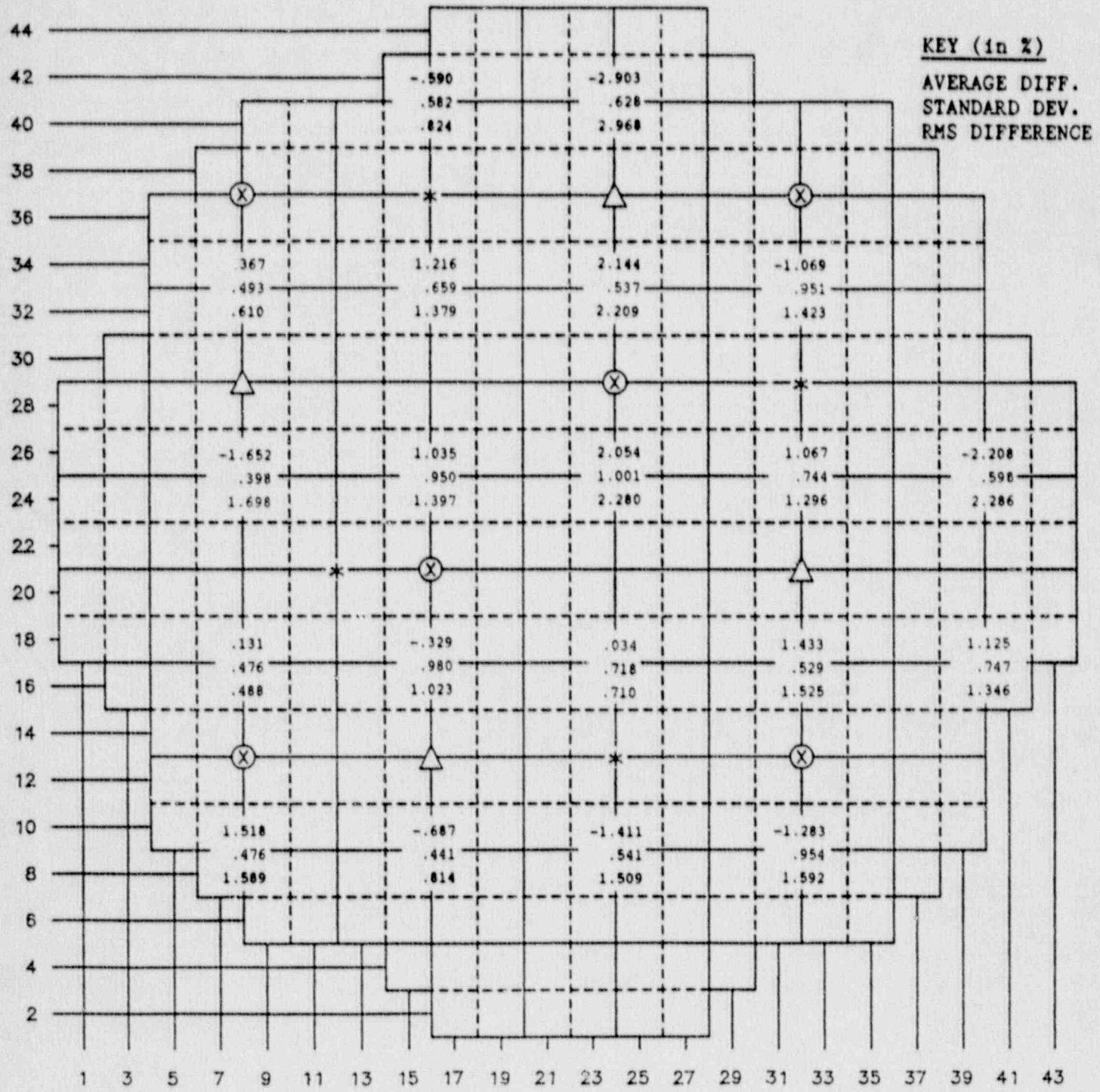

VY CYCLE 12 DEPLETION

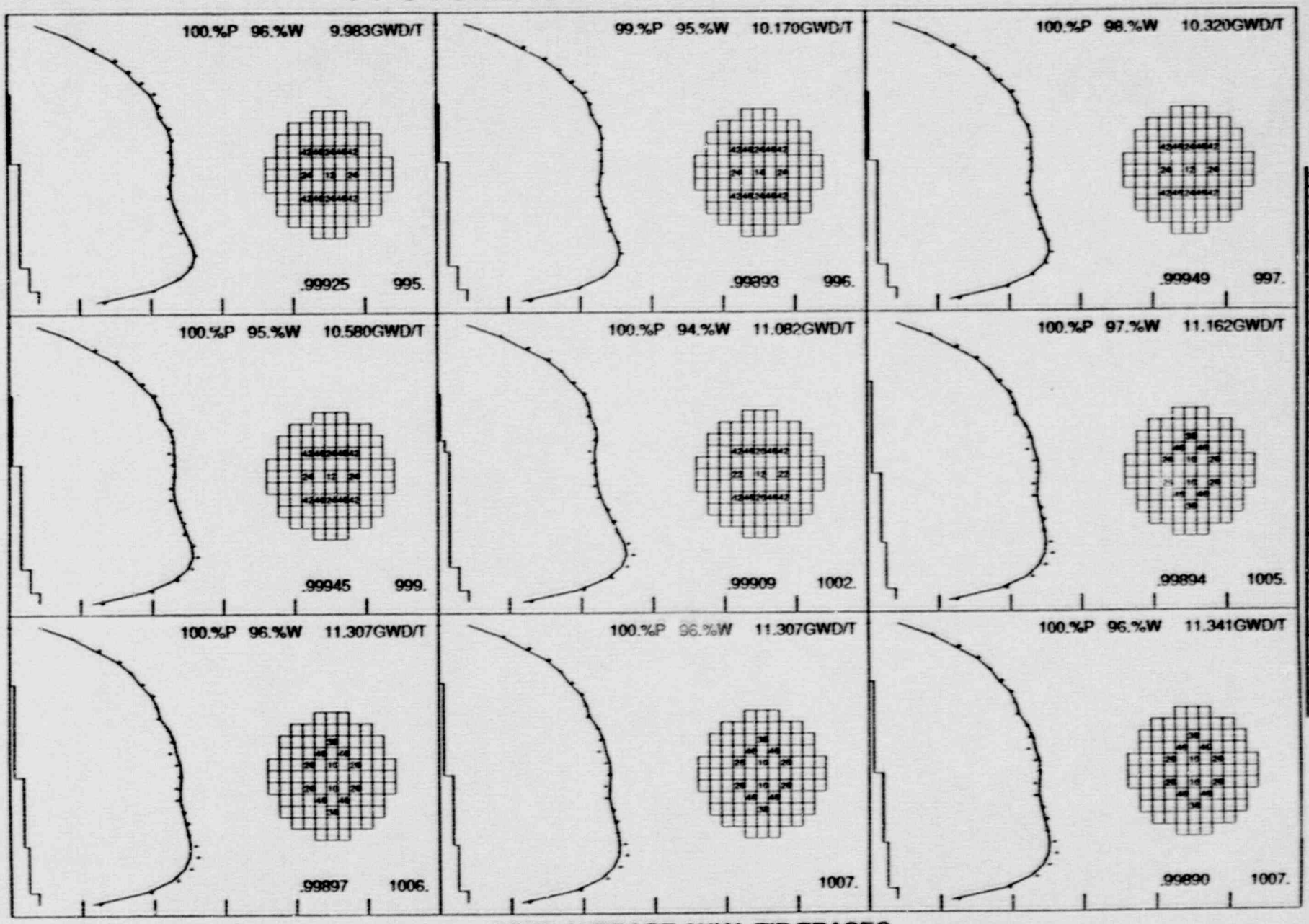

CORE AVERAGE AXIAL TIP TRACES

(*) $USER.DEP6.CYCLE12.S3S206B S3I206B VERMONT YANKEE 01/26/99 08:50:07 2.30-SUN 88/09/09
(X) $USER.DEP6.CYCLE12.S3D206B S3I206B VERMONT YANKEE 01/26/99 08:50:07 2.30-SUN 88/09/09

FIGURE D.8
Cycle 12 Core Average Axial TIP Comparisons by TIP Set

VY CYCLE 12 DEPLETION

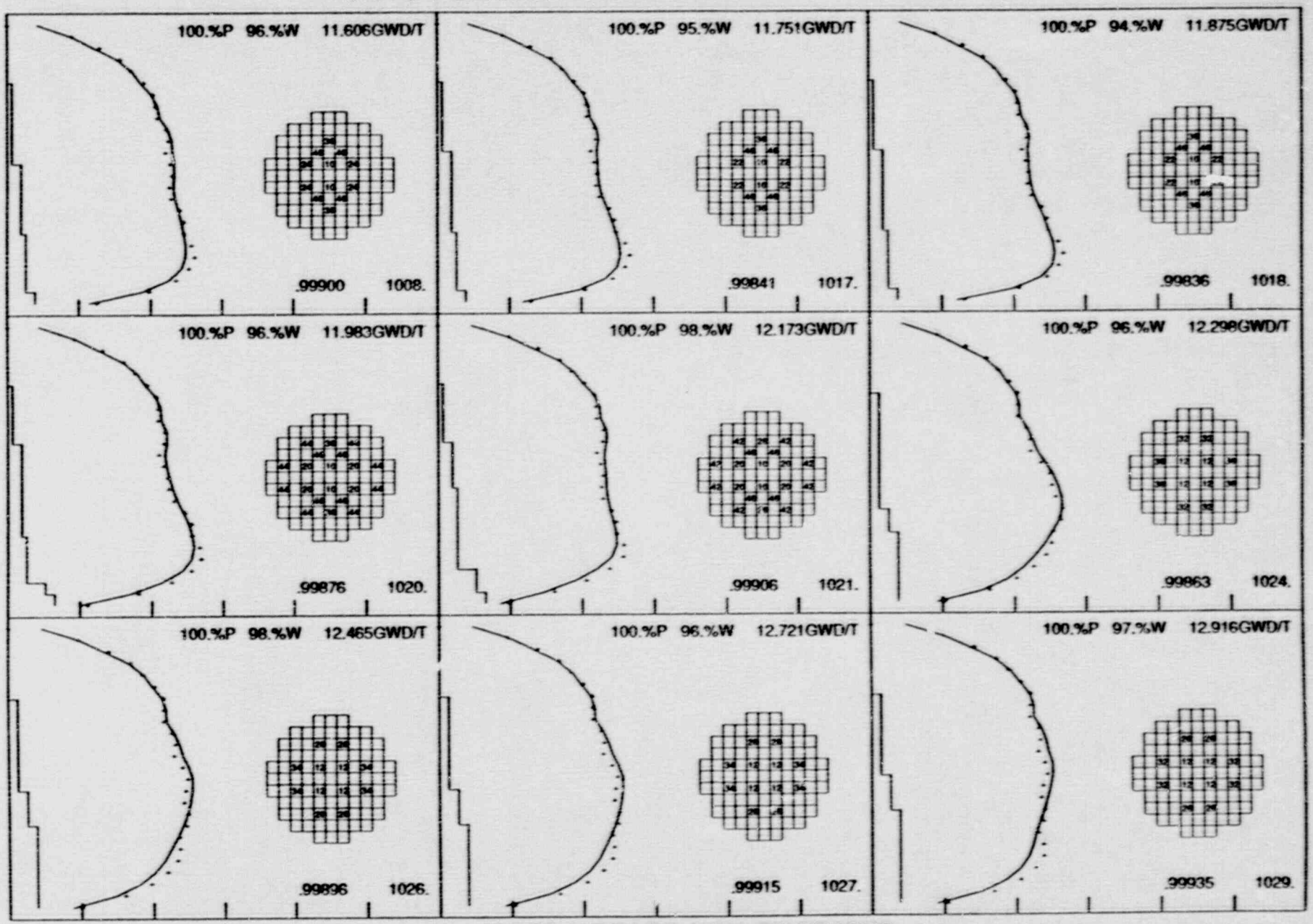

CORE AVERAGE AXIAL TIP TRACES

(*) $USER.DEP8.CYCLE12.S352068 S32068 VERMONT YANKEE 01/26/89 08:50:07 2.30-SUN 88/09/06
(X) $USER.DEP8.CYCLE12.S302068 S32068 VERMONT YANKEE 01/26/89 08:50:07 2.30-SUN 88/09/09

FIGURE D.8 (Continued)

VY CYCLE 12 DEPLETION

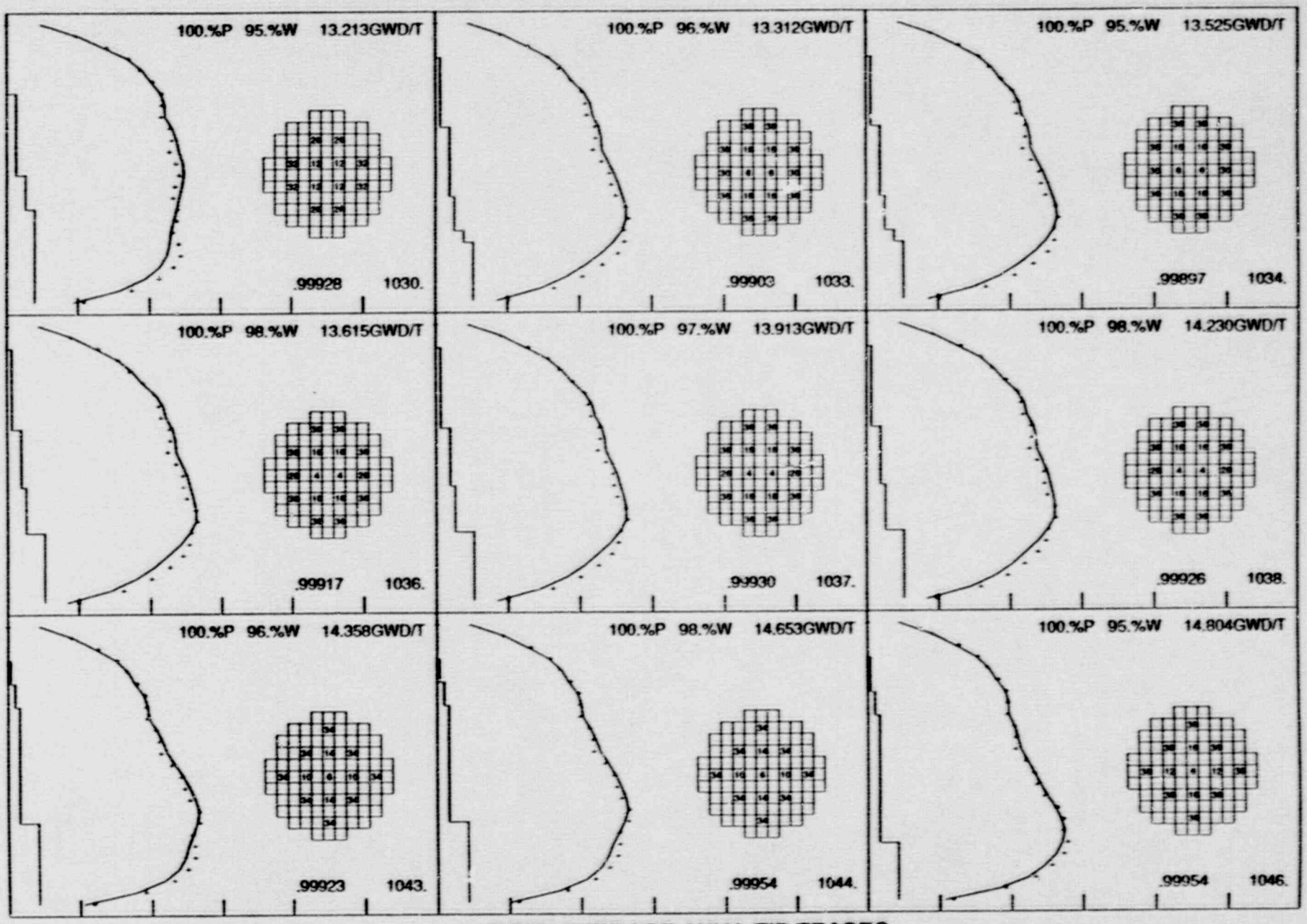

CORE AVERAGE AXIAL TIP TRACES

(*) $USER.DEP8.CYCLE12.S3S206B S3I206B VERMONT YANKEE 01/26/89 08:50:07 2.30-SUN 89/09/09
(X) $USER.DEP8.CYCLE12.S3D206B S3I206B VERMONT YANKEE 01/26/89 08:50:07 2.30-SUN 89/09/09

FIGURE D.8 (Continued)

VY CYCLE 12 DEPLETION

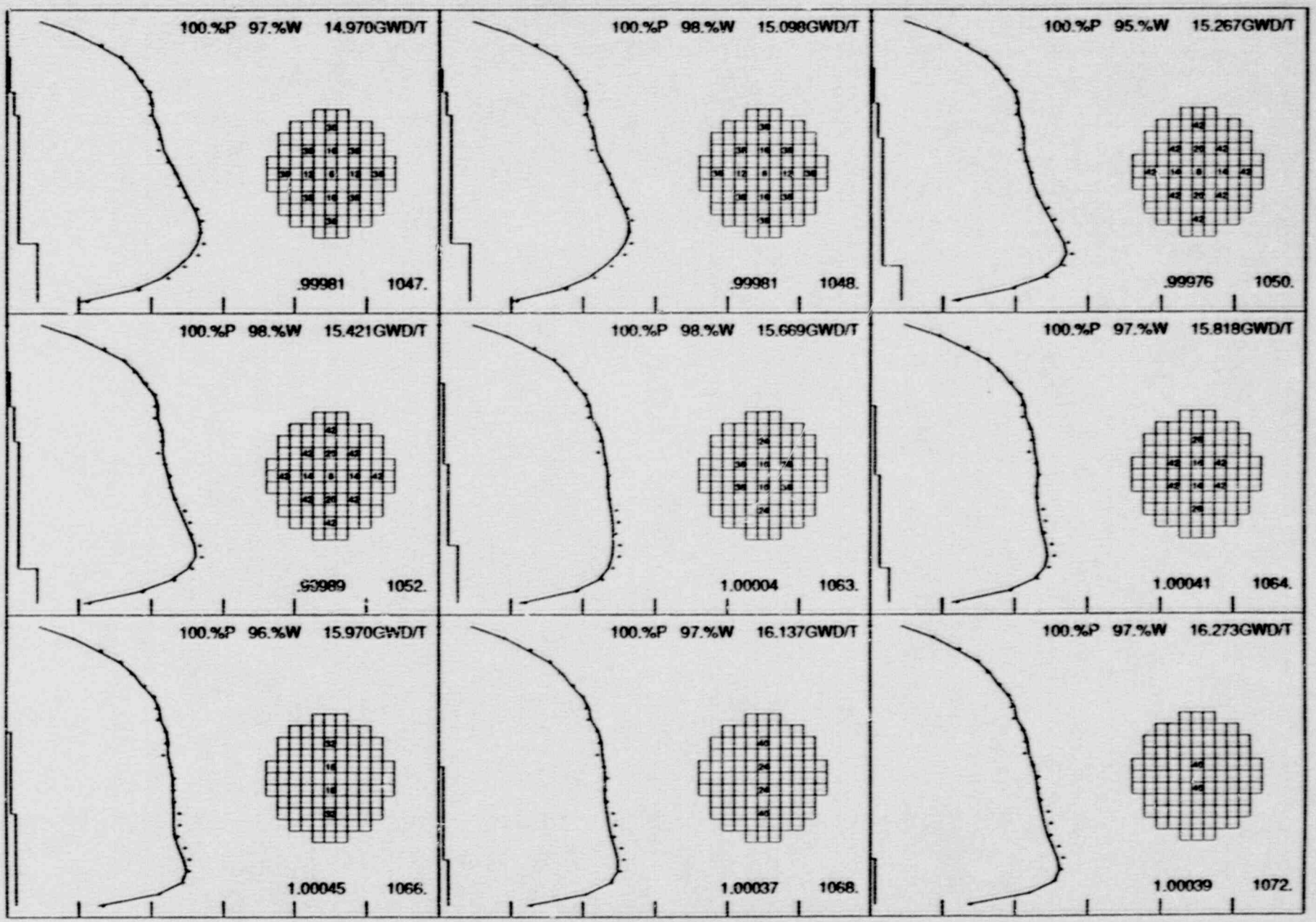

CORE AVERAGE AXIAL TIP TRACES

(*) $USER.DEP8.CYCLE12.S3S208B S3I208B VERMONT YANKEE 01/26/89 08:50:07 2.30-SUN 88/09/09
(X) $USER.DEP8.CYCLE12.S3D208B S3I208B VERMONT YANKEE 01/26/89 08:50:07 2.30-SUN 88/09/09

FIGURE D.8 (Continued)

VY CYCLE 12 DEPLETION

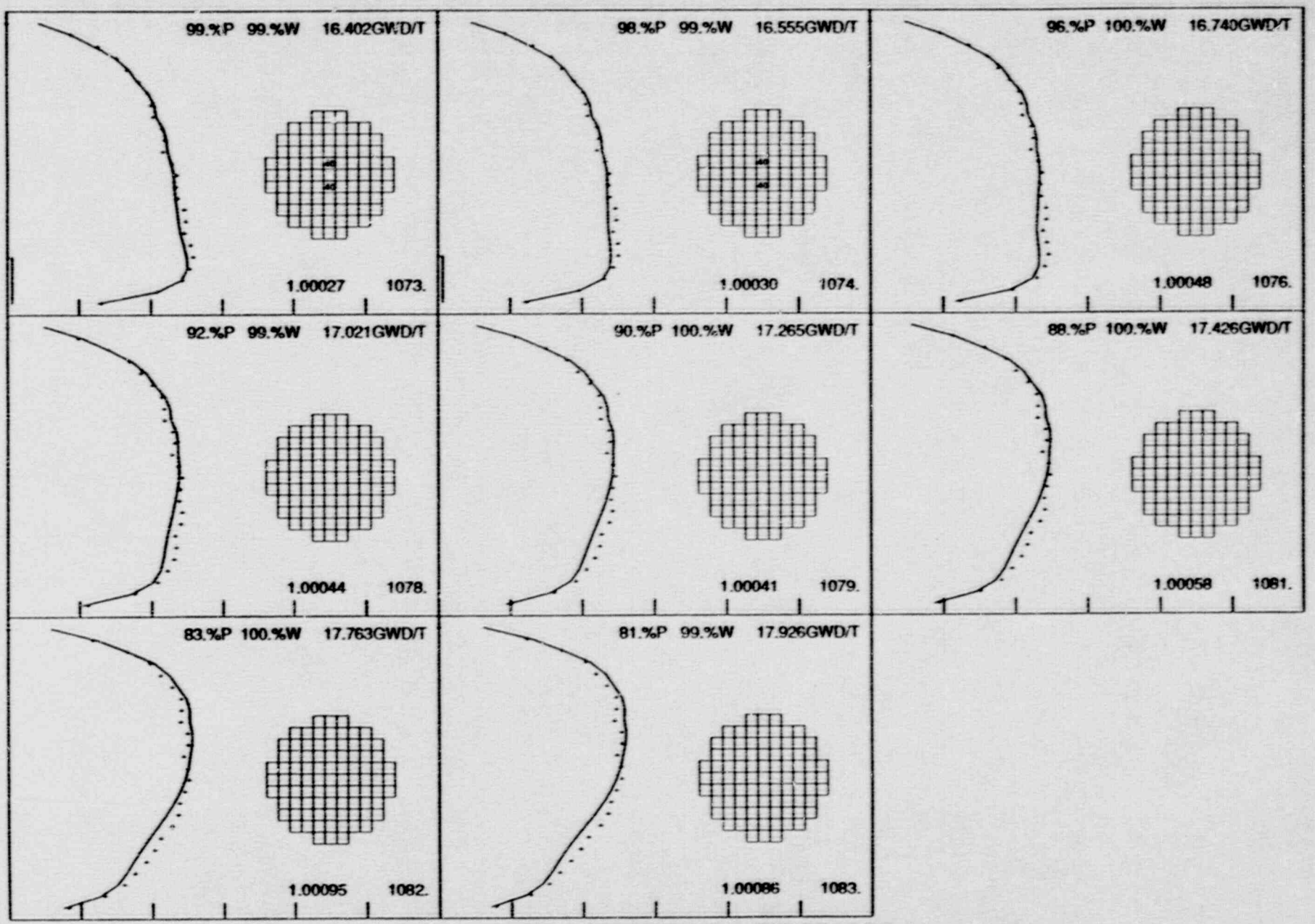

CORE AVERAGE AXIAL TIP TRACES

(*) $USER.DEP8.CYCLE12.S3S206B S3I206B VERMONT YANKEE 01/26/89 08:50:07 2.30-SUN 88/09/09
(X) $USER.DEP8.CYCLE12.S3D206B S3I206B VERMONT YANKEE 01/26/89 08:50:07 2.30-SUN 88/09/09

FIGURE D.8 (Continued)

FIGURE D.9

Cycle 13 Averaged TIP Integral Errors, Standard Deviations, and RMS Errors

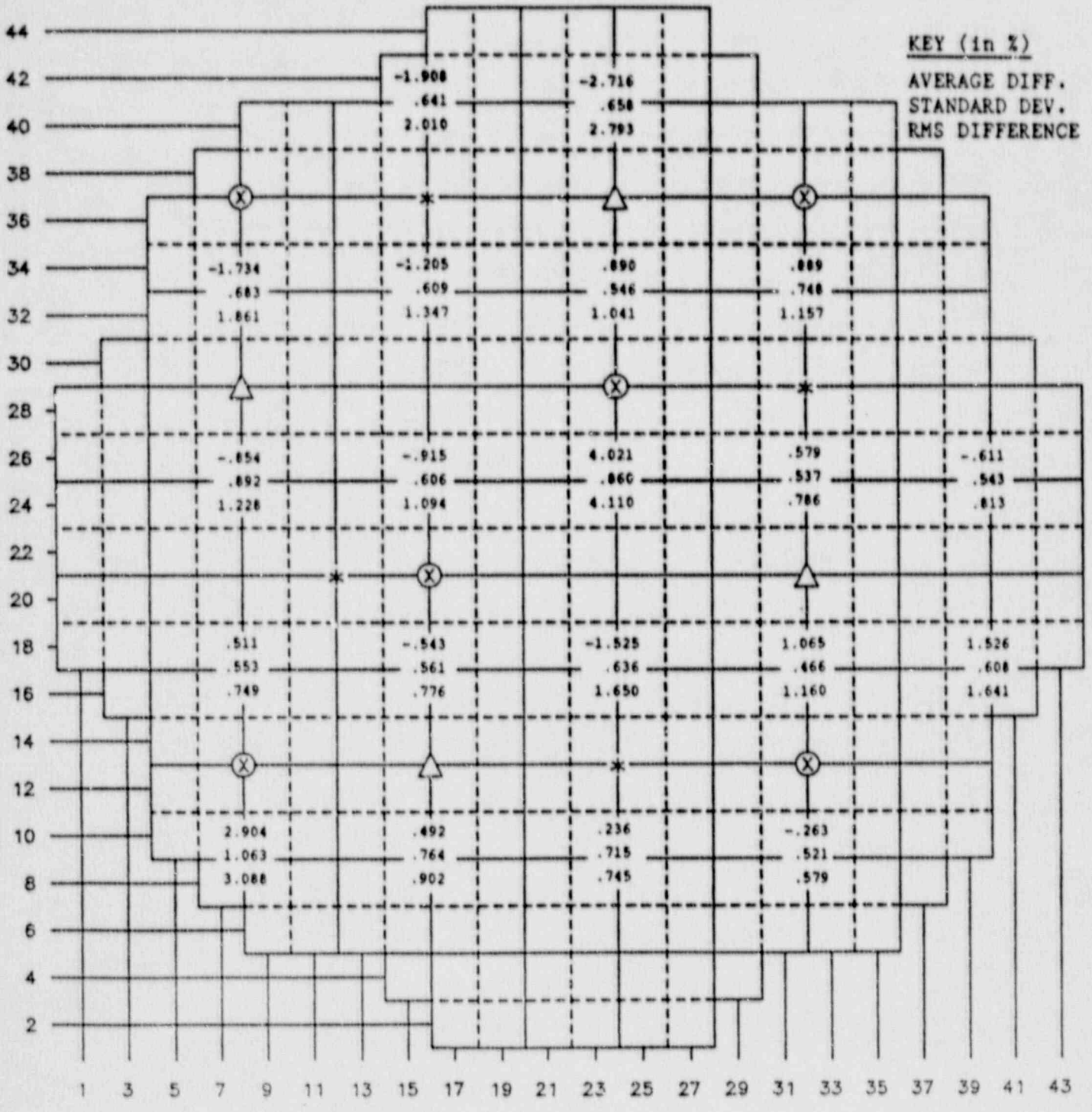

VY CYCLE 13 DEPLETION

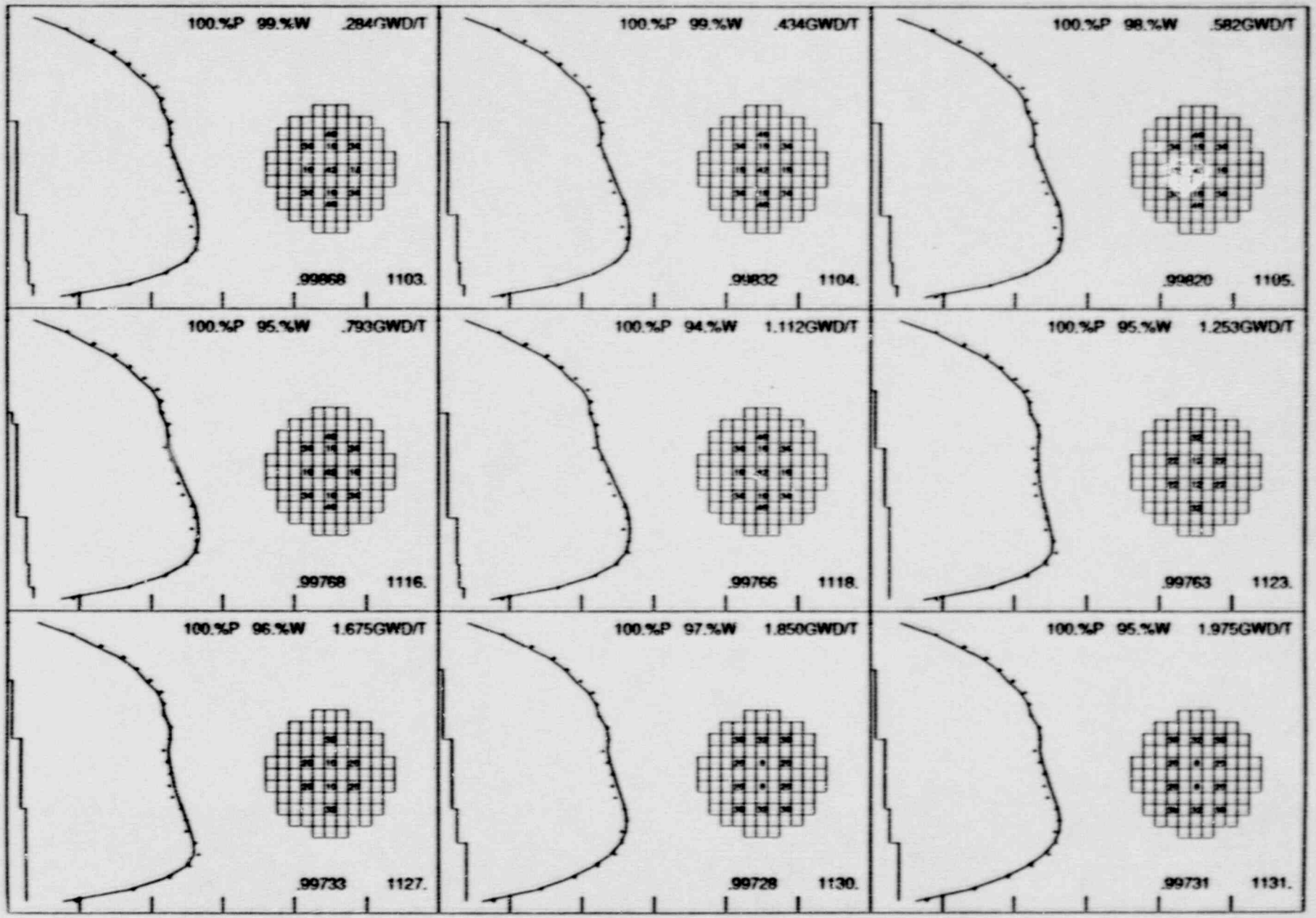

CORE AVERAGE AXIAL TIP TRACES

(*) $USER.DEP8.CYCLE13.TEMP.S3SCY13 S3S08B VERMONT YANKEE 02/21/99 09:39:04 2.30-SUN 99/09/09
(X) $USER.DEP8.CYCLE13.TEMP.S3DCY13 S3S08B VERMONT YANKEE 02/21/99 09:39:04 2.30-SUN 99/09/09

FIGURE D.10
Cycle 13 Core Average Axial TIP Comparisons by TIP Set

VY CYCLE 13 DEPLETION

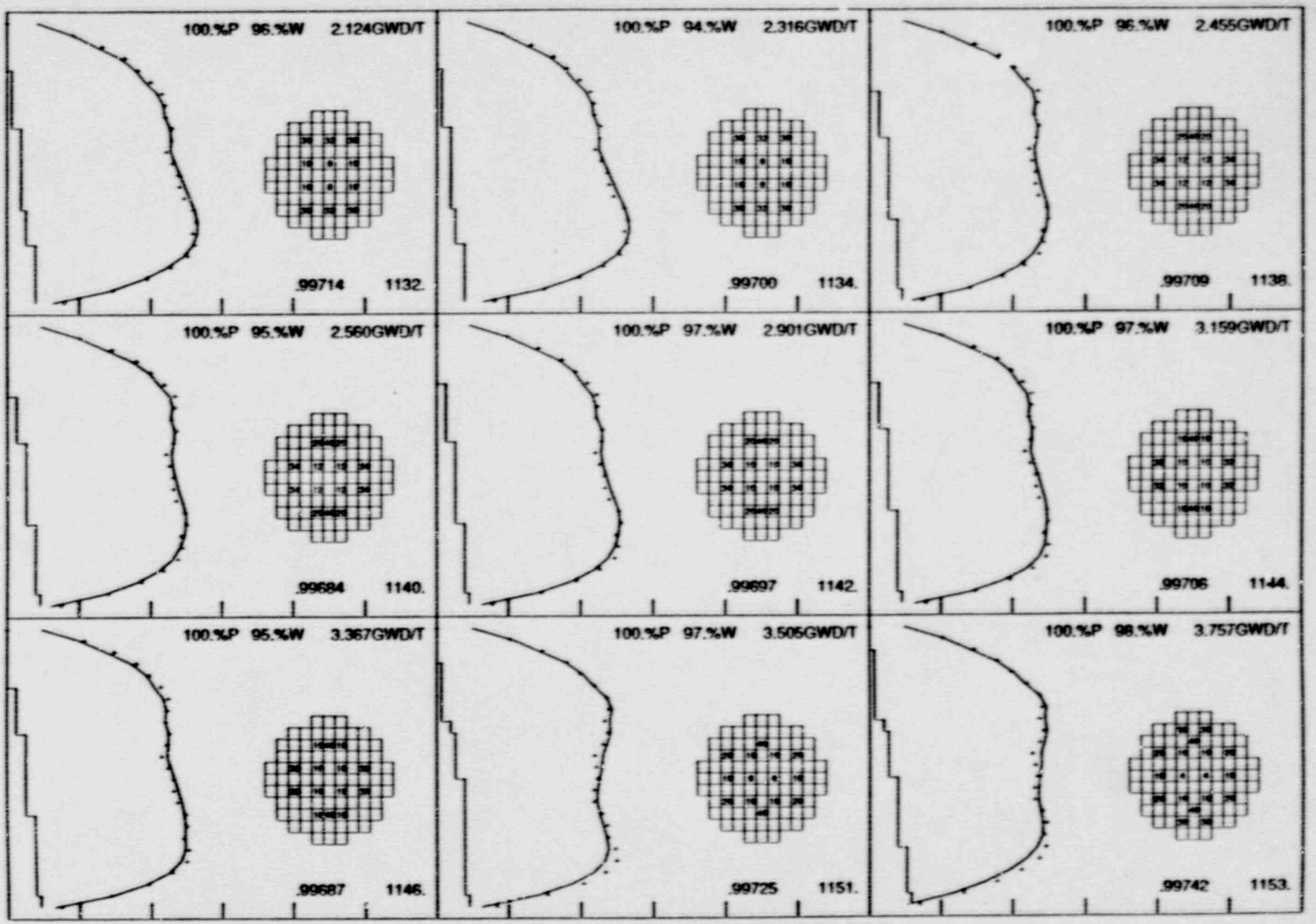

CORE AVERAGE AXIAL TIP TRACES

(*) $USER.DEP8.CYCLE13.TEMP.S35CY13 S353068 VERMONT YANKEE 02/21/89 08:38:04 2.35-SUN 88/08/09
(X) $USER.DEP8.CYCLE13.TEMP.S35DCY13 S353068 VERMONT YANKEE 02/21/89 08:38:04 2.35-SUN 88/08/09

FIGURE D.10 (Continued)

VY CYCLE 13 DEPLETION

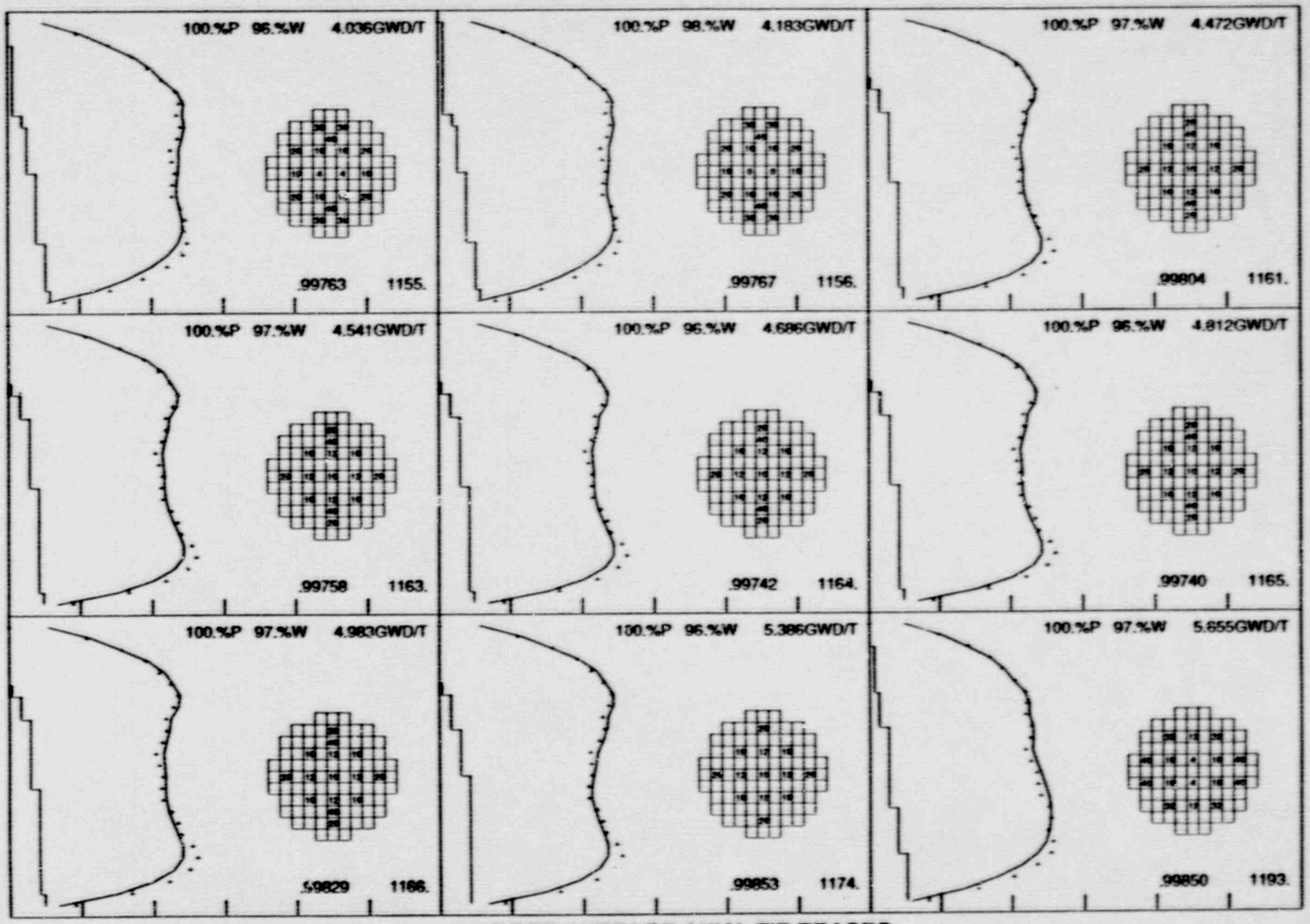

CORE AVERAGE AXIAL TIP TRACES

(*) SUSER:DEP8.CYCLE13.TEMP.S35CY13 S35088 VERMONT YANKEE 02/21/89 09:38:04 2.30-SUN 88/10/09
(X) SUSER:DEP8.CYCLE13.TEMP.S36CY13 S36088 VERMONT YANKEE 02/21/89 09:38:04 2.30-SUN 88/10/09

FIGURE D.10 (Continued)

VY CYCLE 13 DEPLETION

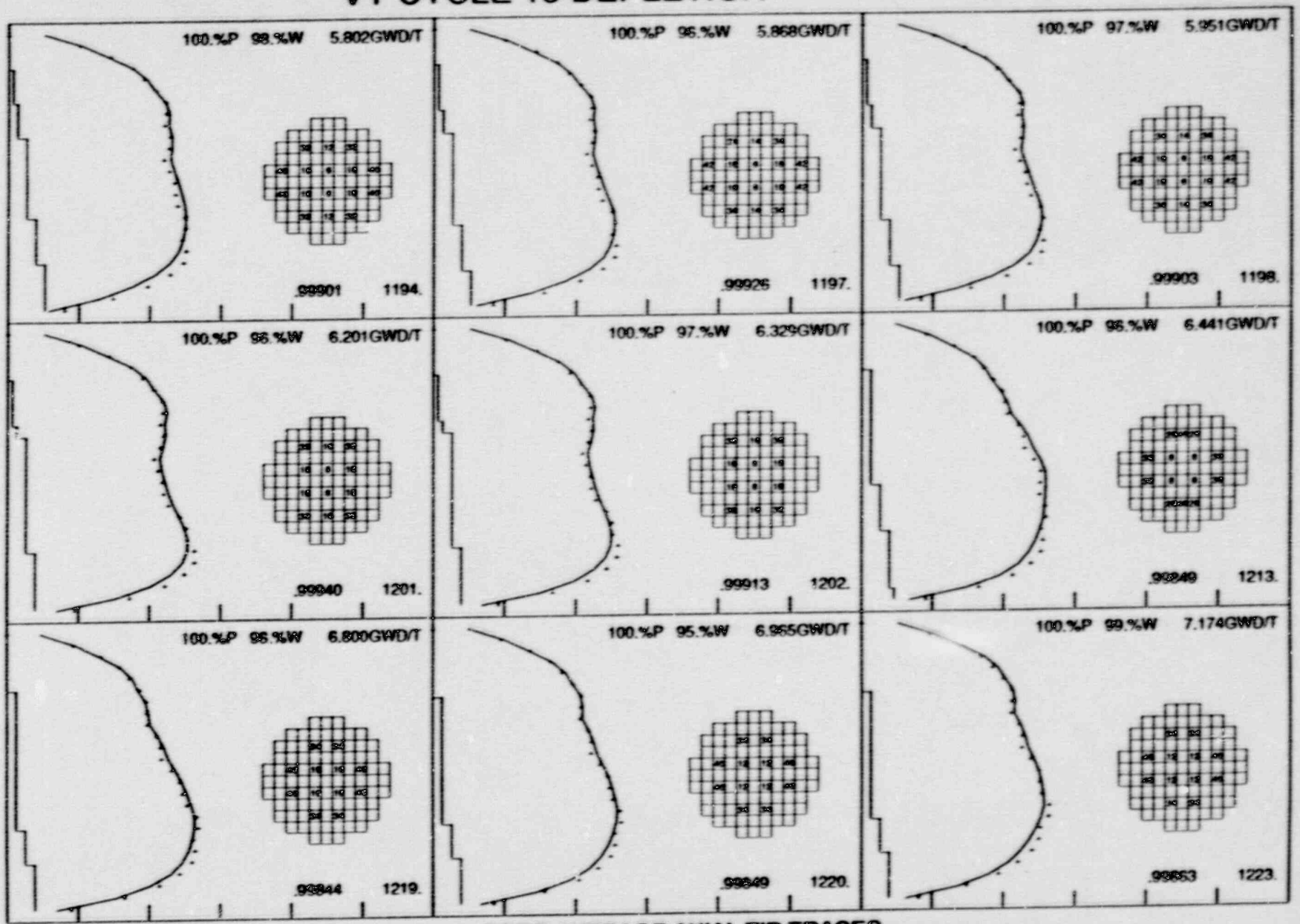

CORE AVERAGE AXIAL TIP TRACES

(*) $USER.DEP9.CYCLE13.TEMP.S3SCY13 S3F9S8 VERMONT YANKEE 02/21/02 09:39:00 2.30-SUN
(X) $USER.DEP9.CYCLE13.TEMP.S3DCY13 S3F9S8 VERMONT YANKEE 02/21/02 09:39:04 2.30-SUN

FIGURE D.10 (Continued)

VY CYCLE 13 DEPLETION

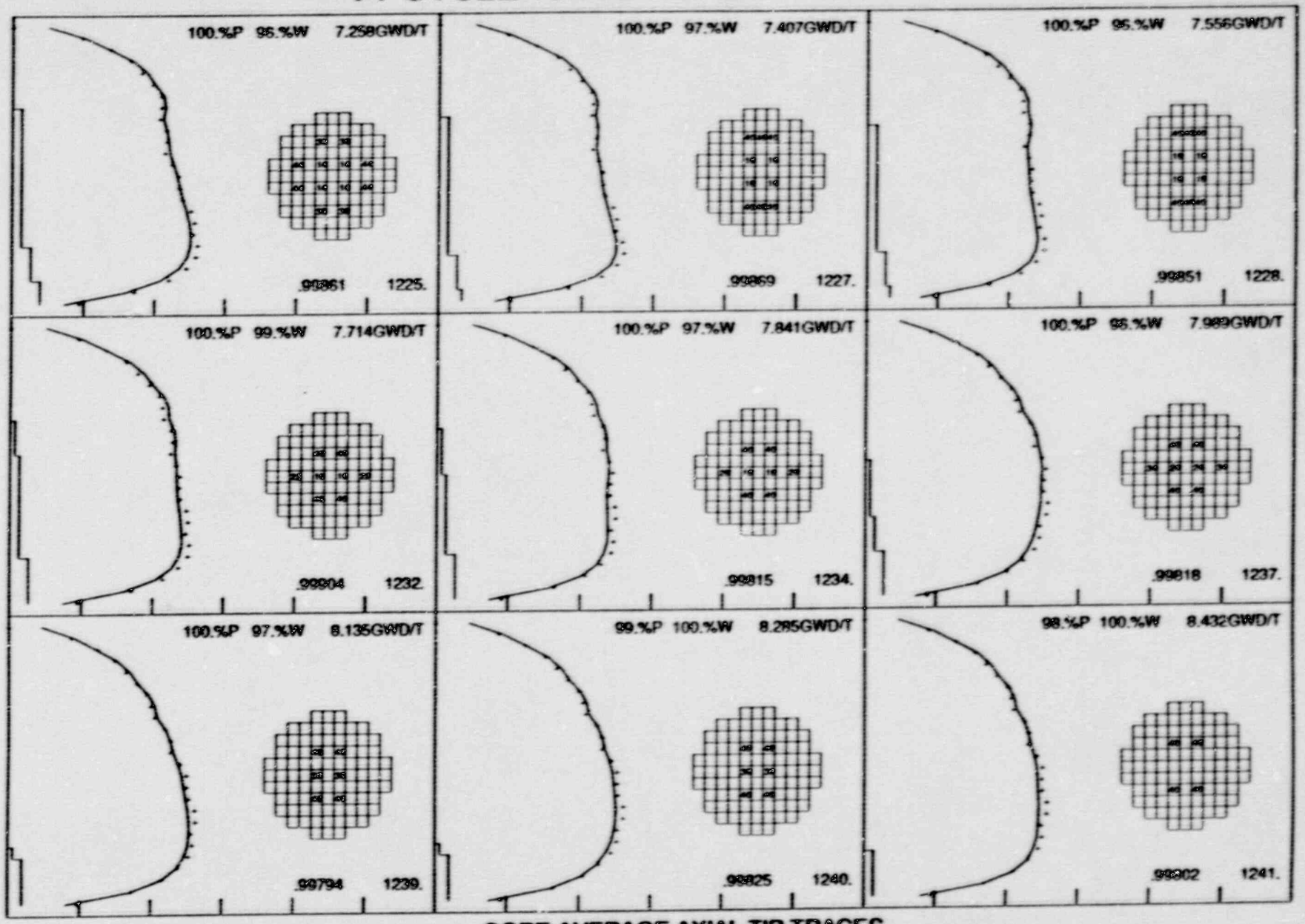

CORE AVERAGE AXIAL TIP TRACES

(*) SUSER:DEP8.CYCLE13.TEXP.S29CY13 S29CY13 VERMONT YANKEE 02/21/00 09:39:00 2.32-SUN
(X) SUSER:DEP8.CYCLE13.TEXP.S30CY13 S30CY13 VERMONT YANKEE 02/21/00 09:39:00 2.32-SUN

FIGURE D.10 (Continued)

VY CYCLE 13 DEPLETION

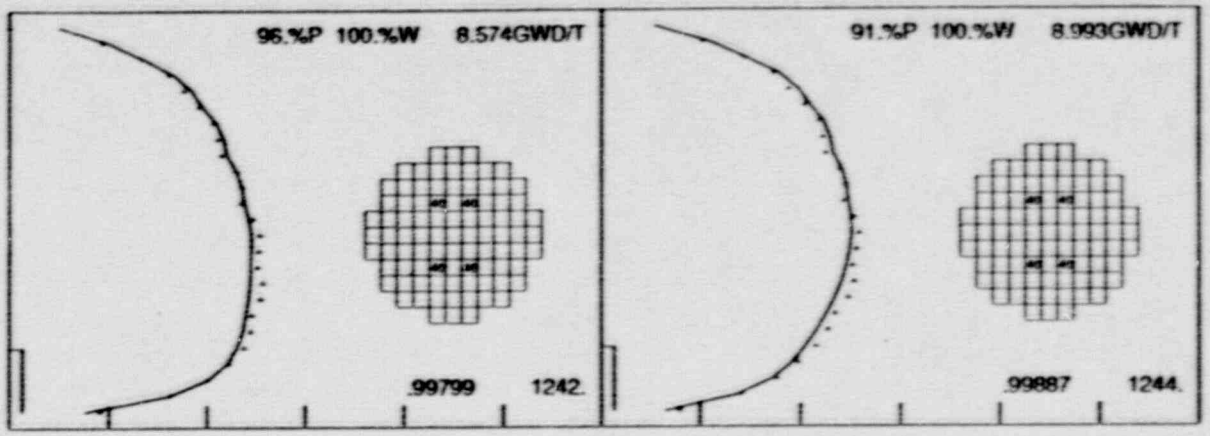

FIGURE D.10 (Continued)

CORE AVERAGE AXIAL TIP TRACES

() $USER:DEP8.CYCLE13.TEMP.S35CY13 S35CY13 VERMONT YANKEE 02/21/89 09:38:04 2.35-SUN 88/09/09

$USER:DEP8.CYCLE13.TEMP.S30CY13 S30CY13 VERMONT YANKEE 02/21/89 09:38:04 2.30-SUN 88/09/09

APPENDIX E

RESPONSES TO REQUEST FOR ADDITIONAL INFORMATION CONCERNING YAEC-1683, MICBURN-3/CASMO-3/TABLES-3/SIMULATE-3 BENCHMARKING OF VERMONT YANKEE CYCLES 9 THROUGH 13

QUESTIONS AND ANSWERS

1) Q. ***How will the reduced K_∞ uncertainty impact the YAEC Licensing Analyses?***

A. On Table 5.7 of YAEC-1683, the hot eigenvalue standard deviation is reduced from ±.00281 with SIMULATE-2 to ±.00098 with SIMULATE-3. Most of this improvement with SIMULATE-3 is caused by a reduction in eigenvalue drift with exposure. As Figure 1.1 illustrates, both SIMULATE-2 and SIMULATE-3 track along well defined paths. It is the consistent behavior of the hot model's eigenvalue path which provides confidence in the predictions made during the licensing (e.g., end of cycle exposure, critical rod patterns for initiating transients, etc.). Since both models have well defined pathways, the hot portion of the licensing will not be affected by this reduction in hot K_∞ uncertainty.

The reduction in cold K_∞ uncertainty with SIMULATE-3 will also not affect the conservatism of the licensing analysis. YAEC does not intend to change the statistical level of confidence or the Technical Specification limit for cold shutdown margin as a result of the reduction in cold K_∞ uncertainty.

2) Q. ***Describe the procedure used to adjust the CASMO-3G pellet densities when the calculated and measured assembly weights for a given fuel type disagree.***

A. A zero depletion step CASMO-3G case is run, for the majority lattice of the fuel bundle, using the nominal pellet stack density as an initial guess. The output from this zero depletion case provides the lattice cell area (cm^2) and heavy metal density (gmU/cm^3). Multiplying these values by the active fuel length (cm) produces an overall HM loading for the assembly (gmU). The latter is compared to the batch average of the as-loaded weights. The ratio of weights (as-loaded to CASMO-3G) provides an adjustment factor to correct the next CASMO-3G input density.

In general, one iteration is sufficient. For the fuel benchmarked in YAEC-1683, this procedure resulted in a 0.2-0.3% increase in stack density to achieve the batch averaged as-loaded weights.

3) Q. ***Will the Vermont Yankee SIMULATE-3 model be applied to fuel types that are not included in the Cycle 9-13 data base and how does the YAEC-1683 benchmarking justify this application? What are these new fuel types?***

A. Yes, the SIMULATE-3 (and CASMO-3G) model benchmarked in YAEC-1683 will be applied to fuel types not included in the Vermont Yankee (VY) Cycles 9-13 data base. Justification is based upon the concept that: This benchmark, along with others performed by YAEC and the code vendor, are consistent over a wide range of fuel parameters; therefore, small extrapolations beyond these ranges should exhibit similar behavior when modelled.

It is not possible, at this time, to define the future fuel types that VY might employ. However, the fuel vendors generally introduce design changes in evolutionary steps, which are usually tested by means of lead test assemblies (LTAs). This provides a long lead time in which to test SIMULATE-3 against vendor results for the LTAs. This should allow YAEC sufficient time to respond to any licensing or operational implications in an orderly manner.

4) Q. ***How do the CASMO-3G and SIMULATE-3 lattice parameters compare in the SIMULATE-3 "Audit" calculation?***

A. The "Audit" calculation of SIMULATE-3 shows that the CASMO-3G cross-sections, etc., are accurately transmitted by TABLES-3. For QA purposes, YAEC has found that the best overall figures of merit are the SIMULATE-3 generated values of K_∞ and M^2 listed in Audit. Typically, the absolute differences observed between CASMO-3G and SIMULATE-3 are less than .02% for K_∞, and less than .07% for M^2.

5) Q. ***Since some "leeway" exists in the specification of the thermal-hydraulic parameters, how were these parameters selected and how sensitive are the calculations to this selection?***

A. The "leeway" referred to on page 24 of YAEC-1683 consists of the following choices:

a.) Whether to use plant process computer generated subcooling as an input, or to use the internal SIMULATE-3 heat balance.

b.) Whether to turn on the spacer correction in SIMULATE-3, or leave it off.

For the benchmark, the plant process computer values of subcooling were used, because they were readily available. A subsequent sensitivity study, using the heat balance, gave virtually identical results to those shown in YAEC-1683.

With regard to the spacer correction, Cycles 9-13 were initially depleted without the spacer correction. Turning on the spacer correction resulted in minor changes: The spacer correction brought the hot eigenvalue closer to 1.0 and slightly improved the comparisons to plant instrument (TIP) readings as illustrated in Figures 4.10-4.12 of YAEC-1683.

6) Q. ***Describe the thermal-hydraulic adjustment made to account for the spacers. Why wasn't this effect accounted for by an adjustment of the local nuclear parameters?***

A. The EPRI-Void model, used in SIMULATE-3, does not account for the highly localized pressure drop and voiding effects in the immediate vicinity of the spacers. The spacer correction is an adjustment which accounts for the local accumulation of steam above the fuel spacers by increasing the local void fraction. The local void adjustment decreases to zero a small distance downstream of the spacer. Since the local accumulation of voids above the spacer is a physical thermal-hydraulic phenomenon it would not be appropriate to model its effect with adjustments to the nuclear parameters.

7) Q. *How was the reactor period converted to reactivity in the cold-critical measurements?*

A. The reactivity correction (-ρ) for reactor period (T) was calculated using the in-hour equation. For large periods, the in-hour equation reduces to:

$$\rho = \sum_{1}^{6} \frac{\beta_i}{+\lambda_i T}$$

The six group β_i and λ_i point kinetics parameters are generated during the licensing of each cycle. The values of β_i change slightly from cycle to cycle, and change with exposure within a given cycle. The use of cycle and exposure specific values for β_i causes some variation in the period corrections used in the benchmark. These are plotted versus stable reactor period in Figure 7.1.

8) Q. *What input does FIBWR provide?*

A. FIBWR is an approved licensing code which provides SIMULATE-3 with the split between active channel flow (moderator in contact with heated fuel rods) and bypass flow (moderator outside the channel plus flow up the water tubes). The split between the two is generated at several different values of total core flow. The bypass flow is input to SIMULATE-3 as a table versus total core flow.

9) Q. *What axial and radial distribution of channel-bow was assumed in the Vermont Yankee calculations? What was the basis for this distribution and did it depend on fuel burnup?*

A. This is described in the answer to Question 14.

10) Q. *Shouldn't the TIP uncertainty be $1\sqrt{2}$ rather than 1/2 of the rms difference between symmetric TIPs?*

A. Yes it should be $1\sqrt{2}$. The description of total TIP uncertainty provided on page 44 of YAEC-1683 is in error. However, the values for total TIP uncertainty shown in Table 5.6 of YAEC-1683 are calculated properly.

11) Q. *How were the non-equilibrium state-points which were excluded from the calculation/measurement comparisons identified? Were other Cycle 9-13 state-points excluded from the benchmark comparisons and, if so, why were they excluded? Why aren't Cycle 11 and 12 EOFPL cold-critical comparisons included?*

A. As part of standard core follow guidelines, YAEC receives TIP data several days to a week following control rod maneuvers at the plant. This data is taken at, or near, xenon equilibrium conditions. The decision regarding the xenon equilibrium status of these transmitted TIP sets is made by Vermont Yankee (VY), based upon the steady behavior of power and flow versus time. All data provided to YAEC by VY, as part of standard core follow, was used in the benchmark. YAEC did not exercise any discretion in eliminating data from the benchmark.

Regarding the cold criticals: Cold criticals were not performed near EOFPL for Cycles 11 and 12 because VY did not scram near EOFPL in these cycles. End of cycle (EOC) cold criticals have not been performed at VY since Cycle 10.

12) Q. ***How did the calculation/measurement difference for the adjacent-rod critical compare with the typical differences obtained for the in-sequence critical measurements?***

A. The adjacent-rod critical (local critical) is the first critical shown on Table 5.4 of YAEC-1683. The local critical eigenvalue is .99258. This compares to an average for all cold criticals of .99680±.00168. Thus, the local critical falls outside the range of the standard deviation.

As a solitary data point, the deviation of the local critical from the average does not indicate a weakness in the methods, per se. As proof that the overall BWR methods are working, refer to the SIMULATE-3 topical YAEC-1659. The benchmark of Quad Cities, shown in Table 4.2 of YAEC-1659, contained 10 local criticals and 8 in-sequence criticals. The local criticals averaged .9983±.0005. The in-sequence criticals averaged .9967±.0026. These statistically overlap, demonstrating that SIMULATE-3 local critical results are consistent with in-sequence critical results.

13) Q. ***The proposed SIMULATE-3 model has essentially no factors for adjusting the model calculations in order to improve agreement with cycle specific measurements. If the calculation/measurement differences for a future cycle increase above the values given in YAEC-1683, how will this increased uncertainty be accommodated? Will the model be adjusted or will the uncertainty margin in the calculations be increased? How will this change be documented?***

A. If the calculation/measurement differences for a future cycle increase above the values given in YAEC-1683, the increased uncertainty would be statistically factored into the data base of those important parameters that affect licensing. The model would not be adjusted under these circumstances. Changes in the uncertainty margins, and how they are implemented to preserve conservatism in licensing, would be documented in the licensing process.

If, for any unforseen reason, changes to approved methods would be required, these would be reported to the USNRC.

14) Q. ***Provide a detailed description of the technique used to incorporate the results of the CASMO-3G calculations for the bowed-channel bundles in the CASMO-3G/SIMULATE-3 model. In addition to the deflection of the channel walls, are the fuel pins in the lattice also assumed to be displaced? How are the effects of channel-bowing on fuel rod power peaking accounted for?***

A. A conscious decision was made, when building the model, to keep it as simple as possible, while including the majority of known physical effects. With regard to channel bowing these physical effects are:

a.) Axially, the channel provides structural rigidity to the fuel. The spacers are in virtual contact with the channel and move with it.

b.) New channels have some bow which averages approximately 30 mils. The manufacturer pre-orients the bow away from the wide-wide corner to preclude any control rod interference.

c.) The fast flux gradient in D-lattices creates a positive feedback in differential Zr growth that causes bowing away from the blade to increase with exposure.

d.) The bowing in exposed channels has an axial shape that seems to follow the axial power distribution history.

Effect (a) is implemented in the model by having the entire lattice, pins and all, deflected in CASMO-3G by the amount of bow. This is achieved in CASMO-3G by simply adding to the dimensions of the wide water gap, while subtracting an equal amount from the dimensions of the narrow gap. Since the pins keep the same geometry relative to the channel walls, they have effectively moved with the channel-bow.

Changing the width of the water gaps affects the magnitude of local peaking as a function of burnup. The local peaking factors that CASMO-3G produces for the deflected lattice are input, via TABLES-3, directly into SIMULATE-3. Therefore, the effects of channel-bowing on fuel rod power peaking are accounted for.

Effect (b) is implemented by modelling the bow in CASMO-3G starting at zero exposure.

Effect (c) is partially implemented by using an amount of channel bow which is greater than the as-manufactured average bow (approximately 30 mils). As stated in Appendix C of YAEC-1683, a value of 40 mils was arbitrarily selected by the investigators to approximate the core average channel bow. Thus, some amount of increase due to burnup is included in the model. However, further change in bow during the cycle is not modelled. The amount of bow is kept fixed for the lifetime of the lattice.

Effect (d) is not included: A detailed axial shape was omitted to keep the model simple. The middle lattices of each fuel type are modelled in CASMO-3G with the same deflection for the 0%, 40% and 70% void depletion cases and branches. Figure 14.1 shows what the effective axial representation of the bowing is in the model. For axially zoned fuel, the top and bottom fuel zones are assumed to have no deflection. All middle fuel zones are run in the CASMO-3G model as if they were uniformly deflected by the full amount of the assumed bow.

To summarize the answer to Question 9, based on the details provided above: The axial and radial distribution of channel-bow in the model is uniform. The amount of bow (uniform deflection) modelled is arbitrarily set at 40 mils. This amount of bow exceeds the as-manufactured amount; therefore, some of the increase in channel-bow with burnup is included in the model. However, the assumed amount of deflection in the model remains fixed during the cycle.

15) Q. ***In view of the wide range in coolant temperatures during the cold critical tests (Table 5.4), is a temperature correction applied to the cold critical eigenvalues of Figure 5.2?***

A. The temperature of each cold critical statepoint is explicitly input into the given SIMULATE-3 case. This is sufficient to allow SIMULATE-3 to interpolate between cross-section sets at 68°F and 300°F. No correction is made to the final SIMULATE-3 answer except for the reactivity adjustment for reactor period (see answer to Question7).

Figure 1.1

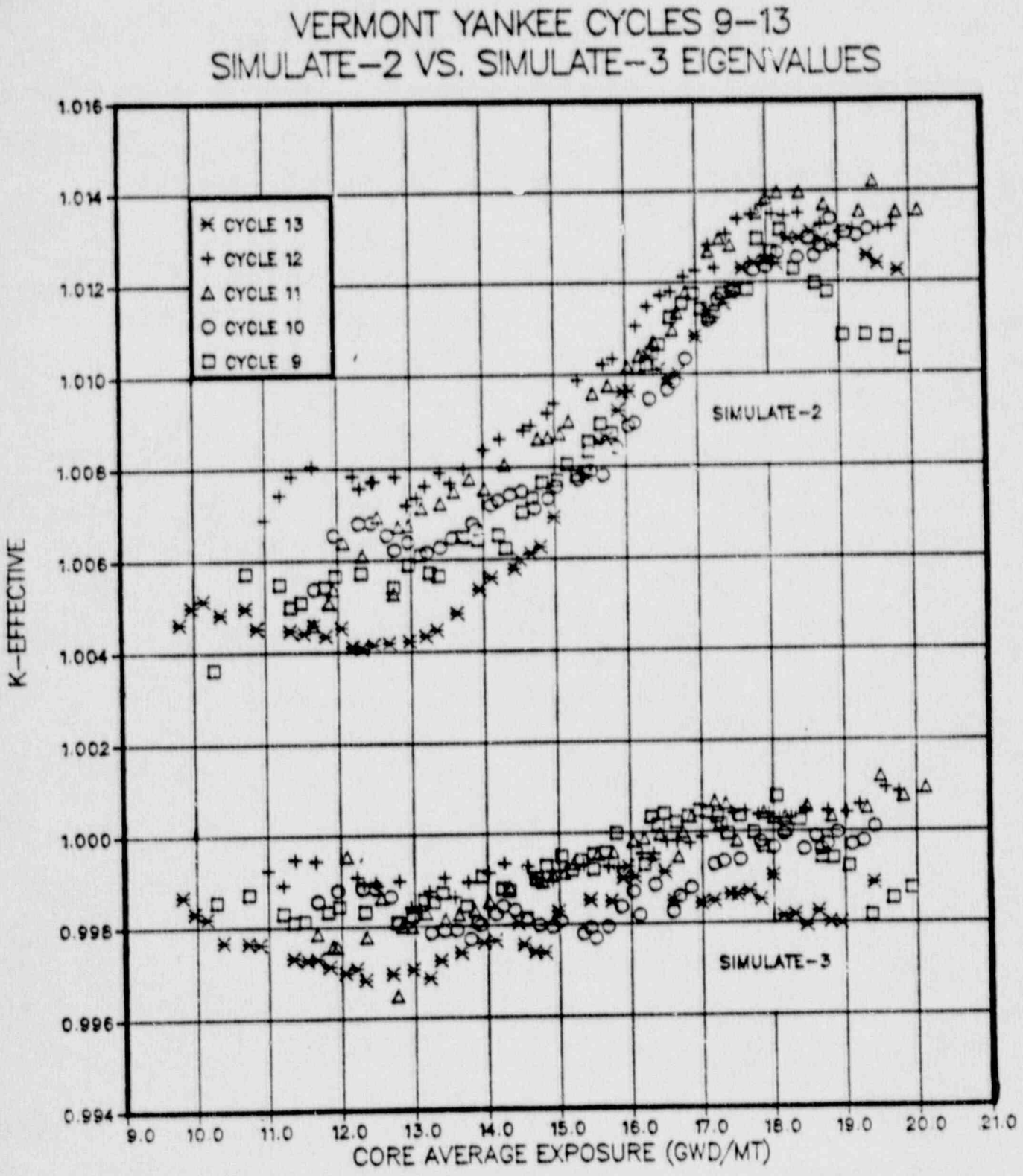
VERMONT YANKEE CYCLES 9–13
SIMULATE–2 VS. SIMULATE–3 EIGENVALUES
K–EFFECTIVE
CORE AVERAGE EXPOSURE (GWD/MT)
CYCLE 13
CYCLE 12
CYCLE 11
CYCLE 10
CYCLE 9
SIMULATE–2
SIMULATE–3
1.016
1.014
1.012
1.010
1.008
1.006
1.004
1.002
1.000
0.998
0.996
0.994
9.0
10.0
11.0
12.0
13.0
14.0
15.0
16.0
17.0
18.0
19.0
20.0
21.0

Figure 7.1

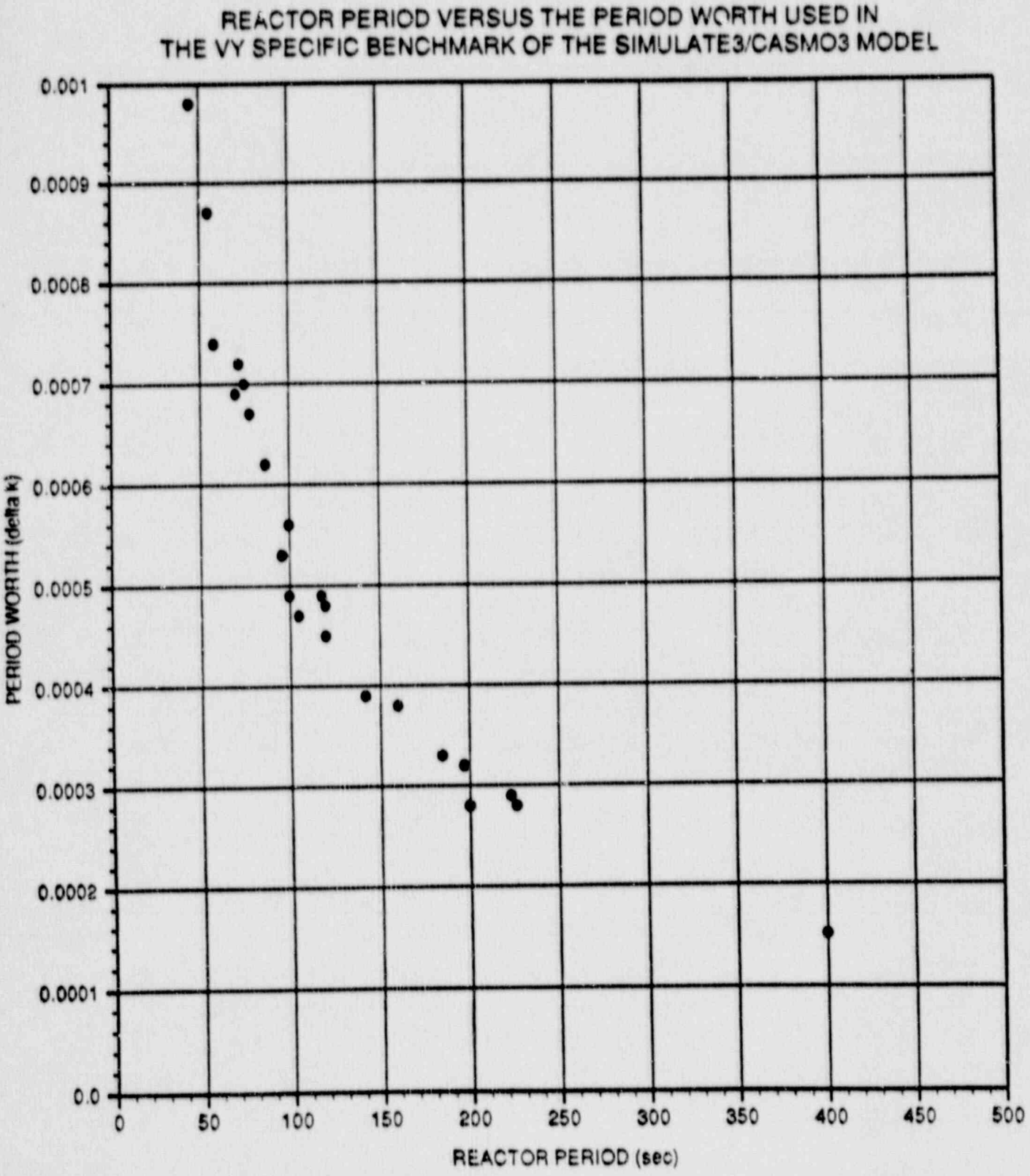
REACTOR PERIOD VERSUS THE PERIOD WORTH USED IN
THE VY SPECIFIC BENCHMARK OF THE SIMULATE3/CASMO3 MODEL
PERIOD WORTH (delta k)
0.001
0.0009
0.0008
0.0007
0.0006
0.0005
0.0004
0.0003
0.0002
0.0001
0.0
0
50
100
150
200
250
300
350
400
450
500
REACTOR PERIOD (sec)

Figure 14.1

UNIFORM DEFLECTION OF THE MIDDLE ZONE AWAY FROM THE WIDE-WIDE CORNER

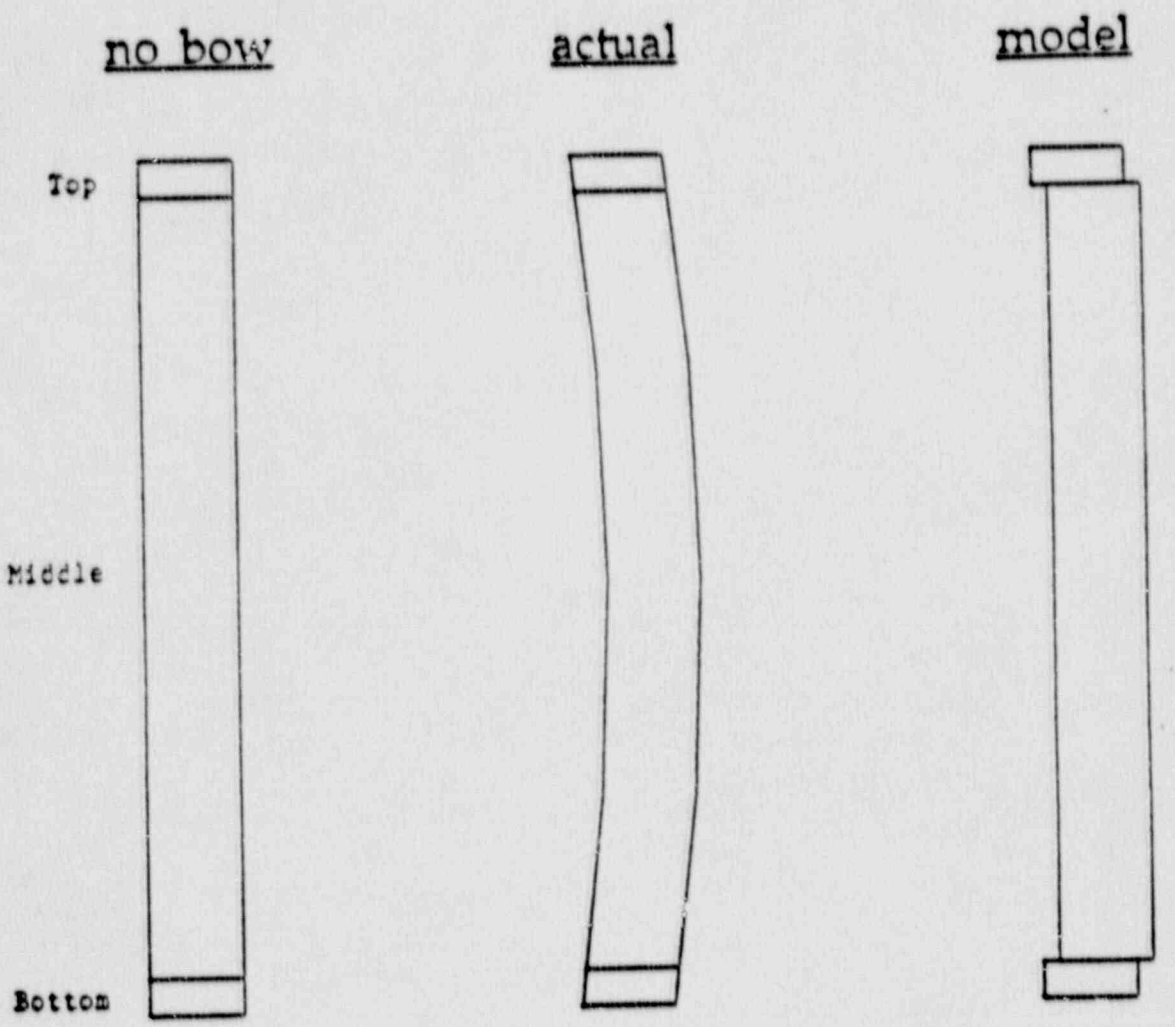

Simple Model For Channel Bowing